2010

JAEA R&D Review

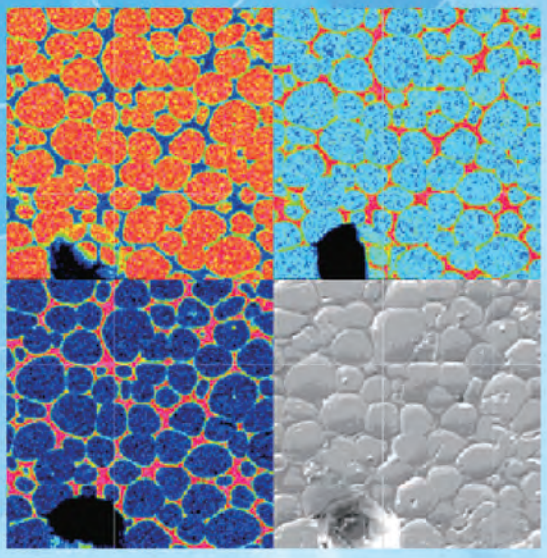

Element mapping images of MOX-6.9wt%SiO_2 analyzed by EPMA

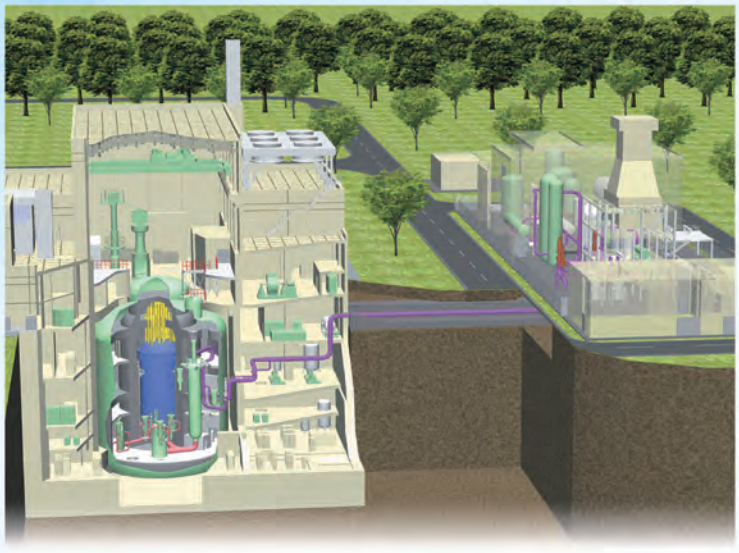

HTTR-IS nuclear hydrogen production system

Message from the President

鈴木篤之

President Atsuyuki Suzuki

Welcome to the fifth issue of the "JAEA R&D Review", informing you of the current R&D activities of the Japan Atomic Energy Agency (JAEA).

This year, JAEA has started its activities under the second 5-year mid-term plan. JAEA was reorganized in 2005 as the sole comprehensive R&D institute for nuclear energy in Japan. JAEA has promoted a wide range of research and development, including establishment of future nuclear fuel cycle technology, basic research and practical application related to nuclear energy.

Recently, the importance of energy security and global environmental issues has become universally recognized, and the role of nuclear technology is significant in supporting the sustained development of mankind.

In this context, on the premise of safety and reliability, we continued R&D of "MONJU" and related techniques toward the completion of fast breeder reactor fuel cycle. In the field of R&D for utilization of applied quantum beams, JAEA continues to put great effort into the operation J-PARC (Japan Proton Accelerator Research Complex) which utilizes the most advanced quantum beam technologies. In the field of fusion energy, the International Fusion Energy Research Center (IFERC) was completed at Rokkasho in March 2010, as the one of the Broader Approach (BA) activities under the International Thermonuclear Experimental Reactor (ITER) Project. Furthermore, we will steadily promote the development of technology for treatment and geological isolation of high-level radioactive wastes, as well as decommissioning engineering for our own nuclear facilities, and disposal of low-level radioactive wastes from research facilities in Japan.

In these ways, we will actively transmit and utilize our R&D results on nuclear engineering, nationally and internationally.

This publication constitutes a review of our achievements in the fiscal year 2009. It provides you with a look at some of the work that has been carried out, and also invites you to check the references listed and contact the researchers if there are any topics that you wish to learn more about. I would be most gratified if I could hear from you with any comments on this publication.

I hope that you enjoy this publication. Thank you for your interest.

JAEA R&D Review 2010

3 Nuclear Fusion Research and Development

4 Quantum Beam Science Research

About This Publication and the Outline of Organization of JAEA

This publication aims to introduce the latest our R&D results in each field, divided into their respective chapters. The R&D results presented in each chapter, correspond to the activities of the relevant R&D Directorates. As shown in the Organization Chart, the various R&D Directorates carry out their activities through R&D Centers or Institutes. Some of these consist of only one site, while others are located two or more locations, depending on the components of their R&D activities. The R&D Centers and Institutes are located all over Japan, as shown in the map below. The following brief introductions give an outline of research undertaken by each R&D Directorate through the various R&D Centers/Institutes.

1. The **Advanced Nuclear System Research and Development Directorate** carries out R&D aimed at commercializing the fast breeder reactor (FBR) and its nuclear fuel cycle. The Tsuruga Head Office undertakes R&D using the prototype fast breeder reactor "MONJU", the Oarai Research and Development Center conducts R&D on reactor technology using the experimental fast reactor "JOYO" and other test facilities, and the Tokai Research and Development Center (Nuclear Fuel Cycle Engineering Laboratories) conducts R&D on manufacturing plutonium fuel and reprocessing FBR fuel, among others.
2. The **Geological Isolation Research and Development Directorate** is carrying out multidisciplinary R&D aimed at improvement in reliability of geological isolation of high-level radioactive waste in Japan. A particular focus involves establishing techniques for investigating the deep geological environment through researches both at the Tono Geoscience Center in crystalline rocks and at the Horonobe Underground Research Center in sedimentary rocks. At the Tokai Research and Development Center, the focus is on improving technologies for designing disposal facilities and safety assessment. In addition, work has been on going to develop a next generation knowledge management system based on the above R&D activities.
3. The **Fusion Research and Development Directorate** operates through two research centers. One of these, the Naka Fusion Institute, takes care of Japan's procurement as a domestic organ of the International Thermonuclear Experimental Reactor (ITER) Project. It also carries out modification planning and core plasma research on the critical plasma test device JT-60 as part of a Japan-EU collaboration and Japanese national program, as well as R&D on various element technologies. The Aomori Research and Development Center, meanwhile, is active as R&D center for fusion computation, DEMO design and R&D, and material irradiation facilities supplementary to the ITER project.
4. The **Quantum Beam Science Directorate** is engaged in research using neutron facilities in the Tokai Research and Development Center (Nuclear Science Research Institute) and J-PARC Center, research using electron beam, gamma ray, and ion beam in the Takasaki Advanced Radiation Research Institute, and research using lasers and synchrotron radiation at the Kansai Photon Science Institute.

Japan Atomic Energy Agency -Outline of Organization-

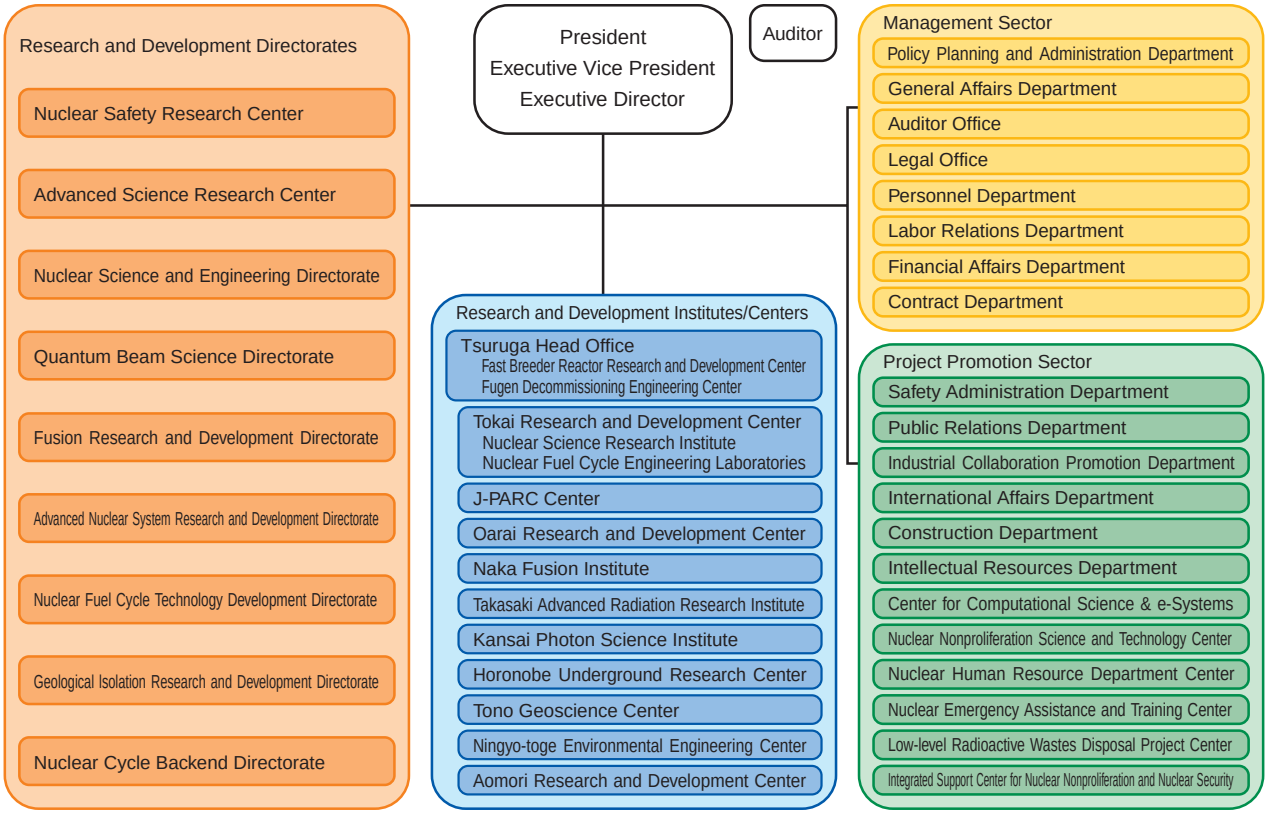

5. Through the Kansai Photon Science Institute, the **Photo-Medical Research Center** conducts R&D on technology for applying lasers to medical treatment, in cooperation with universities and other collaborating research institutions.
6. The **Nuclear Safety Research Center** is in charge of researching for national safety regulations on nuclear power plants, nuclear fuel cycle facilities and radioactive waste disposal facilities, among others, based in the Tokai Research and Development Center and the Tsuruga Head Office.
7. The **Advanced Science Research Center** conducts pioneering research in basic fields of nuclear power science, mainly through the Tokai Research and Development Center (Nuclear Science Research Institute) and Takasaki Advanced Radiation Research Institute.
8. The **Nuclear Science and Engineering Directorate** is engaged in key and basic research on various element technologies that support the use of nuclear power. These efforts are carried out in the Tokai Research and Development Center (Nuclear Science Research Institute) and the Oarai Research and Development Center.
9. The **Nuclear Hydrogen and Heat Application Research Center** conducts R&D on technology for the use of high-temperature heat supplied from high-temperature gas-cooled reactors and technology for hydrogen production using this heat in the Oarai Research and Development Center.
10. The **Nuclear Fuel Cycle Technology Development Directorate** is engaged in developing technology for reprocessing light water reactor spent fuel and processing radioactive waste, and transferring technology to industry, mainly in the Tokai Research and Development Center (Nuclear Fuel Cycle Engineering Laboratories).
11. The **Nuclear Cycle Backend Directorate** develops technology for safe and rational decommissioning of nuclear power facilities as well as measures for processing and disposal of radioactive waste, in the Tokai Research and Development Center.
12. The **Center for Computational Science & e-Systems** develops pioneering simulation technology and basic technology in computational science, as well as operating and maintaining computer equipment, mainly in the Tokai Research and Development Center (Nuclear Science Research Institute).
13. The **Nuclear Nonproliferation Science and Technology Center** develops technology for nuclear nonproliferation and safeguards to ensure the peaceful use of nuclear energy, in the Tokai Research and Development Center (Nuclear Science Research Institute).
14. The **R&D Centers and Institutes** located at 11 sites in Japan, manage and improve the performance of the facilities and equipments to support the above-mentioned R&D Directorates in the safe and efficient R&D activities.

R&D Centers of JAEA

Toward Commercialization of the Fast Reactor Cycle System

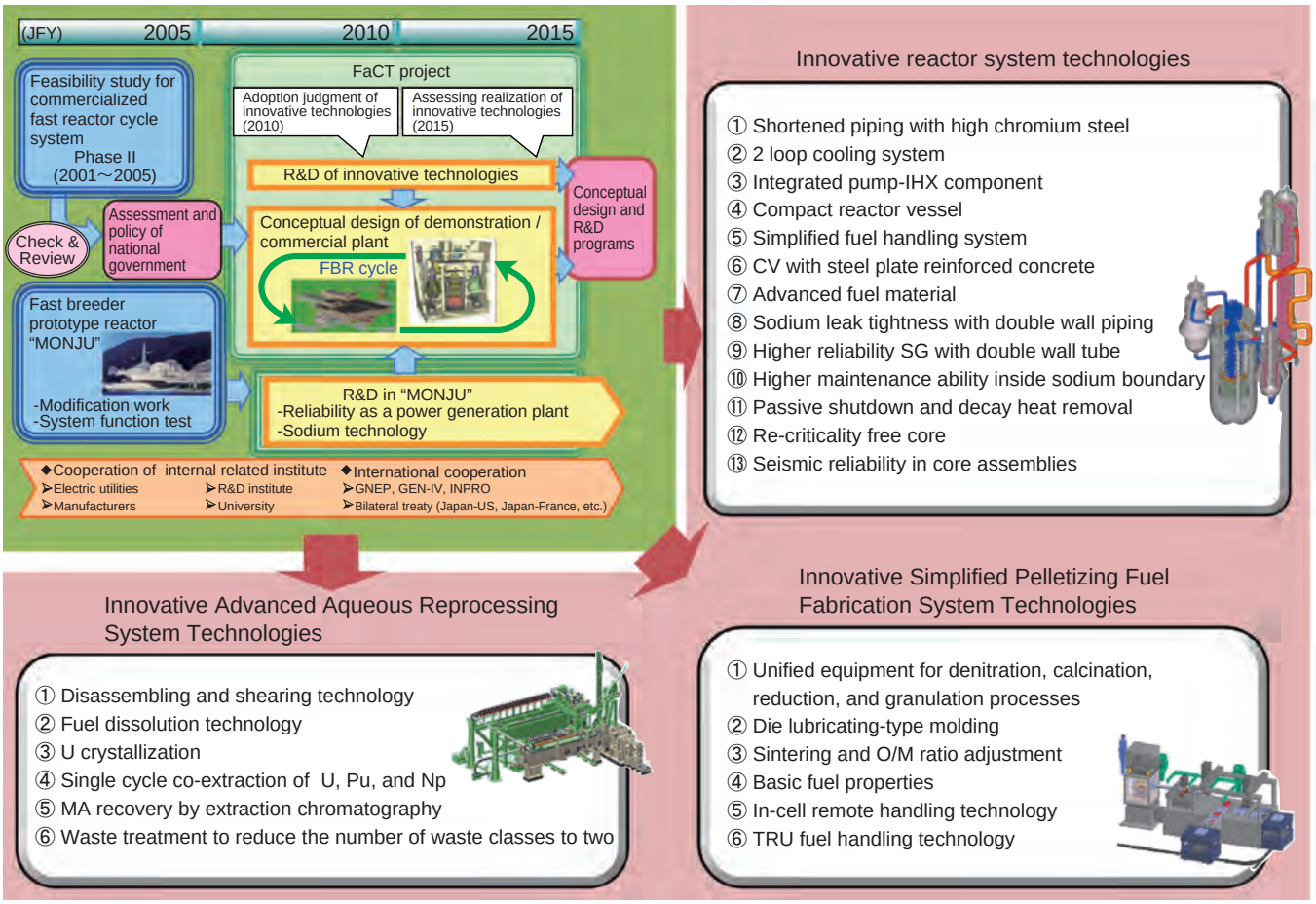

Fig.1-1 Fast Reactor Cycle Technology Development (FaCT Project)
With the aim of starting up a demonstration fast breeder reactor (FBR) around 2025 and introducing it on a commercial basis before 2050, we are now carrying out experimental studies of innovative technologies and design studies. The FaCT project will be implemented in order to decide on which innovative technologies to adopt by 2010 and to present conceptual designs of commercial and demonstration FBR cycle facilities, along with development plans to realize them, by 2015.

With the collaboration of electric utilities and manufacturers, we are now promoting the Fast reactor Cycle Technology (FaCT) development project in order to introduce the commercialization of the Fast Breeder Reactor (FBR) cycle system (Fig.1-1).

As the main concept in the FaCT project, we are developing a combination of a sodium-cooled FBR cycle system utilizing oxide fuel, advanced aqueous reprocessing, and simplified pelletizing fuel fabrication. In FY2009, we advanced the prospects of technologies for the reactor system, the reprocessing system, and the fuel fabrication system. The summary of each topic shown after the next page is as follows.

In the system design of the demonstration reactor and the commercial reactor, the design study and related R&D for the Japan Sodium-cooled Fast Reactor (JSFR) are advancing. We devised the sodium/water boundary concept to improve the reliability of the FBR cooling system (Topic 1-1). In the core design, we evaluated the feasibility of core design methods to enhance nonproliferation characteristics (Topic 1-2).

In terms of developing innovative technologies related to reactor systems, experimental studies on eliminating severe power burst events in core disruptive accidents have been conducted for advancing safety (Topic 1-3), and eddy current simulation technology for detecting defects was developed as a maintenance technology (Topic 1-4).

With regard to innovative technologies development related to reprocessing systems, mechanical disassembly technology for FBR spent fuel was successfully carried out (Topic 1-5). The application of an extraction chromatography system for minor actinides recovery was examined (Topic 1-6). Regarding fuel fabricating system technological development, we investigated the applicability of granulation technology for fuel pellet production (Topic 1-7). We have been analyzing irradiation behavior and the physical properties of FBR fuel (Topic 1-8, Topic 1-9). Furthermore, in the pyrochemical reprocessing process, which was another reprocessing concept (a FaCT project sub-concept), minor actinides were found to be recoverable by a metal electro-refining method (Topic 1-10).

In basic research to support the FaCT project, we discovered a magnetic measurement method whereby irradiation damage is detectable (Topic 1-11), and also a technique to control the chemical activity of liquid sodium by atomic interaction with a nanoparticle surface (Topic 1-12).

1-1 A Reliable Cooling System for a Commercial FBR
－Double Wall Boundary Design Advancing a Commercial FBR－

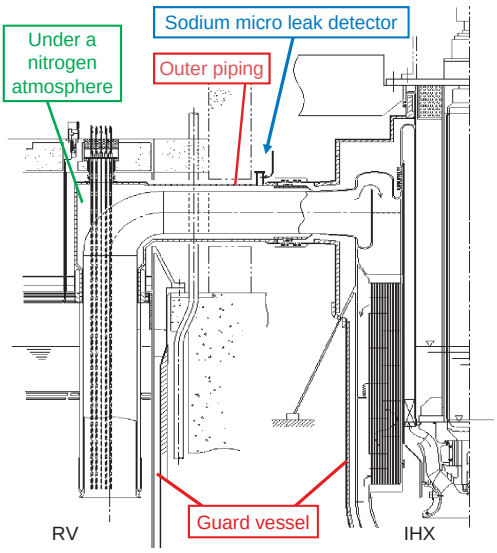

Fig.1-2 Schematic image of a reliable primary cooling system
The primary cooling system has an outer piping and a guard vessel. It contributes to the reliability of the sodium boundary, and is designed to prevent the escalation of accidents by continuously monitoring sodium leak.

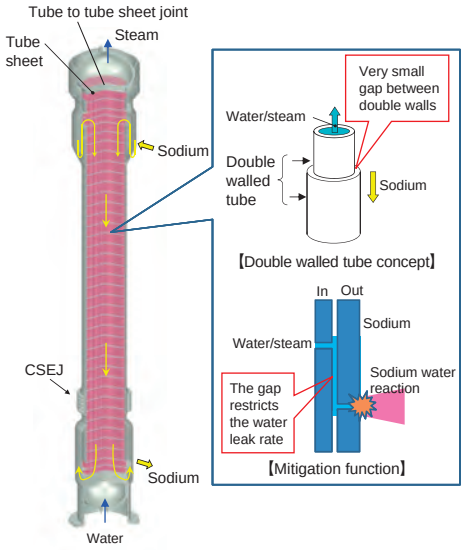

Fig.1-3 Schematic image of reliable SG
A mechanically contacted double walled tube contributes to the reliability of the sodium/water boundary. The gap of the double walled tube can restrict the water leak rate. It contributes to the mitigation of the sodium-water reaction.

In JSFR, we adopted sodium as a coolant because of its good heat transfer capacity properties. However, there is an issue with sodium in terms of its chemical activation, and thus we designed a reliable cooling system using a double wall for all sodium boundaries and sodium/water boundaries. Our design also includes preventing accident escalation by early detection of an emergency boundary failure.

Concerning the sodium boundary, we designed the primary cooling system to provide outer piping as shown in Fig.1-2, and the gap between the piping and the outer piping is under an inert gas atmosphere. Moreover, we designed the reactor vessel (RV) and internal heat exchanger (IHX) to provide a guard vessel to secure a sufficient level of sodium to cool the reactor core. We designed the secondary cooling system to provide an enclosure, and the gap between the piping and the enclosure is under an inert gas atmosphere. Due to these double wall boundary measures, JSFR can prevent thermal damage from the combustion of leaked sodium and chemical damage from the release of sodium aerosol. Moreover, JSFR can provide early stage detection of sodium piping failure by continuously monitoring for sodium micro leaks.

Concerning the sodium/water boundary, we designed a steam generator (SG) tube to eliminate sodium-water reactions by using a double wall tube as shown in Fig.1-3, and we also designed a means to prevent sodium-water reaction accidents by isolating a tube in which a defect is discovered during in-service inspection. Moreover, JSFR can provide early stage detection of tube failure by monitoring of water micro leaks.

To turn these innovative designs into accomplished facts, we are developing a sodium micro leak detector, and adopting Laser Induced Breakdown Spectroscopy (LIBS) as a promising technology to improve signal reliability and sensitivity. We found that the basic functionality of the LIBS technology is attainable. Moreover, we carried out trial fabrication of the double wall SG tube to improve the fablicability by adopting a simple cold drawing manufacturing process and optimized processing conditions. Cold drawing contributes to the reliability of the sodium/water boundary, preventing the penetration of defects by metallurgical separation. The fablicability of a 35 m SG tube is attainable. Moreover, we are developing a water micro leak detector, and adopting a hydrogen sensor as a promising technology to shorten leak detection time. By investigating measures to improve detection time, its basic functionality appears to be attainable.

In the future, we will particularize these design concepts, and determine the base specifications of the demonstration reactor. Moreover, we will advance the demonstration tests of the cooling system and components.

Reference

Kurome, K., Futagami, S. et al., Development of the Main Components for JSFR, Proceedings of 2010 International Congress on Advanced in Nuclear Power Plants (ICAPP'10), San Diego, California, USA, 2010, paper 10247, 8p., in CD-ROM.

1-2 What Core Design Prevents Nuclear Proliferation?
—Commercial FBR Core Study Focusing on a Material Barrier—

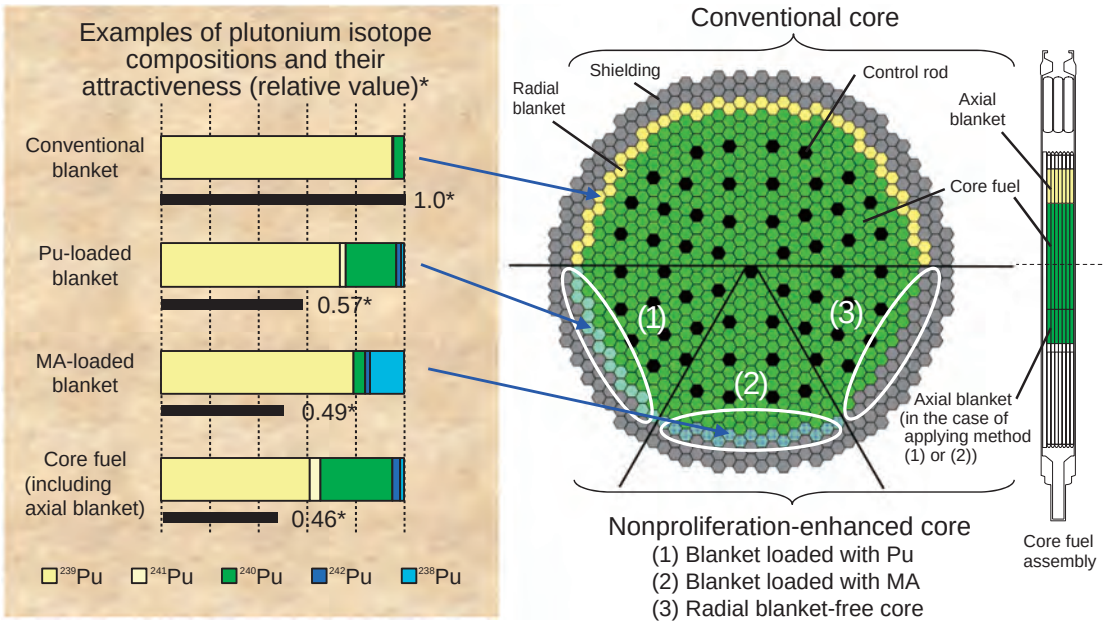

Fig.1-4 Core design methods to enhance the nonproliferation characteristics of the commercial FBR in terms of a material barrier
By means of loading the blanket with plutonium (Pu) or minor actinide (MA), it is possible to reduce the proportion of fissile isotopes and the attractiveness of the Pu produced in the blanket. Moreover, a radial blanket-free core is also possible.

Plutonium (Pu), used as the core fuel of a fast breeder reactor (FBR), consists of around sixty to seventy percent fissile isotopes (^{239}Pu, ^{241}Pu), and the remainder are fertile isotopes (^{240}Pu, ^{242}Pu, ^{238}Pu); this kind of Pu is called "reactor grade." At the same time, in the blanket surrounding the core fuel, uranium is converted into higher grade Pu than reactor grade, in which the proportion of fissile isotopes is more than ninety percent.

As measures in response to concerns about nuclear proliferation due to higher grade Pu, the rigorous safeguards by the International Atomic Energy Agency (IAEA) and the like and the physical protection of nuclear materials essentially keep the system's proliferation resistance at a high level. Moreover, it is possible to keep the Pu products in the fuel cycle system at reactor grade by reprocessing the blanket together with the core fuel. Nevertheless, in a future commercial era when a number of FBRs are deployed, society may come to demand a more enhanced proliferation resistance level. As an example of a way to cope with that situation, we investigated a core design that reduces the attractiveness of nuclear material (that is, which prevents the production of higher grade Pu) while avoiding serious deterioration in core performance, fuel fabrication, fuel handling, and so on. As a result, the three methods (1) to (3) shown in Fig.1-4 were found to be feasible.

Method (1) is to load the blanket with Pu, whereupon the blanket becomes low-enriched fuel with Pu enrichment of 3~5%. No higher grade Pu emerges because from the outset the generated Pu is naturally mixed with the reactor grade Pu added initially. In method (2), minor actinide (MA) on the order of 2~4% produces ^{238}Pu, the decay heat of which is considered to make a large contribution to nonproliferation characteristics. It should be noted that this method is subject to limitations in terms of the MA supply, because MA with low decay heat is necessary from the viewpoint of fuel fabrication and handling. After preliminary evaluation of the attractiveness of Pu for methods (1) and (2), it is foreseen that it is sufficiently possible to reduce the attractiveness of the nuclear material to the same level as core fuel.

Method (3) uses a radial blanket-free core that is made possible by modifications of the core fuel specifications to maintain breeding performance. Method (1) or (2) can be applied to the axial blanket if necessary.

Any of these methods can be expected to enhance the nonproliferation characteristics with respect to the isotope composition of Pu while satisfying the performance requirements of a commercial FBR. We are continuing our efforts to optimize the core concept in consideration of the merits and demerits of each method.

Reference

Ohki, S. et al., FBR Core Concepts in the "FaCT" Project in Japan, Proceedings of International Conference on the Physics of Reactors, Nuclear Power: A Sustainable Resource (PHYSOR'08), Interlaken, Switzerland, 2008, log649, 10p., in CD-ROM.

1-3 For Advanced Safety of Next-Generation FBRs
—Elimination of Severe Power Burst Events in Core Disruptive Accidents—

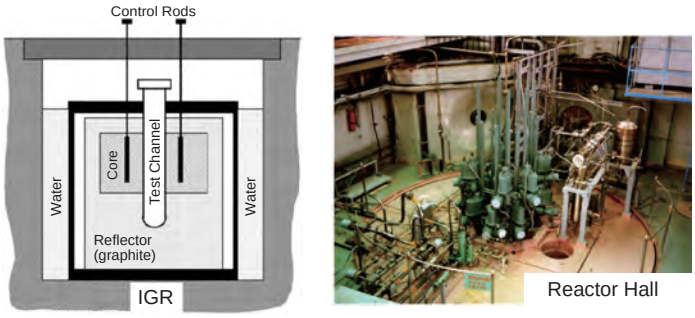

Fig.1-5 IGR and test channel
IGR core concept (left) and above-core structure including control-rod drive mechanism (right).

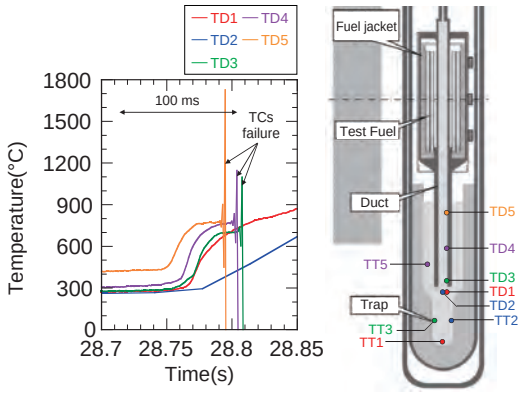

Fig.1-7 An example of EAGLE test data
Thermocouples placed in the lower part of the test channel show a temperature increase corresponding to the arrival of high temperature material.

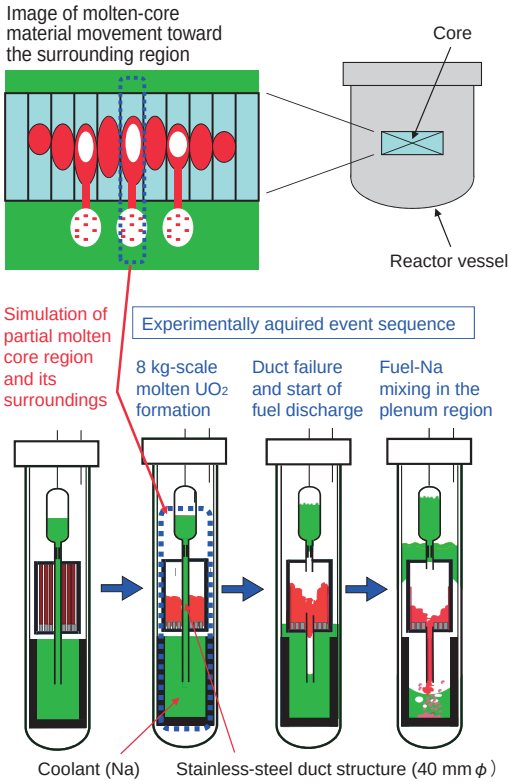

Fig.1-6 Molten core simulation concept in the experiments

In the area of FBR safety research, experimental studies on molten core material behavior in a core-disruptive accident (CDA) have been conducted to confirm that the consequences can be appropriately mitigated, although the possibility of such accidents is extremely low. In conventional CDA evaluations, it is assumed that a large amount of molten fuel remains within the core region, creating the potential for significant power excursion with massive molten fuel movement. With next generation FBRs, however, the intention is to adopt early discharge of molten fuel from the core region (either upward or downward), introducing a duct structure within the fuel subassembly, and to demonstrate the effectiveness of this by experiments.

In collaboration with the National Nuclear Center of the Republic of Kazakhstan, JAEA is conducting the experimental project EAGLE utilizing IGR (Impulse Graphite Reactor). IGR has a central hole as illustrated in Fig.1-5 which can accommodate a test channel equipped with a double-layer pressure vessel enclosing fuel for testing. Four experiments producing approximately 8 kg of molten UO_2 have been performed thus far, and these have provided information on how accidents progress (Fig.1-6). Fig.1-7 shows an example of the data obtained from the experiments. The data showing the response of the thermocouples, TD1 to TD5, placed within the duct, reveal downward movement of high-temperature material. In addition, the thermocouples TT1 to TT3 and TT5, placed in the lower trap, show that the high-temperature material reached to within the lower trap. Coupled with data from pressure gauges, microphones, and the like, the data allowed us to clarify the physical process. In this experiment, the process of duct failure and subsequent molten fuel discharge into the lower trap was implemented.

The JSFR design employs a duct structure option allowing upward fuel discharge, and experiments reflecting this design have also been conducted. Through this EAGLE experimental study with the duct structure, it has been confirmed that early escape of molten fuel prevents large molten fuel pool formation, and thus provides a perspective on how the consequences of accidents can be appropriately mitigated.

Reference

Tobita, Y., Sato, I. et al., Development of Severe Accident Evaluation Technology (Level 2 PSA) for Sodium-Cooled Fast Reactors (3) Identification of Dominant Factors in Transition Phase of Unprotected Events, Proceedings of 2009 International Congress on Advances in Nuclear Power Plants (ICAPP' 09), Tokyo, Japan, 2009, paper 9127, 8p., in CD-ROM.

1-4 The Challenge of Detecting Small Defects in SG Tubes
—3D Numerical Simulations of ISI of FBR SG Tubes Using ECT—

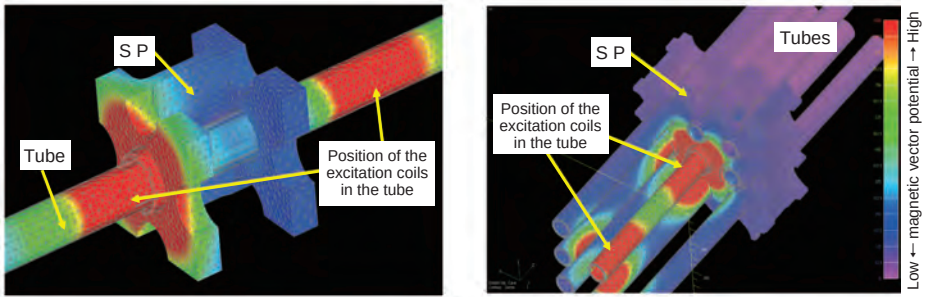

Fig.1-8 Variation in the distribution of the magnetic vector potential in the small (left) and large (right) SP models
In the large SP model, the magnetic field also spreads to the surrounding tubes, which in turn affects the ECT signal.

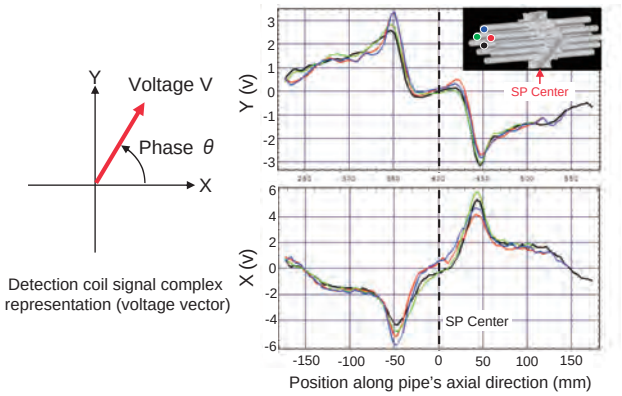

Fig.1-9 Variation in the SP signal according to various tube positions
Variance of analyzed SP signals is not significant among different relative tube positions.

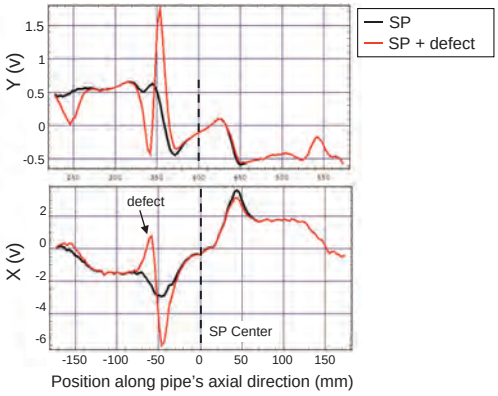

Fig.1-10 ECT signal from a SP when there is or not a defect in the SG tube area under SP
By comparing both signals we can clearly identify the defect in the SG tube (20% thinning of the heat exchange pipe).

One of the methods used in the In-Service Inspection (ISI) of steam generator (SG) tubes of fast breeder reactors (FBRs) is the eddy current technique (ECT). By monitoring changes in the impedance of ECT coils that are inserted in and moved through and along SG tubes, the soundness of the SG tubes can be evaluated. Defects (such as, for example, lack of thickness, cracks, thermal fatigue) in a SG tube are characterized by variations in the electrical conductivity and the magnetic permeability of the monitored region in the SG tube, which leads to interference and disruption in the primary electromagnetic field created by the ECT system.

While simple axisymmetrical models of SG tubes can be modeled in a short time theoretically or in a two-dimensional axisymmetrical approximation, an accurate description of ISI of FBR SG tubes requires a complete three-dimensional (3D) analysis. The interaction of the electromagnetic field and the complex structure of the support plate (SP) of the SG tubes in FBRs is analyzed using a parallel 3D electromagnetic code that has been developed, based on the finite element method, by means of JAEA supercomputers. Numerical 3D simulations are conducted to simulate and to optimize ISI using ECT for a small SP model (as in a mockup), and a large SP model (as in a real reactor) with multiple SG tubes penetrating a large SP (Fig.1-8).

The detectability of smaller defects, resulting from friction between SP and SG tube, originating in areas of SG tubes located under SPs, is analyzed using simulations, and ECT sensor technology is therefore optimized to increase the signal to noise ratio, regardless of the defect location. Variations in the SP signal, interpreted as noise, result either from the position of various SG tubes relative to the SP or from the electromagnetic shielding effect of the surrounding SG tubes (Fig.1-9, Fig.1-10).

Accurate 3D numerical simulations of ISI of FBR SG tubes are used as an effective tool to optimize and enhance the sensitivity of smaller defect detection using ECT, leading to an upgrade in SG tube safety.

Reference

Mihalache, O., Ueda, M. et al., 3D Remote Field-Eddy Current Simulation of the Support Plates of the Magnetic Steam Generator Tubes in FBR, Proceedings of the 7th International Conference on NDE in Relation to Structural Integrity for Nuclear and Pressurized Components, Yokohama, Japan, 2009, p.948-956.

1-5 Reliable Separation of Fuel Pins from the Fuel Assembly
—Development of Mechanical Disassembly Technology for FBR Spent Fuel—

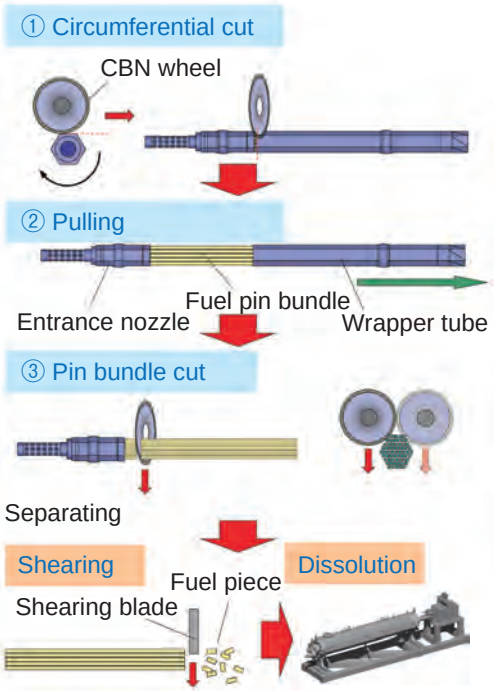

Fig.1-11 Disassembly procedures
The fuel pins are separated from the fuel assembly by cutting and pulling the wrapper tube from the pin bundle.

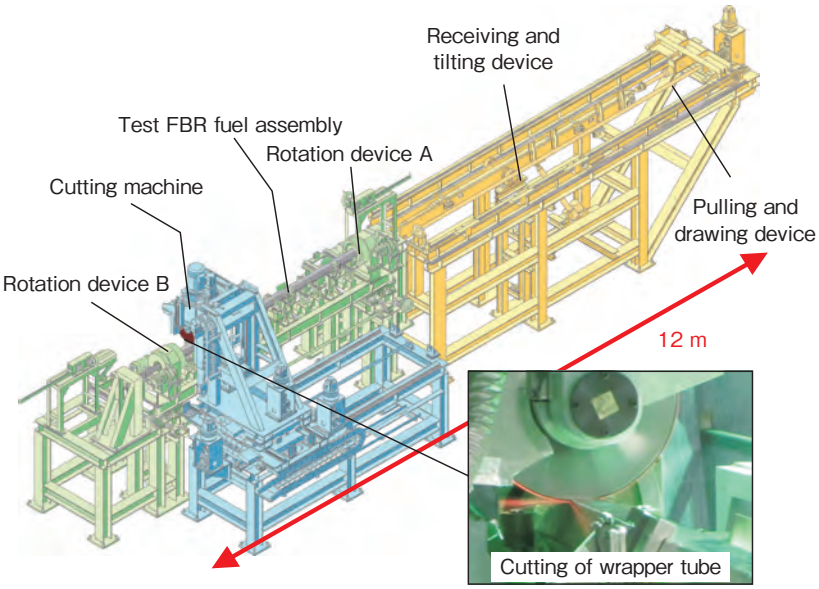

Fig.1-12 Engineering-scale test machine for disassembly operation
This was manufactured for confirmation of the sequential disassembly operation, and performance was evaluated using a mock-up fuel assembly.

FBR fuel pin bundles are arranged in a hexagonal-shaped wrapper tube, and thus the wrapper tube must be disassembled and separated from the fuel pin bundle before shearing. In this technology, the cutting performance is essential for disassembling the wrapper tube, which is made of stainless steel several millimeters thick, and the bundle, which includes a few hundred pins. Accurate control of the cutting depth is required in order not to damage the fuel pins, which are situated below 1 mm from the cutting point. In addition, the effects of irradiation deformation should be considered. Taking these conditions into account, we have developed a mechanical disassembly technology that combines cutting performance with cutting control.

A Cubic Boron Nitride (CBN) wheel was selected as desirable cutting tool. First of all, as shown in Fig.1-11, the wrapper tube is cut around the circumference and pulled from the fuel assembly. Here, if pulling the wrapper tube is not successful owing to the irradiation deformation, cutting toward pulling direction is performed. Next, by crop-cutting at the lower end plug, the fuel pins are separated from the entrance nozzle without being damaged, and they are then passed to the subsequent shearing stage.

We designed and fabricated an engineering-scale test device confirming the sequential disassembly operation using a mock-up fuel assembly (Fig.1-12). A cutting speed control system corresponding to the load on the cutting tool and a measurement system for the wrapper tube surface that takes the deformation into account were prepared in this device. From the test results, it was demonstrated that the cutting performance was good, the damage to the fuel pins was kept as low as possible, and the sequential operation of the overall disassembly procedure was successfully carried out.

In the near future, we will assess a number of points including radiation resistance and remote maintenance to construct a reliable system to be applied to the innovative FBR reprocessing plant.

This work is the result of the study "Developing Technologies for Disassembly and Pin Shearing of FR Spent Fuels," which was entrusted to The Japan Atomic Power Company (JAPC) by the Ministry of Education, Culture, Sports, Science and Technology of Japan (MEXT) in 2009.

Reference

Kitagaki, T. et al., Design and Fabrication of the FBR Fuel Disassembly System, Proceedings of 17th International Conference on Nuclear Engineering (ICONE-17), Brussels, Belgium, 2009, ICONE17-75117, 5p., in CD-ROM.

1-6 Chemical Separation Process Resistant to Decay Heat from Radionuclides
—Extraction Chromatography System for Minor Actinides Recovery—

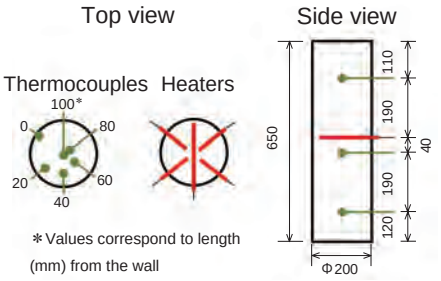

Fig.1-13 Column used for safety tests
The column was 20 cm in inner diameter and 65 cm in height, and equipped with electric heaters and thermocouples inside.

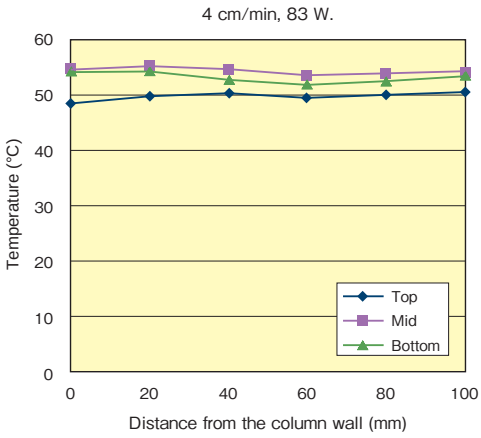

Fig.1-14 Axial distribution of temperatures inside column
Heat was absorbed into water fed to the column at 50 ˚C, and then released from the column.

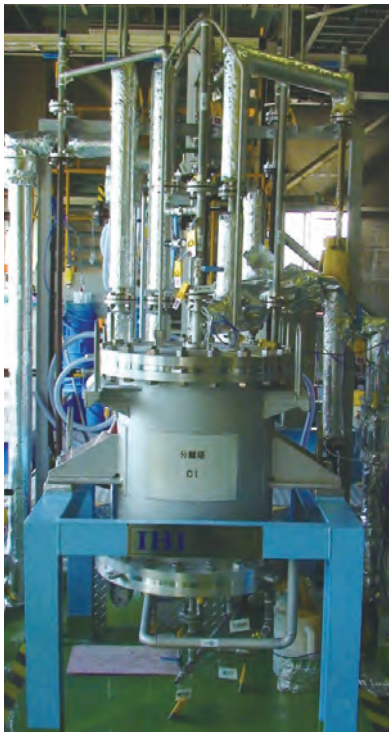

Fig.1-15 Engineering scale testing system
Column 48 cm in inner diameter and 65 cm in height. Procedures were tested for packing and discharging the adsorbents, and recovering from a state of emergency.

Neptunium (Np), americium (Am), and curium (Cm) generated in spent nuclear fuel can be burned to some extent when they are fabricated and used as a MOX fuel. Recycling them will decrease the quantity of these elements that will be contained in highly active radioactive waste. An extraction chromatography technology has been developed in order to separate Am and Cm from highly active liquid waste in nuclear reprocessing. The technique uses a special adsorbent packed in a column. Radioactive waste is fed into the column and the targeted ions are adsorbed and separated from fission products. The high-level liquid waste contains radioisotopes that generate heat and the adsorbent consists of organic extractant; temperature control is thus essential to maintain safety from fire or explosion hazards.

The thermal stability of a number of candidate adsorbents was examined in terms of their pyrolysis behavior to confirm their operational safety. It was also found that, in practical use, there is not a problem with degradation of the adsorbent with exposure to nitric acid solutions as well as γ rays from radioactivity.

When Am and Cm are adsorbed, the possibility of heat accumulating due to their activity should be considered and minimized. The engineering-scale column shown in Fig.1-13 has electric heaters to simulate radioactivity, and was used to investigate temperature distribution inside the column. The temperature inside the column remained constant across the radius as shown in Fig.1-14. The increase in temperature in the axial direction was as small as 3~5 ˚C downstream of the heaters. It was thus confirmed that the separation operation of the column is safely conducted with thermal stability.

Based on this knowledge, an engineering-scale testing system was fabricated, taking remote operation into account, as shown in Fig.1-15. On examination it was found that prevention of abnormal temperature increases is feasible, even supposing a case in which the feeding solutions are forced to a stop.

This series of tests for the engineering column demonstrated its safety properties, and was a step toward the practical application of extraction chromatography in nuclear power.

The present study is the result of "Development of MA Recovery Technology by means of Extraction Chromatography," which was entrusted to us by the Ministry of Education, Culture, Sports, Science and Technology of Japan (MEXT).

Reference

Watanabe, S., Koma, Y. et al., Chromatography Column System with Controlled Flow and Temperature for Engineering Scale Application, Journal of Engineering for Gas Turbines and Power, vol.132, issue 10, 2010, 102903 (7p.).

1-7 Advanced Particle Flowability Measurement for Nuclear Fuel Pellet Production
—Investigation of the Applicability of a Vibrating Tube Method Using Model Particles—

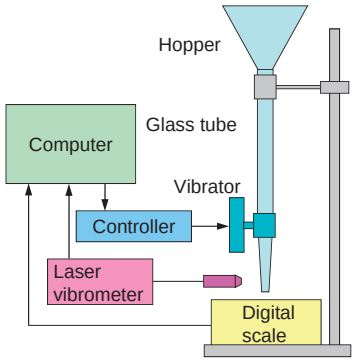

Fig.1-16 Vibrating tube method schematic diagram
Particle flowability is evaluated by measuring the mass flow rate of particles discharged from a vibrating tube while the vibration acceleration is changed.

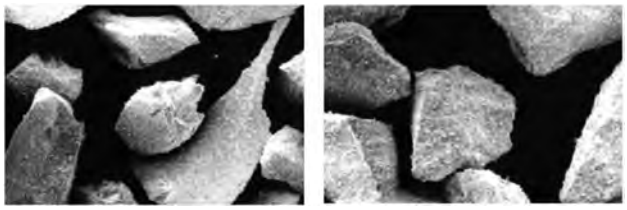

Milling time 0 h (Circularity: 0.78)

Milling time 40 h (Circularity: 0.81)

Fig.1-17 SEM photographs of ZrO_2 particles
The shape and surface state of the particles were changed by mechanical treatment using a ball mill.

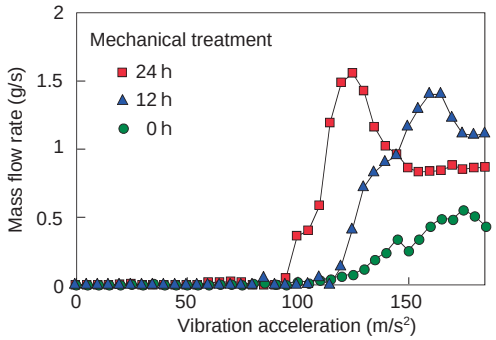

Fig.1-18 Flowability profiles of ZrO_2 smaller than 45 μm
The vibrating tube method can detect differences of shape and surface state among samples.

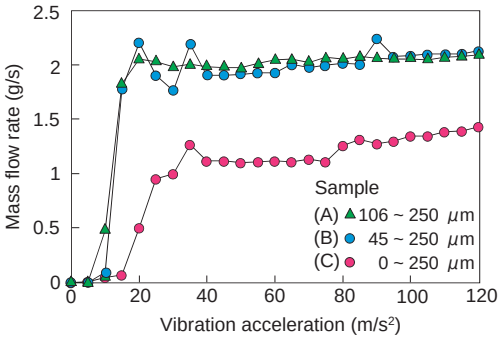

Fig.1-19 Flowability profiles of ZrO_2 smaller than 250 μm
The vibrating tube method can detect fine particles smaller than 45 μm.

It is necessary to employ raw MOX particles having excellent flowability for production of MOX pellets, because flowability affects the output of green pellets, and a non-uniform packed structure of particles in dies sometimes causes defective products. The flowability of MOX particles is currently evaluated by a method based on Carr's flowability index. In order to reduce the measurement time in the glove box, the applicability of a vibrating tube method, which is a new flowability measurement method, was examined using non-radioactive model particles.

The vibrating tube method (Fig.1-16) evaluates flowability based on measurement of the mass flow rate of particles discharged from the vibrating tube while the vibration acceleration is changed. This method has advantages such as a simple structure, easy operation, and short measurement time.

In this experiment, ZrO_2 particles having different shapes and surface states (Fig.1-17) were prepared by changing the milling time, and the particle size distribution was varied by changing the concentration of fine particles.

Fig.1-18 shows the mass flow rate dependence on vibration acceleration (flowability profiles) of ZrO_2 particles smaller than 45 μm in diameter. The flowability of particles with higher circularity (longer milling time) is more excellent, because a smaller vibration acceleration is required to initiate flowing. The vibration tube method can differentiate between samples with higher sensitivity than a method based on Carr's flowability index.

Fig.1-19 shows the flowability profiles of ZrO_2 particles smaller than 250 μm. (A) refers to particles 106 ~ 250 μm in diameter, (B) refers to 45 ~ 250 μm, and (C) refers to 0 ~ 250 μm. Profile (C) is strikingly different from the other profiles, which indicates that vibrating tube method can detect degradation of flowability by fine particles smaller than 45 μm.

For the next step, we are planning to measure the flowability of UO_2 and MOX particles to confirm the applicability of this method to the MOX pellet production line, such as in quality checks of MOX particles before and after granulation.

Reference

Ishii, K. et al., Feasibility Study on Particle Flowability Evaluation in Simplified MOX Pellet Fabrication Process Using Vibrating Tube Method, Journal of the Society of Powder Technology, vol.45, no.5, 2008, p.290-296 (in Japanese).

1-8 Representing the Irradiation Behavior of FBR Fuel
—Development of Np- and Am-Bearing MOX Fuel—

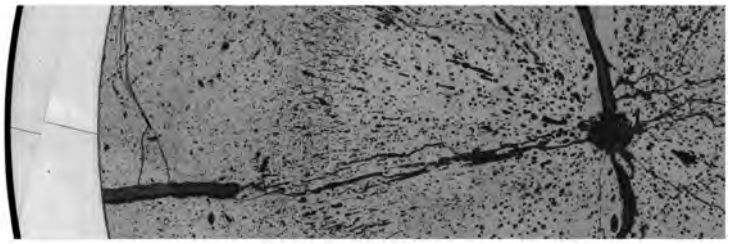

Fig.1-20 Cross-sectional microstructure of Np/Am-MOX pellet irradiated at 430 W/cm for 10 min
Microstructural change and central hole formation were observed.

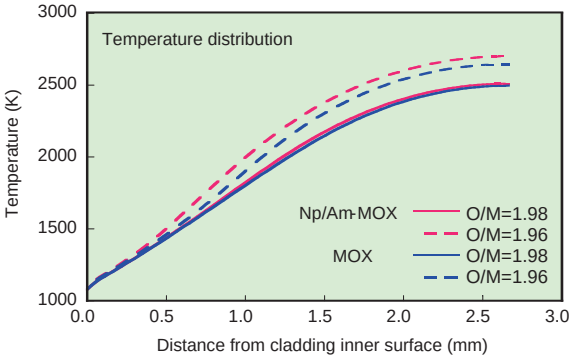

Fig.1-22 Radial temperature distribution in the pellet
A decrease in the O/M ratio caused the pellet temperature to increase.

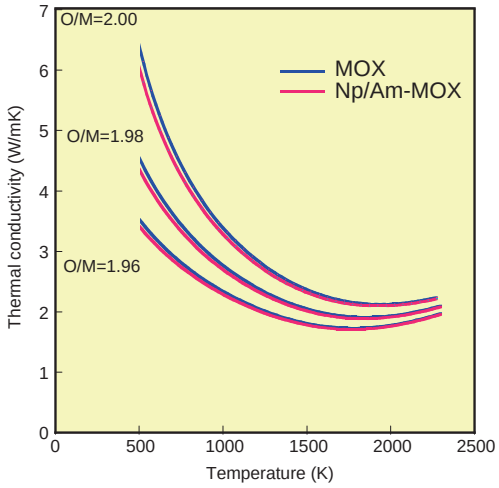

Fig.1-21 Temperature dependence of thermal conductivity
A decrease in the O/M ratio led to a significant decrease in thermal conductivity.

Uranium and plutonium mixed oxide (MOX) fuels containing minor actinide elements have been developed as fuels for Japan sodium cooled fast reactors. The minor actinide elements such as Np and Am are generated by nuclear reaction in reactors; these elements will be recovered from spent fuels and used as fuels in an advanced nuclear cycle. To develop such a new type of fuel, it is essential to describe the irradiation behavior and to evaluate fuel temperature. Irradiation tests of Np- and Am-bearing MOX (Np/Am-MOX) fuel pins were carried out in the fast reactor Joyo as part of this development, and microstructural change and migration of Np and Am were investigated in the irradiated fuel pellets. In addition, the physical properties of Np/Am-MOX pellets (melting temperature, thermal conductivity, oxygen potential, and lattice parameter) were measured, and the irradiation behavior of Np/Am-MOX was analyzed based on the resulting data.

Fig.1-20 shows the cross-sectional microstructure of the irradiated pellets. The oxygen-to-metal (O/M) ratio of the Np/Am-MOX pellets needs to be adjusted to a value lower than that of conventional fuel pellets (O/M≒1.98) for high burnup (for example, to less than 1.97). For this reason the irradiation tests were carried out as a function of the O/M ratio of the fuel pellets.

The fuel pins were operated at a high linear heat rate of 430 W/cm and held at this level for 10 min. A high linear heat rate in FBR fuel causes a large thermal gradient to form in the radial direction and elevates the maximum temperature of the pellets to over 2300 K. Thus it was observed that central hole formation and microstructural change occurred due to pore migration, as shown in Fig.1-20. In addition, the element distribution analysis showed that the concentration of Am and Pu increased around the central hole.

The temperature dependence of the thermal conductivities of Np/Am-MOX and MOX are shown in Fig.1-21. Addition of Np/Am had a small effect on the thermal conductivity, and a decrease in the O/M ratio led to a significant decrease in thermal conductivity. The temperature distribution was evaluated in the irradiated fuel pellets using equations derived from the measured physical properties.

In view of O/M redistribution in the radial direction of the pellet, the fuel temperature was analyzed. Fig.1-22 shows the calculation results. The low O/M fuel attained a higher temperature at the pellet center. In the measurement results, the melting temperature of Np/Am-MOX was over 3000 K, and the fuel pellet did not melt even at a high linear heat rate of 430 W/cm. The microstructural observation results also showed that the fuel pellet was unmelted.

Reference

Morimoto, K., Kato, M. et al., Thermal Conductivity of (U, Pu, Np)O_2 Solid Solutions, Journal of Nuclear Materials, vol.389, issue 1, 2009, p.179-185.

1-9 Investigation of Compounds in the PuO_2-SiO_2 System
—Behavior of Si Impurity Contained in MOX Fuel—

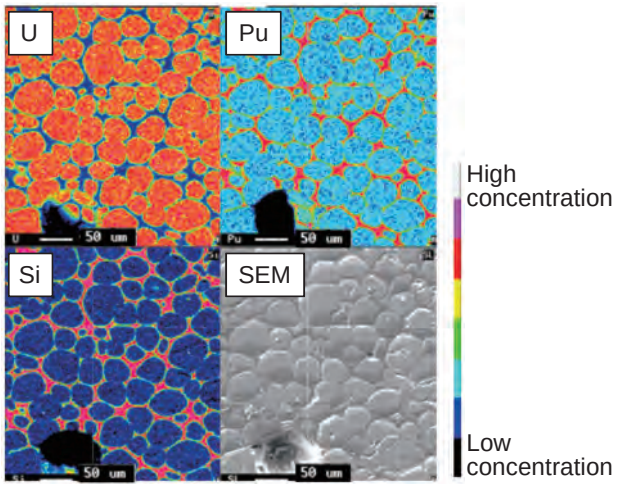

Fig.1-23 Element mapping images of MOX-6.9 wt%SiO_2 analyzed by EPMA
The cross-sectional surface of annealed pellets was analyzed by EPMA. The red area indicates a high concentration area of each element. Pu and Si were highly concentrated in the same areas and spread like network. Microstructural observation by SEM is shown in the lower right.

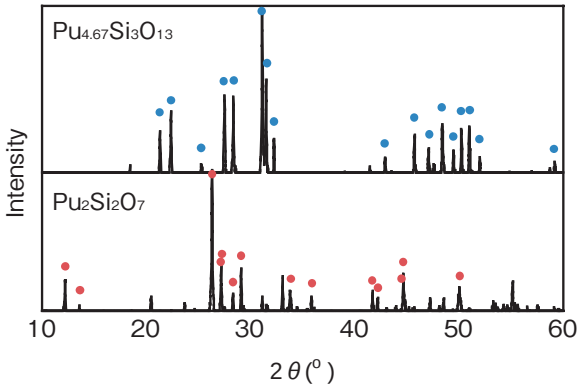

Fig.1-24 X-ray diffraction patterns of PuO_2-SiO_2 mixed powders after annealing
Specimens were analyzed by X-ray diffraction analysis. The $Pu_{4.67}Si_3O_{13}$ phase was precipitated in more conditions than $Pu_2Si_2O_7$. $Pu_2Si_2O_7$ was observed for the first time in this study.

Uranium and plutonium mixed oxide (MOX) fuels have been developed as fast reactor fuel. MOX fuels are fabricated from uranium dioxide (UO_2) and MOX powders by a mechanical blending method. The mixed powder is pelletized and sintered. In the mixing process, there is a possibility that the MOX powder is contaminated with silicon (Si), which is used as part of the ball mill pot. Therefore, it is necessary to evaluate the behavior of Si impurity. In this study, phase states in MOX-SiO_2 and PuO_2-SiO_2 systems were investigated to evaluate the behavior of Si in MOX fuels.

Specimens were prepared by mixing 6.9 wt% SiO_2 powders with MOX, and pelletizing and sintering at 2400 ℃. Fig.1-23 shows a cross-sectional mapping image of a pellet annealed at a low atmosphere (3.0×10^{-7} Pa) oxygen partial pressure (Po_2). Because Pu and Si are enriched in the same area along grain boundaries, Si can be considered to have reacted with Pu and formed compounds.

PuO_2-SiO_2 reaction examinations were carried out to investigate the precipitation conditions and chemical forms of the compounds. Specimens were prepared by mixing powders of PuO_2 and SiO_2 in molar ratios of 3:1, 3:2 and 3:3, and were then annealed as a function of temperature (1350~1700 ℃) and Po_2 (10^{-7}~10^{-10} Pa). X-ray diffraction patterns of the annealed specimens are shown in Fig.1-24. We observed that two kinds of compounds, $Pu_{4.67}Si_3O_{13}$ and $Pu_2Si_2O_7$, were formed as a function of temperature and Po_2. The phase containing $Pu_2Si_2O_7$ was precipitated in the specimens having mixing ratios of 3:2 and 3:3, and precipitation of $Pu_2Si_2O_7$ was limited to the region above 1600 ℃ and a Po_2 below 10^{-7} Pa. However, the $Pu_{4.67}Si_3O_{13}$ phase was precipitated in more conditions in comparison to the $Pu_2Si_2O_7$ phase. In addition to these two regions, there were conditions in which PuO_2 and SiO_2 compounds were not observed. These results show that, as a function of temperature and Po_2, Si impurity in MOX forms three kinds of chemicals: SiO_2, $Pu_{4.67}Si_3O_{13}$ and $Pu_2Si_2O_7$.

Thus, precipitation conditions for each compound were confirmed by investigating the behavior of Si impurity in MOX fuel. The acceptable level of Si impurity in MOX fuel is less than 1400 ppm, and the maximum amount of Si compound precipitated in MOX pellets is estimated to be less than 1 wt%. Therefore, Si impurity is considered to have a small effect on the properties of the fuel.

Reference

Uchida, T. et al., Phase States in the Pu-Si-O Ternary System, IOP Conference Series; Materials Science and Engineering, vol.9, 2010, p.012004-1—012004-5.

1-10 Simultaneous Recovery Technique for Uranium and Transuranic Elements Using Molten Salt Media

—Development of Metal Electro-Refining Pyrochemical Reprocessing—

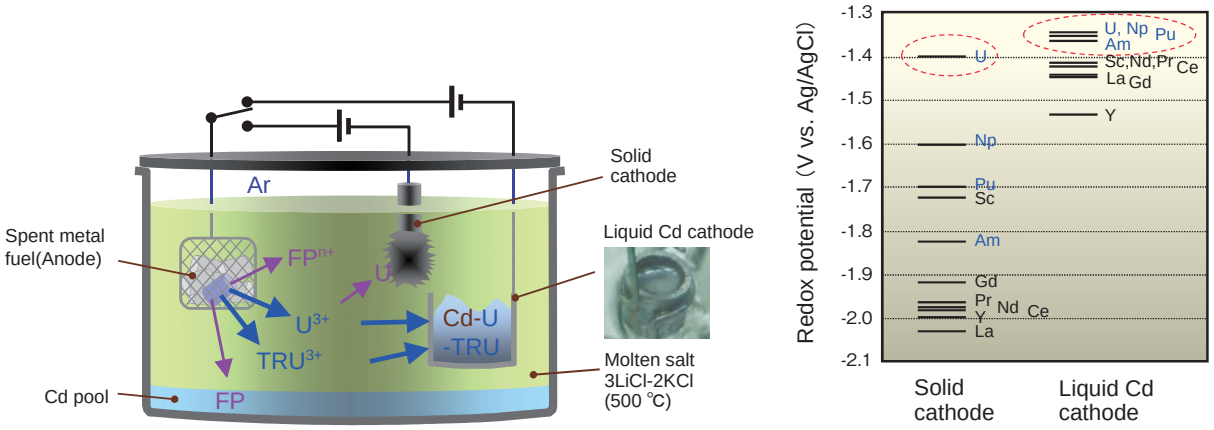

Fig.1-25 Concept of the electro-refining process and standard redox potential of TRU and rare earth elements
Uranium and TRU dissolved in molten salt are separated from FP elements and recovered on a cathode by electrolysis. Uranium metal is deposited on a solid cathode; U and TRU are recovered simultaneously into a liquid cadmium cathode (LCC) by controlling each cathode potential.

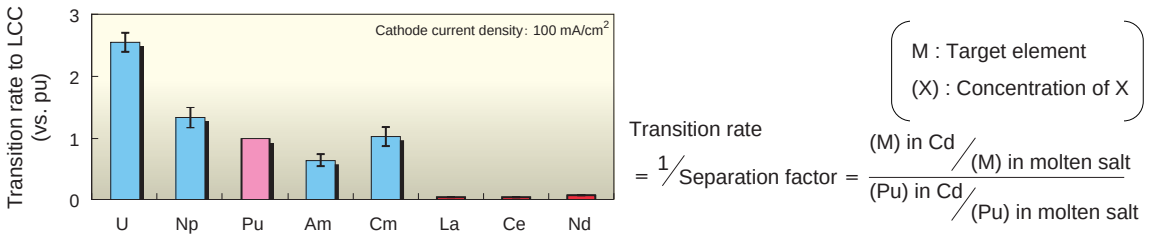

Fig.1-26 Result of the TRU recovery experiment with liquid cadmium cathode
An element with a large transition rate value is recovered into LCC easier than Pu. It was confirmed through the experiments that U, Np, Am, and Cm were recovered with LCC as well as Pu, and they were separated from rare earth elements.

Pyrochemical reprocessing technology (metal electro-refining method) has been developed as a candidate future reprocessing technology. In this process, U and Pu are separated from fission products (FP) and recovered by electrolysis. Fig.1-25 shows the concept of electrolysis at the electro-refining step and the principle of element separation. The deposition potential to a cathode depends on the material of the cathode as well as the element. A molten chloride mixture (LiCl and KCl in this method) is used to lower the electrolyte melting point.

The spent metal fuel pins are chopped into segments and loaded into a steel basket, then the basket is placed in the molten salt as an anode. Moreover, the cathodes consist of two kinds of electrodes: a solid cathode made of iron, and liquid cadmium filled in a ceramic crucible. Uranium, TRU, and some kinds of FP are anodically dissolved into molten salt and deposited on the cathodes by electrolysis. As shown in the right-hand diagram in Fig.1-25, U metal is selectively recovered on the solid cathode by controlling cathode potential. Subsequently, U and TRU are recovered into the LCC by electrolysis as they are dissolved from the anode. The selective recovery of a specific actinide is difficult because their deposition potentials to the LCC are close to each other. FP elements such as rare earth elements (REE) can be separated from actinides due to differences in their deposition potential to the LCC from those of actinides. Thus, the simultaneous recovery of U and TRU is suited to a future nuclear fuel cycle concept that aims to recycle all actinides. The difficulty of separating pure Pu is a desirable feature from the nuclear non-proliferation perspective.

Fig.1-26 shows results indicating that the LCC has these kinds of thermodynamic features. Actinide elements could be recovered simultaneously with the LCC and separated from REE (La, Ce and Nd) by electrolysis, as was expected from the thermodynamic study. We are planning to obtain further experimental data for the development of a superior electrolysis technique.

Reference

Kofuji, H. et al., Electro-Deposition Behavior of Minor Actinides with Liquid Cadmium Cathodes, IOP Conference Series; Materials Science and Engineering, vol.9, 2010, p.012010-1—012010-8.

1-11 Monitoring Irradiation Damage in Reactor Structures

—Development of an Irradiation Damage Evaluation Method Using Magnetic Measurement—

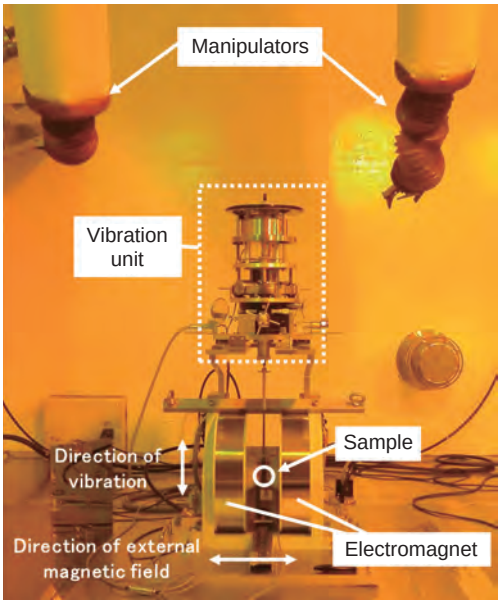

Fig.1-27 Remote operated VSM in a hot cell
We can change samples and align the equipment using manipulators. The photograph looks orange because it was taken through an orange-colored lead glass window.

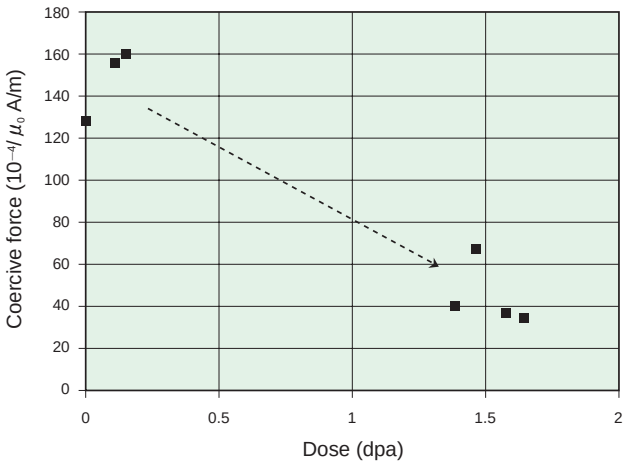

Fig.1-28 Relationship between dose and coercive force (Material: 316FR)
The coercive force was measured for the samples with various doses using the remote operated VSM. We showed that the coercive force decreases with the dose.

Irradiation damage to structural materials such as the reactor vessel of a fast reactor is not as severe as that of core materials such as a cladding tube. However, the structural materials are continuously exposed to irradiation environments for a long period of time, and they are extremely hard to replace. Proper monitoring is thus very important. Our previous studies showed that the dose is effective as an index of irradiation damage. Although the dose can be calculated from plant operating data, there are no methods to evaluate the dose by measuring a sample itself. In this study, we tried to evaluate the dose by means of magnetic measurement. We chose magnetic measurement because magnetic properties may be sensitive to dose-related microstructural change.

We developed a remote operated vibrating sample magnetometer (VSM) for magnetic measurement of neutron irradiated samples. A VSM is a device that evaluates magnetic properties, such as saturated magnetization and coercive force, from induced electromotive force due to vibrating samples in a magnetic field generated by electromagnets. Giving consideration to changing irradiated samples, easy maintenance, reduction of radioactive waste, and so on, we divided the device into two units: a measurement unit and a control unit. The measurement unit was set up inside, and the control unit outside a hot cell. We use manipulators to operate the measurement unit. Fig.1-27 is a photograph of the device we developed (the measurement unit).

The relationship between the coercive force and the dose is shown in Fig.1-28 as an example of the measurement results. The material is 316FR steel, which is a candidate structural material for the next generation fast reactor. We can see that the coercive force decreases with the dose. We revealed that the saturated magnetization is also related to the dose.

These results show that we will be able to monitor irradiation damage in reactor structures by measuring surveillance samples using this device. Measurement takes a short time, so evaluation with higher reliability is possible if we measure a number of samples. In addition, this method is non-destructive, so evaluation is possible for the entire lifetime of the plant with a limited number of samples, if the samples are set in the reactor again after measurement. Furthermore, if we repeatedly measure the same sample during the life of the plant, we can recognize changes in the dose without it being effected by variation in the material properties.

Reference

Takaya, S. et al., Development of Remote Operated Vibratin Sample Magnetometer for Evaluation of Irradiation Damage, Hozengaku, vol.9, no.1, 2010, p.51-56 (in Japanese).

1-12 The Challenge to Control the Chemical Reactivity of Liquid Sodium

— Development of Reactivity Control Using an Atomic Interaction between Nanoparticles and Sodium —

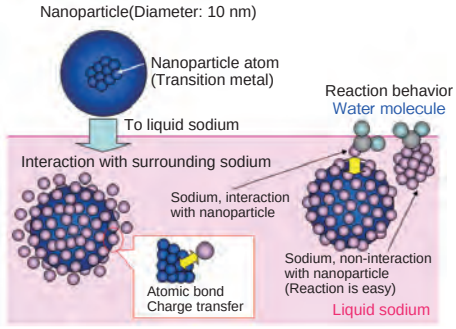

Fig.1-29 The concept of sodium with suspended nanoparticles
An atomic interaction (atomic bond and charge transfer) forms between a nanoparticle and the surrounding sodium atoms when nanoparticles are suspended in liquid sodium. Moreover, it became clear that the reactivity of sodium was suppressed by the atomic interaction.

Table 1-1 Characteristics and changes in the properties of sodium with suspended nanoparticles

		Related properties	
Atomic interaction	Atomic bond N.P. – Na > Na – Na Charge transfer Na → N.P. N.P.: Nanoparticle	Surface tension… Enlargement*1 Evaporation rate…Reduction Reaction property Reaction heat…Reduction Reaction rate…Reduction*2	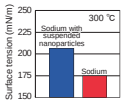 *1 Ex.) Change of property by atomic interaction
Effect of small diameter and low concentration	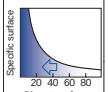	Compared with sodium (by low concentration) Viscosity, Melting temperature, Thermal conductivity …Non-significant change	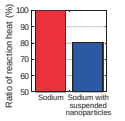 *2 Ex.) Change of reaction property by charge transfer

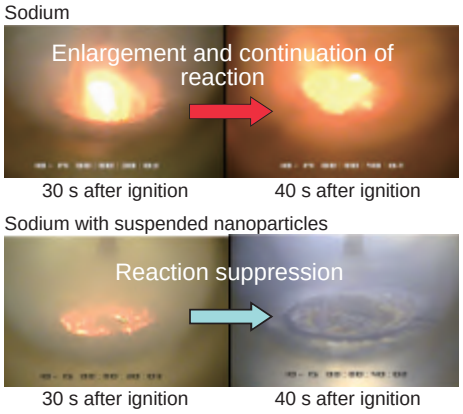

Fig.1-30 Comparison of combustion behavior between sodium and sodium with suspended nanoparticles
The reactivity of pure sodium was enhanced with an increase in time. However, with suspended nanoparticles, sodium inflammation obviously disappeared, and the reaction suppression effect was verified.

Liquid sodium, which is the coolant for the FBR, possesses high thermal conductivity and superior thermal hydraulic properties. However, it also possesses a high chemical reactivity with water or oxygen. For these reasons, satisfactory FBR plant safety is assured based on safety facilities and component design. However, if the reactivity of the sodium itself can be suppressed, it can be expected that safety can be improved independent of the facilities themselves, and that the plant can be made more economical by simplification of the facilities. In this study, we take on the challenge of creative technological development to control the chemical reactivity of sodium itself.

The concept behind this study is shown in Fig.1-29. An atomic interaction (atomic bond and charge transfer) forms between a nanoparticle and the surrounding sodium atoms when nanoparticles are suspended in liquid sodium, and it has become clear that the reactivity of sodium is suppressed by this atomic interaction. Thus there is a possibility that control over reactivity can be achieved without loss of the superior thermal hydraulics demanded of the FBR coolant, because a large amount of atomic interaction can be expected even with a low quantity of nanoparticles, if the diameter of the nanoparticles is smaller and their specific surface area is enlarged.

The charge transfer to a nanoparticle from the surrounding sodium atoms and enlargement of the atomic bond became theoretically clear in a previous study, and the change in the physical properties by the atomic interaction was verified experimentally (the upper part of Table 1-1). Furthermore, the physical properties of sodium with suspended nanoparticles, such as thermal conductivity, melting temperature, and viscosity, were measured and compared with those of sodium to clarify the influence of a small diameter and low quantity of nanoparticles on the thermal hydraulics, as a result of which it was verified that there was no significant change in these properties, and no change in the FBR thermal hydraulics performance (the lower part of Table 1-1). Also, the influence on sodium impurity control was investigated, and the concentration of nanoparticles in sodium did not change before and after trapping impurity elements. From this result, we can predict that the nanoparticle method can be applied to existing process. Moreover, the reactivity control effect in the reaction of water or oxygen and sodium with suspended nanoparticles has been verified, and results with respect to reduction of reaction heat and reaction rate have been obtained (Fig.1-30). In the future, a reactivity control mechanism will become clear, the applicability of this technology to the FBR coolant will be evaluated and the reactivity control effect under FBR operation will be verified, and the applicability of sodium with suspended nanoparticles for practical use will become clear. Furthermore, this kind of technology that uses atomic interactions with the nanoparticle surface is expected to not only control the chemical reactivity of sodium, but can also be applied to improving the properties of other mediums.

The present study is part of the contract research "Development of liquid sodium chemical reaction suppression technology based on nanotechnology" from the Ministry of Education, Culture, Sports, Science and Technology of Japan (MEXT).

Reference

Saito, J. et al., Study on Chemical Reactivity Control of Liquid Sodium -Development of Nano-Fluid and Its Property, and Applicability to FBR Plant-, Proceedings of 16th International Conference on Nuclear Engineering (ICONE-16), Orlando, Florida, USA, 2008, ICONE16-48367, 4p., in CD-ROM.

R&D Supporting the Technology and Reliability of Geological Disposal in Japan

In essence, geological disposal aims to isolate high-level radioactive waste (HLW), which is produced in nuclear power generation, from human environments for a long time. In Japan, spent fuel from power reactors is reprocessed to extract re-useable uranium and plutonium for power generation purposes. The liquids separated from the spent fuel during chemical reprocessing are solidified into a stable glass form. In the Japanese concept, vitrified wastes are encapsulated in a thick steel overpack, which is surrounded by highly compacted bentonite and then placed in a stable geological environment at a depth below 300 m (Fig.2-1).

Geological disposal of HLW will be a long-term project covering more than one hundred years from site selection to repository construction and operation, followed by post-closure monitoring. To launch the repository operation by the Nuclear Waste Management Organization of Japan (NUMO) in the late 2030s, selection of a site for the repository is a critical issue to be solved urgently. It is thus of much significance to proceed with the project efficaciously, as a national responsibility, by continuously reinforcing the technical base and, more importantly, enhancing public confidence. To this end, we have made, and will continue to make, steady progress in research and development (R&D) in various fields, such as geoscientific research, engineering technology and safety assessment, to improve the technology and reliability of geological disposal in Japan. Our efforts also concentrate on promoting public understanding through disseminating relevant information and opening our R&D facilities to the public.

A particular focus of our R&D at present involves projects at two underground research laboratories (URLs), one at Mizunami in crystalline rock and the other at Horonobe in sedimentary formations (Fig.2-2), with the main aim of establishing techniques for investigating if the geological environment provides a suitable environment for installing the engineered barrier system and if it functions as a natural barrier. In March 2010, shaft excavation reached depths of 460 m at Mizunami and 250 m at Horonobe and some research galleries were made available for use. Multidisciplinary investigations are actively ongoing, as the reliability of a variety of investigation techniques should be tested and confirmed before site characterisation begins in earnest. Underground tunnels serve as a place for the public to experience deep geological environments first-hand and

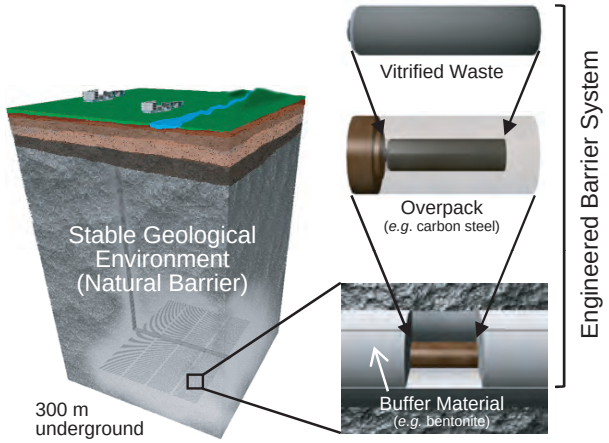

Fig.2-1 Basic concept of geological disposal of HLW in Japan

appreciate our R&D activities. In addition, studies on tectonics, volcanic and faulting activities and so on have been progressing in order to evaluate the long-term stability of geological environments in Japan.

In parallel with such geoscientific research, we are conducting an extensive laboratory programme at the Tokai R&D Center to improve geological disposal technology. Studies have been carried out over a wide range, such as performance assessment of multi-barrier systems and experiments on engineered barrier systems and on the long-term chemical and migration behaviour of radionuclides under actual geological conditions. These studies are linked with the geological environment data obtained from both URLs. In 2009, a methodology for evaluating coupled thermo-hydro-mechanical-chemical processes in the tunnel near-field environment was established and a database for radionuclide sorption/diffusion was improved.

Based on such R&D activities, we have been working intensively on the development of a next generation knowledge management system (KMS) to systematically manage multiple lines of evidence and the R&D results relevant to safety in the form of a knowledge base. In March 2010, a prototype KMS was made publicly available as a website (http://www.jaea.go.jp/04/tisou/toppage/top.html).

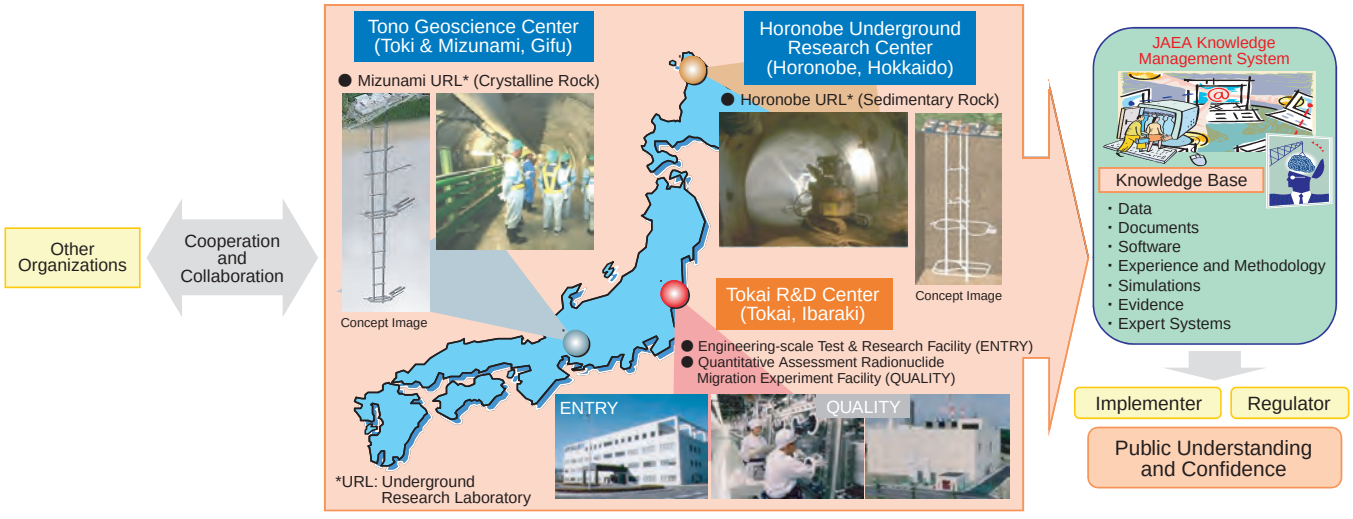

Fig.2-2 JAEA's R&D activities

2-1 Prototype Knowledge Management System
—Challenges for Knowledge and Technology Transfer—

Fig.2-3 Examples of JAEA KMS screenshots
The help and guidance functions including tutorial videos provide support for users.

Because the safety of a geological disposal system cannot be validated by means of operating an actual facility for a long period, it must be verified using various kinds of knowledge. This knowledge includes both explicit and implicit knowledge. Explicit knowledge includes databases, literature, and software, and implicit knowledge includes the experience and know-how of experts, which is called tacit knowledge. As the disposal project progresses, the amount of knowledge is anticipated to continue to grow significantly.

In order to make the verification of safety reliable, all available knowledge needs to be deployed. It is necessary not only to extract and use particular items of knowledge from a vast pool of sources, but also to structure the knowledge on a novel platform so that users can understand the relationship between items of knowledge and share in the knowledge. Therefore the JAEA is developing a knowledge management system (JAEA KMS) that aims to appropriately manage the knowledge that is the key to the geological disposal project. Ten individual tools for the JAEA KMS have been prepared.

The tools include:

1. An argumentation model, which visualizes discussions about safety and the related evidence in the form of a chain of warrants and rebuttals;
2. An expert system, which puts to practical use the implicit knowledge of experts;
3. A case-based system, where examples of past anomalies are retrievable; and
4. A performance assessment integrated report system, which assists users to prepare performance assessment reports.

The JAEA believes that the JAEA KMS can facilitate effective integration and utilization of the knowledge that supports the safety of geological disposal, and that it can be a means to support the steady promotion of the planned geological disposal program in Japan. The JAEA KMS has been publicly available on the JAEA website (http://www.jaea.go.jp/04/tisou/toppage/top.html) since March 2010. Examples of JAEA KMS screenshots are shown in Fig.2-3. The JAEA KMS is currently limited to read-only access, so the system should be regarded as a prototype. There are plans to further reinforce the knowledge base and improve the management function through the operation, maintenance, and management of the system, taking into consideration opinions and comments from a wide range of users.

Reference

Hioki, K. et al., Introduction of JAEA Knowledge Management System and JAEA Mid-Term Report on R&D for Deep Geological Disposal - CoolRep (H22), JAEA-Review 2009-049, 2010, p.24-41 (in Japanese).

2-2 Development of a Coupled THMC Model
—Engineered Barrier Experiment and Analytical Studies Focused on Geochemical Processes in Bentonite Buffer Material—

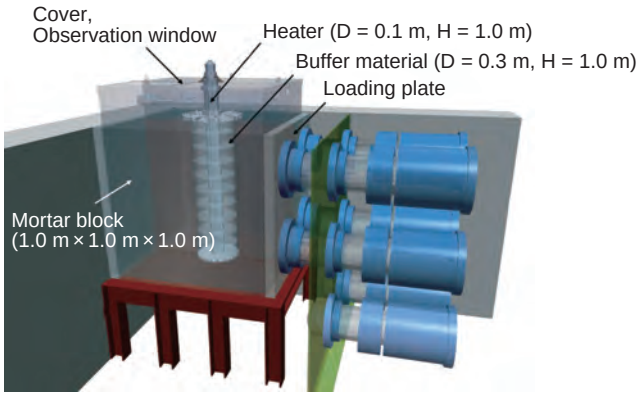

Fig.2-4 Schematic view of the engineered barrier experiment
The specimen consists of mortar block (simulated concrete support), compacted bentonite, and a heater (simulated vitrified waste).

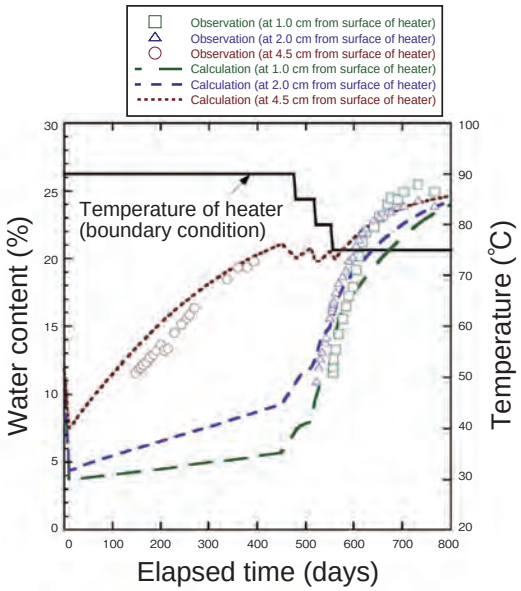

Fig.2-5 Comparison of calculated and measured water content of the buffer material at the depths indicated as a function of elapsed time
There are good agreements between calculated and observed data.

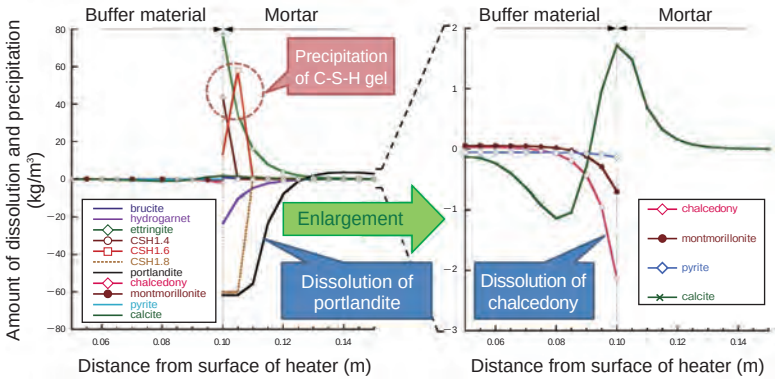

Fig.2-6 Results of mineral dissolution and precipitation in the test specimen
We succeeded in analyzing dissolution and precipitation of minerals using a THMC model.

It is anticipated that thermal - hydraulic - mechanical - chemical (THMC) processes will be coupled in the bentonite buffer material of a repository built for the geological disposal of high-level radioactive waste. The main contributors to these processes are (i) radiogenic heating from the decay of vitrified waste, (ii) infiltration of groundwater from the host rock, (iii) high pH leachate from the cementitious components of the repository, and (iv) the consequent chemical reactions and increase in swelling pressure. Numerical simulations are necessary to evaluate these coupled processes because of the large spatial and temporal scales involved. In order to evaluate these coupled processes, we conducted large scale experiments (Fig.2-4) to assist in the development of a coupled THMC analysis model.

The geochemical processes affecting the dissolution of primary minerals and precipitation of secondary minerals were the main focus of the TMHC model development. In order to confirm the coupled analysis model, we carried out an engineered barrier experiment (Fig.2-4), and compared the results of the experiment to the results of the coupled analysis.

Comparison between the experimentally measured and numerically simulated water content shows that they agree well (Fig.2-5). The THMC model in development predicted precipitation of a calcium silicate hydrate gel as a secondary mineral because the solution was saturated with respect to portlandite ($Ca(OH)_2$) and chalcedony (SiO_2) (Fig.2-6), thereby providing some confidence in the chemical features of the developing THMC model.

Reference

Suzuki, H. et al., Engineered Barrier Experiments and Analytical Studies on Coupled Thermal-Hydraulic-Chemical Processes in Bentonite Buffer Material, Genshiryoku Bakkuendo Kenkyu, vol.16, no.1, 2009, p.43-56 (in Japanese).

2-3 Evaluating the Solubility of Radionuclides with Speciation in Groundwater

— Development of the Thermodynamic Database for Safety Assessment of Geological Disposal —

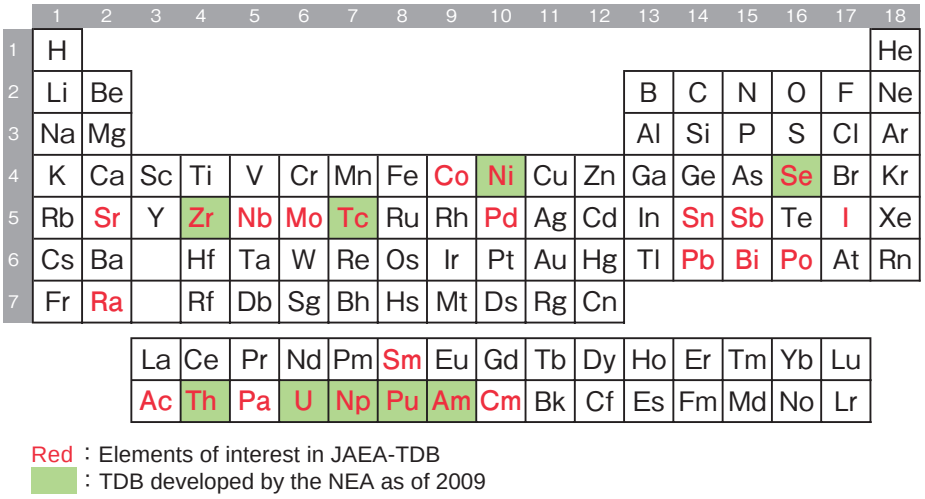

Fig.2-7 Periodic table showing the elements of interest in the JAEA-TDB

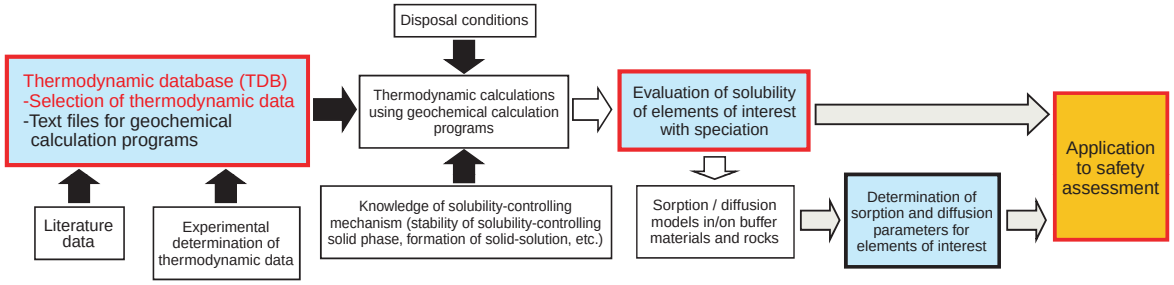

Fig.2-8 Schematic view of the status of the thermodynamic database for safety assessment of geological disposal

The first process of radionuclide release from vitrified waste will be via dissolution of radionuclides into groundwater. The speciation and solubility of radionuclides are fundamental to performing geological disposal safety assessment. Although many studies on radionuclide solubility have been performed, it is not easy to use the solubility data directly, because solubility depends on groundwater compositions that are usually more complex than those in most solubility studies, and thus we need to compile a database which consists of thermodynamic constants for chemical equilibrium calculations.

Development of a thermodynamic database (TDB) is accepted in several countries as well as in Japan. For example, the Nuclear Energy Agency (NEA) of the Organisation for Economic Co-operation and Development has carried out a TDB project in which we have been participating since 1984, and TDBs for 9 elements had been developed as of 2009.

We developed our TDB (the JAEA-TDB) through reviewing and selecting thermodynamic data based on the NEA guidelines while enhancing the guidelines applicable to selecting thermodynamic data for the 25 elements shown in Fig.2-7, which are important for geological disposal safety assessment. As a result, we collected 880 items of thermodynamic data respecting the elements of interest for safety assessment, 180 of which pertain to groundwater composition, and 140 of which pertain to geochemical reactions at the mineral/water interface. Furthermore, we confirmed the reliability of the JAEA-TDB through checking internal consistencies from several points of view. Using the JAEA-TDB permits us to evaluate the solubility of radionuclides with speciation, which provides basic information for determining sorption and diffusion parameters; these values are fundamental to performing safety assessment, as shown in Fig.2-8.

JAEA-TDB text files for some geochemical calculation programs, such as PHREEQC, are available on our website (http://migrationdb.jaea.go.jp/). We appreciate your access and feedback.

Reference

Kitamura, A. et al., JAEA Thermodynamic Database for Performance Assessment of Geological Disposal of High-Level Radioactive and TRU Wastes, JAEA-Data/Code 2009-024, 2010, 84p.

2-4 Modeling of Radionuclide Migration in Actual Surface and Near-Surface Environments
—Approach to Develop a Biosphere Model for Geological Disposal Safety Assessment—

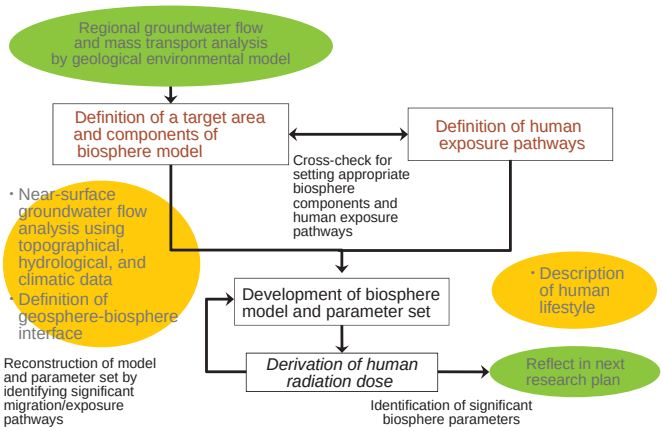

Fig.2-9 Biosphere model in surface and near-surface environments: development overview flow chart
Target area and components of the biosphere model are defined based on the results of groundwater flow analysis in surface and near-surface environments using topographical, hydrological, and climate data. Additionally, exposure pathways are defined by description of human lifestyles (e.g., land use, water resources). The biosphere model and its parameter set are developed through these definitions.

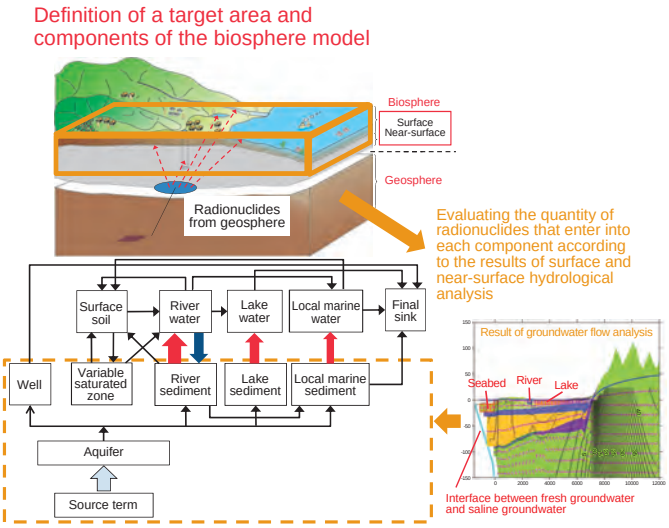

Fig.2-10 Image of biosphere model development using the information acquired at actual surface and near-surface environments
The quantity of radionuclides that enter into each component is evaluated and the geosphere-biosphere interface is defined according to the results of surface and near-surface hydrological analysis. Biosphere components are also selected.

In the safety assessment of a deep geological disposal system for high-level radioactive waste (HLW) and transuranic waste (TRU), there is a need to consider the surface and near-surface environment (biosphere) into which future releases of radionuclides via groundwater might occur and associated future human behavior. This is called "biosphere assessment." In biosphere assessment, it is often necessary to estimate future human radiation exposure doses.

The radioactive waste disposal project is currently at the repository site selection stage. We need to develop a methodology for developing site-specific biosphere models and a priority list of the biosphere parameters that should be acquired at the repository site. It is especially important to indicate a practical procedure for developing biosphere models based on information acquired at specific surface and near-surface environments. Fig.2-9 shows a flow chart for developing a biosphere model based on information required at a specific environment. The top left side of this chart shows the practical procedure for evaluating groundwater flow in the near-surface environment in order to define a target area and components of the biosphere model. This is one of the most important procedures, because this result points to the area where radionuclides enter into the biosphere. Fig.2-10 shows the concept for developing a biosphere model based on information acquired at a specific environment.

In parallel to the development of this flow chart, we prepared a list of the data required to develop the biosphere model at each stage of the radioactive waste disposal project. This list shows the data and their sources (references) required to define a target area, biosphere components, and exposure pathways. The chart and the list provide a practical procedure for handling the data acquired at a specific site environment, and this would serve as a guide for biosphere modeling at the site. We should develop a procedure specific to biosphere assessment in Japan, because the data required for biosphere modeling and the importance of that data differ from country to country. Our goal is to put this methodology to practical use as a knowledge base that indicates a systematic approach to biosphere modeling.

Reference

Itazu, T., Kato, T. et al., Development of Biosphere Assessment Methodology in View of Surface and Near-Surface Environment, JAEA-Review 2009-015, 2009, 59p. (in Japanese).

2-5 Exploring Chemical Environments 1000 m Underground Using Microbiological Characterization —In Situ Microbiological Properties of Toki Granite—

Table 2-1 Major microbial metabolism types
Microorganisms acquire energy via metabolic activity utilizing various electron acceptors, such as oxygen (O_2), nitrate (NO_3^-), ferrous ion (Fe(III)), sulfate (SO_4^{2-}), carbon dioxide (CO_2), and so on, and from donors such as organics, methane, hydrogen, and so on. They can be classified into groups based on their electron acceptors and metabolic processes.

Group	Electron acceptor		Product
Aerobe	O_2	→	H_2O
Nitrate reducer	NO_3^-	→	NO_2^-
Iron reducer	Fe(III)	→	Fe(II)
Sulfate reducer	SO_4^{2-}	→	H_2S
Methanogen	CO_2	→	CH_4

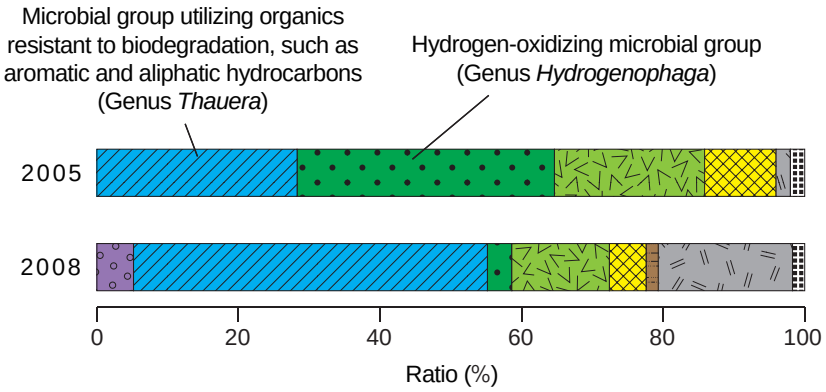

Fig.2-11 Microbial composition of groundwater samples collected between 1148 and 1169 m underground in Toki granite
Blue and green bars respectively indicate the genus *Thauera* and genus *Hydrogenophaga* microbial groups. The other bars are sorted into phylum or class, rather than genus, due to the phylogenetic diversity of the samples.

Recent studies have revealed that deep subsurface environments harbor many microorganisms, despite seeming to be too severe for organisms to survive. Understanding these microorganisms contributes to developing technologies and methods for evaluating subsurface environments. Organisms acquire energy using electron acceptors and electron donors. Human beings utilize, for instance, oxygen as an electron acceptor and organics as electron donors. Unlike surface environments, oxygen and organics are scarce in deep subsurface environments. Nevertheless, there appear to be various microorganisms that can utilize other electron acceptors and donors as energy sources (Table 2-1). Their energy acquisition rates depend on the coupling of electron acceptor and donor. In a limited energy source environment, microbial species that can sustain metabolic activity associated with a high rate of energy acquisition will adapt to the environment and dominate. Therefore, microbial composition shifts accompany a change in the chemical environment. This means that we could interpret the chemical environment transition by determining the microbial energy source and the shift in microbial composition. Few studies, however, describe the relationship of chemical environments to microbial compositions and metabolic activities in crystalline rocks.

In this study, we conducted geochemical analyses (anionic and cationic species, trace elements, organic acids, and dissolved gasses) of granitic groundwater collected in 2005 and 2008 from a depth segment between 1148 and 1169 m to determine the microbial energy source, as well as analyzing microbial composition and evaluating metabolic activities. Geochemical analyses showed that electron acceptors and organic acids, which are easily degradable by microorganisms, were scarce in the groundwater samples. The results of microbial composition analysis indicated that the microbial community was dominated by microorganism that could utilize organics resistant to biodegrading (Fig.2-11). Although concentrations of the main components did not change from 2005 to 2008, the hydrogen-oxidizing microbial group decreased. These results suggest that the hydrogen concentration in groundwater collected in 2005 (not measured) could be higher than in 2008, and thus indicate that there was a shift in the chemical environment. The exact cause of the shift is under investigation.

From these investigations, we were able to evaluate change in a deep subsurface environment that was assumed to be analogous to a geological disposal site.

This research was a collaborative project with the National Institute of Advanced Industrial Science and Technology (AIST).

References

Fukuda, A. et al., Geomicrobiological Properties of Ultra-Deep Granitic Groundwater from the Mizunami Underground Research Laboratory (MIU), Central Japan, Microbial Ecology, vol.60, no.1, 2010, p.214-225.

2-6 Elucidating Crustal Evolution

—Inferred Formation of Granitic Rock Based on 3D Petrological Evidence—

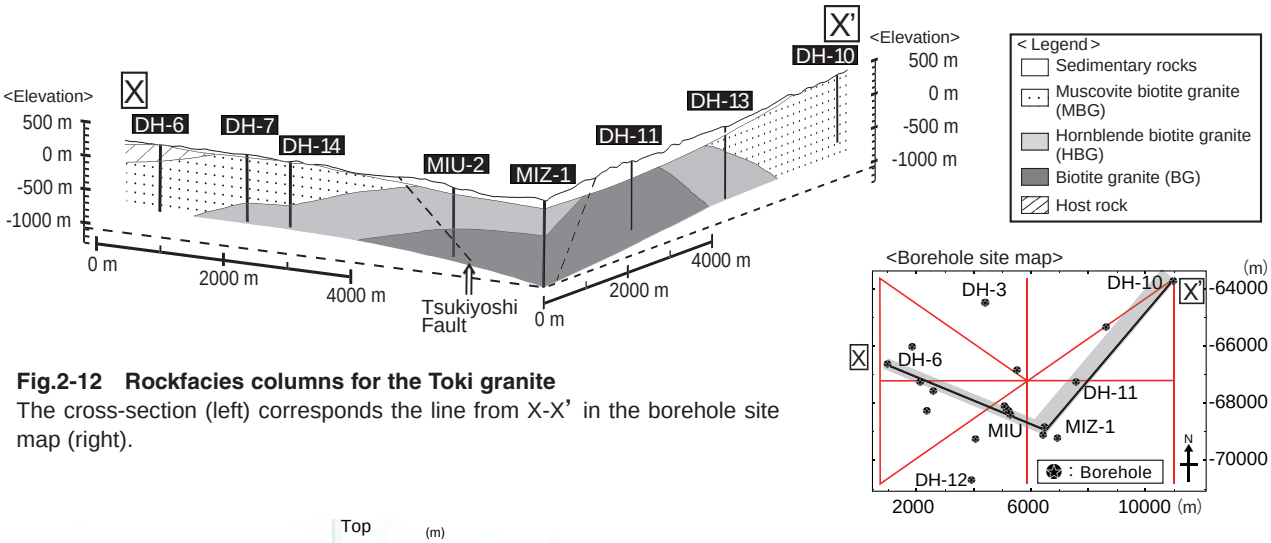

Fig.2-12 Rockfacies columns for the Toki granite
The cross-section (left) corresponds the line from X-X' in the borehole site map (right).

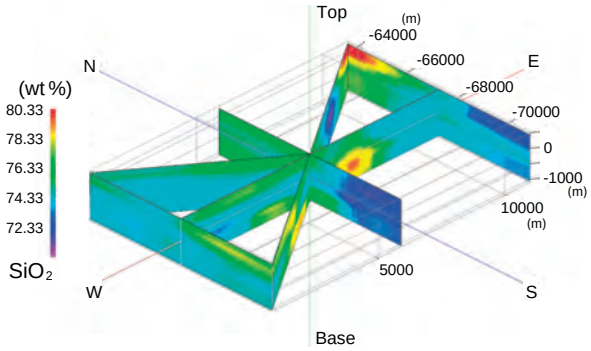

Fig.2-13 Contoured spatial distribution of SiO_2 concentration in a fence diagram along the red lines in borehole site map (Fig.2-12)
To make the diagrams, the data were interpolated and converted to 3D data for visualizing using RockWorks 14.

An important subject in studies of crustal evolution is the development of an understanding of the formation (intrusion and emplacement processes) of granitic plutons. Heat transfer to the surrounding host rock during intrusion of granitic magma plays a vital role in the development of metamorphic rock. Granitic and metamorphic rocks account for a large part of the continental crust. That is, knowing how granitic plutons form is a "keystone" to understanding the evolution of the continental crust. Differences in formation processes are likely reflected in petrophysical properties, which eventually effects fracture formation.

This study presents the results of petrographical studies of spatial variations in rock facies (mineral assemblage and mode) and chemistry recorded in the Toki granite of central Japan, and evidence from the formation of this pluton. Samples collected from 19 boreholes in the Toki granite display spatial variations in both rock facies (Fig.2-12) and chemistry (Fig.2-13). Based on these variations, the Toki granite is divisible into three rock facies ranging from muscovite biotite granite (MBG) at the margin, to hornblende biotite granite (HBG), and to biotite granite (BG) in the interior (Fig.2-12). Spatial SiO_2 distribution in the granite shows high concentrations in the upper NE margin, lower concentrations in the central part of the intrusion, and the lowest concentrations in the intervening region (Fig.2-13). The chemistry of the body is related to the change in rock facies from the upper margin, the lower central region, and the intermediate region between them, which respectively correspond to the MBG, BG and HBG.

These petrographical variations could be due to two different formation possibilities: either assimilation of crustal host rocks into the granitic magma during intrusion, or simultaneous intrusion of different magmas. Assimilation would be evident in zonal variations in which rock facies and chemistry are closer to the host rock, towards the margin of the body. Simultaneous intrusion of different magmas can also yield zonal variations, as the three rock facies and the corresponding chemical variation are derived from three different magmas.

The addition of isotope and trace element examination to this study will enable us to further understand the formation process. This study will also contribute to the safety evaluation of a geological disposal system, through understanding the characteristics of fracture formation.

Reference

Yuguchi, T. et al., Zoning of Rock Facies and Chemical Composition in the Toki Granitic Body, Central Japan, Ganseki Kobutsu Kagaku (Japanese Magazine of Mineralogical and Petrological Sciences), vol.39, no.2, 2010, p.50-70 (in Japanese).

2-7 Heat Source for Hot Springs in the Noto Peninsula
—An Amagmatic Hydrothermal System in a Non-Volcanic Region—

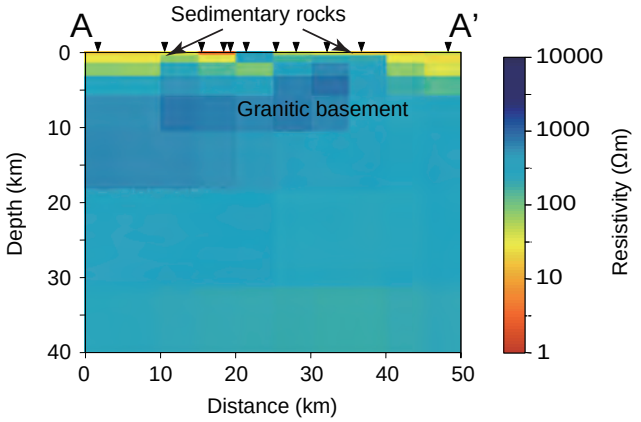

Fig.2-14 Electrical resistivity structure beneath the Noto Peninsula
A near-surface conductive layer corresponding to sedimentary rocks is visible, however, conductive anomalies representing magma are not seen below the depth of several km.

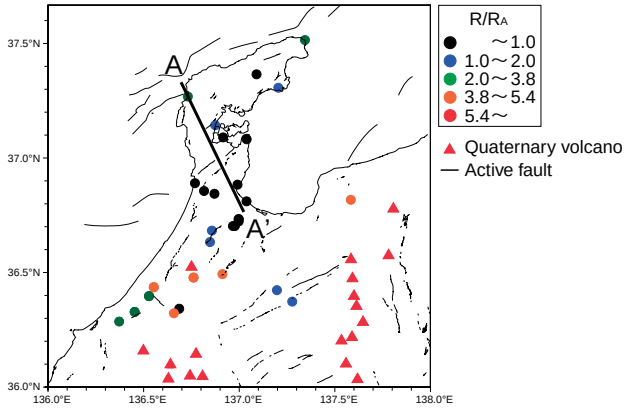

Fig.2-15 Geographical distribution of helium isotope ratios in and around the Noto Peninsula
The helium isotope ratios ($R=^3He/^4He$) of hot springs located in a volcanic region are higher than that of the atmospheric value (R_A), whereas in the Noto Peninsula, most are similar to R_A.

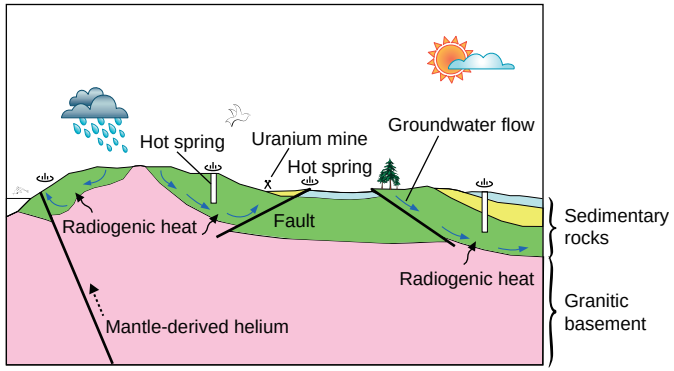

Fig.2-16 Schematic illustration of the hydrothermal system in the Noto Peninsula
A plausible heat source for high-temperature hot springs in this area is radiogenic heat production derived from the decay of U, Th, and K within the granitic basement, and heat transfer with groundwater advection.

Hydrothermal system related volcanism is one of the most important factors affecting the long-term stability of a geological disposal system, because it could cause significant changes in groundwater flow and temperature. Therefore, we have been developing magma and high-temperature fluid detection technologies to evaluate the possibility of renewed volcanism in a given site. For this purpose, we characterized a plausible heat source of high-temperature hot springs in the Noto Peninsula using magnetotelluric (MT) soundings and measurement of the helium isotope ratio ($^3He/^4He$) of hot springs.

It has long been recognized that the Noto Peninsula is unusual for a non-volcanic region, in that it has anomalously high-temperature hot springs similar to those in volcanic regions. Electrical conductivity is the physical property most sensitive to the configuration of magma. According to MT soundings in this region, the electrical resistive zone corresponding to granitic rock is visible below a depth of several km; however, conductive body anomalies representing magma do not exist beneath the Noto Peninsula (Fig.2-14). The observed $^3He/^4He$ ratios of most hot springs in this region are similar to that of the atmospheric value (Fig.2-15). These results indicate that the high temperature of the hot springs in this region is not due to the supply of heat from magma. What, then, is the heat source of the amagmatic hydrothermal system in the Noto Peninsula? The granitic rocks revealed as the electrical resistive zone contain elevated concentrations of U, Th, and K. These findings indicate that a plausible heat source for the high-temperature hot springs can be attributed to radiogenic heat production derived from the decay of U, Th, and K within the granitic basement, and heat transfer with groundwater advection (Fig.2-16).

Reference

Umeda, K. et al., Heat Source for an Amagmatic Hydrothermal System, Noto Peninsula, Central Japan, Journal of Geophysical Research, vol.114, 2009, B01202-1—B01202-10, doi:10.1029/2008JB005812.

2-8 Establishment of a Practical Guide for Construction Management in Deep Shaft Sinking
—A Rock Mass Behavior Classification Proposal for Deep Shaft Sinking—

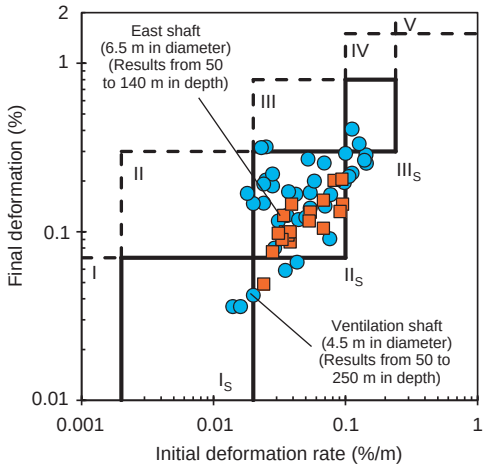

Fig.2-17 Relationship between initial deformation rate and final deformation observed in shaft sinking at the Horonobe URL
The relationships observed in conventional tunnel excavation (Class I to V) and in shaft sinking at the Horonobe URL (Class I_S to III_S) are illustrated by dotted lines and by solid lines, respectively.

Table 2-2 Rock mass behavior classification for deep shaft sinking
Where an initial deformation categorized into Class IIIS is observed, it is estimated that, in the earlier steps of shaft excavation, significant inelastic deformation of rock would occur until a shaft stabilizes.

Class	Initial deformation rate (%/m)	Final deformation (%)	Modulus of elasticity ratio *)	Inelastic deformation ratio **)
I_S	less than 0.02	less than 0.07	more than 400	less than 0.2
II_S	0.02～0.1	0.07～0.3	300～400	0.2～0.5
III_S	more than 0.1	more than 0.3	less than 300	more than 0.5

*) Ratio of the modulus of elasticity of rock to the initial stress
**) Ratio of the inelastic deformation to the final deformation

(Notes)
1) The classification is applied to middle-sized shaft excavation.
2) The classification is applied to the results of convergence measurement in diatomaceous mudstone distributed around the Horonobe area.
3) The initial values of convergence measurement should be observed within 0.5 m in the relative distance between a face and measurement section.
4) The modulus of elasticity ratio is calculated using the results from the dilatometer test.
5) The inelastic deformation ratio is applicable in the case of measurements in excavations with a road-header.

In deep underground tunneling, it is difficult to properly estimate rock mass properties and the initial stress conditions on the basis of a surface-based investigation. The quantity of support elements in the design phase should be modified at the construction phase based on the results of observation of rock mass properties in the excavation face and monitoring of rock deformation. The mechanical stability of support elements and rock around a tunnel are usually estimated based on monitoring of the deformation caused by excavation work. The total deformation which occurs until rock stabilizes (the final deformation) is predicted based on the deformation observed in the earlier excavation steps (the initial deformation rate). In tunneling in deep geological disposal sites, control over changes in the hydraulic conductivity of rock around a tunnel is required so that the rock can function as a natural barrier. Specifically, in the construction phase, a practical guide would be needed to predict and estimate not only the stability of the rock but also changes in the hydraulic conductivity of the rock around a tunnel based on monitoring of rock deformation.

In this study, at the Horonobe URL, we investigated the relationship between rock deformation and rock mass deformability during the sinking of the ventilation shaft (4.5 m in diameter) and the east shaft (6.5 m in diameter). It was found that rock deformation was controlled well compared with conventional tunneling, because the rock around a shaft was supported by a 400 mm thick concrete lining installed in the early stages of excavation. Based on the indexes used in conventional tunneling in rock, we proposed a relationship between the initial deformation rate and the final deformation in shafts sunk at the URL. It consists of 3 classes (Class I_S, Class II_S, and Class III_S) (Fig.2-17). To a significant extent, changes in the hydraulic conductivity of rock around a shaft are caused by inelastic deformation of the rock. We analyzed the relationship between the ratio of inelastic deformation to final deformation and rock mass deformability in each class. The relationship is shown in Table 2-2 as a rock mass behavior classification in shaft sinking. The classification helps us estimate excessive inelastic deformation of rock based on monitoring of rock deformation conducted in the earlier stages of excavation, and to make decisions on the installation of additional support elements. We establish a practical guide for shaft sinking in deep geological disposal sites by analyzing the relationship between the inelastic deformation of rock and the hydraulic conductivity of rock around a tunnel.

Reference

Tsusaka, K., Proposal of Rock Mass Behavior Classification Based on Convergence Measurement in Shaft Sinking Through Sedimentary Soft Rocks, Doboku Gakkai Ronbunshu F, vol.66, no.1, 2010, p.181-192 (in Japanese).

2-9 Deformation and Failure Behavior in Deep Sedimentary Rocks
—Evaluation of Sedimentary Rocks Based on Laboratory Tests—

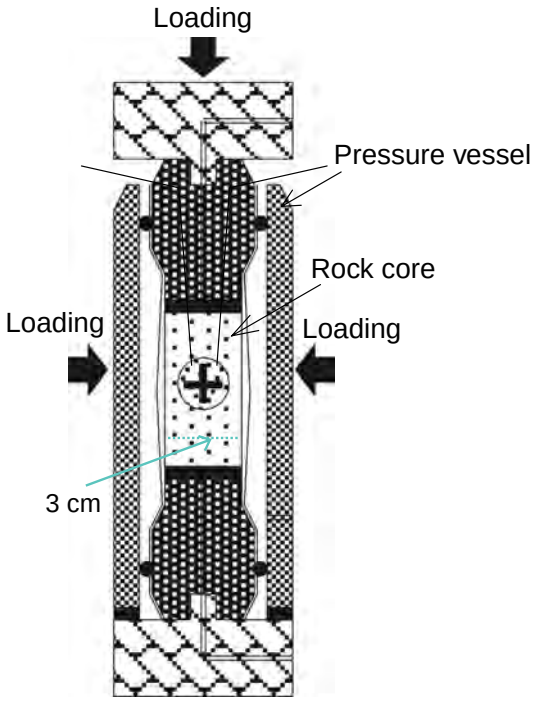

Fig.2-18 System of laboratory testing
Under the rock specimen in the triaxial pressure cell.

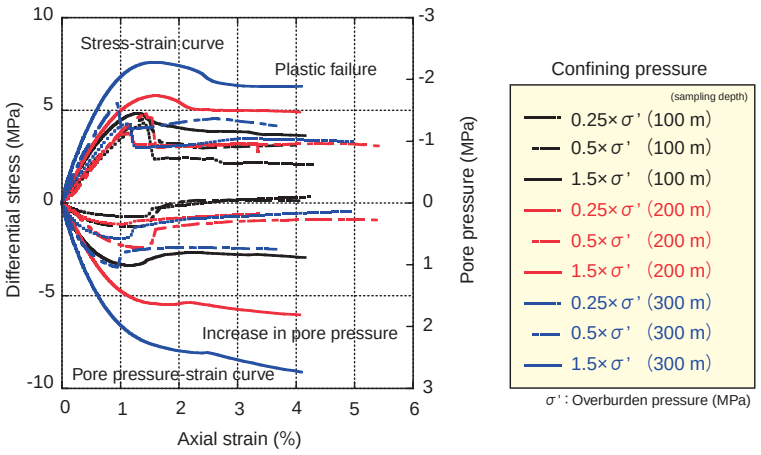

Fig.2-19 An example of laboratory test results
Behavior of stress, strain and pore pressure during shear. Pore pressure is increased during shearing of the rock specimen.

Several tunnels will be required in a repository of high-level radioactive waste (HLW) due to transportation of the HLW and engineered barriers, and ventilation openings. When tunnels deep underground are excavated, stress in the surrounding rock mass is increased due to stress redistribution. Deformation and failure around tunnels are then estimated to occurred. Therefore, it is necessary to understand rock mass failure and deformation for excavation and planning of a repository site.

Compared with other countries, the sedimentation period of sedimentary rock in Japan is so recent that their mechanical features are porous and weak. Therefore, it can be anticipated that microstructural failure and changes in hydraulic parameters such as pore pressure and hydraulic conductivity with stress variation will occur. Accordingly, we carried out rock mechanical testing such as tri-axial compression tests using rock cores taken from deep boreholes in the Horonobe URL Project to clarify the deformation and failure properties of sedimentary rocks. In addition, the relationship between mechanical behavior and microstructure was investigated via microscopic observations.

Examples of laboratory tests are described in Fig.2-18 and Fig.2-19. After rock cores were sampled, they were set in a pressure vessel and crushed under a load. Because the pore pressure and volumetric strain in the rock core during the pressure loading were recorded, volumetric dilatancy and pore pressure behavior could be evaluated. Fig.2-19 shows stress-strain curves for diatomaceous mudstone from the Koetoi formation. The Koetoi formation is composed of diatom including numerous tiny pores, and it possesses features of porosity and low permeability. According to the test results, the stress-strain shape switched from strain softening to ductile behavior with an increase in confining pressure. In addition, a large confining pressure led to an increase in pore pressure. Increasing pore pressure during shearing can be expected to lead to microstructural failure and shrinkage with an increase in confining pressure.

Mine-by experiments are being conducted in the Horonobe URL Project, and technical insights taken from the laboratory tests were used for interpretation of mine-by experiments and rock mechanical modeling.

Reference

Sanada, H. et al., Influences of Sedimentary History on the Mechanical Properties and Microscopic Structure Change of Horonobe Siliceous Rocks, Journal of MMIJ, vol.125, no.10-11, 2009, p.521-529 (in Japanese).

2-10 Estimating Long-Term Changes in Deep Subsurface Hydrochemical Conditions
—Research into Water - Mineral - Microbe Interactions—

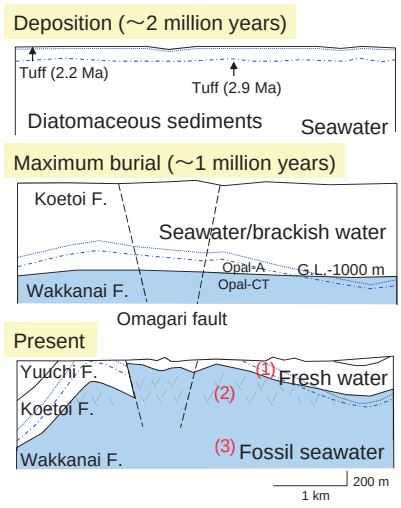

Fig.2-20 Long-term hydrogeological evolution
Distinct hydrogeological properties were evolvedbysedimentation,burialdiagenesis, and subsequent uplift/erosion in the area.

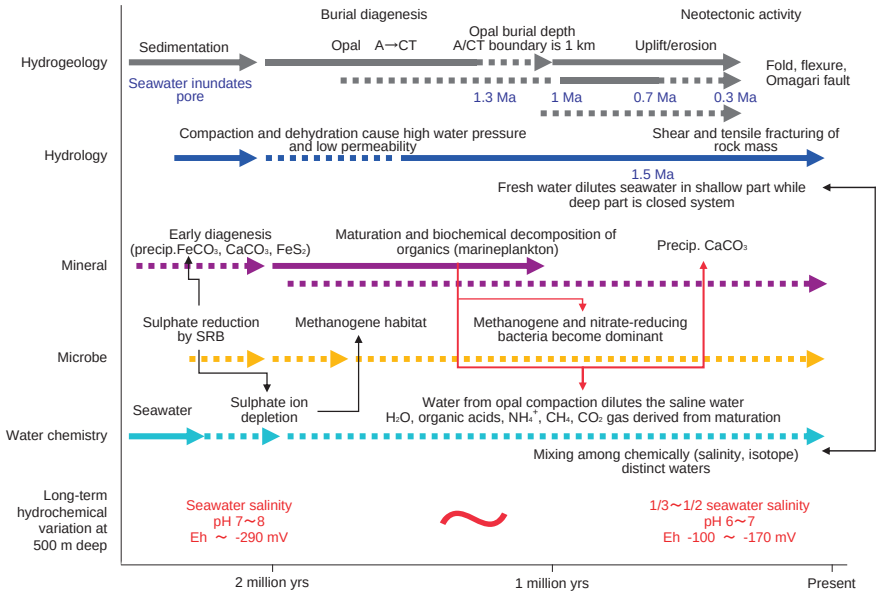

Fig.2-21 Interrelationships among geological features, events, and processes
It is possible to estimate the dominant hydrochemical processes and long-term variation based on consideration of geological phenomena and their relations in each epoch.

A methodology to estimate long-term hydrochemical evolution deep underground is indispensable for the safe geological isolation of high-level radioactive waste (HLW). This study demonstrates a methodology for this by illustrating scenarios of past geological events and processes, and their interrelationships with present-day hydrochemical conditions. In addition, this study makes inferences regarding long-term variations in groundwater chemistry in Horonobe, Hokkaido, Japan.

The study area is underlain mainly by Neogene to Quaternary marine sedimentary rock, (the Wakkanai Formation and the overlying Koetoi Formation: siliceous and diatomaceous mudstones). During various events in the geological past, such as deposition, compaction, uplift, and denudation, and the more recent Neotectonic activities in this area, highly permeable hydrogeological structures formed at depths not more than 400 m below ground level in the Wakkanai Formation. The hydrogeological system can be subdivided into three hydrogeological sub-systems: (1) the overlying, relatively low permeability Koetoi Formation, (2) the highly permeable, upper Wakkanai Formation at depths less than 400 m, and (3) the relatively low permeability Wakkanai Formation, at depths greater than 400 m (Fig.2-20). The present-day hydrochemical conditions in each sub-system have been influenced by hydrogeological properties and hydraulic conditions over a long period. In subsystems (1) and (2), recharging with meteoric water flushed connate seawater during uplifting and denudation during the last million years. In contrast, fossil seawater with one-third to one-half the salinity of present-day seawater has been preserved in subsystem (3).

The relatively low permeability sequence in sub-system (3) was formed by the compaction of diatomaceous mudstone during subsidence prior to one million years ago. After that, changes in climatic conditions and geographical features would not have influenced groundwater flow. The groundwater chemistry evolved from seawater during long-term geochemical diagenesis in a relatively closed system (Fig.2-21). The long-term variations in salinity probably range from that of seawater to that of present-day groundwater. The occurrence of secondary minerals shows that the buffer reactions of carbonate and sulphide minerals have preserved a near neutral pH and reducing condition since initial diagenesis immediately after deposition of the rock formation. Furthermore those processes seem to have continued for several hundred thousand years. It is possible to extrapolate the hydrochemical processes and conditions into the future based on the interrelationships among geological features, events, and processes.

Reference

Iwatsuki, T. et al., Scenario Development of Long-Term Evolution for Deep Hydrochemical Conditions in Horonobe Area, Hokkaido, Japan, Chigaku Zasshi, vol.118, no.4, 2009, p.700-716 (in Japanese).

3 Nuclear Fusion Research and Development

Toward Practical Use of Fusion Energy

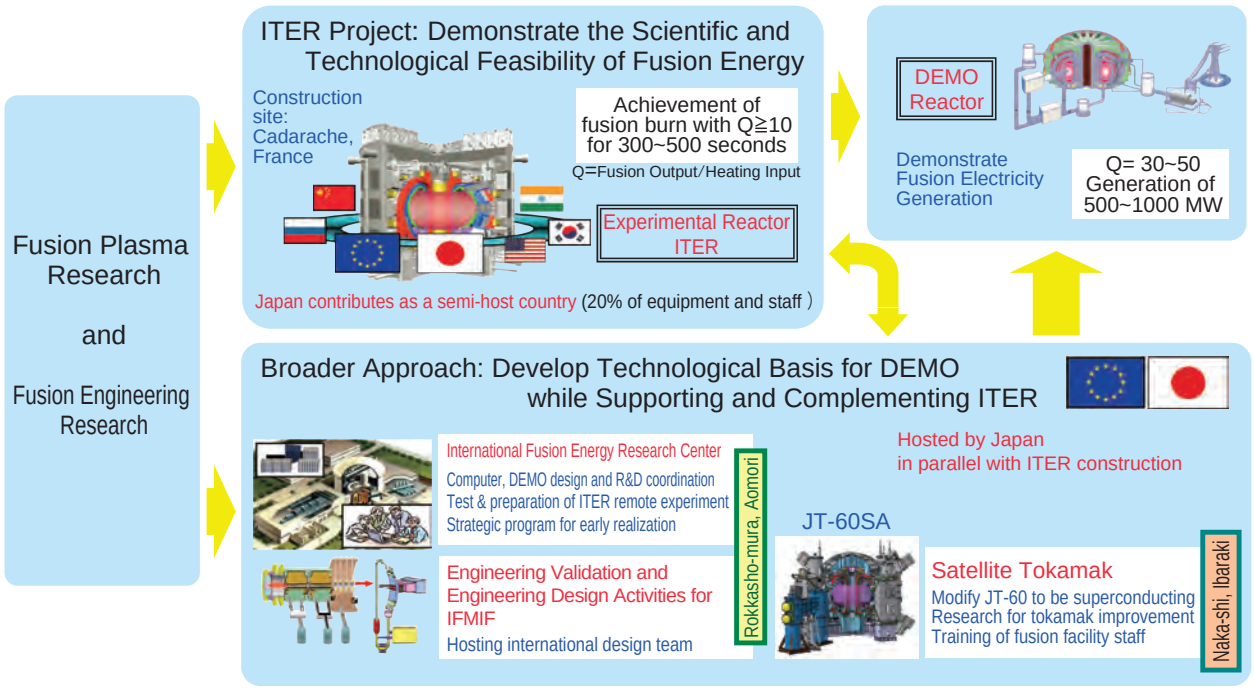

Fig.3-1 Development Steps Toward the Fusion DEMO Reactor

In the Fusion Research and Development Directorate, crucial R&D toward the practical use of fusion energy (fusion plasma and fusion engineering R&D) is being pursued through intensive international cooperation such as the International Thermonuclear Experimental Reactor (ITER) project, Broader Approach (BA) activity, and so on, aiming to make the fusion DEMO reactor a reality (Fig.3-1).

ITER Project

The ITER project is an international cooperative project to demonstrate the scientific and technological feasibility of fusion energy through the construction and operation of an experimental reactor. The ITER agreement came into force in October 2007, and JAEA was designated as the domestic agency of the ITER project in Japan. JAEA has proceeded with preparing the equipment that Japan was allotted to provide, has achieved various results in terms of technological development (Topics 3-2, 3-3, and 3-4), has completed an advanced conductor manufacturing factory in cooperation with the world of industry, and has started mass production of a superconducting coil conductor (Topic 3-1) ahead of any other country participating in ITER.

BA Activity

The BA activity is a joint project by Japan and the EU for executing support research for ITER and research and development for a DEMO reactor, which is the next step of ITER, aiming for early realization of fusion energy. The BA agreement came into force in June 2007, and JAEA was designated as the implementing agency of BA activity in Japan. BA activity consists of three projects: the activities of the International Fusion Energy Research Center, the engineering validation and engineering design activities of the international fusion material irradiation facility (IFMIF/EVEDA), and the Satellite Tokamak Program. The International Fusion Energy Research Center buildings were completed in March, 2010, and its real activity began. Topic 3-11 describes the results achieved in research related to IFMIF/EVEDA. In the Satellite Tokamak Program, Japan and the EU began joint construction of the advanced superconducting tokamak JT-60SA (Topic 3-5). Moreover, Topic 3-6 describes a result that also contributes to the JT-60SA.

Fusion Plasma Research

The critical requirement for a future fusion reactor is attaining a high level of economic efficiency: namely, to sustain high fusion power in a reactor core of compact size. It is necessary to improve the plasma pressure to accomplish this. Topics 3-7 and 3-8 describe results that can indicate guiding principles for achieving high plasma pressure.

Fusion Engineering Research

In a fusion reactor, it is necessary to maintain an ultra high temperature plasma of 100 million degrees or more in the vacuum vessel. Topics 3-9 and 3-10 relate results achieved regarding development of equipment for this.

3-1 Start of Manufacture of the Superconductors for the ITER Magnets
—Development of Exacting Quality Assurance Techniques—

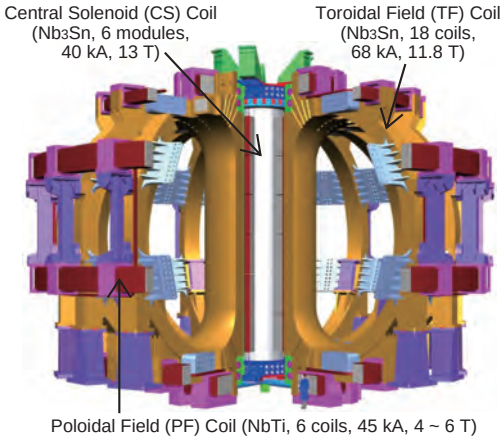

Fig.3-2 ITER superconducting magnet system
The system consists of 18 toroidal field (TF) Coils, 6 central solenoid coils and 6 poloidal field coils.

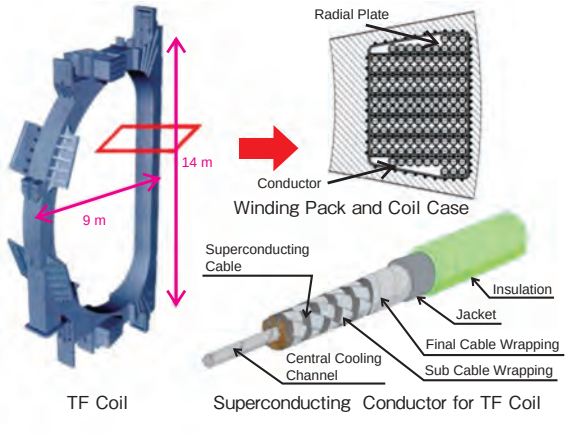

Fig.3-3 Structure of TF coils and their superconductor
A circular, multistage superconducting cable, consisting of around 1000 superconducting strands, is inserted into a circular stainless steel jacket. The superconductor is subsequently inserted into the groove of a radial plate.

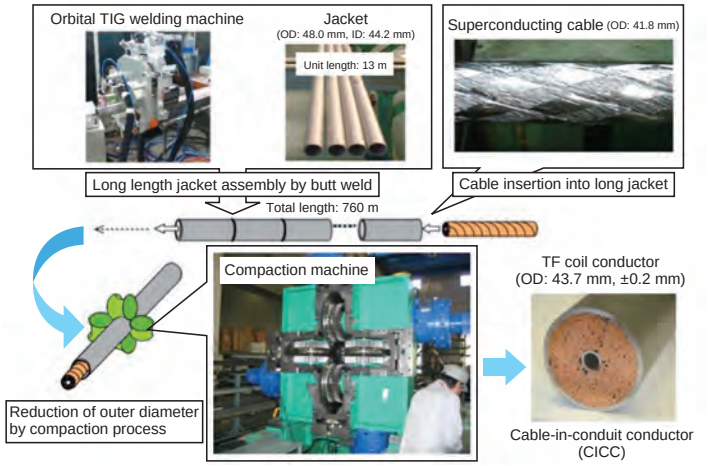

Fig.3-4 Fabrication process of the TF conductor
Jackets with a length of 13 m are butt-welded by an automatic welding machine to create a jacket whose total length is 760 m. The superconducting cable is inserted into the jacket. The jacket is then compacted to a diameter of 43.7 mm.

The ITER device being constructed by Japan, China, the EU, India, Korea, Russia and the US, will have a field of 10 T in order to confine and control a very high temperature plasma. Huge superconducting coils are necessary for this purpose (Fig.3-2). The height, width and weight of a toroidal field (TF) coil, which generate the magnetic field, are 14 m, 9 m and about 300 tons, respectively (Fig.3-3). Japan is procuring 9 TF coils and 25% of all TF superconductors, and is the first to begin manufacturing the TF conductors.

A circular superconducting cable, consisting of around 1000 superconducting strands, is inserted into a circular stainless steel jacket (Fig.3-4). The jacket is composed of tubes, each 13 m in length, that are butt-welded by an automatic welding machine to create a single length of 760 m. The gap between the cable and the jacket is approximately 2 mm. The pulling force on the cable is approximately 4 tons. Following cable insertion, the jacket is compacted to the specified diameter in a single step. After welding, a helium leak test, radiographic inspection and a dye penetrant test are carried out on the welds. Following the compaction, outer diameter tolerances of 0.2 mm, corresponding to 0.5% of the outer diameter (43.7 mm), are confirmed through continuous laser measurement. The conductor is wound as a one-layer solenoid with a diameter of 4 m, and a helium leak test is carried out in a vacuum tank. Demanding specifications have required the development of exacting quality assurance techniques. These techniques were confirmed as valid during the fabrication of a 760 m Cu dummy conductor, as a result of which we have started fabrication of actual superconductors at the rate of approximately one conductor per month.

Reference

Nabara, Y., Takahashi, Y. et al., Procurement of Nb_3Sn Superconducting Conductors in ITER, Journal of Plasma and Fusion Research SERIES, vol.9, 2010, p.270-275.

3-2 Development of an In-Vessel Remote Handling Robot for the ITER

—Demonstration for Automatic Assembly and Installation of the Remote Handling Robot—

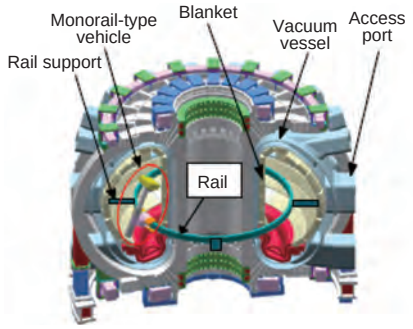

Fig.3-5 In-vessel remote handling robot for the ITER
A monorail-type vehicle that is equipped with a telescopic manipulator (maximum 5 m long) travels on the rail.

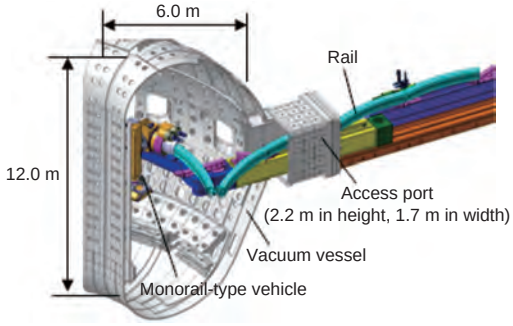

Fig.3-6 Conditions for installation of the maintenance robot in the vacuum vessel
One of the conditions is that it must pass through an access port.

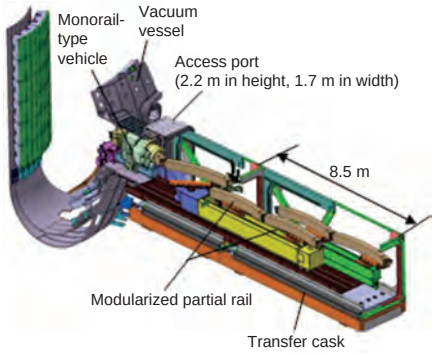

Fig.3-7 Equipment for installing the maintenance robot into the vacuum vessel
Modularized devices will be assembled to perform maintenance operations according to their purpose.

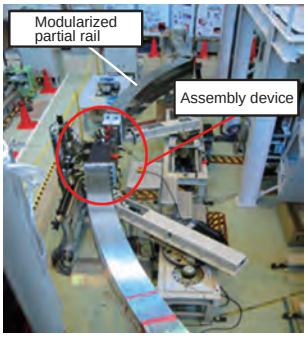

Fig.3-8 Demonstration for assembly of modularized partial rail
A hook, which strengthened the hinge between partial rails in the previous design, enables precise assembly by guiding the relative position of the partial rails in the new design.

In the ITER, an international experimental fusion reactor, in-vessel components such as the blanket will be maintained by remote equipment. The blanket of the ITER is divided into 440 modules so as to make possible easy maintenance and exchange; each module is a heavy (4.5 tons) and large (1.4 m ×1.0 m×0.5 m) component. Therefore, development of a maintenance robot for remote maintenance of the blanket is necessary to maintain this tokamak device.

The main features of the robot system are high mobility of the robot and high stiffness of the rail, on which a monorail-type vehicle travels equipped with a manipulator, and which is supported by four supports every 90 degrees (Fig.3-5). Thus far, high precision heavy component handling technology has been demonstrated via a prototype of the robot system. In the future development of the robot system, the important technical issue to be solved to put the system into practice is the robot system installation method.

The requirements for the installation method are: (1) that the robot system can be installed into the vacuum vessel through the access port (2.2 m, 1.7 m), which is narrow compared to the maintenance area (12.0 m, 6.0 m), and (2) that the robot system can be transported by means of a transfer cask (8.5 m in length, 2.5 m in width, 3.0 m in height) (Fig.3-6). In order to satisfy these two requirements, the rail and the rail assembly/deployment device are modularized and separated. Modularization makes it possible to install the robot system through the narrow access port and transport the robot system by the transfer cask (Fig.3-7).

A technical issue for the modularization is the highly precise (0.1 mm) assembly of the modularized partial rails. Moreover, position sensors cannot be used because of the radiation environment near the access port, and thus the only possibility is to utilize passive positioning with a guiding mechanism. To solve this issue, a new assembly device was developed to enable high precision assembly, and the device shown in Fig.3-8 reduced the positioning error to 0.1 mm. As a result, the automatic assembly technology for the installation of the robot system through the narrow access port was established, and the technical issues were therefore resolved for fabrication of the actual machine.

Reference

Takeda, N. et al., Mock-Up Test on Key Components of ITER Blanket Remote Handling System, Fusion Engineering and Design, vol.84, issues 7-11, 2009, p.1813-1817.

3-3 Demonstration of Voltage Holding with the World's Largest Fine Ceramic Ring

—Progress on Development of a 1 MV Accelerator for Heating and Current Drive in ITER—

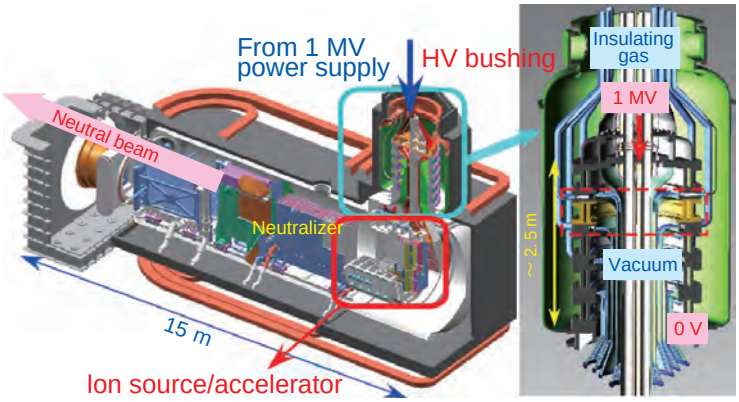

Fig.3-9 ITER NBI system and high voltage bushing
The high voltage bushing acts as a bulkhead between the gas region and a vacuum. While providing 1 MV insulation, the bushing is also a feedthrough for supplying electric power and cooling water for the ion source and accelerator in vacuum.

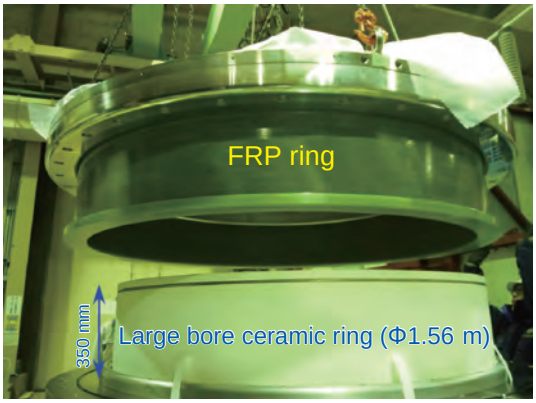

Fig.3-10 Full-size mockup of high voltage bushing
A full-size double-layered insulator consisting of a ceramic ring and FRP ring was manufactured. This simulates one stage of the high voltage bushing in the ITER NBI.

Neutral beam injection (NBI) is one of the key technologies for plasma heating and current drive in ITER. In the ITER NBI, a 1 million volt (MV) electrostatic accelerator is equipped to produce deuterium negative ion beams. A conventional insulation method to sustain high voltage in an accelerator is gas insulation with SF_6 gas. However, the accelerator in the ITER NBI is exposed to a radiation environment and electric current is induced in the insulating gas in such an environment, which results in power dissipation, and thus the accelerator must be installed in a vacuum. A high voltage (HV) bushing is then required to be mounted between the transmission line from the 1 MV power supply in the SF_6 gas and the accelerator in the vacuum. The HV bushing, which acts as a bulkhead and a feedthrough, is composed of a five-stage insulator to sustain 1 MV insulation (Fig.3-9). Since many conductors must be located inside the ceramic ring sustaining 1 MV insulation, the dimensions of the ceramic ring must be 1.56 m in diameter, 29 cm in height, and 5 cm in thickness. However, in conventional manufacturing methods the diameter has been limited to less than 1 m, and hence to establish a manufacturing method for the large ceramic ring has been a long-standing issue, for over ten years. To make the HV bushing a reality, JAEA and Kyocera Cooperation succeeded in manufacturing the world's largest ceramic ring (1.56 m in diameter) with a newly-developed forming method. A joining technique by brazing of the large ceramic ring with Kovar (a nickel alloy) was also developed in collaboration between JAEA and Hitachi Haramachi Electronics Co., Ltd.

JAEA manufactured a full-size mockup with the brazed ceramic, which simulated one stage of the HV bushing, as shown in Fig.3-10. To suppress breakdown triggered at the joint of the ceramic and metal, stress rings developed in R&D activity for the ITER accelerator in JAEA were installed in the mockup.

In the high voltage test of the mockup, 240 kV were sustained stably for over 1 hour. This is 20% higher than the rated voltage for each ceramic ring (200 kV), and thus the voltage holding capability required in the ITER NBI was verified for the first time. The present result supports development of the ITER NBI. Application of the vacuum insulation technique is expected to promote development of a "SF_6 gas free" high voltage component, which will be useful in the power industry.

Reference

Tobari, H. et al., Development of the High Voltage Bushing for the ITER NBI, Journal of Plasma and Fusion Research SERIES, vol.9, 2010, p.152-156.

3-4 Robust Leak Tight Box with Thin Wall Membrane Structure

—Demonstration of a Tritium Breeder Pebble Container for the ITER Test Blanket Module—

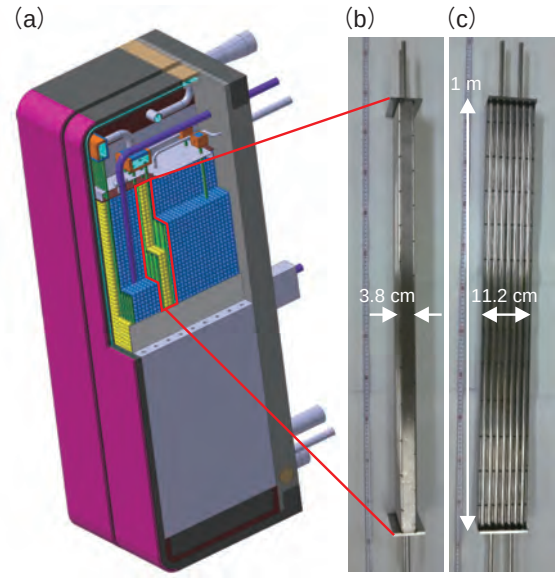

Fig.3-11 Internal structure of a water cooled ceramic breeder blanket
Views from (a) the cross section, (b) the side, and (c) the front of the BPC. The blanket contains tritium breeder pebbles (yellow) and neutron multiplier pebbles (blue). The full-scale BPC withstood 0.5 MPa of internal pressure.

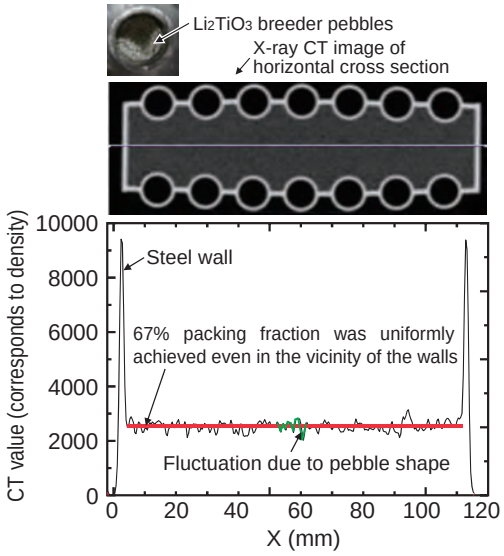

Fig.3-12 X-ray CT image of the interior of the BPC and packing fraction of breeder pebbles
The X-ray CT image reveals a uniform distribution of pebbles and confirms a 67% packing fraction.

The blanket is located in the vacuum vessel of a fusion reactor, surrounding the fusion plasma. Its functions are to extract heat from fusion energy, and to generate the fusion fuel tritium using fusion neutrons. Tritium is generated by a nuclear reaction between neutrons and the tritium breeder: lithium meta titanate (Li_2TiO_3) pebbles. Li_2TiO_3 pebbles are contained in a breeder pebble container (BPC) in a blanket module. Since the BPC is expected to attain high efficiency in tritium production and heat extraction, it is required to be leak-tight and robust with a thin wall structure to minimize the structural material mass in order to maximize tritium breeding efficiency.

We have succeeded in fabricating a full scale mockup of a BPC with reduced activation ferritic martensitic steel, using a fiber-laser welding (FLW) method (Fig.3-11). Generally, in welding, the structural material shows softening induced by heat input during welding. FLW has a high laser beam focusing capability, and therefore it can minimize the softened region. This FLW method was successfully applied to welding plates 1.5 mm thick to tubes 1 mm thick and 11 mm in diameter, without penetration of the weld bead through the tube. The width of the softened region was less than 0.2 mm, which is small enough to maintain robustness together with the thin wall structure. Its leak-tightness and robustness were confirmed with 0.5 MPa helium (He) gas.

Breeder pebbles 1 mm in diameter were packed into the BPC for evaluation of the packing fraction and packing uniformity. By measurement of the total volume of the BPC and total weight of the Li_2TiO_3 pebbles, the average packing fraction was confirmed to be 67%, which is sufficient for the expected heat transfer and tritium production. Fig.3-12 shows a horizontal cross-sectional image of X-ray computer tomography (CT) of the BPC. The X-ray CT image shows uniform packing of the pebbles. The observed CT value showed no major porosity, which would degrade heat transfer, in the central region or near the walls.

This achievement presents a bright prospect for efficient tritium breeding and high grade heat extraction by the blanket.

Reference

Hirose, T., Seki, Y., Tanigawa, H. et al., Packing Experiment of Breeder Pebbles into Water Cooled Solid Breeder Test Blanket Module for ITER, Fusion Engineering and Design, vol.85, issues 7-9, 2010, p.1426-1429, doi: 10.1016/j.fusengdes.2010.03.066.

3-5 Progress in the Satellite Tokamak Program Project for Broader Approach Activities
—Europe-Japan Joint Construction of the JT-60SA Tokamak Launched—

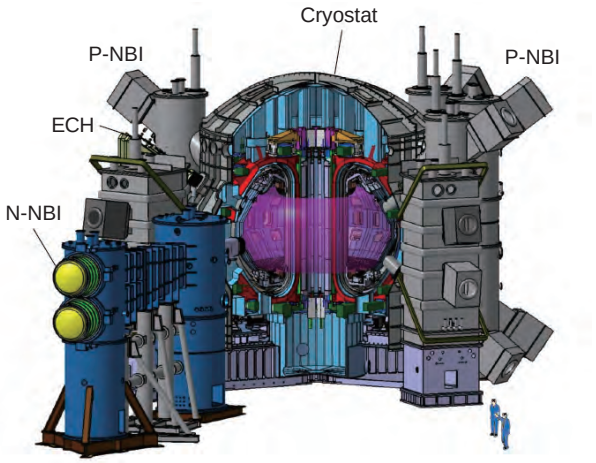

Fig.3-13 Bird's eye view of JT-60SA
Superconducting coils of the toroidal field, equilibrium field coils, the center solenoid, and the vacuum vessel are enclosed by a cryostat with thermal shields surrounded by additional heating systems for negative and positive ion neutral beam injection and electron cyclotron heating.

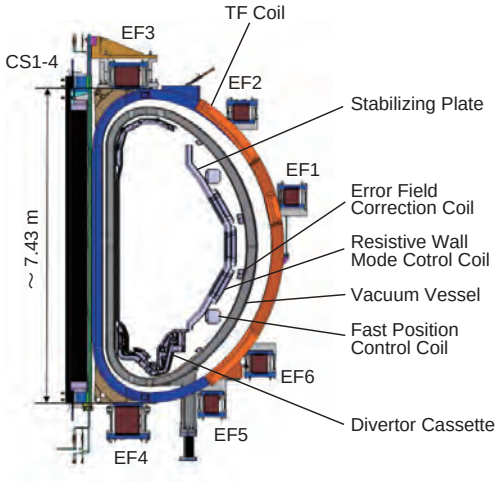

Fig.3-14 Cross-sectional view of JT-60SA
Copper coils consisting of fast plasma position control coils, error field correction coils and resistive wall mode control coils, divertor cassettes, stabilizing plates, and so on, will be installed in the vacuum vessel.

Construction and exploitation of the JT-60SA (JT-60 Super Advanced) are being implemented at the JAEA Naka site under the Satellite Tokamak Program, which is to be undertaken as part of the Broader Approach agreement jointly implemented by Europe and Japan from 2007, and the Japanese national program. The mission of the JT-60SA project is to contribute to the early realization of fusion energy by supporting the exploitation of ITER and research towards DEMO by addressing key physics issues associated with these machines. The JT-60SA will be capable of confining break-even equivalent class high-temperature deuterium plasmas at a plasma current I_P of 5.5 MA, a major radius of ~3 m and a toroidal field of 2.25 T, lasting for a duration ~100 s longer than the time scales characteristic of plasma processes such as current diffusion. It will pursue full non-inductive steady-state operation, with high plasma beta close to and exceeding no-wall ideal stability limits, and will establish ITER-relevant high density plasma regimes well above the H-mode power threshold (Fig.3-13).

Re-baselining of the project has been prompted by cost concerns and has been developed intensively since late 2007. In order to satisfy the plasma performance requirements, the machine has been coherently re-designed to cover the following specifications: a wide range of plasma equilibria with divertor configurations covering a higher plasma shaping factor of S~7, a lower aspect ratio of ~2.5, a high triangularity of κ_x~0.5, and a high elongation of δ_x~1.9; an inductive plasma current flattop and additional heating up to 41 MW for 100 s; divertor targets to withstand up to 15 MW/m^2; N-NBI having high beam energy up to 500 keV; internal coils for RWM stabilization equipped with a stabilizing shell; and in-vessel components such as divertor cassettes to be compatible with remote maintenance (Fig.3-14).

The re-baselining was completed in December 2008. The newly designed machine preserves all the scientific missions of the JT-60SA project, and is expected to meet its cost objectives, comply with additional design requirements, and add further flexibility features. In accordance with Procurement Arrangements between the Implementing Agencies of Fusion for Energy in Europe and JAEA in Japan, in 2009, manufacturing activities commenced with facilities for superconducting coils on the JAEA Naka site and a prototype vacuum vessel in the manufacturing factory. Thus, the JT-60SA project made a large step forward toward completion, in which the first plasma is foreseen to be in 2016.

Reference

Kamada, Y., Ishida, S. et al., Progress of JT-60SA Project towards an Integrated Research for ITER and DEMO, Journal of Plasma and Fusion Research SERIES, vol.9, 2010, p.641-649.

3-6 High Energy and Large-Area Negative Ion Beams Successfully Produced
—Progress with the JT-60SA Neutral Beam Injector—

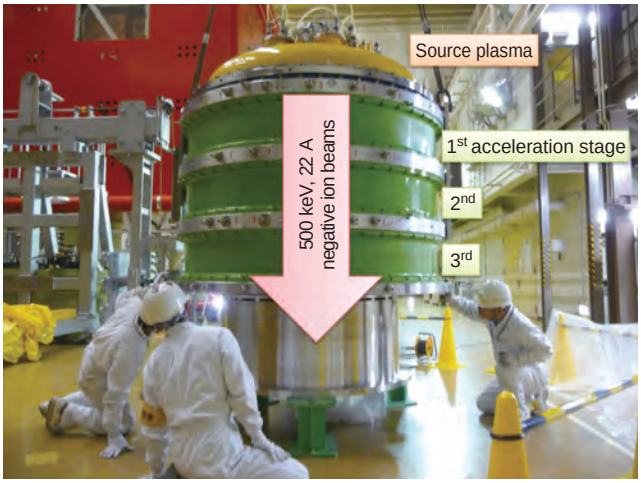

Fig.3-15 Modification of 500 keV negative ion source for JT-60U
The JT-60U negative ion source is the world's largest negative ion source (height 1.8 m, diameter 2 m, weight 6.5 t), and produces 500 keV beams at a negative ion current of 22 A.

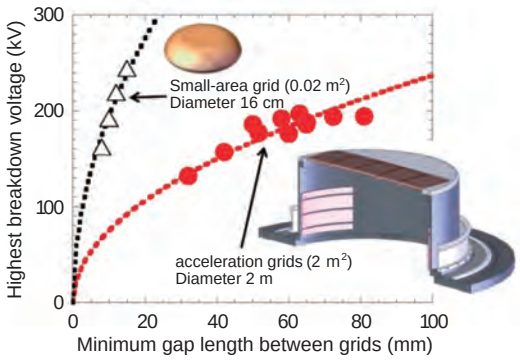

Fig.3-16 Voltage holding capability of the acceleration grids and small-area grid
The voltage holding of each acceleration stage has been investigated. The JT-60 negative ion source is designed to sustain 500 kV with three stages.

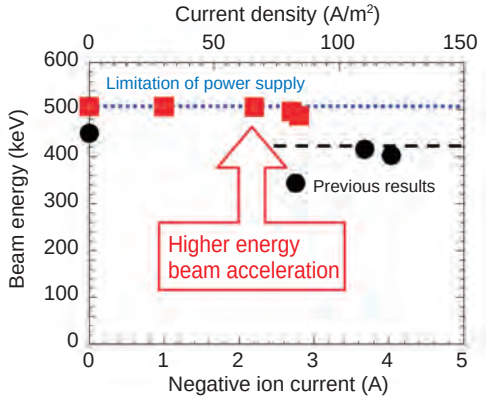

Fig.3-17 Progress in negative ion source development
Based on the result of Fig.3-16, the ion source was modified, after which 500 keV, 3A negative ion beams were obtained having energy that satisfies the JT-60SA requirement.

In fusion devices, neutral beam injectors are widely used to drive plasma current externally and to heat fusion plasmas efficiently. In particular, for ITER and JT-60SA, higher energy beams (above 100 keV) are required to heat the high density fusion plasmas. The JT-60U negative-ion-based neutral beam injector (N-NBI) with rated energy of 500 keV was the first constructed in the world. The use of high-energy neutral beams has contributed to improvement in the plasma performance.

However, the achieved beam energy was limited to 420 keV due to the low voltage holding capability of the ion source, which was designed to have three acceleration stages with large acceleration grids (Fig.3-15). The vacuum insulation distance between the acceleration grids was designed based on existing data, which were not sufficient to predict the required vacuum insulation distance of such large-area girds as the JT-60 negative ion source (2 m^2).

Recently, in order to achieve high energy beam acceleration, we investigated the voltage holding capability of the ion source by changing the vacuum insulation distances (Fig.3-16). As a result, we found that the required vacuum insulation distance of the large-area grids is much longer than that of the small-area grid. This large difference in the voltage holding capability was also found to be affected by a local strong field around the grid aperture and/or the corner of the grid support. By modifying the ion source based on the newly obtained database, an acceleration voltage of 500 kV has been stably sustained, and a stable H- ion beam acceleration of 3 A up to 500 keV has been achieved (Fig.3-17).

This is the highest beam energy of a beam over 1 A in the world. This success is driven by our understanding of the vacuum insulation distance between the large acceleration grids. Development for the JT-60SA ion source has thus advanced, and this also contributes to the ITER ion source. In addition, new findings for vacuum insulation physics have also been obtained.

Reference

Kojima, A. et al., Achievement and Improvement of the JT-60U Negative Ion Source for JT-60 Super Advanced, Review of Scientific Instruments, vol.81, issue 2, 2010, p.02B112-1—02B112-5.

3-7 New Instability Observed in High Pressure Plasmas

—Exploitation of Stability Physics toward High Pressure Burning Plasmas—

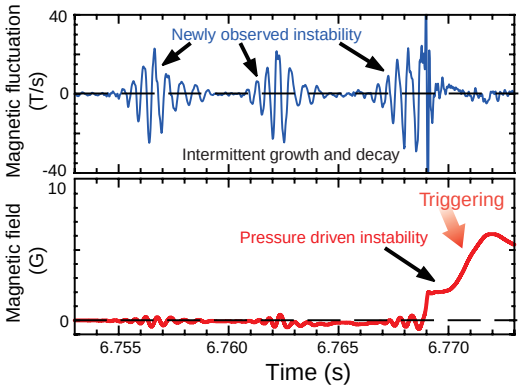

Fig.3-18
Waveforms of the new energetic particle-driven instability (above) and its triggered pressure-driven instability (below). Intermittent appearance of the energetic particle-driven instability ultimately triggers pressure-driven instability and plasma is terminated.

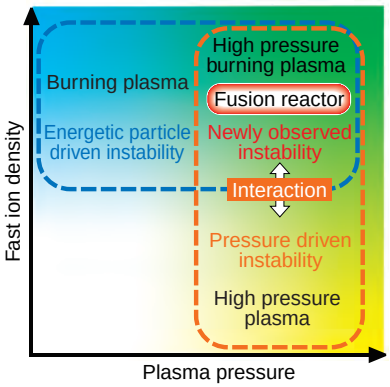

Fig.3-20
The newly observed energetic particle-driven instability is predicted to occur in burning plasma at high pressure, and interacts with pressure driven instability that limits the achievable plasma pressure. This discovery means that we have opened up a new region of stability physics in the predicted burning plasma, high pressure fusion reactor.

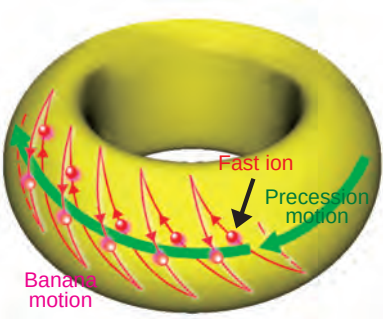

Fig.3-19
Schematic drawing of the motion of energetic particle (fast ions) that is thought to be the driving source of the new instability. Fast ions go around the torus (precession motion) in a zigzag motion (banana motion) in the plasma. This phenomenon is predicted to occur because many fast ions exit in the burning plasma.

With an economically attractive fusion reactor, high fusion output should be achieved. Since the fusion output is proportional to the square of plasma pressure (= temperature times density), operations with plasma pressure as high as possible are required. However, in magnetic confined plasma, there is an upper limit to plasma pressure called the pressure limit. When the plasma pressure reaches the pressure limit, the plasma is distorted and plasma confinement is degraded. Plasma distortion driven by high pressure is called pressure-driven instability. On JT-60U, we have exploited and developed the operation region near the pressure limit while suppressing these instabilities.

Thus far, pressure-driven instability has been successfully stabilized by rotating the plasma on JT-60U. However, a sudden occurrence of pressure-driven instability has been observed despite there being sufficient plasma rotation. As shown in Fig.3-18, it was found that this phenomenon is associated with another new instability that intermittently grows and decays repeatedly with an oscillation of several kilohertz. According to detailed analyses, the new instability appears only in high pressure plasmas, and it is found that the instability is an energetic particle-driven instability, the driving source of which is energetic particles (fast ions) in the plasma. The motion of fast ions is schematically described in Fig.3-19. In the plasma, the fast ions go around the torus (precession motion) in a zigzag motion (banana motion). Because the frequency of the observed instability is close to the precession frequency of the fast ions, the new instability is thought to be driven by resonance with the precession motion of the fast ions.

The triggering of pressure-driven instability by the new instability, thus energetic particle-driven instability, is expected to be a serious problem in fusion burning plasmas at high pressure (Fig.3-20). At the same time, a beneficial interaction, such that the new instability could mitigate against energy loss due to the edge localized mode that intermittently appears in the peripheral region, has also been observed. This discovery of this new instability that is predicted to occur in fusion reactors is based on the realization of high pressure plasma on JT-60, and is a world-leading result.

Reference

Matsunaga, G. et al., Observation of an Energetic-Particle-Driven Instability in the Wall-Stabilized High-β Plasmas in the JT-60U Tokamak, Physical Review Letters, vol.103, issue 4, 2009, p.045001-1—045001-4.

3-8 Investigating Complex Patterns of Tokamak Edge Plasma Flow

—Pioneering Plasma Physics with First-Principles Advanced Particle Simulation—

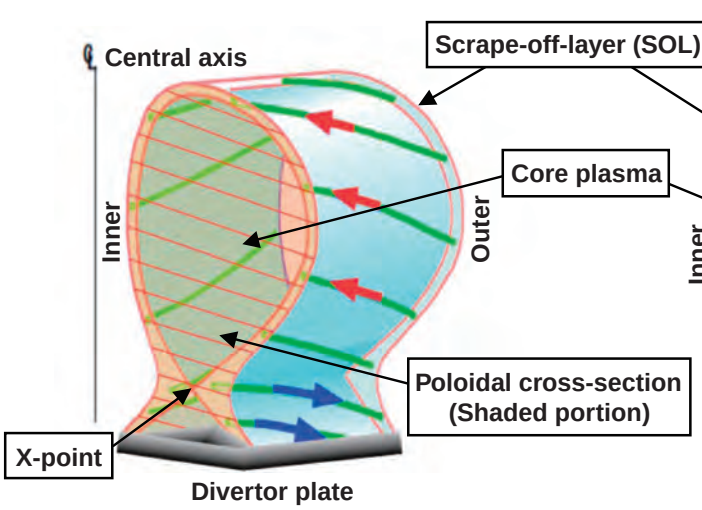

Fig.3-21 Schematic of plasma flow in the tokamak edge SOL

Plasma in the SOL, which surrounds the core plasma, mainly flows along the magnetic field line (green line), and finally reaches the divertor plate (blue arrow), but the reverse flow was observed as shown by the red arrow.

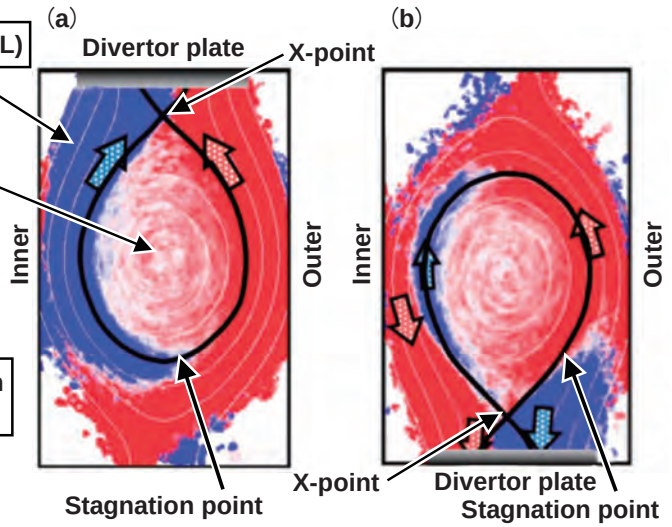

Fig.3-22 Two-dimensional structure of plasma flow for (a) upper X-point and (b) lower X-point cases

(a) In the upper X-point case, the plasma flows symmetrically into the inner part and outer part of the divertor plate.
(b) In the lower X-point case, plasma flow is directed away from the divertor plate in the outer SOL region. The black line represents the magnetic separatrix with an X-point.

Plasma flow in the scrape-off-layer (SOL) of the tokamak edge plays an important role for heat and particle control in fusion reactors. Energy and helium ash generated by fusion reactions in the hot core region are diffused across the closed magnetic surfaces to the open-field SOL region. The flow is expected to efficiently expel helium ash and to retain impurities enhancing radiative cooling in the divertor region, if the flow is directed towards the divertor plate (blue arrow in Fig.3-21). It has been experimentally observed, however, that the flow direction is sometimes the opposite: from the plate side to the middle of the SOL in the outer SOL region (red arrow in Fig.3-21). Many fluid model simulation studies have been carried out with regard to this flow structure problem. The simulation results were compared with experimental results, but satisfactory agreements were not achieved.

We believe that this may be caused by the particle behavior. We therefore investigated the SOL flow patterns using the advanced first-principles particle simulation code PARASOL, and found that the major mechanism of the pattern variation was due to the X-point location. The PARASOL code traces behaviors of a large number of ions and electrons in the whole tokamak region, consisting of hot core and SOL-divertor regions. Particle orbits including gyro-motion are fully solved under the influence of the electric field self-consistently calculated by a particle-in-cell method. Coulomb collisions between particles are accurately simulated by a Monte-Carlo binary collision model. Fig.3-22 shows the two-dimensional structure (poloidal projection on a poloidal cross-section) of the plasma flow ($V_{//}$) parallel to the magnetic field. For the upper X-point case (a), $V_{//}$ is directed to the diverter plate both in the inner (central axis side) and outer SOL regions, and the stagnation point ($V_{//} = 0$) is located symmetrically at the bottom. On the other hand, for the lower X-point case (b), $V_{//}$ in the outer SOL region has a backward flow pattern (counterclockwise flow near the outer mid-plane). The stagnation point moves below the mid-plane of the outer SOL. In comparison with experimental results, the simulation produced very similar flow patterns both qualitatively and quantitatively. Performing various parametric surveys, we found that the complex edge plasma flow pattern is governed mainly by the ion orbits in the toroidal geometry of the tokamak magnetic field.

Reference

Takizuka, T. et al., Two-Dimensional Full Particle Simulation of the Flow Patterns in the Scrape-Off-Layer Plasma for Upper- and Lower-Null Point Divertor Configurations in Tokamaks, Nuclear Fusion, vol.49, no.7, 2009, p.075038-1—075038-9.

3-9 Investigation of Impurity Transport in Plasma

—Development of Accurate Quantitative Analysis for Tungsten on the Plasma Facing Wall—

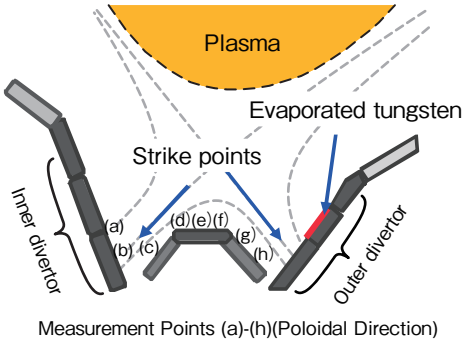

Fig.3-23 Poloidal cross-sectional view of the divertor in JT-60U and measurement positions
After all the plasma discharge shots, the amount of tungsten on the CFC divertor tile along the poloidal direction was analyzed.

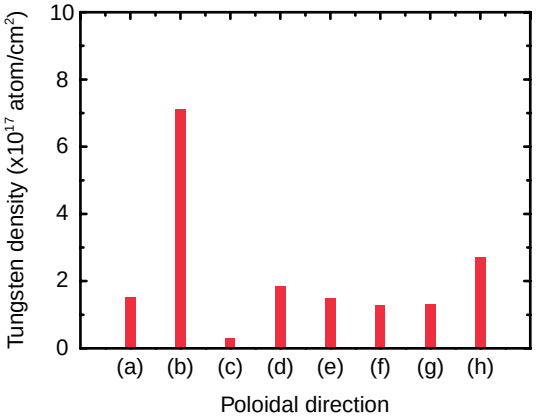

Fig.3-25 Surface density distribution of deposited tungsten along the poloidal direction
From the tungsten distribution obtained via the activation analysis, it was discovered that tungsten sputtered by the plasma tended to accumulate at the strike point (Fig.3-23(b)) where exhaust particles concentrated.

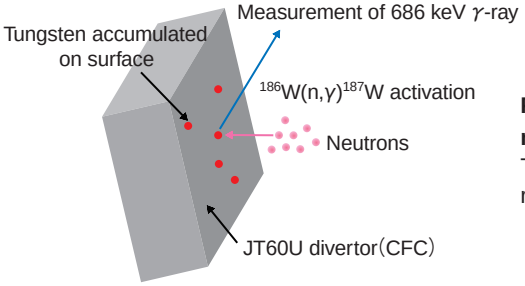

Fig.3-24 Principle of the activation analysis method using the ^{186}W(n, γ)^{187}W reaction
The measurement of γ-rays emitted from ^{187}W produced in the ^{186}W(n, γ)^{187}W reaction is employed for analysis of the tungsten.

Tungsten is one of the most promising candidate materials for the plasma facing wall and divertor in nuclear fusion reactors, but when tungsten becomes sputtered and transported into the plasma as an impurity, it significantly cools the plasma due to the radiation effect, and the plasma performance degrades. In order to prevent tungsten being transported into the plasma, it is essential to clarify the transport mechanism of tungsten that is evaporated and/or sputtered from the plasma facing components. This requires accurate measurement of tungsten deposited on the plasma facing wall and divertor. Thus far ion and electron beams have been typically used as the measuring method, but the quantitative measurement of such traces of tungsten has been technically so difficult that developing a new method has been a significant issue. In this study, we focused on γ-rays emitted from ^{187}W produced in the ^{186}W(n, γ)^{187}W reaction and developed a new measurement method for trace amounts of tungsten with an activation analysis method. Fig.3-23 shows the poloidal cross sectional view of the divertor in JT-60U and measurement positions. The principle of the activation analysis method using the ^{186}W(n, γ)^{187}W reaction is illustrated in Fig.3-24.

A tungsten divertor, composed of carbon fiber composite (CFC) tiles on which tungsten 50 μm in thickness was evaporated, was set up in the outer divertor region, and plasma discharge experiments were conducted involving more than 1000 shots in JT-60U. After all the plasma discharge shots, the CFC tiles near the tungsten divertor were removed (Fig.3-23(a) ~ (h)) and were cut into pieces about 1 cm square and 2 mm thick as analysis samples. They were then irradiated with DT neutrons at the Fusion Neutronics Source (FNS) facility in JAEA. The sample pieces were surrounded by beryllium metal blocks to improve the measurement accuracy of the ^{186}W(n, γ)^{187}W activation analysis by providing enhanced thermal neutrons. After neutron irradiation, we measured the 686 keV γ-rays emitted from the ^{187}W isotope produced in each sample, and thus the tungsten atom density on the CFC divertor surface was finally deduced. Fig.3-25 shows the distribution of tungsten density along the poloidal direction. Using this activation method, we were able to provide the first experimental observation that tungsten sputtered by the plasma tended to accumulate at the strike point where exhaust particles concentrated.

Reference

Ueda, Y., Ochiai, K. et al., Localized Tungsten Deposition in Divertor Region in JT-60U, Nuclear Fusion, vol.49, no.6, 2009, p.065027-1—065027-7.

3-10 Further Improvement of the Fusion Reactor Structural Material
—Inclusion Control in Reduced Activation Ferritic/Martensitic Steel F82H—

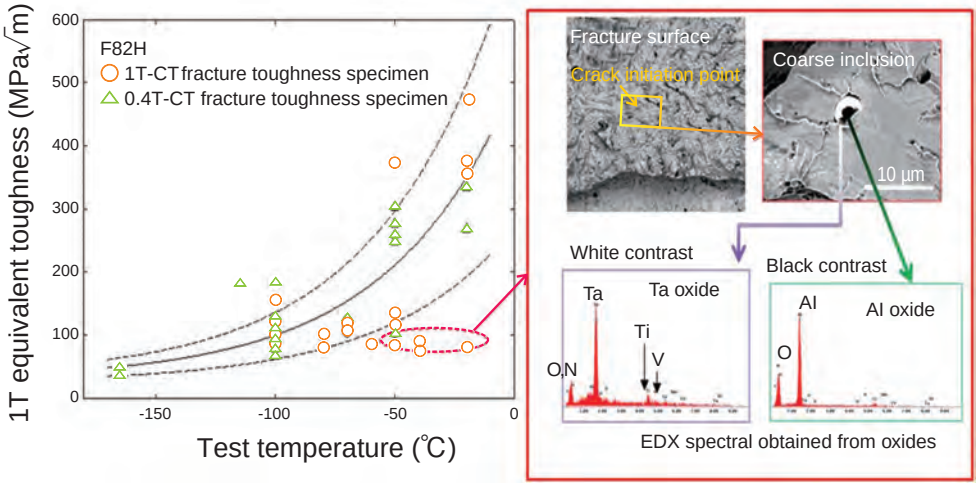

Fig.3-26 The influence of inclusions on the toughness of F82H
A coarse inclusion was found at a crack initiation point on the fractured surface of a specimen that showed low toughness beyond the dispersion latitude in the ductile brittle transition temperature region.

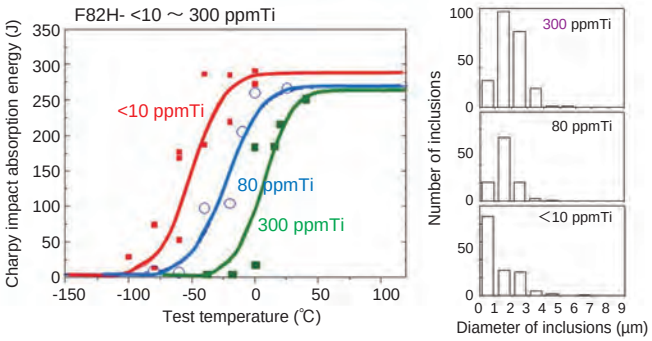

Fig.3-27 The impact of Ti contamination level in F82H
F82H with controlled Ti content was prepared to evaluate the impact of the Ti contamination level, and it was proven that the Charpy impact property was improved (left) and the formation of coarse inclusions was suppressed (right) as the Ti quantity was reduced.

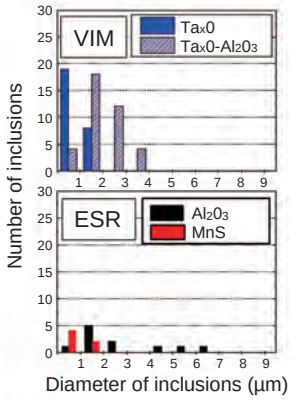

Fig.3-28 Inclusion removal by ESR
ESR was conducted after VIM for further removing inclusions, and no Ta oxide was observed in ESRed F82H except for low numbers of Al_2O_3 and MnS.

Reduced activation ferritic/martensitic (RAFM) steels are recognized as the primary candidate structural materials for fusion blanket systems, based on massive industrial experience with high chromium heat resistant steels and its high resistance to irradiation effects. F82H (Fe-8Cr-2W-0.2V-0.04Ta-0.1C) was designed with an emphasis on high temperature properties and weldability, and now F82H has the most extensive database among RAFM steels.

Ta, which is not used as an additive in conventional steels, is used to provide toughness and creep strength. A recent study revealed that Ta had formed coarse inclusions, which are a compound oxide of Al oxide and Ta oxide with Ti and N, and which have an undesirable influence on the toughness and fatigue properties (Fig.3-26).

Based on the fact that the coarse inclusions contained Ti, the impact of the Ti contamination level in F82H was examined, and improvement of the Charpy impact property and reduction of coarse inclusion formation were proven (Fig.3-27). Electroslag remelting (ESR) was also implemented as a secondary refinement after vacuum induction melting (VIM), and it was proven that ESR could remove Ta rich inclusions (Fig.3-28).

Reference

Tanigawa, H. et al., Effect of Ta Rich Inclusions and Microstructure Change During Precracking on Bimodal Fracture of Reduced-Activation Ferritic/Martensitic Steels Observed in Transition Range, Journal of ASTM International (JAI), vol.6, issue 5, 2009, JAI101728 (10p.).

3-11 For Validation of Materials for the Fusion DEMO Reactor

—Development of Small Specimen Test Technology in the International Fusion Materials Irradiation Facility/Engineering Validation and Engineering Design Activities (IFMIF/EVEDA)—

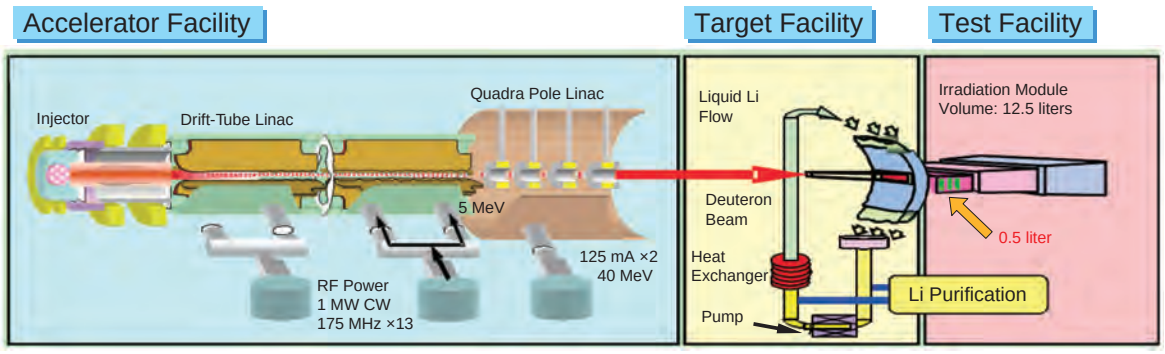

Fig.3-29 Acceleration-driven type neutron irradiation facility for fusion materials
In the IFMIF, 40 MeV deuteron beams (two lines, 125 mA) are irradiated to a 20 m/s Li flow, and high intensity neutrons are produced by a D-Li nuclear reaction. In the irradiation module set in the test facility, materials data about structural and functional materials are obtained for the design of fusion DEMO reactors.

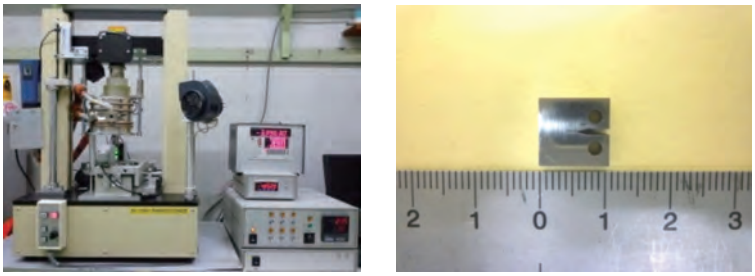

Fig.3-30 We developed test equipment (left) of fracture toughness for small size specimens (right)
The testing equipment can perform fracture toughness tests for stress and displacement with highly controllable accuracy.

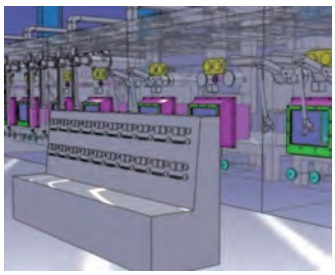

Fig.3-31 IFMIF Post Irradiation Examination (PIE) facility
Designs for a PIE facility, for testing irradiated specimens in IFMIF, are being evaluated.

The International Fusion Materials Irradiation Facility/Engineering Validation and Engineering Design Activities（IFMIF/EVEDA）was initiated in 2007 under the BA (Broader Approach) agreement. The main purpose of IFMIF is to build a database for the design of fusion DEMO reactors. As shown in Fig.3-29, the neutron production method in IFMIF makes use of a deuterium-lithium reaction, which is performed by accelerating deuteron beams to lithium target flow, and high intensity neutron sources are produced. The irradiation volume of the IFMIF is about 12.5 liters (L) in total, and the highest displacement damage is more than 20 dpa (displacement per atom)/year in a volume of 0.5 L. Therefore, we need to use small-size specimens, and a small specimen test technique or technology (SSTT) is very important.

In the IFMIF/EVEDA program, some SSTT testing, such as for fracture toughness, fatigue, and fatigue crack-growth measurement, are performed in collaborative research with a number of universities. Mechanical tests using small specimens should demonstrate highly accurate controllability of the applied stress and displacement, but commercial test machines are not typically designed to cover controllability. Fig.3-30 shows a test machine that has been specially designed and manufactured for fracture toughness tests of very small specimens, such as a compact type specimen with a length of about 10 mm. Guidelines for mechanical tests such as those of ASTM-international and the ISO have already been prepared, but they do not match up with the results of some recent research, such as the master curve method for fracture transition behavior, and so there is a need to modify and develop the standards.

In addition, we are also developing the irradiation modules and the design of a PIE facility as shown in Fig.3-31. The engineering design of the IFMIF will be finished in the middle of 2013, and then we will be able to move to the IFMF construction phase.

Reference

Wakai, E., Kogawara, T. et al., Design Status of Post Irradiation Examination Facilities in IFMIF/EVEDA, Journal of Plasma and Fusion Research SERIES, vol.9, 2010, p.242-247 .

Development of Quantum Beam Technology

Characteristics of quantum beams

Quantum beams such as neutrons, ions, electrons, high intensity lasers, and synchrotron X-rays have a creative function, allowing us to process materials on a nanometer level (atomic or molecular level) as they interact with constituent atoms of a material to change their configuration, composition, and electronic state. Such quantum beam interactions also cause changes in the beams themselves, such as the beam direction and energy, and sometimes generate different types of quantum beams. Thus quantum beams have a probe function as well, whereby we can obtain atomic or molecular level information by observing alteration of the beam parameters.

Application of quantum beams

At JAEA, we are performing advanced beam technology R&D using our beam facility complex, which includes research reactors, accelerators, and so on (Quantum Beam Platform), as shown in Fig.4-1. By utilizing the creative and probe functions of quantum beams, we are promoting fundamental and applied research in a wide range of fields, such as (1) materials science, (2) environment and energy, and (3) life science, advanced medicine and biotechnology, which are listed as the priority fields to be promoted in the Science and Technology Basic Plan of Japan. We are intensively performing these R&D activities to contribute to progress in science and technology as well as the promotion of industry.

Recent achievements

In the materials science field, we clarified the structure and kinetics of water molecules under extremely high temperature and pressure conditions, newly observed the orbital structure of molecules using tunnel ionization, and found Fermi surfaces formed by heavy electrons in metal. We also developed a soft X-ray laser interferometer and first observed the behavior of metal fine particles in a catalyst using time-resolved X-ray absorption spectroscopy. These activities are introduced in Topics 4-1 to 4-5. In Topics 4-6 and 4-7, we describe the origin of the rarest isotope in the solar system, Ta-180, and the identification of noble gas components in meteorites.

In the environment and energy field, we successfully synthesized high performance polymer electrolyte membranes to be applied in fuel cells, fabricated radiation resistant transistors based on SiC semiconductors, and developed a new welding system for inspection and repair of the inner walls of nuclear plant tubes using lasers. These results are shown in Topics 4-8 to 4-10.

In the life science, advanced medicine, and biotechnology field, we succeeded in elucidating the catalytic mechanism of protease using neutron diffraction, and developed a new technique to obtain global conformational changes of ribosome based on electron microscopy data. We also developed a novel radiopharmaceutical that enables us to find very small tumors a few millimeters in size. These achievements are described in Topics 4-11 to 4-13.

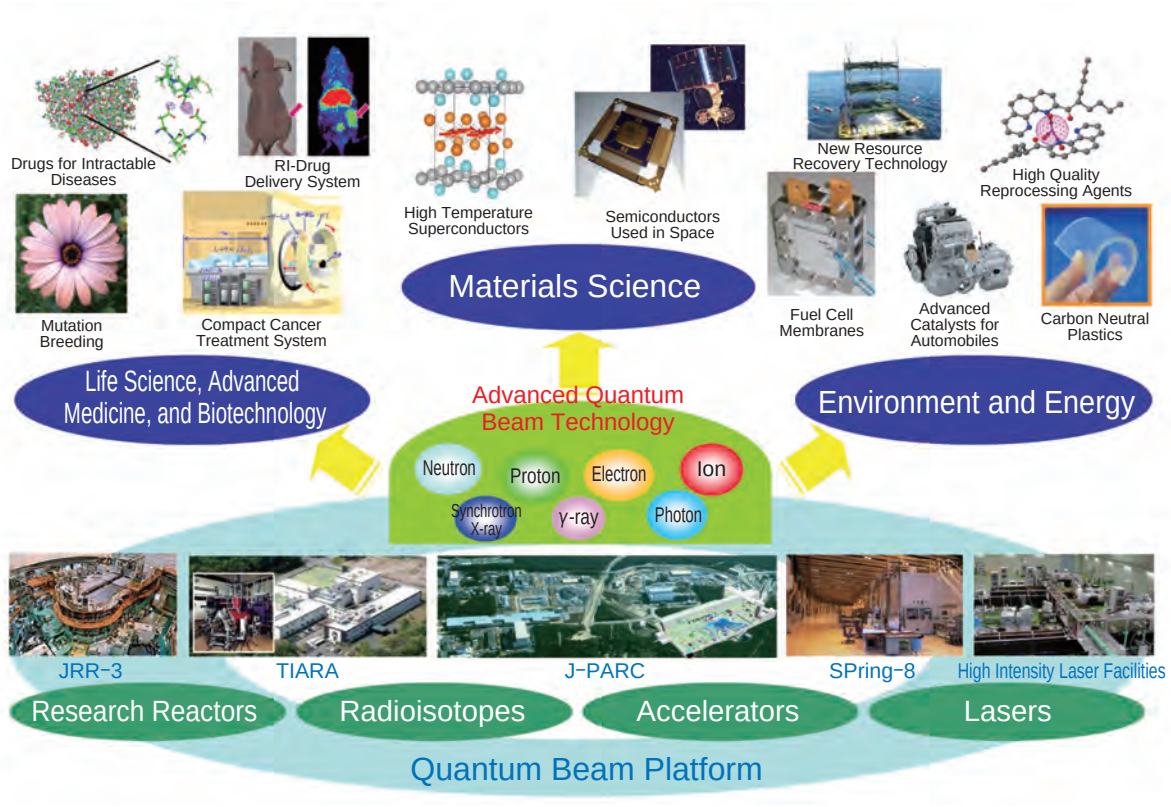

Fig.4-1 JAEA quantum beam facilities and the R&D done there

4-1 Success in Gaining a New Insight into High-Temperature Water under Pressure —Toward Full Understanding of Water—

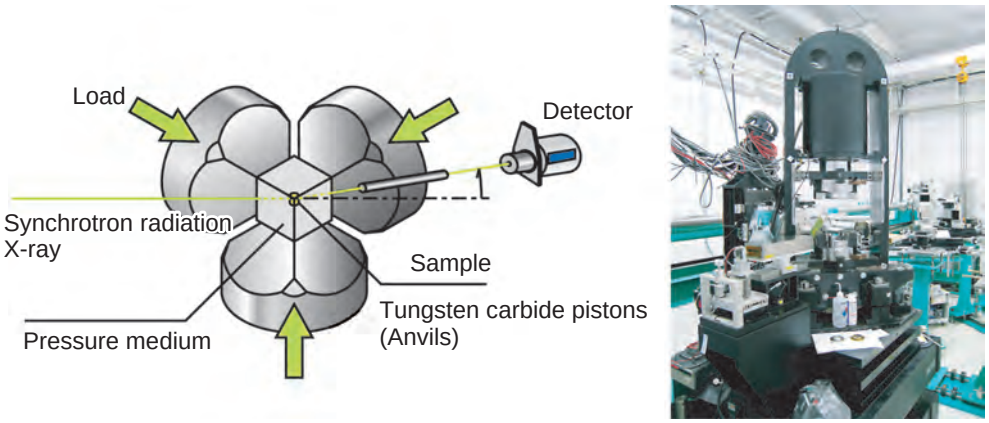

Fig.4-2 Apparatus for high temperature and pressure X-ray diffraction experiment
Schematic view (left) and photograph (right) of the cubic-type multianvil press installed on BL14B1 of SPring-8, where the present experiment was conducted.

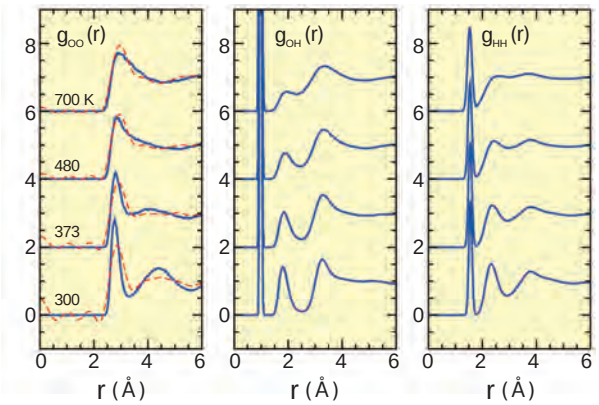

Fig.4-3 Theoretical and experimental radial distribution functions compared
Radial distribution functions $g_{XY}(r)$ (X, Y = O or H) for 1.0 g/cm^3 obtained from our first-principles molecular dynamics simulation and in situ X-ray diffraction experiment are shown as solid and dashed lines, respectively. For clarity, the vertical axis for data obtained at different temperatures is shifted up.

Although liquid water is one of the most abundant materials on earth and one of the most familiar to all of us, the present understanding of liquid water that exhibits various anomalous properties around ambient conditions is still far from satisfactory. A joint research team of the Quantum Beam Science Directorate has successfully reproduced fluid water at multi-extreme conditions of pressures (~1 GPa) and temperature (> 400 ℃) corresponding to the Earth's interior, at a depth ~30 km, by both advanced first-principles molecular dynamics simulations and in situ X-ray diffraction experiments (Fig.4-2). Thus we found that high-temperature water under pressure exhibits a characteristic structure of simple liquids (Fig.4-3), resulting from anomalously fast rotational motions, which turn out to be typically two orders of magnitude faster than in ambient liquid water. The present results will contribute to the understanding of the fundamental role of water in the (de)composition of various materials occurring in the high temperature and high pressure conditions of the Earth's interior.

Further advancement can be expected to be attainable by realizing neutron diffraction experiments at corresponding extreme conditions, which enables us to observe hydrogens as well. For this purpose, a new beamline is being actively developed in J-PARC.

This research was partially supported by a Grant-in-Aid for Scientific Research on Innovative Areas, "Earth Science Based on High Pressure and Temperature Neutron Experiments" from the Ministry of Education, Culture, Sports, Science and Technology of Japan (MEXT), Grant Nos. 20103004 and 20103005.

References

Ikeda, T., Katayama, Y. et al., High-Temperature Water under Pressure, Journal of Chemical Physics, vol.132, issue 12, 2010, p.121102-1—121102-4.
Katayama, Y. et al., Structure of Liquid Water under High Pressure Up to 17 GPa, Physical Review B, vol.81, issue 1, 2010, p.014109-1—014109-6.

4-2 Observation of Tunnel Ionization from an Orbital Lower than HOMO

— First Determination of Ionized Orbital by Comparing the Experiment with the Computer Simulation —

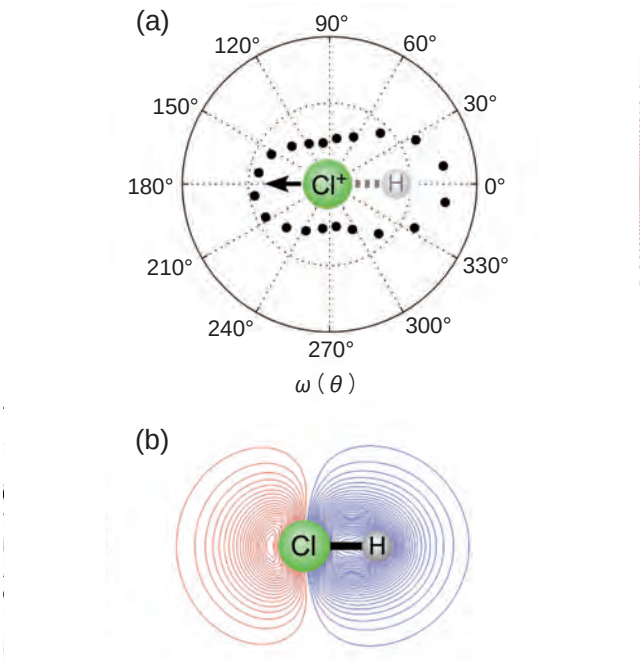

Fig.4-4 (a) Molecular - frame photoelectron angular distribution (MFPAD) obtained for Cl^+ ion production. (b) HOMO-1 of HCl, calculated by the full valence CASSCF procedure using the TZV basis sets with polarization functions.

The obtained MFPADs are similar to the shape of the HOMO-1, indicating the ionization proceeds from the orbital, not from the HOMO.

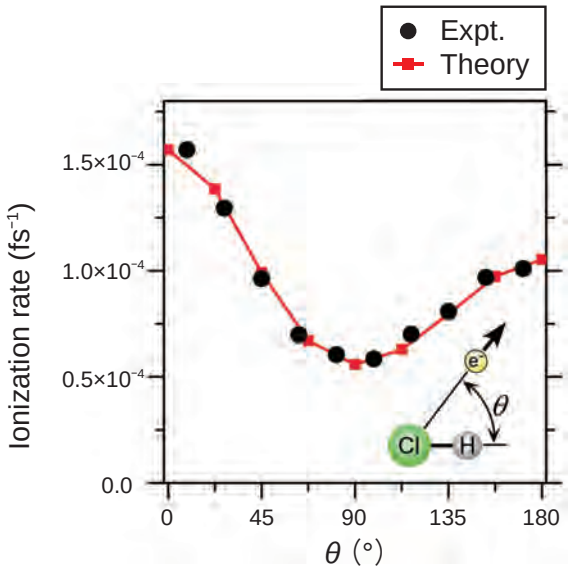

Fig.4-5 Comparison of experimental data and DFT simulation of angular dependence of ionization probability with HCl

The DFT simulated angular distribution is in nearly perfect agreement with the experimental one. Based on this agreement, we conclude that we have actually observed the ionization from the HOMO-1, not from the HOMO.

In the present work, we observed that electrons can tunnel out of orbitals at a lower energy level than previously realized. Recent advances in ultrafast laser technology enable us to obtain an intense laser field as high as 10^{15} W/cm^2. Since the intensity is comparable in magnitude to the Coulomb field generated by the atomic nucleus, the potential barrier of an atom (or a molecule) is drastically distorted, leading to quantum mechanical tunneling of electrons from the atom or the molecule.

In the case of tunnel ionization from a molecule, scientists have traditionally believed that the electron is ejected only from the highest occupied molecular orbital (HOMO). Ionization from the lower orbitals might be possible, but the probability would be much lower than that for the HOMO, and hence ionization from the lower orbitals has not been observed.

In the present work, we simulated angular dependence of tunnel ionization probability of a hydrogen chloride (HCl) molecule based on the latest computational theory, as shown in Fig.4-5. The simulated result perfectly agrees with the experimentally obtained angular dependence (Fig.4-4(a)), indicating electron ejection from the HOMO-1, the next-highest orbital.

The HOMO of a HCl molecule is a lone-pair 3p orbital of the Cl atom and is not involved in bonding. Thus, the ionization from the HOMO produces a stable HCl^+ ion. In contrast, the HOMO-1 is formed by the overlap of the H 1s and Cl 3p orbitals and accounts for the H-Cl bond. Consequently, a HCl^+ ion produced by the ionization from the HOMO-1 is unstable and easily fragments. Hence, the breakup of a HCl molecule after ionization is a direct signature for tunneling from the HOMO-1.

By measuring the fragment ion and the tunneled electron in coincidence, we determine the molecular frame photoelectron angular distribution, as shown in Fig.4-4(a), that identifies the HOMO-1 of HCl. An intense, circularly polarized laser pulse singly ionizes and subsequently dissociates an unaligned molecule. The ejected electron drifts perpendicular to the electric field direction at the moment of ionization, while the fragment ion trajectory reflects the orientation of the molecule. The obtained angular distribution (Fig.4-4(a)) is similar to the HOMO-1 (Fig.4-4(b)), and the DFT simulated angular distribution is in nearly perfect agreement with the experimental one, as shown in Fig.4-5.

This research is the first observation of tunnel ionization from lower orbitals than the HOMO. We found that the overall probability for an electron to come from the HOMO-1 is only 0.2%, but if an electron is removed specifically along the molecular axis, away from the H atom, the probability is at least 10%. We expect that tunneling from lower-energy orbitals should be more prevalent in molecules larger than HCl. In such molecules, the energy difference between the HOMO and lower-lying orbitals is generally smaller than that for HCl and would favor lower-energy tunneling.

Reference

Akagi, H., Otobe, T. et al., Laser Tunnel Ionization from Multiple Orbitals in HCl, Science, vol.325, no.5946, 2009, p.1364-1367.

4-3 Direct Observation of Fermi Surfaces Formed by Heavy Electrons

—Clue to the Mechanism of Anomalous Superconductivity Coexisting with Magnetism—

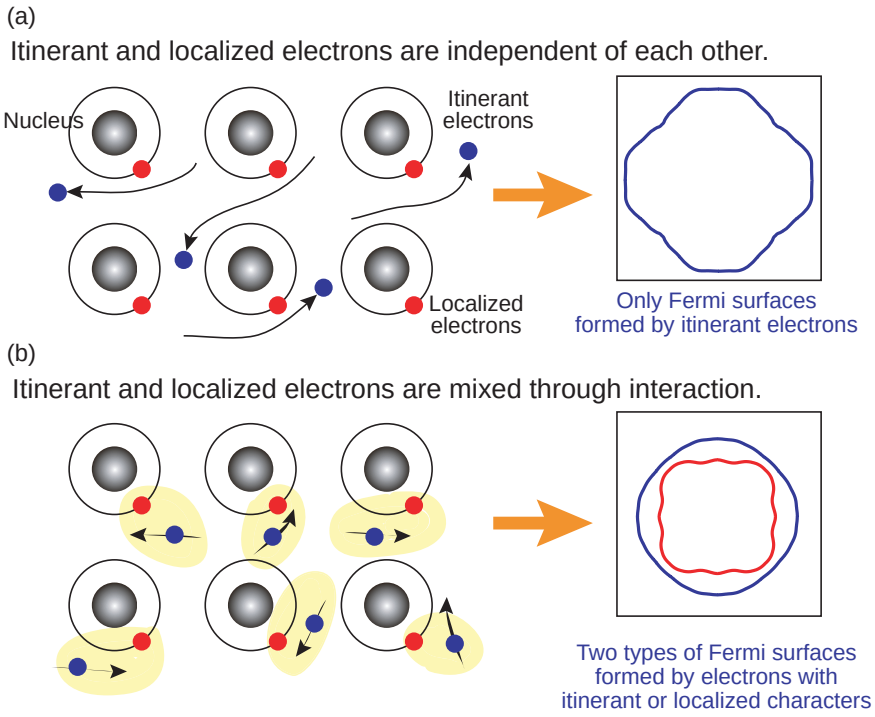

Fig.4-6 Formation of Fermi surfaces (FSs) related to heavy electrons
(a) When localized f electrons (●) and itinerant conduction electrons (●) are independent of each other, only the FSs formed by itinerant electrons are observed.
(b) When f electrons hybridize with itinerant electrons, two types of FSs formed by electrons with itinerant or localized characters are observed.

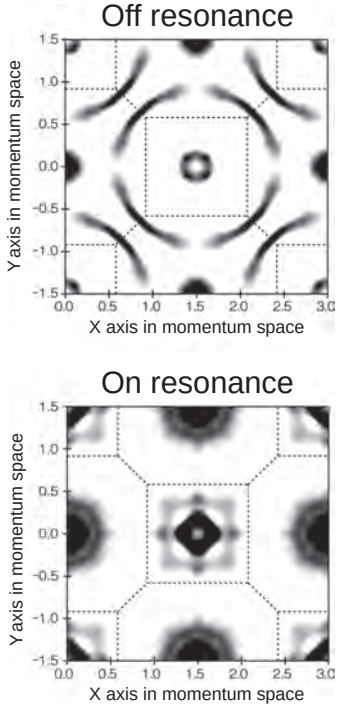

Fig.4-7 FSs observed by RARPES
Itinerant nature FSs (circular shape) and localized nature FSs (square shape) are selectively observed by off-resonance and on-resonance data, respectively.

Electrons in metals are classified into two types: itinerant electrons, which contribute electrical conductivity, and localized electrons, which contribute magnetism. When the two types of electrons are mixed through strong interaction, heavy electrons are formed, which have an effective mass up to 1000 times the free-electron mass. The nature of heavy electrons is a key to understanding the mechanism of anomalous superconductivity coexisting with magnetism. The Fermi surface (FS), which is derived from the periodicity and symmetry of the crystalline lattice and from the occupation of the electronic energy bands, is useful for predicting the thermal, electrical, magnetic, and optical properties of metals. Experimental observation of the overall shape of FSs formed by heavy electrons had not been successful yet.

In this study, we succeeded in direct observation of FSs formed by heavy electrons by means of Resonant Angle-Resolved PhotoElectron Spectroscopy (RARPES), which enables us to make electron-orbital-selective measurements, using the JAEA soft X-ray beamline BL23SU at SPring-8. Fig.4-6 illustrates the formation of two types of FSs in a situation in which heavy electrons are formed through a strong hybridization between localized and itinerant electrons. By means of RARPES, we have selectively observed the FSs having itinerant and localized natures, in off-resonance and on-resonance measurements, respectively, as shown in Fig.4-7. In future studies, RARES will clarify the characteristics of FSs in the magnetic order related to superconductivity, which should contribute to progress in understanding the mechanism of superconductivity in heavy electron systems.

Reference

Okane, T. et al., 4f-Derived Fermi Surfaces of $CeRu_2(Si_{1-x}Ge_x)_2$ near the Quantum Critical Point: Resonant Soft-X-ray ARPES Study, Physical Review Letters, vol.102, issue 21, 2009, p.216401-1—216401-4.

4-4 Observation of Dynamical Surface Morphology with One-Nanometer Resolution —Development of the Soft X-ray Laser Interferometer—

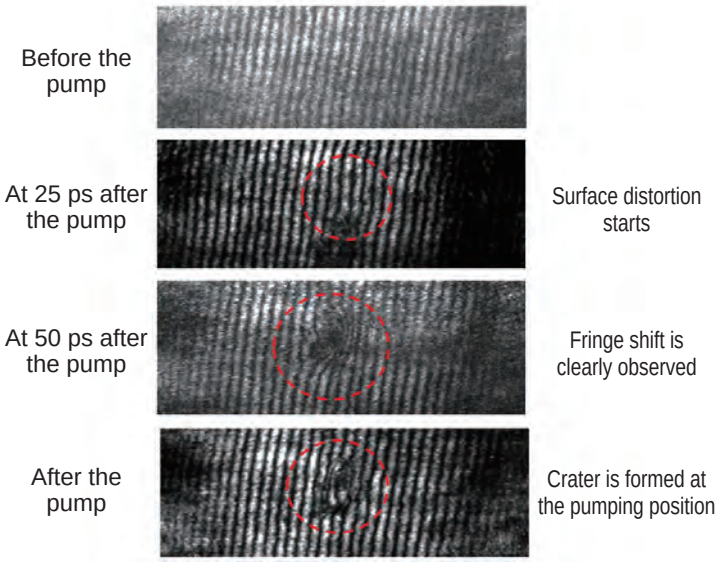

Fig.4-8 Soft X-ray interferogram of platinum surface pumped by ultra-short laser pulse
From top to bottom: the X-ray laser proves the surface before the pump; at 25 ps after the pump; at 50 ps after the pump; and after several seconds. The fringe shift can be seen in the red dotted circle area.

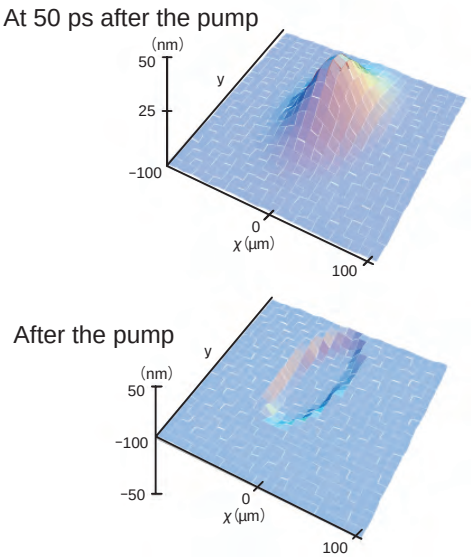

Fig.4-9 Retrieved surface profile from the interferogram
The surface profile of platinum at 50 ps after the pump (top), and after several seconds (bottom).

The dynamics of photo-induced phenomena, namely laser-induced melting, annealing, ablation, and ripple formation on solid surfaces, is the central issue in photon-aided advanced technologies for nanometer-scale fabrication. Photo-induced phase transitions, as well as photochemical and biological processes in nanometer space, also have to be clarified from a dynamic point of view. These phenomena often accompany changes in surface morphology proceeding in a very short (nano- to femtosecond) time scale, and thus are hard to explore using ordinary experimental techniques. The nonreversible and nonrepetitive nature of these phenomena adds more difficulties to time-resolved observation. In spatial resolution, it is directly related to the wavelength of the probe, and drastic improvement in resolution is being sought in extreme ultraviolet and soft X-ray regions by utilizing new light sources to investigate the structures of biological cells, magnetic domains, nano-particles/tubes, and fabricated devices.

The laser-driven plasma soft X-ray laser is an attractive light source for this purpose, because it has outstanding properties such as high monochromaticity, coherence, and short duration. We developed a pump-and-probe X-ray laser interferometer under the collaboration with Institute of Solid State Physics (ISSP) and University of Tokushima. The spatially coherent 13.9 nm laser illuminates a sample at a grazing angle of 24 degrees. The sample image is then transferred onto an X-ray CCD by a concave imaging mirror with a magnification factor of 21.3. The soft X-ray from the sample is divided into two parts by a double Lloyd's mirror placed between the imaging mirror and the CCD, and is focused on the CCD with a small angle to produce interference fringes. The spatial resolution of this interferometer reaches 1 μm for lateral directions and 1 nm in depth, and the temporal resolution is the duration of the X-ray laser (~7 ps). This performance is sufficient for observing the surface dynamics of the initial stage of laser processing.

Using this interferometer, we demonstrated observation of the surface dynamics of a platinum (Pt) sample pumped by a 100 fs-duration infrared laser pulse. Fig.4-8 and Fig.4-9 show the temporal evolution of the interferogram of the Pt surface and the retrieved surface profile, respectively. After irradiation, a very small but substantial deformation starts at around 25 ps. At around 50 ps, apparent expansion of the surface is shown and the height of the peak reaches 30 nm, and finally a crater is generated. This is the first observation of the initial stage of laser processing or laser welding, and the result provides useful information to deep understanding of the fundamental processes in the laser-matter interaction. Our next objective is to improve the lateral resolution to ~100 nm by replacing the imaging mirror with a Fresnel zone plate.

Reference

Suemoto, T., Kawachi, T. et al., Single-Shot Picosecond Interferometry with One-Nanometer Resolution for Dynamical Surface Morphology Using a Soft X-ray Laser, Optics Express, vol.18, no.13, 2010, p.14114-14122.

4-5 Behavior of Metal Fine Particles during Automotive Emissions Control

— Direct Observation of a Catalytic Reaction by Time-Resolved X-ray Absorption Spectroscopy —

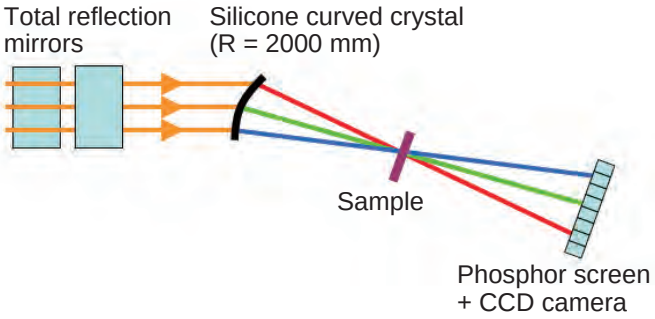

Fig.4-10 Schematic of the dispersive XAFS system
In the conventional XAFS system, plane crystals need to rotate in order to change the energy of X-rays. On the other hand, in the dispersive XAFS system, X-rays of suitable band energy are formed from a curved crystal illuminated by white X-rays. This enables us to obtain the XAFS spectra without mechanical motion of the optics.

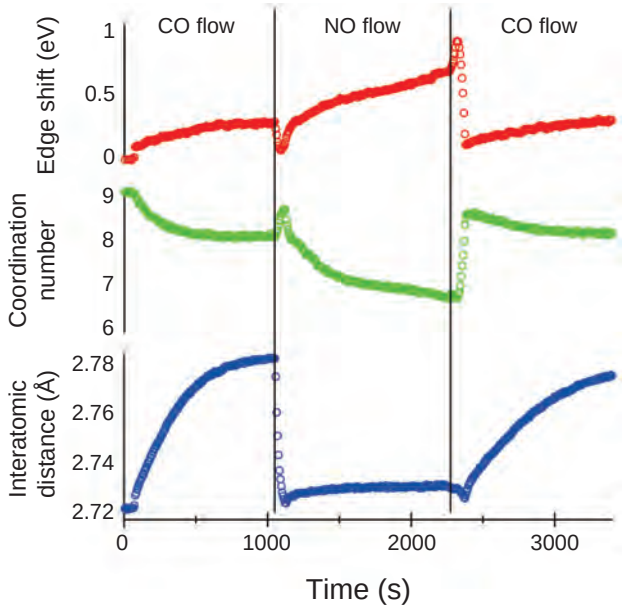

Fig.4-11 Variations of XAFS parameters
Time-resolved XAFS parameters for Pd metal fine particles on aluminum oxide at 400 ℃ during a CO/NO catalytic reaction. From the variations in the parameters, we can determine the structure, shape, and oxidation state of the Pd metal fine particles.

Removal of NO by reaction of CO on metal fine particles is an important process in automotive exhaust catalysts. During this reaction, it has been pointed out that the metal particle shows a rapid change of structure. An X-ray absorption fine structure (XAFS) technique having an element-selective feature is suitable for the direct observation of supported fine particles. This advantage was used to study the CO/NO catalytic reaction on Pd metal fine particles.

The main optical equipment system is displayed in Fig.4-10. The dispersive XAFS system has no mechanical motion process, which is different from a conventional system that requires a change in the X-ray incident angle to obtain the XAFS spectra. Fast and stable observation is achieved using this dispersive XAFS system.

Fig.4-11 shows the variations of the XAFS parameters during successive flow of CO and NO for Pd metal particles on aluminum oxide. From this figure, we determined the changes of structure, shape, and oxidation state for the Pd metal particles during the catalytic reaction. Because the relative accuracy for the interatomic distance is as fine as 0.002 Å, a precise determination of the metal particles has been realized.

Here we explain how the metal particles change during the catalytic reaction. By CO first flow, the interatomic distance is elongated about 0.07 Å. Part of the adsorbed CO is considered to dissociate, and the lattice is expanded by atomic C. The coordination number gradually decreases at the same time scale as the increase in the interatomic distance, which means that CO dissociative adsorption can induce the dispersion of the Pd metal fine particles. Just after NO flow, these parameters rapidly recover their original values. The edge shift denotes a gradual increase after CO removal by NO flow, which indicates that the surface of the Pd particles is gradually oxidized by NO. This surface-oxidized layer is smoothly removed by the next CO flow with a slight positive shift indicating the particular adsorption state.

Direct and time-resolved information on metal particles during a catalytic reaction has revealed the dynamic structure of the Pd metal particles. We believe that such a new viewpoint can aid in the discovery of a catalyst possessing new reaction properties.

Reference

Matsumura, D. et al., Dynamic Structural Change of Pd Particles on $LaFeO_3$ under Redox Atmosphere and CO/NO Catalytic Reaction Studied by Dispersive XAFS, Journal of Physics: Conference Series, vol.190, no.1, 2009, 012154 (6p.).

4-6 Supernova Neutrino-Process Nucleosynthesis
—Astrophysical Origin of ^{180}Ta, the Rarest Nuclide in the Solar System—

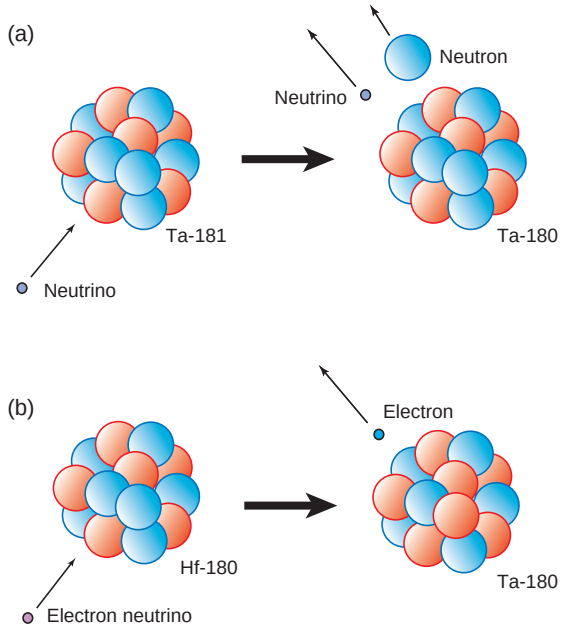

Fig.4-12 Schematic view of production of ^{180}Ta by neutrino transitions induced reactions
^{180}Ta is produced by (a) a neutrino-induced reaction in which a neutron is evaporated and by (b) a charge exchange reaction where a neutron is changed to a proton.

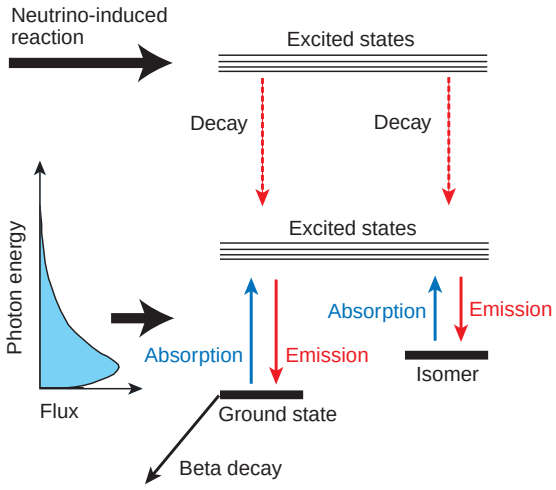

Fig.4-13 Schematic views of nuclear structure of ^{180}Ta and between the ground state and the isomer
The neutrino-induced reaction produces the ground state and isomer in ^{180}Ta. These two states are linked by an interaction of photon absorption and emission.

The astrophysical origins of about 290 nuclides have been studied but the nucleosynthesis of ^{180}Ta has remained an unsolved problem. A unique feature of this nuclide is that it is the rarest in the solar system. Over the past 30 years many processes such as rapid neutron capture reactions in supernova explosions, photon-induced reactions in supernovae, and galactic cosmic ray production have been proposed as the origin of ^{180}Ta. However, previous theoretical calculations based on these proposed models could not reproduce the solar abundance of ^{180}Ta.

Neutrino-induced reactions in supernovae have been proposed as the origin of ^{180}Ta. A proto-neutron star formed in the early stage of a supernova emits huge neutrinos; these neutrinos produce ^{180}Ta by neutrino-nucleus reactions on ^{180}Hf and ^{181}Ta in outer layers (Fig.4-12). However, the theoretical calculation overproduces the solar abundance of ^{180}Ta. This overproduction problem originates from the fact that previous models could not calculate a meta-stable isomer residual ratio using a time-dependent model. The nuclear structure of ^{180}Ta has a feature that the ground state beta decays with a half-life of about 8 hours, whereas the isomer at 77 keV is meta-stable.

In extremely high temperature environments in supernovae, the ground state is linked through highly excited states by (gamma, gamma$'$) reactions. The transition probability from the ground state (isomer) to the isomer (ground state) is a function of temperature. In supernova explosions, the temperature of the neutrino process layers becomes higher than 10^9 K and suddenly decreases in a time scale of several seconds.

For our purposes we can model the excited-state structure as consisting of two sets of nuclear states: (1) the ground state structure, which consists of the ground state plus the excited states with strong transitions to the ground state; and (2) the analogous isomeric structure (Fig.4-13). The time-dependent evolution of the residual isomeric ratio is developed using the two structure model. The resulting isomeric residual population ratio isomer/(ground state + isomer) is found to be 0.39.

We also found that the final result, namely that the isomer residual ratio is 0.39, is nearly independent of a number of astrophysical parameters such as the progenitor mass, the supernova explosion energy, the neutrino energy spectrum, or the peak temperature of the nucleosynthesis environment. Using the ratio of 0.39, we found that the solar abundance of ^{180}Ta can be reproduced by the neutrino process with average electron neutrino energy of 12 MeV.

Reference

Hayakawa, T. et al., New Estimate for the Time-Dependent Thermal Nucleosynthesis of ^{180}Ta^{m}, Physical Review C, vol.81, issue 5, 2010, p.052801-1—052801-4.

4-7 Kerogen as a Noble Gas Carrier Phase of Meteorite
—The Origin of the Solar System Revealed by Synchrotron Radiation—

Table 4-1 Quasi-saturated Ar concentrations determined by X-ray absorption spectra
Powder and chip coals were measured. Some coals were treated with pyridine to extract bitumen.

Target	Ar (atom %)
Fullerene	0.41
Carbon nanotube	0.40
Graphite	0.79
Diamond	0.74
Coal (Shin-sarufutsu)	0.06
Coal (Mitasui Ashibetsu)	0.08
Coal (Mitsui Bibai)	0.05
Coal (Tomiuchi Fukuyama)	0.07
Coal (Nukibetsu, treated with pyridine)	0.05
Coal (Obihiro)	0.05
Coal (Taiheiyo Kushiro)	0.07

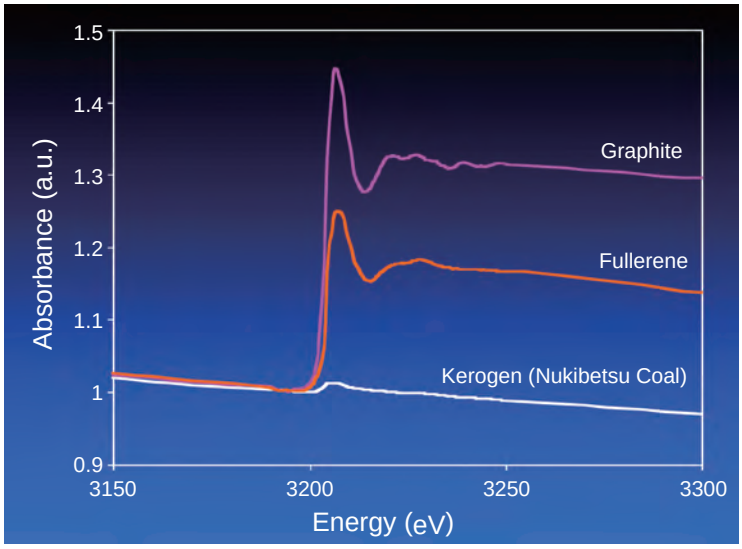

Fig.4-14 X-ray absorption spectra of graphite, fullerene, and kerogen

Primordial trapped components of noble gases preserved in meteorites provide important information on the early solar system. A large number of trapped noble gas components are preserved in distinctive phases of meteorites. Of these, Q-noble gases are the most important component because heavy noble gases in primitive chondrites are mainly hosted by phase Q, which is an oxidizable phase of a residue of treatment with hydrochloric acid and hydrofluoric acid. Although the nature of the residual material after HCl/HF treatment is ill identified, phase Q seems to be a carbonaceous phase, and insoluble organic matter in the meteorite is analogous to terrestrial Type III kerogen, which is a mixture of organic material formed from terrestrial plant matter. Phase Q must have very high noble gas retentivity based on the presence of extremely large amounts of heavy noble gases in a very minor fraction of the meteorite.

To verify that kerogen is a carrier phase of Q-noble gases, X-ray absorption spectroscopy (XAS) and X-ray photoelectron spectroscopy (XPS) using synchrotron radiation were carried out on kerogens (coals) and carbon allotropes that had been bombarded by 3-keV Ar ions, and the Ar retentivities of the two materials were compared. This comparison of the estimated Ar concentrations in the target materials revealed that carbon allotropes (graphite, fullerene, carbon nanotube, and diamond) have a much higher Ar retentivity than kerogens (Table 4-1 and Fig.4-14). This unexpected result clearly shows that the terrestrial kerogens tested in this study are not suitable as a carrier phase of Ar and, consequently, that phase Q may not be similar to the terrestrial kerogen tested. If heavy noble gases are really concentrated in carbonaceous components of primitive meteorites, phase Q may have a more ordered structure than terrestrial kerogen based on the fact that the greatest difference between terrestrial kerogen and carbon allotropes is the degree of order of the molecular structure.

Reference

Osawa, T. et al., Argon Retentivity of Carbonaceous Materials: Feasibility of Kerogen as a Carrier Phase of Q-Noble Gases in Primitive Meteorites, Earth, Planets and Space, vol.61, no.8, 2009, p.1003-1011.

4-8 New Graft Polymerization of High Performance Polymer Electrolyte Membrane

—Synthesis of Block Graft Type Membrane by Radiation / Living Graft Polymerization—

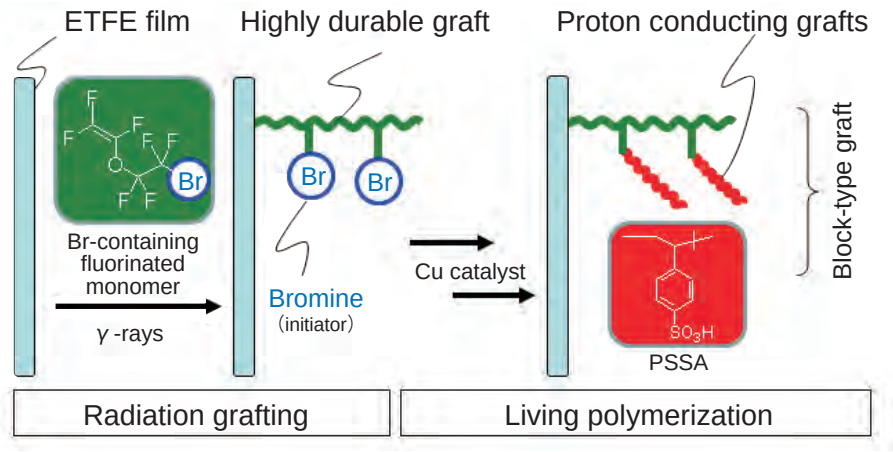

Fig.4-15 Schematic scheme for the synthesis of a block type graft membrane
For synthesis of highly durable PEM, fluorinated monomers with a bromo group (-Br) were grafted into ETFE film by a simultaneous grafting method. The subsequent living polymerization of styrene proceeded from the Br-initiator in the grafts, by means of controlling the reaction conditions, such as the proportions of the Cu catalyst, ligand, and initiator.

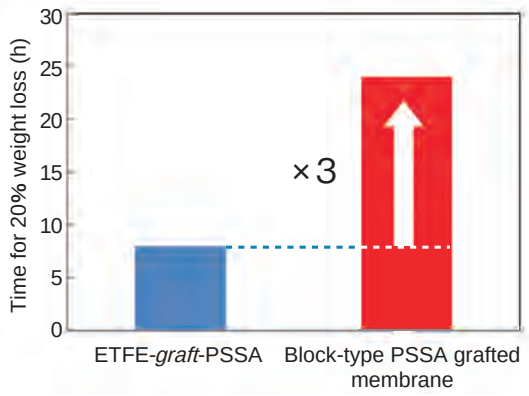

Fig.4-16 Oxidative stability of ETFE-*graft*-PSSA and the block type graft membrane
In oxidation conditions (3% H_2O_2 aqueous solution, 60 ℃), the durability of block-type PEM was 3 times higher than that of ETFE-*graft*-PSSA.

Polymer electrolyte membrane fuel cells have been intensively investigated for application in domestic cogeneration systems and fuel cell vehicles. Both high proton conductivity and thermal durability are required in a polymer electrolyte membrane (PEM), which determines fuel cell performance.

Radiation-induced graft polymerization has been widely recognized as a preparation method for a high performance fuel cell PEM because in graft polymerization, the characteristics of substrate polymer films, such as thermal stability and mechanical strength, are retained in introduction of the new functional polymer phase as a grafting chain into the substrate polymer films. Many PEMs having poly (styrene sulfonic acid) (PSSA) grafts have been synthesized by radiation grafting of styrene into fluorinated polymer films, such as poly (ethylene-*co*-tetrafluoroethylene) (ETFE), followed by sulfonation of the grafts. Although a PEM with PSSA grafts possesses high proton conductivity, the PSSA is less durable because it consists of different chemical components: hydrocarbon polymers from the fluorinated ETFE.

Thus, given that fluorinated monomers with a bromo group (-Br) can be grafted into ETFE, it should be possible to improve the affinity of the grafts with the ETFE substrate, as well as to introduce proton conducting groups using living radical graft polymerization from the Br initiator of the grafts (Fig.4-15). Although there have been few reports about graft polymerization of perfluorinated vinyl ether into polymer substrate films, Br containing perfluorinated vinyl ether could be grafted into ETFE film by a simultaneous grafting method with a degree of grafting (*DG*) of 25%. The subsequent living radical polymerization of styrene proceeded from the Br-initiator in the grafts by means of controlling the reaction conditions, such as the proportions of the Cu catalyst, ligand, and initiator. A newly developed PEM with a *DG* larger than 15% showed higher conductivity than that of Nafion 117. Furthermore, in oxidative conditions (3% H_2O_2 aqueous solution, 60 ℃), the block type PEM exhibited durability three times higher than a conventional ETFE-*graft*-PSSA (Fig.4-16).

In conclusion, we have succeeded in preparing the first block type grafts consisting of highly durable perfluorinated polymer and proton-conducting hydrophilic grafts. This new preparation technique for block type graft polymers shows promise as a synthesis method for high performance fuel cell PEMs.

Reference

Zhai, M., Hasegawa, S., Maekawa, Y., Synthesis of Fluorinated Polymer Electrolyte Membranes by Radiation Grafting and Atom Transfer Radical Polymerization Techniques, Polymer, vol.50, issue 5, 2009, p.1159-1165.

4-9 Semiconductor Devices Can Be Operated in Harsh Radiation Environments in Nuclear Plants

—Development of SiC Transistors Having Radiation Hardness—

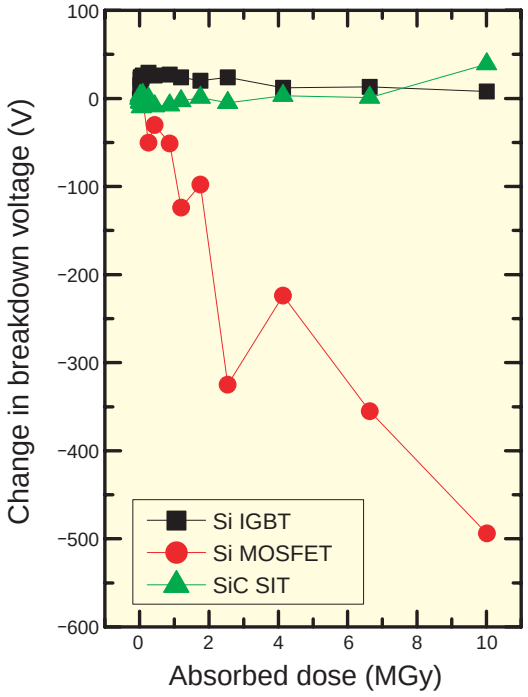

Fig.4-17 Relationship between absorbed dose and breakdown voltage
For SiC SITs and Si IGBTs, no significant change in the breakdown voltage is observed even after a high irradiation dose, such as 10 MGy.

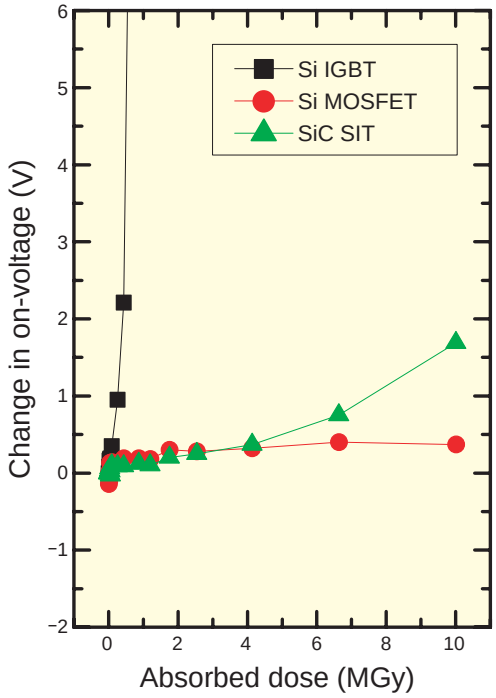

Fig.4-18 Relationship between absorbed dose and on-voltage
For SiC SITs and Si MOSFETs, no significant change in the on-voltage is observed even after a high irradiation dose, such as 10 MGy.

Silicon carbide (SiC) is a candidate semiconductor material for devices having lower loss and higher energy conversion efficiency than Silicon (Si). SiC has thus attracted much attention for next-generation energy-saving devices. In addition, SiC devices can be operated in harsh environments that exceed the physical properties of Si. Taking advantage of features of SiC, we are developing SiC devices which can be operated in harsh radiation environments, such as nuclear facilities and in space.

In this study, we carried out ^{60}Co γ-ray irradiation of SiC Static Induction Transistors (SiC-SITs) up to a total dose of 10 MGy. For comparative purposes, Si Metal Oxide Semiconductor Field Effect Transistors (Si MOSFETs) and Si Insulated Gate Barrier Transistors (Si IGBTs) were also irradiated with γ-rays. After irradiation, the current-voltage characteristics of these devices were investigated. The following results were observed. (1) There was no significant change in the breakdown voltage for SiC SITs and Si IGBTs observed after 10 MGy irradiation. For Si MOSFETs, however, the breakdown voltage decreased with an increase in the absorbed dose (Fig.4-17). (2) The on-voltages for SiC SITs and Si MOSFETs did not significantly change. On the other hand, the on-voltage for Si IGBTs dramatically increased after irradiation at several hundred kGy (Fig.4-18).

The decrease in the breakdown voltage indicates degradation of reliability. The change in on-voltage leads to unexpected circuit operations because the voltage for turning on the device fluctuates. These phenomena are crucial issues for devices used in radiation environments. Although obvious degradation of the electrical performance of Si IGBTs and MOSFETs is observed after γ-ray irradiation, SiC SIT shows stable performance after 10 MGy irradiation, which is the target value. Therefore, we can conclude that SiC transistors with high radiation hardness have been successfully developed.

This study was carried out under the Strategic Promotion Program for Basic Nuclear Research by the Ministry of Education, Culture, Sports, Science and Technology of Japan (MEXT).

Reference

Tanaka, Y., Onoda, S. et al., Radiation Hardness Evaluation of SiC-BGSIT, Materials Science Forum, vols.645-648, 2010, p.941-944.

4-10 Inspection and Repairing Welding System for an Inner Tube Wall
—Combination Laser Processing Technique and Eddy Current Testing—

Fig.4-19 Control system
The control system was stowed in a small portable rack.

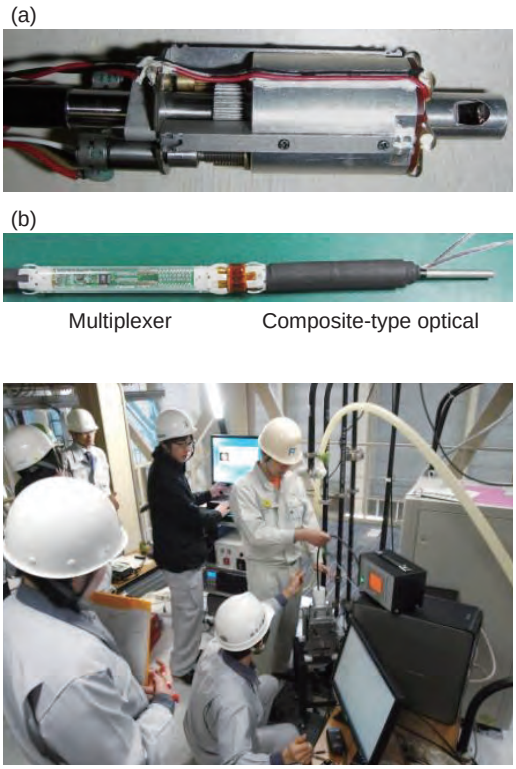

Fig.4-20
(a) Laser processing head
The laser processing head with a composite-type optical fiber scope can inspect 1-inch diameter heat exchanger tubes and repair cracks by laser welding.
(b) ECT coil sensor
The Eddy Current Testing (ECT) coil sensor mounted on a composite-type optical fiber cable can detect cracks on the inside wall of the 1-inch diameter heat exchanger tubes.

Fig.4-21 Demonstration of heat exchanger tube inspection and repair
The mock-up facility at Shiraki in Tsuruga city was used for the demonstration. The performance of the prototype was confirmed in a maintenance drill.

Sodium cooled Fast Breeder Reactors (FBRs) use water as a heat exchanger for steam generation. For this reason, countermeasures against water-corrosion deterioration of the heat exchanger tubes is very important. Especially at welding portions where frequent deformations are superimposed due to residual stress and thermal expansion, it is thought that cracks may occur along welding beads.

Japan Atomic Energy Agency (JAEA) developed a new probing system which makes it possible not only to inspect cracks on the inner tube wall but also to repair them at the same time. Three major technologies were successfully integrated: eddy current testing (ECT), a composite-type optical fiber scope, and laser processing. To put it in general terms, all that could be done previously was to plug the heat exchanger tube where any defect was detected. The new probing system can grant us the possibility to repair the heat exchanger tubes to extend their service life.

Fig.4-19 shows the appearance of the control system stowed in a small portable rack. The backbone of the probing system consists of a composite-type optical fiberscope which has a unique coaxial design. The fiberscope can deliver a high energy laser beam for welding along the center fiber, which is surrounded by thousands of image fibers. A laser processing head is connected at the end of the fiberscope, which is shown in Fig. 4-20. The laser processing head can attain 360 degree round-trip scanning of the inner wall of heat exchanger tubes with fine adjustment for the laser irradiation position. Just beside the laser processing head, an ECT multi-coil sensor is mounted on a composite-type optical fiber cable, which is shown in Fig.4-20. In addition, a CCD camera for image capture and a temperature monitor recorder for key optical components are included. In order to complete the system, a high energy ytterbium fiber laser is integrated into the control system rack as a tightly focused welding heat source.

To confirm the performance of the system, a maintenance demonstration for 1-inch diameter heat exchanger tubes was carried out in the mock-up facility of the Monju steam generator heat exchanger unit. Fig.4-21 shows the demonstration where both ECT inspection and laser welding repair for cracks in 1-inch heat exchanger tubes were carried out. This system can grant us new possibilities for wall maintenance in complex piping facilities such as chemical plants or steam boilers as well as atomic power stations. We will apply this technology to decontamination of scaling deposited on the inner wall of piping.

The present study includes the results of "Development of maintenance technologies with a new probe system for FBR heat exchanger tubes" entrusted to the Japan Atomic Energy Agency by the Ministry of Education, Culture, Sports, Science and Technology of Japan (MEXT).

Reference

Oka, K., Nishimura, A. et al., Development of a Laser Processing Head Using a Composite-Type Optical Fiberscope to Inspect and Repair 1-inch Heat Exchanger Pipes, Hozengaku, vol.8, no.4, 2010, p.37-42 (in Japanese).

4-11 Elucidation for Catalytic Mechanism of Elastase by Neutron Diffraction
—Success in Observing the Oxyanion Hole in Serine Protease—

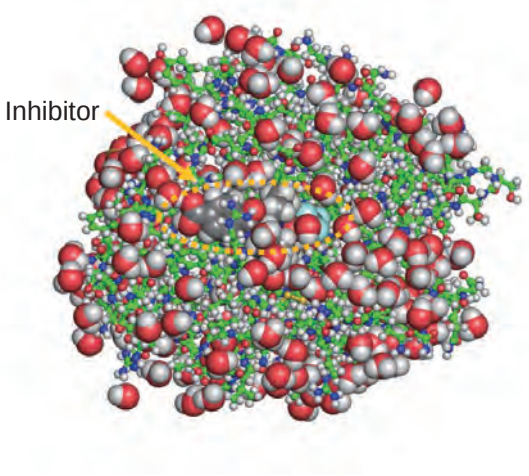

Fig.4-22 Whole atom positions in elastase complexed with inhibitor
Colors represent hydrogen (white), carbon in protein/inhibitor (green/gray), nitrogen (blue), oxygen (red), sulfur (yellow), and fluorine (light blue). Inhibitor and protein bound waters are shown as sphere models.

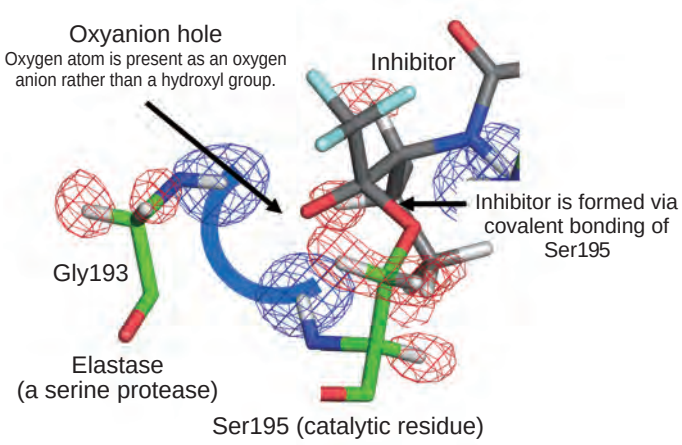

Fig.4-23 Oxyanion hole in the active center of elastase observed by neutron diffraction
The meshed maps represent nuclear density and show the location of hydrogen (red) and deuterium (blue) atoms. In this study, some hydrogens were substituted to deuterium, which had similar chemical properties.

Almost one third of all proteases can be classified as serine proteases, named for the nucleophilic serine residue at the active site. The tetrahedral intermediate in catalytic reactions is considered to stabilize electrostatically though hydrogen bonds with the backbone amides of Gly193 and Ser195, which together form an "oxyanion hole." However, the state of the oxygen atom of the substrate in the oxyanion hole has not been confirmed yet. To help resolve long-standing questions regarding the catalytic activity of the serine proteases, the structure of porcine pancreatic elastase (PPE), which has been frequently used for research in structure-based drug design (SBDD), was analyzed by high-resolution neutron crystallography, because neutrons strongly interact with hydrogen and deuterium atoms and the neutron scattering lengths of hydrogen and deuterium atoms are very similar to those of other atoms.

We have succeeded in determining the positions of all the atoms of PPE complexed with its inhibitor by neutron crystallography at 1.65 Å resolution using the BIX-3 diffractometer installed at the 1G-A port of the research reactor JRR-3 (Fig.4-22). The inhibitor used in this study was covalently bound to the side chain of the Ser195 of the PPE. In this covalent complex, the carbonyl structure in the inhibitor was converted to a tetrahedral structure mimicking the catalytic transition intermediate state.

The carbonyl oxygen of the oxopropyl group of the inhibitor was converted to a hydroxyl oxygen that interacts with the oxyanion hole, comprising two hydrogen atoms from the backbone amides of Gly193 and Ser195. These two hydrogen atoms (deuterium in the neutron structure) were clearly confirmed in the F_o-F_c nuclear density maps (Fig.4-23). The nuclear density maps also show that the oxygen is present as an oxygen anion rather than a hydroxyl group, supporting the role of the oxyanion hole in stabilizing the tetrahedral intermediate in catalysis.

This is the first case in which an oxyanion of an intermediate analogue has been directly observed at an oxyanion hole. The precise structural information including hydrogen positions will contribute to further elucidation of the catalytic mechanism of serine protease. In addition, the structural information including hydrogen positions will provide additional knowledge to improve inhibitor design for therapeutic application with the fatal disease pancreatitis.

Reference

Tamada, T. et al., Combined High-Resolution Neutron and X-ray Analysis of Inhibited Elastase Confirms the Active-Site Oxyanion Hole but Rules against a Low-Barrier Hydrogen Bond, Journal of the American Chemical Society, vol.131, no.31, 2009, p.11033-11040.

4-12 Global Conformational Changes of Ribosome Revealed from Low-Resolution Structural Data

—A New Technique for Building Molecular Models from Electron Microscopy Data—

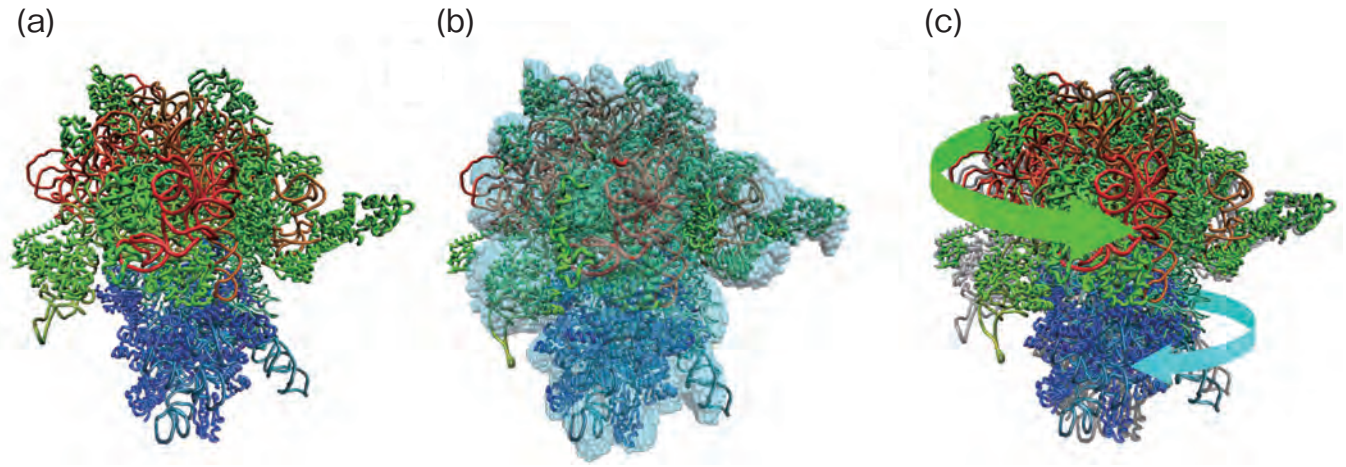

Fig.4-24 Three-dimensional structures of a ribosome determined by different methods
(a) X-ray crystal structure of the ribosome. It is composed of large (red, green) and small (blue) subunits.
(b) 3D electron microscopy structure (cyan), shown overlaid upon a best-fit molecular model.
(c) Comparison of (a) the X-ray crystal structure (gray) with (b) the best-fit molecular model. The latter is twisted along the direction of the arrows with respect to the former.

Due to the emergence of more and more antibiotic-resistant bacteria, the development of new antibiotics is an urgent necessity. Different antibiotics attack bacteria in different ways. Some kinds of antibiotics inhibit the growth of bacteria by preventing their protein synthesis. In a cell, protein synthesis is performed by huge macromolecular complexes called ribosomes. For effective development of antibiotics, it is important to reveal the three-dimensional (3D) structure of ribosomes in functional states at the atomic level.

The atomic structure of a biological molecule such as protein and DNA is usually determined by a method called X-ray crystallography. This method requires the crystallization of the molecule, and for the crystallization, many conditions must be satisfied. Thus, it is not easy to determine the structure of the molecule in a specific functional state, and it is especially difficult for a huge molecular complex like a ribosome. The atomic structures of ribosomes in a few functional states have hitherto been determined (Fig.4-12(a), (c)), but this is not enough for understanding the whole molecular mechanism.

In recent years, the use of an electron microscope (EM) has been a popular method for determination of the 3D structure of biological molecules. In this method, the 3D structure is reconstructed from many EM images of the molecule taken from different angles. The resolution of the reconstructed structure is too low to identify the constituent atoms. However, because crystallization is unnecessary, determination of the 3D structure is relatively easy, and the 3D structures of ribosomes in many functional states have already been determined (Fig.4-12(b)).

We have developed a computational technique for building a molecular model from a 3D-EM structure (Fig.4-12(b), (c)). In this technique, the atomic structure determined by X-ray crystallography is deformed so that it fits into the 3D-EM structure. Thus, using this technique, we can determine the atomic structure of a molecule in a specific state, where the structure is known from EM, but not from X-ray crystallography. We have applied this technique to many 3D-EM structures of ribosomes and built molecular models. By analyzing these models statistically, we were successful in clarifying conformational change in ribosomes during protein synthesis.

The structural information that we obtained in this study will contribute to the development of new antibiotics.

Reference

Matsumoto, A., Ishida, H., Global Conformational Changes of Ribosome Observed by Normal Mode Fitting for 3D Cryo-EM Structures, Structure, vol.17, issue 12, 2009, p.1605-1613.

4-13 Development of a Novel Radiopharmacutical Finding Even Very Small Tumors
—Success in PET Imaging of Pheochromocytomas Using ^{76}Br-MBBG—

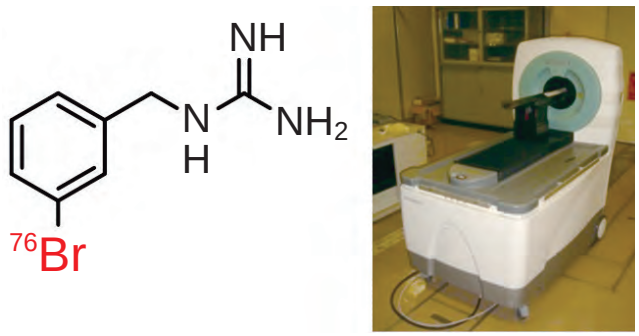

Fig.4-25 Chemical structure of ^{76}Br-MBBG (left) and photo of a small-animal PET (right)
^{76}Br-MBBG (^{76}Br-*meta*-bromobenzylguanidine) is a positron emitter ^{76}Br (half-life: 16.1 h) labeled compound which shows specific uptake into pheochromocytoma. ^{76}Br-MBBG was administrated to pheochromocytoma bearing mice, and PET scans were performed using a small-animal PET for 20 min emission scanning.

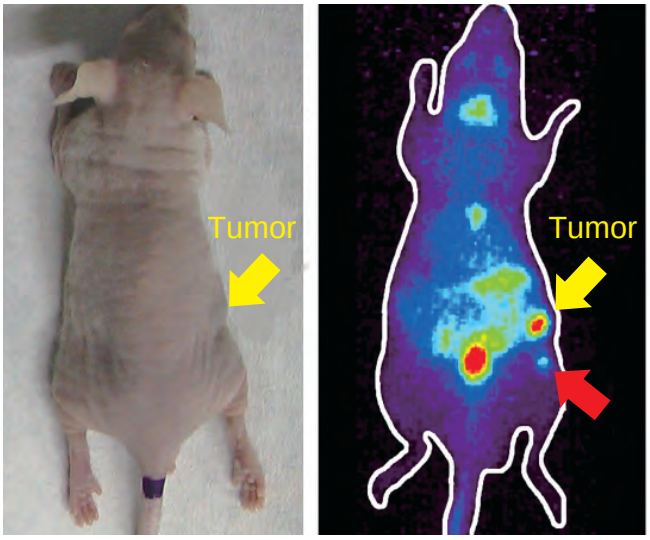

Fig.4-26 Photo of a pheochromocytoma-bearing mouse (left) and PET imaging at 3 h after administration of ^{76}Br-MBBG (right)
Yellow arrows indicate the position of implanted pheochromocytoma. ^{76}Br-MBBG showed higher accumulation in tumor compared to normal tissues (green or purple regions). High accumulation in the center of the mouse showed urine in the bladder. The red arrow shows a very small tumor (size: 2 mm) undetected before PET.

Pheochromocytoma is a tumor in the medulla of the adrenal glands. This tumor secretes excessive amounts of catecholamines such as epinephrine (adrenaline), which causes heavy hypertension. Although pheochromocytoma is usually curable by surgical resection, patients with small lesions or multiple metastases will be fatal because other treatments are not effective. Thus, early detection is critical to cure the pheochromocytoma. However, it is difficult to detect a small lesion or early metastasis using X-ray computed tomography (CT) or single photon emission computed tomography (SPECT) due to their lower spatial resolution.

We focused on positron emission tomography (PET) to overcome the above-mentioned problems. PET is a nuclear imaging technology that images distribution of lesions or metabolic activity in tissues of interest by detecting γ-rays from positron emitters. PET has a high potential to detect small tumors, since it has a higher spatial resolution compared to CT and SPECT. A positron emitter labeled compound that shows specific uptake into pheochromocytoma thus can be a promising tracer for detecting small pheochromocytoma using PET. We synthesized the positron emitter Br-76 (^{76}Br) labeled ^{76}Br-*meta*-bromobenzylguanidine (^{76}Br-MBBG), which has high affinity to pheochromocytoma.

^{76}Br-MBBG was administrated to tumor bearing mice and PET scans were performed at 3 h after administration (Fig.4-25). As a result, transplanted tumors were successfully imaged using ^{76}Br-MBBG. Furthermore, a small tumor (size: 2 mm) undetected before PET scans was clearly imaged (Fig.4-26). These results indicated that ^{76}Br-MBBG is a potential radiopharmaceutical for imaging pheochromocytoma and detecting very small tumors.

^{76}Br-MBBG could be a powerful tool for early detection of pheochromocytoma. Furthermore, ^{76}Br-MBBG could also be provided for imaging neruoblastoma, medullary thyroid carcinoma, and carcinoid which specifically accumulate ^{76}Br-MBBG like pheochromocytoma.

Reference

Watanabe, S. et al., PET Imaging of Norepinephrine Transporter-Expressing Tumors Using ^{76}Br-*meta*-Bromobenzylguanidine, The Journal of Nuclear Medicine, vol.51, no.9, 2010, p.1472-1479.

Toward Development of a Laser-Driven Ion Beam Apparatus

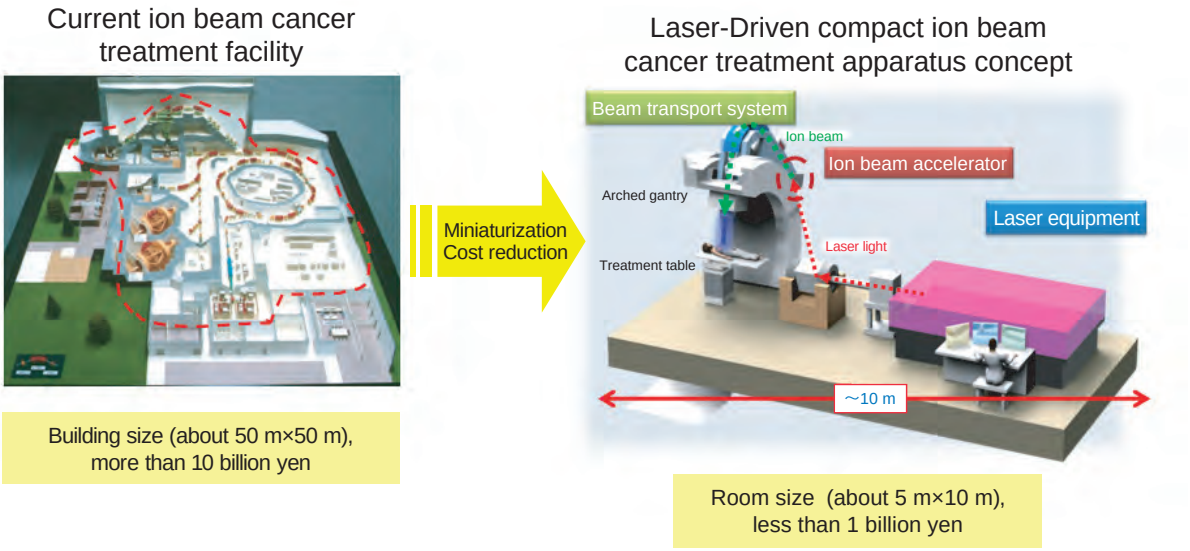

Fig.5-1 The current ion beam medical facility and outline of a laser-driven ion beam apparatus

The JAEA Photo-Medical Research Center (PMRC) is promoting innovative development of a laser-driven ion beam apparatus for medical applications. This device employs ion acceleration by a high power laser in order to significantly reduce overall size and cost, which can then facilitate wider access to ion beam cancer treatment (Fig.5-1). (http://wwwapr.kansai.jaea.go.jp/pmrc_en/)

The PMRC project has been pursued since 2007 in collaboration with ten partners (Fig.5-2), and is funded by the Special Coordination Fund for Promoting Science and Technology commissioned by the Ministry of Education, Culture, Sports, Science and Technology.

Development of a treatment and diagnostic device

To advance development of a laser-driven ion beam medical device, we conducted research and development to produce a proton beam suitable for cancer therapy. We verified the world's first laser-driven ion acceleration method using a nanoparticle target. This research mainly targeted a key for the success of the PMRC project, namely a significant increase in the number of accelerated protons. Laser irradiation of nanoparticle targets has accelerated ions to maximum energies that exceed 20 MeV per nucleon (Topic 5-1). We also conducted studies of other target types and laser irradiation conditions. Thin film targets have yielded protons that were accelerated up to kinetic energies of 14 MeV.

Verification of the effects of treatment with a laser-driven proton beam

To verify that a laser-driven proton beam can be effective in cancer therapy, we completed experiments to determine the effect of proton irradiation of cancer cells. For the first time in the world, we successfully induced DNA double strand breaks in human-derived cancer cells by irradiating them with laser-driven proton beams. We also evaluated the biological effect of cell irradiation and measured self-activated gamma emission from phantom targets using a proton irradiation research chamber. This apparatus was built at the Hyogo Ion Beam Medical Center to determine if there is any difference in the irradiation effect between a laser-driven ion beam and an ion beam delivered by an existing accelerator.

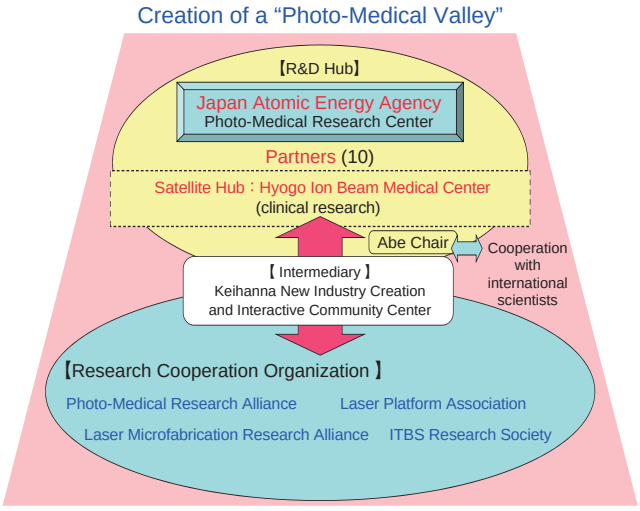

Partners (FY2009): Hyogo Ion Beam Medical Center (HIBMC), Hamamatsu Photonics K.K., Ushio Inc., Toshiba Corporation, Shimadzu Corporation, Toyota Central R&D Labs., Inc., HOYA Corporation, Fujikura Ltd., Nippon Advanced Technology Co., Ltd., HOC

Fig.5-2 Common research initiative for creation of a "Photo-Medical Valley"

Studies toward prototype development

As part of our efforts with industrial applications, we investigated the specifications of equipment and implementation of proton-induced radio-activation to study wear on metal surfaces. We also initiated clinical tests of a minimally invasive fiber-based medical device, together with development of integrated software to smoothly control it.

Based on these results, we will advance this project during this fiscal year and resubmit our proposal for program evaluation by the Special Coordination Fund for Promoting Science and Technology commissioned by the Ministry of Education, Culture, Sports, Science and Technology of Japan (MEXT).

5-1 Demonstration of a New Method for Ion Acceleration Aiming at a Development of a Compact Laser-Driven Hadron Therapy System

—Ion Acceleration Using Subcritical-Density Plasma Created Using a Nanoparticle Target—

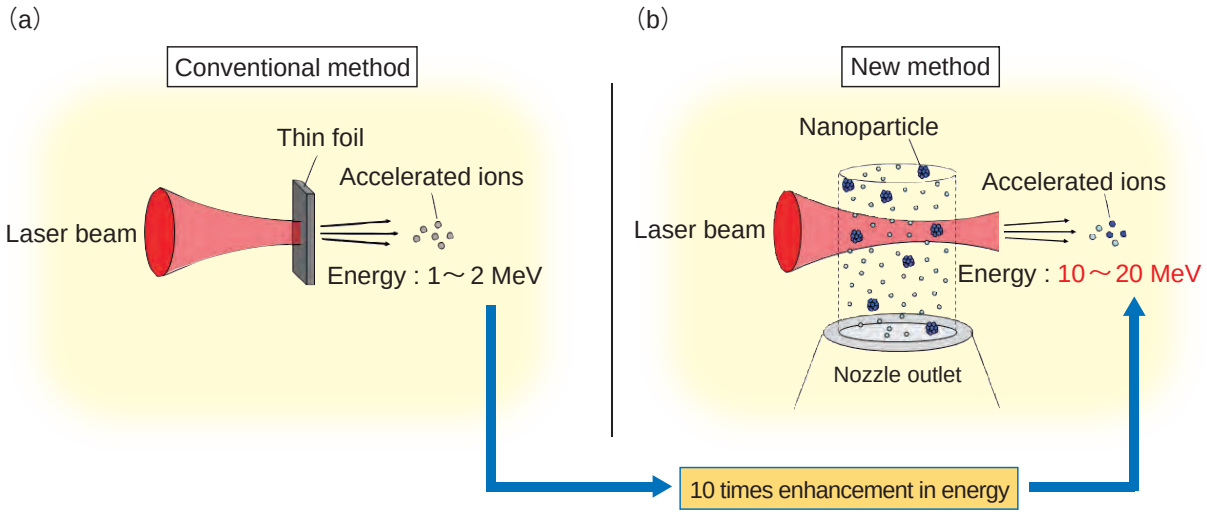

Fig.5-3 Schematic of laser-driven ion acceleration
In a conventional method (a), high energy ions are generated by irradiation of a focused laser beam onto a micron-thick foil target. In the new method (b), instead of using thin foil targets, the laser beam is focused onto a nanoparticle target. In the case of the nanoparticle target, it is easy to create a state of matter that effectively absorbs laser energy, called subcritical-density plasma. As a result, we demonstrated efficient generation of high energy ions whose energies are ten times higher than those in previous experiments with thin foil.

Extremely strong electromagnetic fields at micron scale are created by irradiation of a strong focused laser beam onto matter. Laser-driven ion acceleration, which utilizes such strong electromagnetic fields, has attracted much attention in terms of hadron therapy system downscaling and cost reduction. A laser-driven ion beam with energies of 80~250 MeV is required for the purpose of a medical application. However, if we used the conventional ion acceleration method using a thin foil target (Fig.5-3(a)), it would require an enormous amount of laser energy from a newly-developed large-scale laser system. Therefore, in order to downscale the whole treatment unit including the laser system, we have to discover a new method for ion acceleration using the compact laser systems which are widely used around the world.

In the Photo-Medical Research Center (PMRC), instead of using a thin foil target but by irradiating a laser beam onto a nanoparticle target, we successfully created a state of matter (called "subcritical-density plasma") which can effectively absorb laser energy (Fig.5-3(b)). As a result, we demonstrated efficient generation of high energy ions with energies up to 10~20 MeV. This corresponds to an approximately tenfold improvement in accelerated ion energy compared to previous experiments (1~2 MeV) with thin foil targets.

The experimental results and computer simulations estimate that ions greater than 200 MeV could be generated at a laser intensity of 10^{20} W/cm^2 with the nanoparticle target, which is one of the milestones of the PRMC's research program. The laser intensity of 10^{20} W/cm^2 could be attainable using the compact laser system at the PMRC, if its beam quality can be further improved. Moreover, the new method is replenishable and has a small divergence angle, which makes it possible to shorten the treatment time with an increase in the dose rate, and to construct a compact beam transport system.

In summary, the method we demonstrated has the potential to enhance development of a compact laser-driven hadron therapy system.

Reference

Fukuda, Y. et al., Energy Increase in Multi-MeV Ion Acceleration in the Interaction of a Short Pulse Laser with a Cluster-Gas Target, Physical Review Letters, vol.103, issue 16, 2009, p.165002-1—165002-4.

5-2 Unlimited Particle Acceleration by Photon Pressure Was Proposed
—Synchronized Thin Foil Plasma Acceleration Due to Photon Pressure—

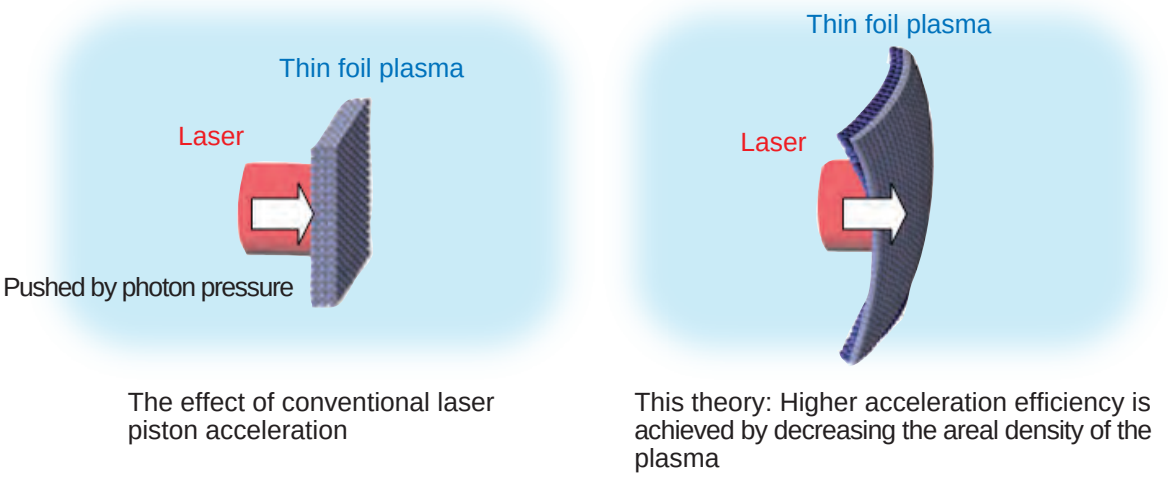

Fig.5-4 Laser piston acceleration of thin foil plasma
Thin foil plasma was stretched and made thinner under pressure from a laser piston. The areal density decreases during acceleration. Finally, unlimited particle acceleration is shown to be theoretically possible.

We have proposed a new theory, which points to the possibility of producing much higher energy particles using a modified laser piston method (Fig.5-4).

In the Photo-Medical Research Center (PMRC), laser driven particle acceleration is studied in order to make a compact particle cancer therapy machine, and it is necessary to realize theoretical calculations in the study. We must pay attention to laser piston acceleration, in which a thin foil is directly accelerated by the strong photon pressure generated by focusing a high peak power laser pulse on the foil. In conventional laser piston theory, the thin foil is accelerated while maintaining a constant areal density, as shown in the left figure in Fig.5-4. In this study, it was found that much higher energy can be obtained if we take into account a condition in which the areal density is decreased during the acceleration, even though the number of accelerated particles decreases. When the areal density of accelerated thin foil plasma is decreased, the velocity of the plasma is thought to become higher. This effect may cause the velocity of the thin plasma bulk to be almost the same as the velocity of laser propagation in the plasma. In such a case, the laser pulse cannot overtake the thin foil plasma, and continuously pushes the thin foil while locking this acceleration phase. Therefore, unlimited particle acceleration could be possible, imparting the momentum to the particles which constitute the thin foil plasma.

If we succeed in controlling areal density based on this theory, generation of the 200 MeV protons needed for cancer therapy is seen to be attainable by focusing a 200 TW laser pulse on a nanometer-size thin foil. The size of the laser driver could then be downscaled to be one fifth of the conventionally estimated scale.

This study is supported by the Special Coordination Fund (SCF) for Promoting Science and Technology commissioned by the Ministry of Education, Culture, Sports, Science and Technology of Japan (MEXT), and Grant-in-Aid for Scientific Research No. 20244065.

Reference

Bulanov, S.V. et al., Unlimited Ion Acceleration by Radiation Pressure, Physical Review Letters, vol.104, issue 13, 2010, p.135003-1—135003-4.

To Promote Advanced Use of Light Water Reactors

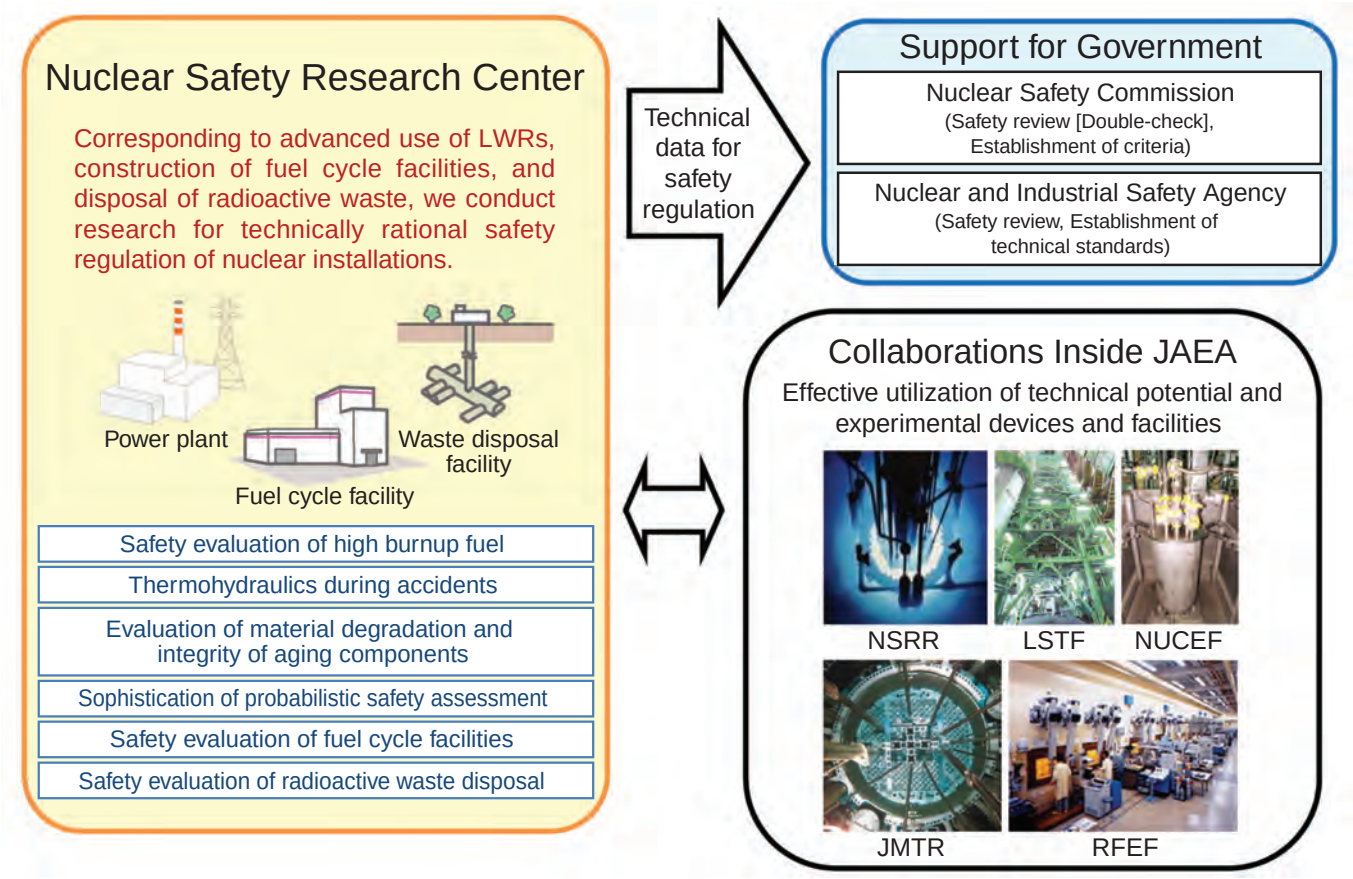

Fig.6-1 Main subjects, utilization of results, and collaboration for nuclear safety research

Advanced use of light-water reactors (LWRs) such as long-term fuel use (high burnup) and power plant aging management are required from the viewpoint of energy and environmental issues. The advanced use of LWRs must be promoted while confirming the safety of the reactors. The objective of our safety research is to provide scientific and technical data as the basis for regulatory judgments in safety reviews and in the establishment of safety criteria. We are conducting research into the safety of LWRs regarding high burnup fuel behavior under accident conditions, material degradation and the integrity of aging components, thermohydraulics during accidents, probabilistic safety assessment, safety of fuel cycle facilities, and radioactive waste disposal, according to the Prioritized Plan for Nuclear Safety Research produced by the Nuclear Safety Commission (NSC), as shown in Fig.6-1. Recent results in these subject areas are briefly described below.

For the study of the high burnup fuel behavior, valuable data were obtained on fuel failure under accident conditions (Topic 6-1) and on the thermal properties of high burnup mixed oxide (MOX) fuel (Topic 6-2). For the study of the integrity of aged components and materials, hydride precipitation, which would affect the dimension stability of the hafnium for control rods, was investigated (Topic 6-3). On the safe long-term service of the reactor pressure vessel (RPV), useful data on the embrittlement mechanisms of RPV materials were obtained from systematic observation of microstructural changes due to neutron irradiation (Topic 6-4). In addition, we performed residual stress analysis to evaluate the effect on the RPV integrity of weld-overlay cladding on the inner surface of the RPV (Topic 6-5). A new importance measure was proposed for identifying input factors that contribute to uncertainty in risk analysis output obtained from a probabilistic safety assessment, and a computer code was also developed to implement this new importance measure (Topic 6-6). Regarding thermohydraulics during accidents, the production of volatile iodine due to radiation chemical reactions was examined for better quantitative evaluation of the proportion of radioactive iodine released to the environment in the case of an accident with severe core damage (Topic 6-7). Relating to the safety evaluation of fuel cycle facilities, a new analysis method for criticality safety evaluation was validated and basic data were produced, which was reported in the revised data collection for the criticality safety handbook (Topic 6-8). For a reliable safety assessment of radioactive waste disposal, sorption data for radionuclides on rocks were obtained under disposal conditions (Topic 6-9).

6-1 Toward Fuel Safety Regulations with Improved Rationality

—Study of High Burnup Fuel Behavior in RIA Using the NSRR High Temperature Capsule—

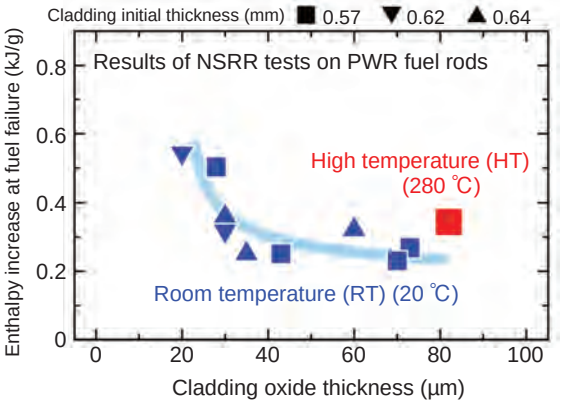

Fig.6-2 Relation between fuel enthalpy increase at failure and cladding oxide thickness
The fuel enthalpy increase at which a high burnup fuel rod fails was evaluated in RIA simulation tests at NSRR. Previous tests at a room temperature (RT) had revealed a strong correlation between the fuel enthalpy at failure and cladding oxide thickness. A new result was obtained at a high temperature (HT).

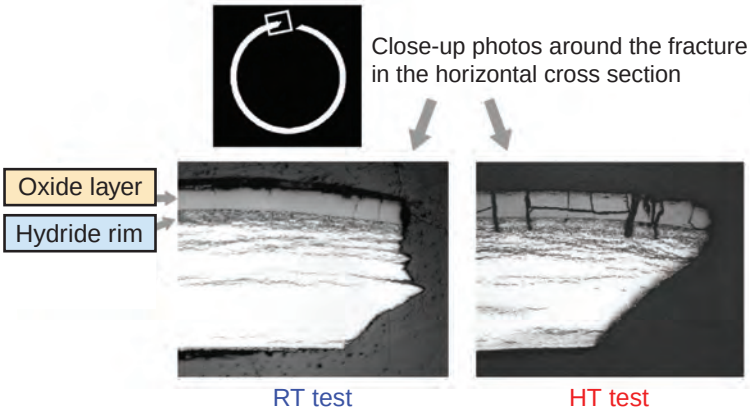

Fig.6-3 High burnup PWR fuel cladding that failed in the room temperature and high temperature tests at NSRR
Cross sections of failed cladding are compared. In the both cases, one of the radial cracks generated in the outer brittle zone (oxide layer and hydride rim) grew into a fracture. Comparison of the shapes of non-penetrating cracks between the RT and HT tests suggests that a larger hoop strain could occur at HT.

To confirm the safety design of a reactor, safety reviews are performed under various accident conditions as well as under normal operation conditions. One of the hypothesized accidents is the reactivity initiated accident (RIA), which is a power excursion typically caused by control rod ejection. The safety review needs criteria to judge fuel failure in RIAs. The current Japanese criteria for fuel failure are based on the results of RIA simulation tests carried out at a room temperature (RT) of ~20 ℃ in the Nuclear Safety Research Reactor (NSRR), with consideration of a sufficient safety margin. These criteria are applied also to RIAs at a reactor operation temperature of ~280 ℃. However, since the metal ductility generally increases with temperature, the fuel failure limit can be elevated at high temperature (HT) in case of mechanical failure of highly corroded and embrittled cladding, which is typical with high burnup fuels. Accordingly, the current criteria could have a too wide safety margin for RIAs at HT.

A new test capsule which can attain 280 ℃ was developed to investigate the temperature effect on the failure limit. In a HT test with a high burnup PWR fuel rod, the failure limit was successfully evaluated and the elevation of the failure limit was demonstrated. Fig.6-2 shows the relation between the failure limit and cladding corrosion level, which are represented by the enthalpy increase at fuel failure and the cladding oxide thickness, respectively. The figure shows that fuel failure occurs at higher enthalpy at HT, if compared at the same oxide thickness. Fig.6-3 compares the cross sections of failed cladding between RT and HT tests. In both cases one of the surface cracks would have grown into a fracture. As for the crack shapes which did not penetrate, the tips are seen to be rounded in the HT test, which suggests that the fracture occurred after a large plastic deformation. These are valuable results, and were first obtained with the HT capsule. Further achievements are foreseen for NSRR tests using the HT capsule.

Utilization of the present results permits advanced fuel failure criteria to be established with an appropriate safety margin corresponding to the temperature conditions. That is, safety regulations with improved scientific rationality are expected, which will provide both safety and economic efficiency.

Development of the HT capsule and the HT tests were conducted under a contract with the Nuclear and Industrial Safety Agency (NISA), the Ministry of Economy, Trade and Industry (METI).

Reference

Sugiyama, T. et al., Effect of Initial Coolant Temperature on Mechanical Fuel Failure under Reactivity-Initiated Accident Conditions, Proceedings of Top Fuel 2009, Paris, France, 2009, Paper 2086, p.489-496, in DVD-ROM.

6-2 Evaluation of Thermal Properties of High Burnup MOX Fuel for LWRs
—Thermal Conductivity Change in MOX Pellets Due to Long-Term Use—

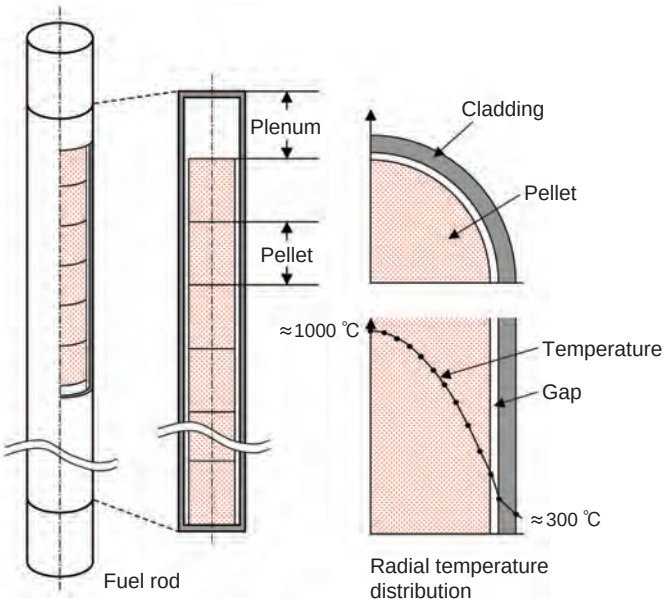

Fig.6-4 Schematic diagrams of a LWR fuel rod and radial temperature profile in the fuel rod
The fuel rod consists of fuel pellets and zirconium alloy cladding, and is used in LWRs. The fuel pellet temperature is dependent on pellet thermal conductivity and fuel rod power. The radial temperature profile in the pellet is close to a parabolic shape.

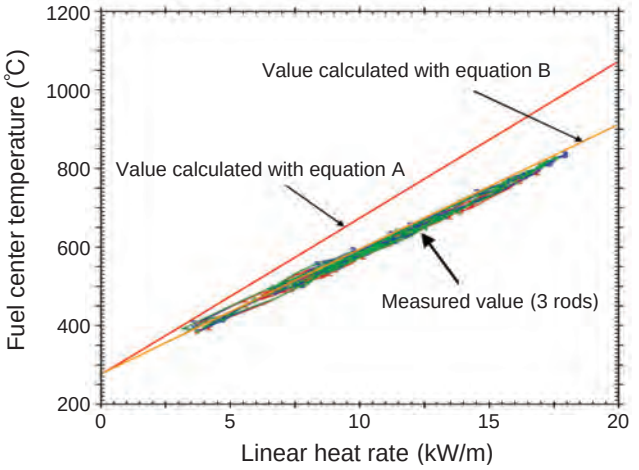

Fig.6-5 Comparison between measured and calculated fuel temperatures of high burnup MOX fuels
The fuel center temperatures measured in high burnup MOX fuel rods are close to the values calculated by equation B, in which only the effect of burnup on the thermal conductivity of UO_2 pellet is considered.

From the perspective of the effective use of resources, high burnup of LWR (Light Water Reactor) fuel and the use of plutonium (Pu) as MOX (Mixed Oxide) fuel are being promoted stepwise with LWRs.

Schematic diagrams of a LWR fuel rod are shown in Fig.6-4. Fuel behaviors such as fission gas release from pellet strongly depend on the pellet temperature during irradiation. In terms of the safety evaluation of fuel, since the fuel temperature during irradiation is strongly related to the thermal conductivity of the fuel pellet, it is necessary to evaluate the thermal conductivity of pellet with high accuracy in order to properly evaluate the pellet temperature during irradiation.

The thermal conductivities of uranium dioxide (UO_2) have been investigated up to the high burnup region. However, thermal conductivity data of MOX pellet are not yet satisfactory, especially at high burnup. In this study, MOX fuels irradiated up to high burnup in European LWRs were re-irradiated in a test reactor, and data concerning the thermal conductivity change in high burnup MOX fuel (about 80 GWd/tHM) were obtained by measuring the fuel center temperatures.

The fuel center temperatures of the MOX fuel rods were measured while changing the heat generation rate per unit length of the fuel rod (Linear Heat Rate: LHR) during irradiation. The measured fuel center temperatures were compared with values calculated by a fuel performance analysis code (Fig.6-5). The thermal conductivity models of MOX pellet proposed in the literatures were used in the calculation. Equation A is an equation in which the degradation effects of Pu addition and burnup on the thermal conductivity of UO_2 are considered. Equation B is an equation in which only the degradation effect of burnup on the thermal conductivity of UO_2 is considered. Here, the validity of equation B with respect to UO_2 pellet was confirmed by the fuel center temperature measurements of high burnup UO_2 pellet that were also conducted in this study. As seen in Fig.6-5, the measured fuel center temperatures of the MOX fuel rods are close to the values calculated by equation B rather than those calculated by equation A. These results suggest that the difference of thermal conductivity between MOX and UO_2 pellets becomes small in high burnup region. This also suggests that the fission products and irradiation defects accumulated in the crystal lattice during irradiation have a greater effect on the thermal conductivity of MOX fuel pellet than does the Pu added at fabrication. This information is useful for improving the accuracy of safety evaluations for high burnup MOX fuel.

The present study was performed as part of a program sponsored and organized by the Nuclear and Industrial Safety Agency (NISA), the Ministry of Economy, Trade and Industry (METI).

Reference

Nakamura, J. et al., Thermal Conductivity Change in High Burnup MOX Fuel Pellet, Journal of Nuclear Science and Technology, vol.46, no.9, 2009, p.944-952.

6-3 For Safe and Long-Term Utilization of Control Rods
—Evaluation of the Properties of Hafnium—

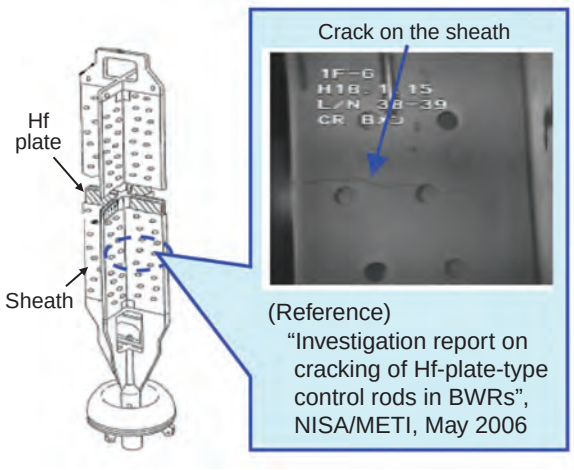

Fig.6-6 Structure of hafnium (Hf)-plate-type control rods and example of sheath cracking
Hf plates for control rods are covered by stainless steel sheaths. In January, 2006, cracks on the sheaths, etc., were found at the Fukushima Daiichi Nuclear Power Station of Tokyo Electric Power Co., Inc. Countermeasures such as a replacement of the control rod, etc., are made based on the results of investigating the cracking.

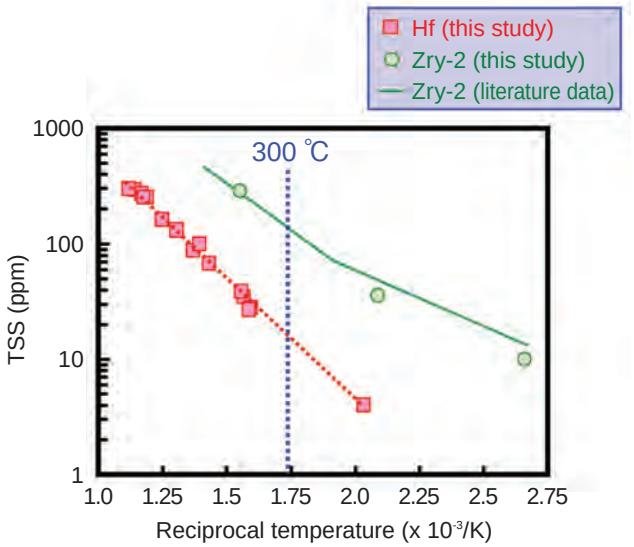

Fig.6-7 Temperature dependence of terminal solid solubility of hydrogen (TSS): a comparison between Hf and zircaloy-2 (Zry-2)
The TSS for Hf at an operational temperature of 300 ℃ was about 20 ppm (1/7 the TSS for Zry-2). Hydrides in Hf were found to precipitate under lower hydrogen concentration conditions than Zry-2.

Control rods in a reactor core are exposed to a severe environment, such as high pressure water at high temperature and high radiation, for a long time. Control rods made of boron, which is a neutron absorber, usually have to be exchanged frequently, leading to the production of high-level radioactive waste. Because hafnium (Hf) has a considerably longer nuclear lifetime than boron and is resistant to corrosion, it has been used as a neutron absorber for long-life control rods.

Recently, cracking which may have resulted from irradiation-assisted stress corrosion cracking was found in the stainless steel cladding (sheath), etc., of Hf-plate-type control rods (Fig.6-6). Size change of the Hf plate due to irradiation growth and hydride precipitation is considered to be a possible cause of the cracking. Countermeasures such as replacement of the control rod, etc., were performed. In order to use Hf control rods safely for a long time, we investigated the quantitative evaluation of Hf size stability.

Hf absorbs hydrogen through a corrosion reaction, and then part of the absorbed hydrogen precipitates as hydrides. Because the hydride precipitation causes size change (volume expansion), it is important to know both the temperature and hydrogen concentration conditions at which hydrides precipitate in Hf. Fig.6-7 shows the terminal solid solubility of hydrogen (TSS) in Hf, i.e., the lower limit of the hydrogen concentration at which the hydrides precipitate. Results for zircaloy-2 (Zry-2), which has similar chemical properties and is used for fuel claddings, is also shown in this figure for a comparison. The TSS for Hf shows similar temperature dependence to that for Zry-2. The TSS for Hf at 300 ℃, which corresponds to the operational temperature of control rods, is about 20 ppm. The hydrides were found to precipitate in Hf under a lower hydrogen concentration condition than Zry-2. We will clarify the effect of hydride precipitation on the size change of Hf.

This research is a part of a program of the Nuclear and Industrial Safety Agency (NISA) of the Ministry of Economy, Trade and Industry (METI).

Reference

Ogiyanagi, J. et al., Terminal Solid Solubility of Hydrogen in Hafnium, Journal of Nuclear Science and Technology, vol.47, no.2, 2010, p.197-201.

6-4 Toward Safe Long-Term Service of Reactor Pressure Vessels
—Prediction of the Service Life Based on Nano-Scale Structural Analysis—

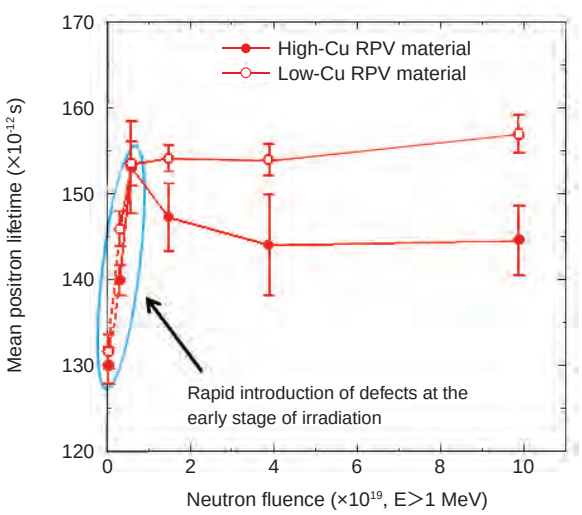

Fig.6-8 Mean positron lifetimes as a function of neutron fluence
Neutron fluence is proportional to the operation period of an RPV. Defects are formed in RPV materials by neutron irradiation. Since the positron lifetime tends to increase with the amount of defects, the amount of defects is seen to rapidly increase in the early stages of irradiation.

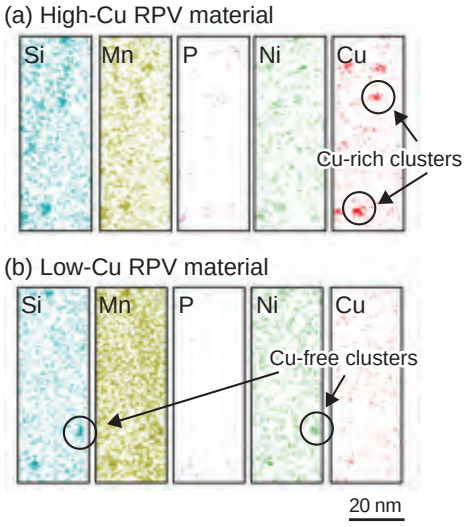

Fig.6-9 Solute clusters observed by 3DAP
RPV materials are an iron-base alloy containing slight amounts of various solutes. Research into the process of solute-clustering due to neutron irradiation has shown that Cu-rich clusters were formed in high-Cu material and Cu-free clusters were formed even in low-Cu material.

The first generation of domestic nuclear power plants has already been in operation for 40 years, and such long-term operation will increase in the near future. Although long-term service of existing plants is desirable from the viewpoints of global warming and the stable supply of energy, the most important factor is to assure the safety of the plants. Nuclear power generation is accompanied by neutron emission from the reactor core. The reactor pressure vessel (RPV), therefore, tends to become brittle due to neutron irradiation, resulting in reduction in its service life.

The degree of neutron irradiation embrittlement is generally evaluated by mechanical tests on specimens made from the RPV materials and inserted in the RPV. Prediction of future embrittlement is performed based on the trend curve of embrittlement with respect to neutron fluence. However, since the main causes of embrittlement are considered to be neutron irradiation-induced defects (i.e., fine displacement of atoms and voids) and clusters (i.e., nano-scale aggregations of atoms), microstructural observations are necessary to understand the embrittlement mechanism. An embrittlement prediction method using information from microstructural observations of irradiated RPV materials has now been incorporated in the domestic code for testing RPV materials.

We are conducting research to clarify the mechanism of neutron irradiation embrittlement using positron annihilation lifetime spectroscopy (PALS) and three-dimensional atom probe tomography (3DAP), which are methods for analyzing nano-scale structures in materials. PALS can provide information on the kinds and amounts of defects. Irradiation experiments with a high neutron flux were performed using two kinds of materials with high- and low-Cu contents in the Japan Materials Testing Reactor. For the first time, this revealed a rapid introduction of defects at the early stage of irradiation (Fig.6-8). Moreover, 3DAP can observe clusters. Cu is considered to play a central role in clustering, and Cu-rich clusters were observed in the high-Cu material. In addition, it was also revealed that Cu-free clusters were formed in the low-Cu material (Fig.6-9). Although the mechanical tests suggest that the magnitude of neutron embrittlement is roughly proportional to the Cu content of the materials, the nano-scale observations suggest the necessity of predicting neutron embrittlement while considering clustering even in low-Cu materials.

We aim to further improve the prediction of embrittlement of RPVs in order to contribute to their safe, long-term service.

Reference

Takeuchi, T. et al., Effects of Chemical Composition and Dose on Microstructure Evolution and Hardening of Neutron-Irradiated Reactor Pressure Vessel Steels, Journal of Nuclear Materials, vol.402, issues 2-3, 2010, p.93-101.

6-5 Assessing the Structural Integrity of Reactor Pressure Vessels

—Fracture Mechanics Assessment Considering the Effect of Weld-Overlay Cladding—

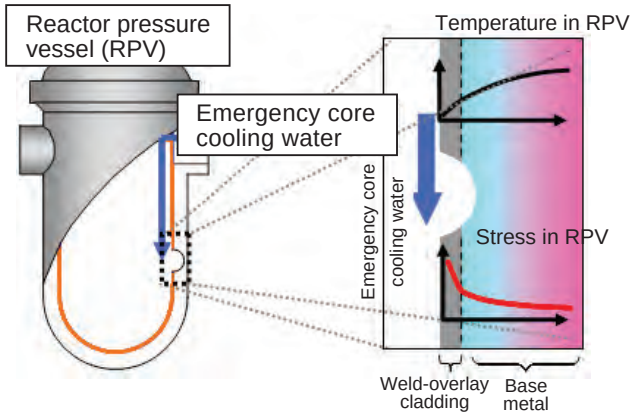

Fig.6-10 RPV pressurized thermal shock event of RPV
High tensile stress is generated by rapid cooling of the wall of the RPV as a result of injecting emergency core cooling water into the RPV after a loss of coolant accident.

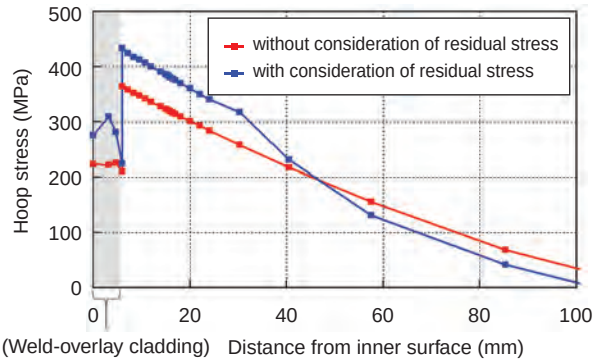

Fig.6-11 Hoop direction stress with or without consideration of residual stress due to overlay welding during PTS
The RPV structural integrity assessment was performed on the assumption that a crack existed on the inner surface. The stress in the wall of an RPV during a PTS event was higher with consideration of the residual stress due to overlay welding than it was without consideration of the residual stress.

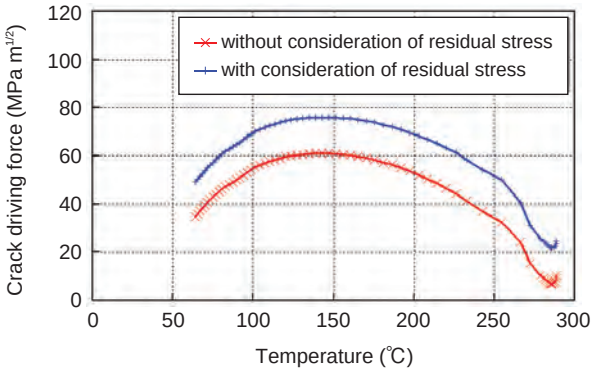

Fig.6-12 Comparison of crack driving force
Assuming that a semi-elliptical crack existed on the inner surface of an RPV, the crack driving force was calculated with and without the residual stress. The results showed that the crack driving force with residual stress was larger than the force without consideration of residual stress.

For the safe operation of nuclear power plants, whatever may happen, the structural integrity of the reactor pressure vessels (RPVs) must be maintained. Therefore, it is necessary to assure the structural integrity of the RPV while taking into account the possible degradation of its materials. Pressurized thermal shock (PTS) is one of the most severe events in assessing the structural integrity of RPVs in a pressurized water reactor (Fig.6-10). A PTS event generates high tensile stress in the inside of the RPV wall. In order to protect the RPV walls against corrosion, stainless steel is overlay-welded as cladding on the inner surface of the RPV exposed to coolant. Residual stress will be generated in the vessel wall near the cladding due to this weld-overlay cladding and this may affect assessment of the structural integrity of the RPV. Because cladding is not structural material, treatment of the residual stress has not been provided in the current domestic assessment method of the structural integrity of RPVs.

Numerical simulations by thermal-elastic-plastic-creep finite element analysis have been performed to evaluate residual stress distributions near the cladding. The analysis results reveal that the weld-overlay cladding produced tensile stress comparable to the yield stress of stainless steel in the cladding. Next, stress analyses during PTS events were performed. The analysis results showed that the stress in the inner surface of RPVs with consideration of weld residual stress was higher than the stress without consideration of residual stress (Fig.6-11). The effect of the residual stress on crack driving force was assessed based on fracture mechanics that assumed the existence of a crack on the inner surface of the RPV during a PTS event. The result indicates that the crack driving force with residual stress may become higher depending on the kind of PTS event than that without residual stress (Fig.6-12).

In the current structural integrity assessment method, safety factors and/or margins are used in order to consider uncertainties such as residual stress that might influence structural integrity. The accuracy of structural integrity assessment can be improved by considering the residual stress due to weld-overlay cladding.

Reference

Nishikawa, H. et al., Effects of Weld-Overlay Cladding on the Structural Integrity of Reactor Pressure Vessels during Pressurized Thermal Shock, Yosetsu Gakkai Ronbunshu, vol.27, no.2, 2009, p.245s-250s.

6-6 Which Model Inputs Are More Important?

—Development of a New Importance Measure and the GSALab Code—

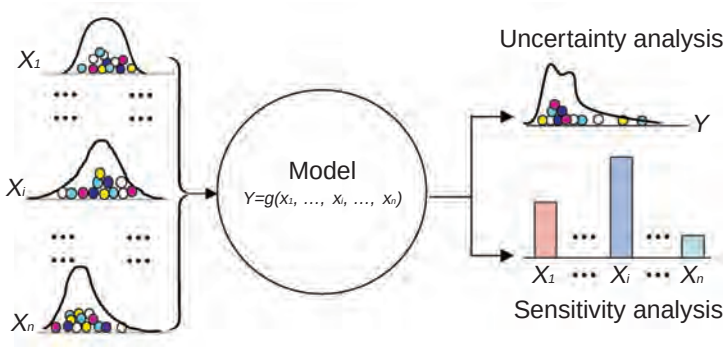

Fig.6-13 Concept of uncertainty and sensitivity analysis
Uncertainties in the model inputs {X_1, ⋯ , X_i, ⋯ , X_n}(n is the number of model inputs) propagate through the model and result in uncertainty in the model output Y (the uncertainty of a model input or a model output is characterized by a probability distribution). While uncertainty analysis refers to the determination of the uncertainty in Y, sensitivity analysis refers to the determination of the contributions of the individual inputs to the uncertainty of Y.

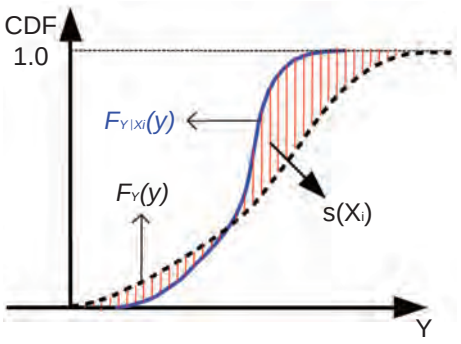

Fig.6-14 Basic idea of the new importance measure
$F_Y(y)$ represents the cumulative distribution function (CDF) of the model output Y obtained with all model inputs {X_1, ⋯, X_i,⋯, X_n} being sampled randomly in their uncertainty ranges. $F_{Y|Xi}(y)$ represents the conditional CDF of Y obtained with the model input of interest X_i being fixed and all other inputs being sampled randomly. The difference between $F_Y(y)$ and $F_{Y|Xi}(y)$ is evaluated by $s(X_i)$, the area closed by these two CDFs.

Probabilistic Safety Assessment (PSA) is a systematic methodology to quantitatively evaluate the probabilities of occurrences of accidents and their consequences.

Given a PSA model of a nuclear power plant, there are uncertainties in the model inputs (e.g., the failure rates of components), which are usually characterized by probability distributions. Generally, Monte Carlo simulations are adopted to propagate input uncertainties through the PSA model and to obtain the probability distribution of the model output as well as its statistics, such as the variance and the mean. This process is called uncertainty analysis (UA) (Fig.6-13).

To reduce the uncertainty of Y, it is necessary to identify the model inputs that highly affect it. This is done through sensitivity analysis (SA) (Fig.6-13). The importance measure mostly used for SA is to find contributors from the model inputs to the variance of Y. If the variance of Y is greatly reduced due to reducing the variance of an input of interest, this input will be an important contributor to the variance of Y. In this method, it is implicitly assumed that the variance of Y is sufficient to describe the uncertainty of Y. However, if the distribution of Y is highly skewed, its variance will not be a good statistic to represent its uncertainty.

In our work we proposed a new importance measure, in which the quantified shape change of the CDF of Y is adopted as an indicator to evaluate the importance of each model input. As shown in Fig. 6-14, the area $s(X_i)$ is used to evaluate the difference between $F_Y(y)$ and $F_{Y|Xi}(y)$. It is obvious that $F_{Y|Xi}(y)$ is dependent on X_i, and so is $s(X_i)$. Because there is uncertainty in X_i, each time we change the value of X_i in its uncertainty range and propagate the uncertainties of other model inputs through the model, we will obtain a new $F_{Y|Xi}(y)$ as well as a new $s(X_i)$. Repeating the above procedures thousands of times, we can obtain thousands of $s(X_i)$. The expected value of $s(X_i)$ can then be computed. We define this expected value as the importance measure of X_i.

This new importance measure was implemented in a computer code GSALab (Global Sensitivity Analysis Lab). In addition to PSA models, GSALab can also be applied to UA and SA of other models, such as atmospheric dispersion models and thermal-hydraulic models.

Reference

Liu, Q., Homma, T., A New Importance Measure for Sensitivity Analysis, Journal of Nuclear Science and Technology, vol.47, no.1, 2010, p.53-61.

6-7 How Much Radioiodine Is Released in a Severe Accident?
—Chemical Production of Volatile Iodine in Radiation Conditions—

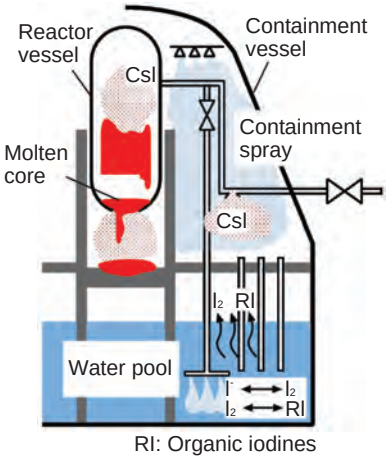

RI: Organic iodines

Fig.6-15 Iodine release during a severe accident
Iodine is likely to be transferred into the containment mostly as cesium iodide (CsI) and absorbed in water. It is then partially converted into volatile I_2 and organic iodines by radiation chemical reactions.

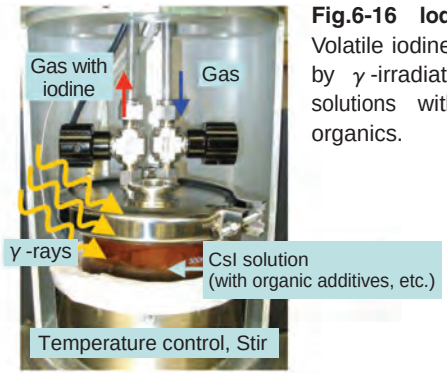

Fig.6-16 Iodine release experiment
Volatile iodine release was examined by γ -irradiating cesium iodide (CsI) solutions with additives such as organics.

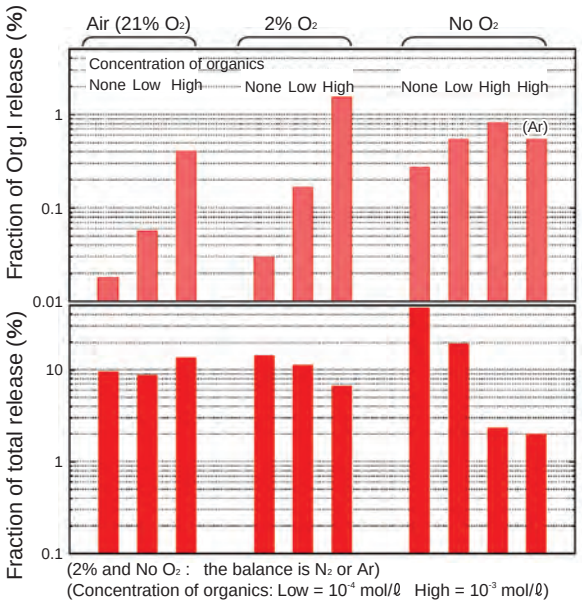

Fig.6-17 Experimental results on the influence of organic impurity and oxygen concentration
A thinner retained in the wall paint in the containment, methyl isobutyl ketone (MIBK), was added at various concentrations, and oxygen concentration in the sweeping gas was changed. The "air" and "2% O_2" cases represent the PWR and BWR containment atmospheres, respectively. (The release fractions here are not directly comparable to the fraction of release during an accident based on the core inventory.)

The safety of a nuclear power plant means that its risk to the public is adequately managed. If severe core damage occurs, the radioactives in the core may be released into the environment. What kinds of radioactives they are, and how much of them there are, are important factors in evaluating the public risk.

Among such radioactives, iodine can become volatile and is easily released, and also has strong biological impacts. Thus it is regarded as most important in terms of heath consequences. The iodine accumulated in the containment atmosphere is important, because it is released into the environment if the containment fails.

Iodine is likely to be transferred into the containment mostly as cesium iodide (CsI), which is readily absorbed in water. It is, however, partially converted into volatile I_2 and organic iodines by chemical reactions under strong radiation in the containment in accident conditions (Fig.6-15). The organic iodines are produced by reactions between iodine and organic compounds such as solvents leaching from the wall paint. Methyl iodide is a highly volatile kind and is relatively inert; it is not trapped and easily released.

We conducted experiments on such volatile iodine release by radiation chemical reactions. As shown in Fig.6-16, we prepared CsI solution in a vessel with various additives relevant to the containment environment, irradiated it, and measured the iodine release fractions. The cover gas in the vessel was swept and the gaseous iodine was transferred downstream, where iodine was trapped by filters. The percentages released as I_2 or organic iodines were measured by this method.

Fig.6-17 compares the results of experiments with an organic additive, methyl isobutyl ketone (MIBK), which is a kind of thinner that is retained in the wall paint, and various oxygen concentrations in the sweeping gas. Data on the influence of the concentrations of organics and oxygen on iodine release were obtained through this experiment. This is useful for improving chemical reaction models and for reducing uncertainties in the evaluation of iodine release fractions in severe accidents.

This is part of a contract research program funded by the Japan Nuclear Energy Safety Organization (JNES).

Reference

Moriyama, K. et al., Experiments on the Release of Gaseous Iodine from Gamma-Irradiated Aqueous CsI Solution and Influence of Oxygen and Methyl Isobutyl Ketone (MIBK), Journal of Nuclear Science and Technology, vol.47, no.3, 2010, p.229-237.

6-8 Analysis Method Validation and Criticality ata roduction
—Revision of Data Collection for the Nuclear Criticality Safety Handbook—

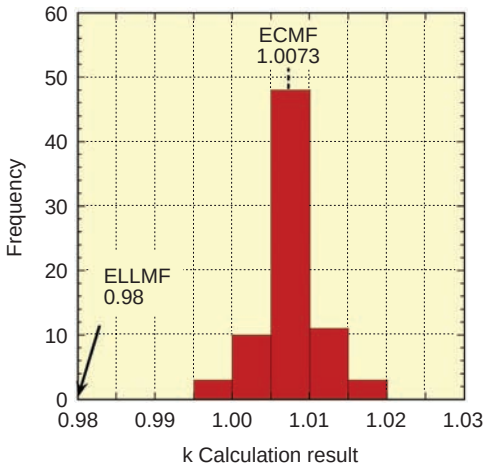

Fig.6-18 Distribution of critical benchmark calculation results (homogeneous low-enriched uranium system)
Analysis of critical mass measurements of homogeneous low-enriched uranium with MVP and JENDL-3.2 gives ks distributed from 0.995 to 1.020. Statistical testing concluded that the Estimated Criticality Multiplication Factor (ECMF), which is the value estimated to be most probably critical, is 1.0073, and that the value 0.98 can be employed as the Estimated Lower Limit Multiplication Factor (ELLMF) k_{lim}.

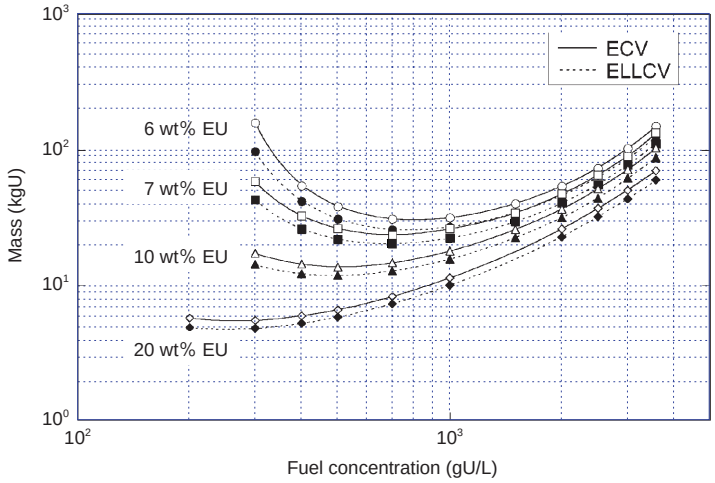

Fig.6-19 Critical mass data for homogeneous ADU(II)-H_2O (with water reflector)
This is an example of the results of calculation with MVP and JENDL-3.2, showing, for various uranium concentrations, Estimated Critical Values (ECVs), which are calculated minimum critical masses, and Estimated Lower Limit Critical Values (ELLCVs), which are calculated minimum masses whose ks are 0.98, of a homogeneous mixture of ammonium diuranate ADU(II) and water H_2O handled in the re-conversion process. Handling a mass smaller than the ELLCV avoids criticality.

Fission chain reactions linked by neutrons are maintained in a nuclear reactor by keeping its nuclear fuel critical, and energy and radiation emitted from the reaction are utilized. The nuclear fuel must not, however, be critical in places other than a nuclear reactor. Safety management for this purpose is generally known as criticality safety.

Due to advances in computation technology, it has become feasible to analyze nuclear interactions between neutrons and nuclei in materials such as nuclear fuel, and to judge with pretty good accuracy if a condition is critical, wherein a fission reaction can continue, or is safely sub-critical. The analysis computes the effective neutron multiplication factor k, which is the ratio between the neutron production rate by fission and the annihilation rate by absorptions, etc. Theoretically, $k = 1$ and $k < 1$ indicate criticality and sub-criticality, respectively. It is indispensable to know the accuracy quantitatively before practical applications of the analysis method; therefore a validation was conducted for a combination of the continuous energy Monte-Carlo code MVP and the nuclear data library JENDL-3.2, both of which were developed in Japan.

A validation needs critical masses of various nuclear fuels measured in critical experiments as references. The data used for the present validation came from the database of the International Criticality Safety Benchmark Evaluation Project (ICSBEP) of OECD/NEA. The results of critical mass measurements conducted in many countries are registered in the database; conditions such as the kinds, structures, and dimensions of nuclear fuels that became critical are described in detail for each measurement.

Analysis based on this information gives distributions of k around 1 as shown in Fig.6-18, which may be caused by uncertainties in the ICSBEP data and the nuclear data library. The important fact is that a case may be critical in reality even if the computed k is < 1. If, however, a value sufficiently smaller than the lowest limit in the distribution is chosen as the Estimated Lower Limit Multiplication Factor (ELLMF) k_{lim}, and if the computed k is $< k_{lim}$, then it can be judged as being actually sub-critical. A statistical test of the distribution concluded that the value 0.98 could be employed as k_{lim}. This is a good improvement on the value 0.95 employed for the analysis method approximately two decades ago.

Moreover, the minimum mass, dimensions, concentrations, etc., of various nuclear materials whose ks are 1 and 0.98 were computed with the same method, and published as a revised data collection for the nuclear criticality safety handbook, to be used as references for designing equipment and procedures to handle nuclear fuel. The new version has become more useful than the old one by adding new kinds of data, as shown in Fig.6-19, for example.

Reference

Okuno, H., Suyama, K., et al., Second Version of Data Collection Part of Nuclear Criticality Safety Handbook (Contract Research), JAEA-Data/Code 2009-010, List of errata, 2009, 175p.（in Japanese）.

6-9 Mass Transport Retardation Studies in Bedrock
—Sorption Experiments under Anoxic Conditions—

Fig.6-20 Collection of rock and groundwater samples
To minimize oxidation, groundwater and rock samples were collected with special care to avoid exposure to the air. Boreholes were drilled with degassed water obtained by bubbling argon gas into the local surface water.

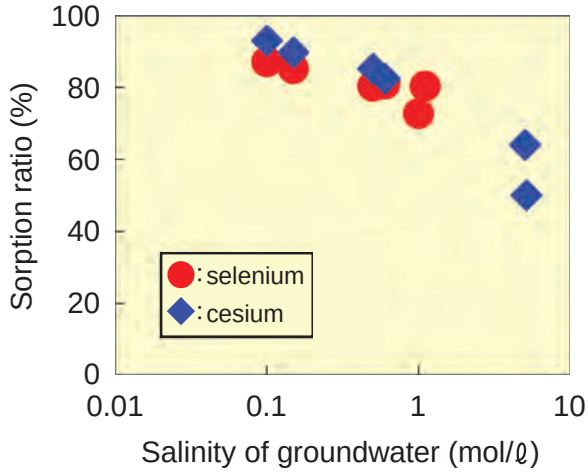

Fig.6-21 Influence of salinity on the sorption of selenium
The influence of salinity on the sorption of selenium was slightly negative, but the effect was not striking.

In Japan, high-level radioactive waste (HLW) is vitrified, encapsulated in a metal container called an overpack, surrounded by engineered buffer material, and emplaced in a repository constructed in stable rocks at a depth of 300 m or greater. In safety assessments of this disposal system, the possibility that long-lived radionuclides may be leached from the wastes and may subsequently be transported through surrounding rock masses must be considered. Retardation of radionuclide migration by sorption onto a host rock is one of the main geologic factors that influence the performance of a radioactive waste disposal system. It is therefore necessary to evaluate the sorption of radionuclides in rocks surrounding the repository. Since the chemical conditions deep underground are likely to be anoxic, it is possible that the sorption behavior of radionuclides under disposal conditions is different from that under atmospheric conditions. In addition, sorption behavior of radionuclides would change depending on the salinity of the groundwater.

In this study, sorption experiments were carried out under anoxic conditions to study the influence of salinity on the sorption of radionuclides. The rock and groundwater samples employed were collected with special care to avoid exposure to the air (Fig.6-20). The experiments were performed in an argon gas atmosphere glove box (O_2 < 1 ppm).

Fig.6-21 shows the sorption behaviors of selenium and cesium, which are the dominant long-term radiological hazard in safety assessment calculations for hypothetical HLW. The sorption ratio of selenium, which forms low sorbable anionic species in groundwater, was as high as cationic cesium, suggesting a specific bonding of selenium species with surface sites of rocks under anoxic conditions. The influence of salinity on the sorption of selenium was slightly negative, but the effect was not striking.

We demonstrated the sorption behavior of radionuclides on rocks under anoxic conditions and confirmed that the sorption was not inhibited even at high salinity. Sorption data for radionuclides on rocks under disposal conditions have thus been obtained and accumulated for reliable radioactive waste disposal safety assessments.

This research project has been conducted as regulatory-supporting research funded by the Nuclear and Industrial Safety Agency (NISA), the Ministry of Economy, Trade and Industry (METI).

Reference

Iida, Y. et al., Sorption Distribution Coefficients of Selenium on a Sandy Mudstone under Reducing Conditions of Underground, Genshiryoku Bakkuendo Kenkyu, vol.15, no.2, 2009, p.57-67 (in Japanese).

Advanced Science Pioneers the Future

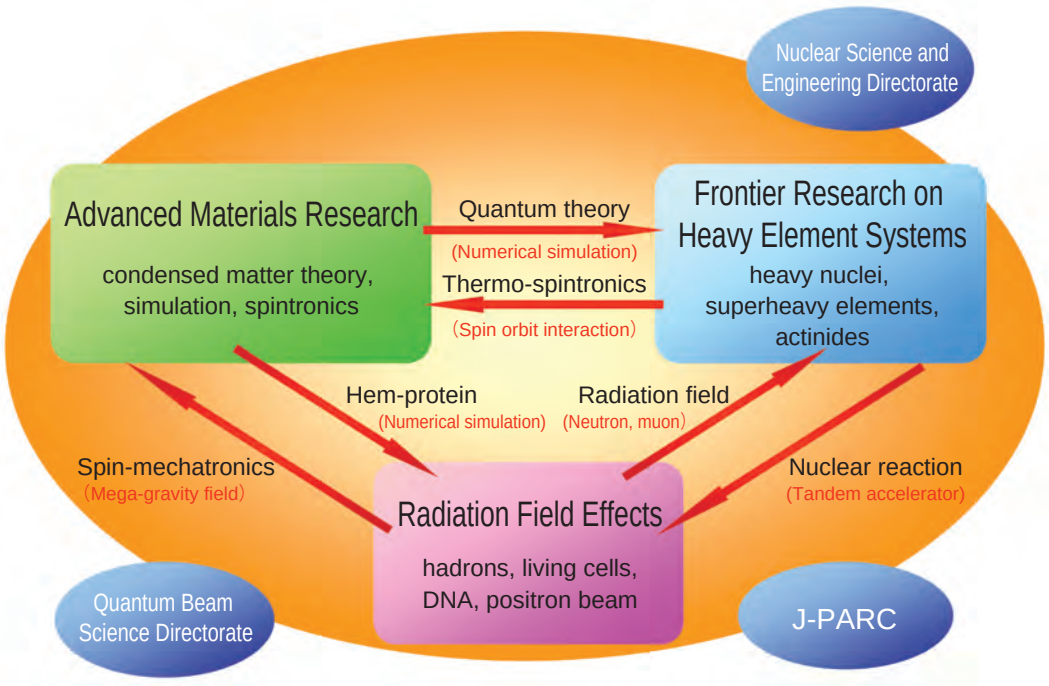

Fig.7-1 Cooperative framework of the Advanced Science Research Center (ASRC)

Atomic energy science is essentially based on comprehensive research and development that covers the entire range from basic research to practical applications. It is thus particularly important to promote both goal-oriented and fundamental research programs to deal with a new phase of atomic energy in the coming decades as well as to solve today's energy problems.

The Advanced Science Research Center (ASRC) has been conducting leading-edge research related to atomic energy sciences, for the discovery of new principles and phenomena, the creation of new materials, and for the development of innovative technologies. In FY2009, we achieved some prominent results: the analysis of superheavy atoms on an atom-at-a-time scale, the successful clarification of the mysterious properties of the uranium compounds, the development of isotope separation in a mega-gravity field, the exploration of amazing functions of microbes, and the development of a novel technique for investigating radiation damage in DNA. Details will be shown in the following sub-sections.

As a plan for the next 5-year term starting from FY2010, the ASRC intends to dedicate itself not only to conducting world leading basic research, but also to establishing an international center of excellence (COE) in basic sciences. To attain this ambition, we have decided to take up the following three research fields: (1) advanced materials science research, (2) frontier research on heavy element systems, and (3) research on radiation field effects.

The first research field consists of three themes: creating new functions of materials by means of numerical simulations, spin - transport mechanism and design in molecular spintronics systems, and spin - mechatronics combining quantum interaction between electron spin and mechanical torque in solids. For the second field, the following four subjects have been set up: surrogate reactions via nucleon-transfer reactions in heavy nuclei, the valence electronic structure and nuclear shell structure of superheavy elements, preparation of new actinide compounds with exotic behavior, and foundation of a new concept in condensed matter physics for heavy element systems. The third field involves four themes: the structure of nuclei and hadrons with strangeness, the formation of actinide nanoparticles in biological reaction environments, the biophysical study of molecular and cellular responses to radiation, and surface low-dimensional materials study using advanced positron beams (Fig.7-1).

In order to promote the above leading-edge research and development, we cooperate not only within the ASRC and other divisions of JAEA but also with external scientific communities. In addition, through implementation of the Reimei Research Program, we conduct new research programs on a global basis and investigate innovative subjects together with other institutes (Fig.7-2).

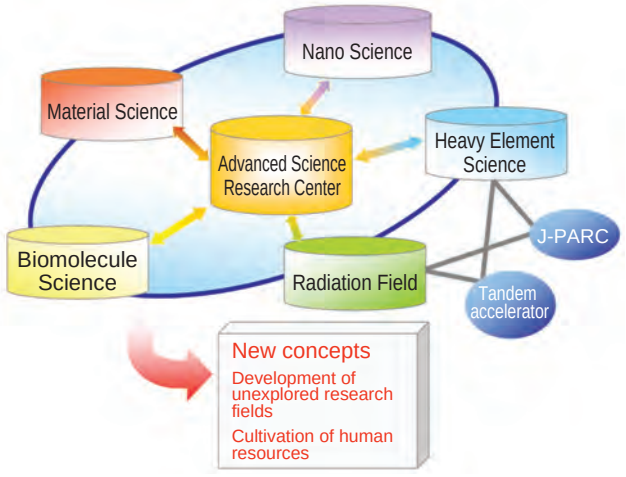

Fig.7-2 ASRC as a center of excellence (COE)

7-1 Analyzing Supherheavy Atoms on an Atom-at-a-Time Scale
—Oxidation of Nobelium with Flow Electrolytic Chromatography—

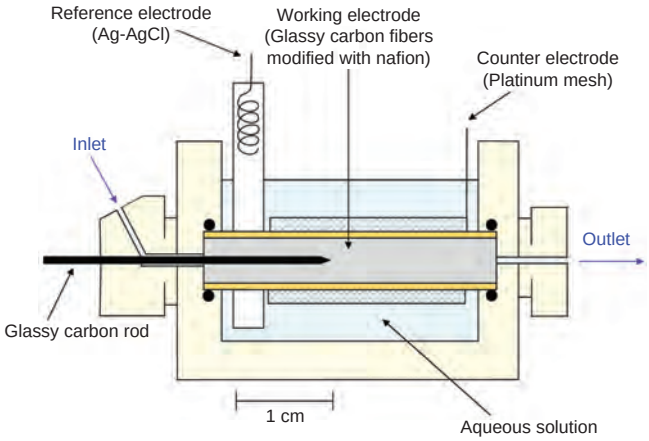

Fig.7-3 Flow electrolytic chromatograph apparatus
Single atoms injected from the inlet pass through the column-type working electrode modified with Nafion cation-exchanger, where single ions are electrolyzed and chemically separated.

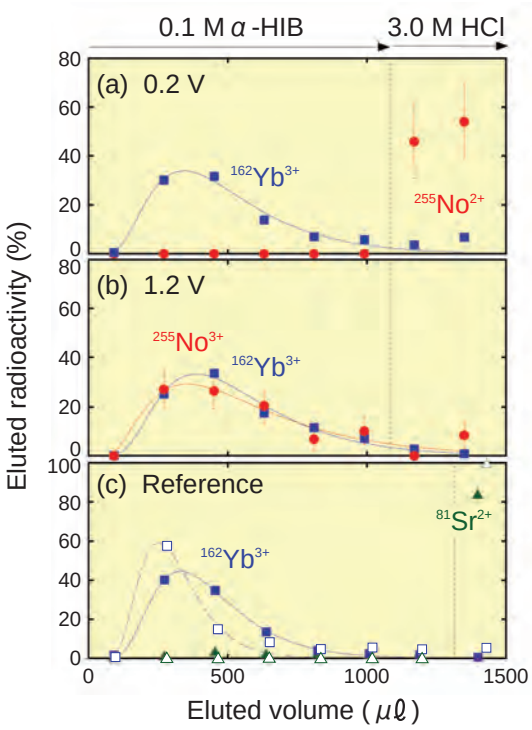

Fig.7-4 Elution behavior of No, Sr^{2+}, and Yb^{3+}
Elution behavior of No(●) and Yb^{3+}(■) at the applied potentials of (a) 0.2 V and (b) 1.2 V. (c) Behavior of Sr^{2+} (0.2 V: △, 1.2 V:▲) and Yb^{3+} (0.2 V:□, 1.2 V:■).

The electron configuration of superheavy elements placed at the uppermost end of the periodic table is predicted to be intensely affected by strong relativistic effects. Redox properties sensitive to the electron configuration are, therefore, important in elucidating the influence of the relativistic effects. Because an atom-at-a-time scale is used with these elements, however, their redox properties had not been studied previously. Here we report the oxidation of element 102, nobelium (No), using flow electrolytic chromatography on an atom-at-a-time scale.

We produced nobelium-255 (^{255}No) with a half-life of ~3 min in a nuclear reaction of carbon-12 (^{12}C) and curium-248 (^{248}Cm) at the JAEA tandem accelerator. No was dissolved with 0.1 M α-hydroxyisobutyric acid (α-HIB) and was then injected into the flow electrolytic chromatography apparatus shown in Fig.7-3. The No^{2+} ion passed through a column-type working electrode composed of thin carbon fibers modified with Nafion cation-exchanger where No^{2+} is electrolyzed to No^{3+} and these ions are separated from each other. After elution with α-HIB, adsorbed ions on the electrode were stripped with 3.0 M HCl.

In Figs.7-4(a) and (b), the elution behavior of No and Yb^{3+} are shown, while that of Sr^{2+} and Yb^{3+} are plotted as a reference in Fig.7-4(c). Quite different behavior between Sr^{2+} and Yb^{3+} indicates clear separation between +2 and +3 ions under the given conditions. At the applied potential of 0.2 V, No is not eluted with α-HIB and is stripped with 3.0 M HCl. This behavior is quite similar to that of Sr^{2+}, showing that No is bound in a stable +2 state. On the other hand, at 1.2 V, No is eluted with α-HIB at the position of Yb^{3+}, which unambiguously indicates that No is oxidized to the +3 state. These results demonstrate successful electrochemical oxidation on an atom-at-a-time scale for the first time.

In the future, we will clarify the redox properties of other superheavy elements by applying this newly developed electrochemistry approach.

Reference

Toyoshima, A. et al., Oxidation of Element 102, Nobelium, with Flow Electrolytic Column Chromatography on an Atom-at-a-Time Scale, Journal of the American Chemical Society, vol.131, no.26, 2009, p.9180-9181.

7-2 Challenges for the Mysterious Properties in the Uranium Compounds
—New Physical Properties in a Super High Quality Single Crystal of URu_2Si_2—

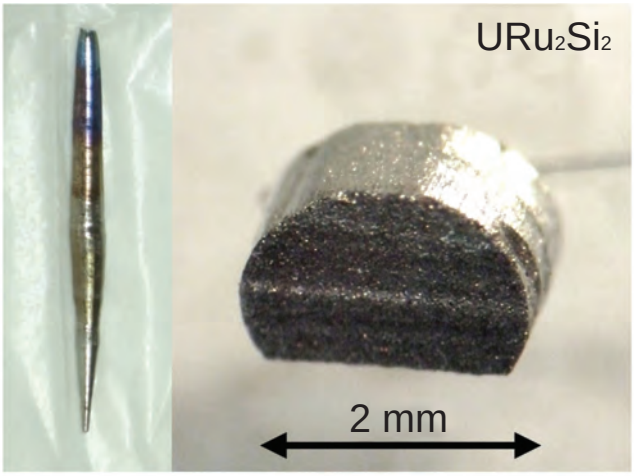

Fig.7-5 Single crystal of URu_2Si_2
The picture on the left shows an ingot of the single crystal. The picture on the right shows a sample cut out for measurement.

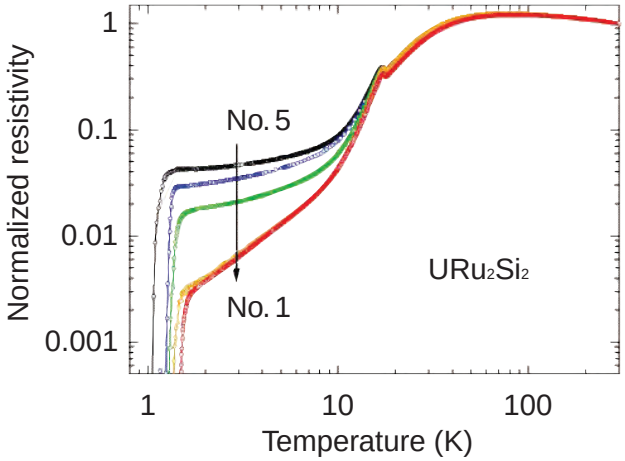

Fig.7-6 Electrical resistivity in the single crystal of URu_2Si_2
The vertical axis was normalized to the value at room temperature. The No. 1 sample corresponds to the highest quality sample. The steep decrease at 1.5 K is due to the phase transition of the superconductivity.

The properties of actinide elements are governed by the behavior of 5f electrons. Because of the degrees of freedom that 5f electrons have, actinide compounds show a variety of ordered states. The well-known examples include the ordering of magnetic moments and the ordering of the electron charge distribution. These conventional orderings have been revealed by microscopic experimental probes such as neutron / X-ray scattering, NMR, and so on. However, the origins of the ordered state of the actinide compound URu_2Si_2 have not been resolved since its discovery in 1985, despite exhaustive experimental efforts. It is hence described as a "hidden-order" state.

One of the key experiments to tackle this problem would be detailed measurement of the electrical resistivity as a function of temperature (T). Generally, electrical resistivity reflects the electronic state and ordering state through the scattering process. For example, strong electron-electron scattering gives the T^2 term of resistivity. However, a high quality single crystal sample is required to avoid large scattering contributions from impurities, dislocations, lattice defects, and so on. Establishing a technique of high quality single crystal growth is a key point for this investigation.

We succeeded in growing a highly purified single crystal of URu_2Si_2 by a combination of a solid-state electro-transport method for the refinement of the uranium raw metal and a Czochralski-pulling method for growing a single crystal of URu_2Si_2 (Fig.7-5). Fig.7-6 shows the temperature dependence of the electrical resistivity for 5 pieces that were cut out from that ingot. The residual resistivity of the No.1 sample has the smallest value, which is one-tenth that of No.5. The temperature dependence in the No.1 is different from that of the No.5. Although the No.5 sample has good quality compared to samples reported from other groups in the world, it is still dominated by impurity scattering at low temperatures. On the other hand, in the No.1 sample, the electrical resistivity follows the $T^{1.5}$. This anomalous behavior cannot be explained by the usual electron-electron scattering process, as mentioned previously. It indicates that the resistivity strongly reflects the electronic state of the "hidden-order" state. These results are unmistakably crucial to clarifying the order parameter in URu_2Si_2.

Although actinides are very important elements in nuclear science and technology, some diverse characteristics of 5f electrons have not been well-understood, as in URu_2Si_2. Advances in such research are expected to be connected to understanding the electronic state of actinides.

Reference

Matsuda, T. D. et al., Super Clean Sample of URu_2Si_2, Journal of the Physical Society of Japan, vol.77, suppl.A, 2008, p.362-364.

7-3 Breakthrough for Isotope Separation
－Separating Isotopes in Solids or Liquids Using a Centrifuge－

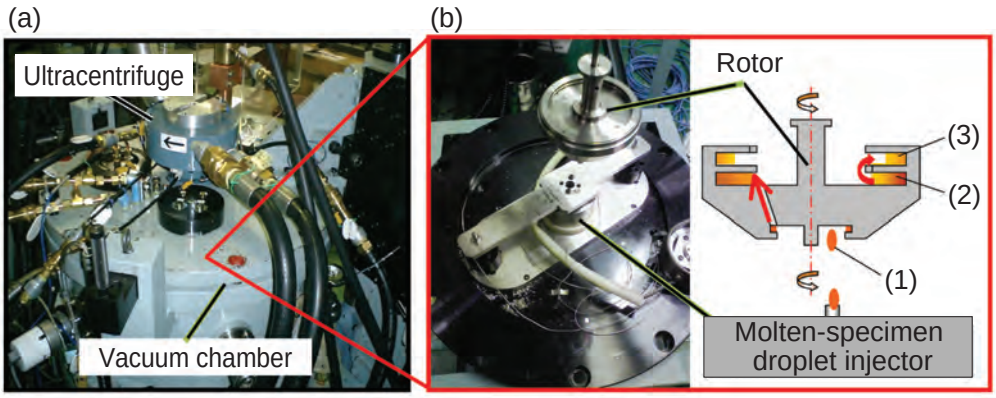

The transferring of indium in the rotor
(1) is the initial state of a molten-indium droplet (0.1g-In/shot)
(2) ^{113}In-enriched move to (3) by overflow

Physical properties of In
Melting point : 156.4 ℃
Specific gravity : 7.9

Natural percentage of isotopes :
^{113}In : 4.3%, ^{115}In: 95.7%

Fig.7-7 (a) Ultracentrifuge (b) Unit developed for separating isotopes in solids or liquids (rotor and molten-specimen droplet injector)
A strong gravitational field can be generated by rotating the rotor at very high speed in an ultracentrifuge. The rotor temperature can be raised up to 400 ℃ using a heater in a vacuum chamber.

Table 7-1 Percentage of ^{113}In in pure indium before and after centrifugation
(1) Before centrifugation. (2), (3) In the separation grooves after centrifugation.

Experimental conditions (Centrifugal acc. 370,000 *g*)	^{113}In percentage in pure indium before and after centrifugation (Calculated from the measurement result of ^{113}In/^{115}In isotope ratio by Secondary Ion Mass Spectrometry. The errors represent one standard deviation.)		
	(1)	(2)	(3)
Solid (temp.148 ℃, time interval of specimen feed 0.1 g / 45 min, Total processing time 60 h)	4.300±0.012%	4.285±0.009% (0.345% ↓)	4.319±0.011% (0.435% ↑)
Liquid (temp.170 ℃, time interval of specimen feed 0.1 g / 5 min, Total processing time 5 h)	4.300±0.009%	4.287±0.010% (0.308% ↓)	4.318±0.011%(0.411% ↑)

Under a strong centrifugal acceleration field of around several hundred thousand *g*(*g*= 9.80665 m/s^2), in the case of two component alloys, the atoms of heavier and lighter elements move in the direction of centrifugal acceleration and in the opposite direction, respectively. That is to say, sedimentation of atoms results. To study mass dependence in sedimentation of atoms, we developed an ultracentrifuge to generate a centrifugal acceleration up to 1 million *g* at elevated temperature. Recently (in a collaborative study with Kumamoto University), we have been successful in the sedimentation of constitutional isotopes in a single element, i.e., sedimentation of isotopes, where the sedimentation is dependent only on a small difference in mass among the relevant isotopes. We have confirmed the sedimentation of isotopes in solid or liquid states of pure elements such as Se, In, and Sn.

A centrifugal isotope separation process for solids or liquids had not yet been proposed, although a process in the gaseous state (gas centrifugation) has already been put to practical use to enrich stable isotopes and uranium isotopes. We have devised a technique to show that the sedimentation of isotopes should be the principal phenomenon to realize the other two processes. First, we developed a rotor having 2 grooves for the multi-stage centrifugal isotope separation (in a collaborative study with Maruwa Electric Inc., supported by JAEA's Reimei Research). Indium was chosen for the isotope separation experiment for the reason that natural indium consists of only two isotopes, and a relatively simple procedure was expected for verification of mass dependent isotope fractionation.

Fig.7-7 (b) shows the rotor we developed and a molten-specimen droplet injector for intermittent specimen feeding, and Table 7-1 shows the percentages of ^{113}In in pure indium before and after centrifugation. The time interval for specimen feeding in the case of a solid was set about 10 times longer than that of a liquid state, to take into consideration the approximate difference in time required to reach a steady state of isotope fractionation in the separation groove, which was attributed to the difference in the diffusion coefficients between the two states. Although there was a difference in the specimen feeding time interval, almost the same separation ratios were obtained in the case of both a solid and a liquid at the same magnitude of acceleration. This indicates that the sedimentation of isotopes occurs according to the same principle in the case of both solids and liquids.

With this development, it has become clear that the sedimentation of isotopes can be used as the principal phenomenon to realize a centrifugal isotope separation process in solids or liquids.

Reference

Ono, M. et al., Development of Special Rotor for Centrifugal Separation of Isotopes in Solid Pure Metals, Review of Scientific Instruments, vol.80, issue 8, 2009, p.083908-1－083908-6.

7-4 Exploring Amazing Functions of Microbes
－Formation of Biogenic Nanoparticles of Precious Metals－

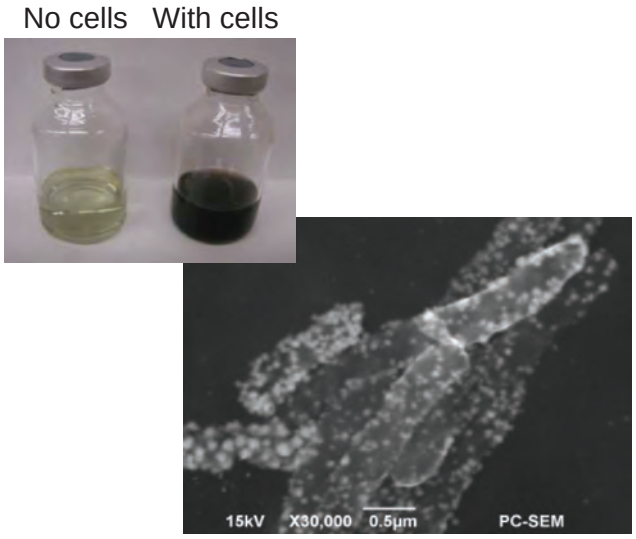

Fig.7-8 Photographs of platinic acid solution with and without iron reducing bacteria (upper left), and SEM of iron reducing bacteria after exposure to a platinic acid solution (lower right).
Bright spots indicate nanoparticles of platinum, and ellipsoids are cells.

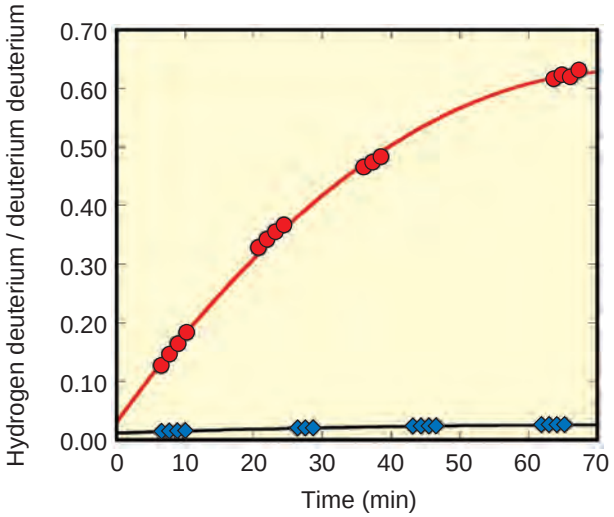

Fig.7-9 Time course of HD/D_2 ratios in gas passed through columns containing biogenic (●) and abiotic Pt nanoparticles
The HD/D_2 ratio obtained with the biogenic Pt nanoparticles was 6.1 times higher than that in the abiotic Pt precipitates.

We developed a new biological technique to form nanoparticles (smaller than 1/10000 mm) of platinum and palladium using iron reducing microorganisms.

How nanoparticles can be applied depends on diverse magnetic, electronic, and optical properties, which vary on the basis of their shape, size, and composition. The platinum-group metals (PGM) comprising palladium, platinum, and rhodium have been used in the industrial production of fuel cells, as catalytic converters to reduce gaseous emissions in vehicle exhausts, and in the catalytic separation of hydrogen isotopes.

Microorganisms posses various functions for obtaining energy. In particular, the functions of metal ion accumulation and selection have been applied to the recovery and separation of actinides in the nuclear fuel reprocessing process and in the evolution of a mathematical model for estimating migration of actinides in groundwater.

In this study, PGM ions were recovered by means of reductive precipitation by iron reducing bacteria. We found that platinum and palladium chloride ions were reduced to form nanoparticles by electron transfer from the bacteria, as expressed by the following equations.

$PdCl_4^{2-} + 4e^- + 2H_2O \rightarrow Pd\ (prep) + 4HCl + O_2$

$PtCl_6^{4-} + 6e^- + 3H_2O \rightarrow Pt\ (prep) + 6HCl + 3/2O_2$

SEM observation showed the formation of nanoparticles containing PGMs on the cell surface (Fig.7-8). XRD and XAFS analyses indicated that the oxidation state of the PGMs was 0 and that the crystal form was face centered cubic.

We applied these biogenic PGM nanoparticles to the catalysis of hydrogen isotope exchange. The results showed a formation ratio of HD from H_2 and D_2 mixed gas approximately 6 times higher than with nanoparticles formed abiotically (Fig.7-9). The iron reducing bacteria alone did not cause the hydrogen isotope exchange. These results are the first indication that biogenic Pt nanoparticles formed on the cells of iron reducing bacteria have high catalytic activity in the exchange of hydrogen isotopes.

Reference
Suzuki, Y., Ohnuki, T. et al., Effects of Citrate, NTA, and EDTA on the Reduction of U(VI) by Shewanella Putrefaciens, Geomicrobiology Journal, vol.27, issue 3, 2010, p.245-250.

7-5 A Novel Technique for Investigating Radiation Damage in DNA
—Selective Induction of DNA Damage by Synchrotron Soft X-rays—

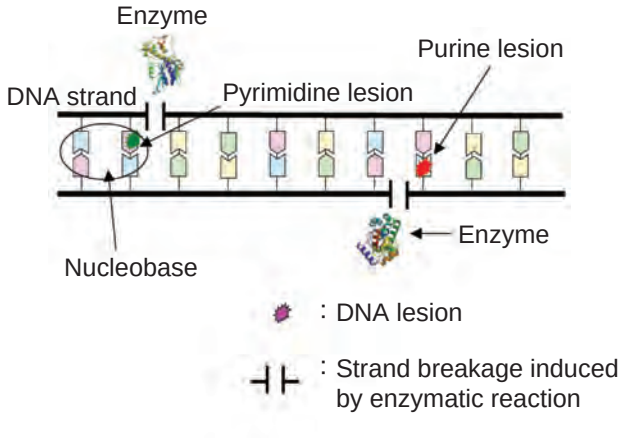

Fig.7-10 Detection of nucleobase lesions by enzymes
Nucleobase lesions are converted to DNA strand breakage by enzymes.

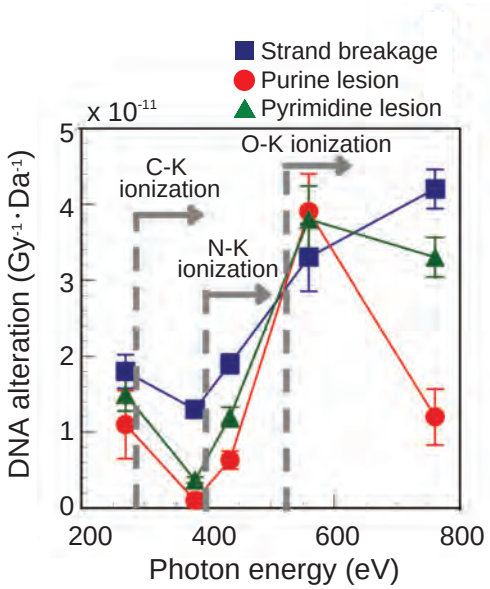

Fig.7-11 DNA alterations are selectively induced by monochromatic soft X-rays
By tuning the irradiated photon energy, different atoms can be selectively ionized. The chart shows the type of DNA damage (strand breakage (■), purine (●) or pyrimidine lesion (▲)) that can be selectively induced by monochromatic soft X-rays.

Molecular damage to cellular DNA, and in particular the induction of mutation, is thought to be among the most critical biological effects of radiation. Therefore, the study of radiation-induced DNA damage can be expected to enhance our understanding of the selective induction of specific molecular changes in DNA. The DNA molecule consists of a helical double-stranded sugar-phosphate backbone and nucleobases, which consist of purine (adenine (A) and guanine (G)) and pyrimidine (thymine (T) and cytosine (C)) pairs. Although double-strand breakage of the DNA double helix results in cell death, nucleobase lesions are thought to be one of the principal factors in the induction of mutation. Accordingly, we investigated the yield of DNA strand breakage and nucleobase lesions due to monochromatic soft X-rays. We selected typical photon energies for the K-shell ionization of carbon, nitrogen, and oxygen, then attempted a novel technique to selectively induce DNA alterations. Base excision repair enzymes (Fpg and Nth) were used to detect base lesions efficiently (Fig.7-10). The results revealed that selective induction of specific DNA alteration can be achieved by tuning the soft X-ray energy (Fig.7-11). The K-shell ionization of oxygen most likely contributes to the induction of nucleobase lesions. On the other hand, single-strand breakage of DNA is preferably produced just below the N K-edge. Therefore, we concluded that the specific types of DNA alterations can be selectively induced by tuning monochromatic soft X-ray irradiation. In general, purine and pyrimidine bases are known to function as efficient trapping sites of holes and electrons, respectively, which are produced in the DNA molecule by ionizing radiation. These holes and electrons subsequently induce molecular damage to the DNA. Strand breakage results from the decomposition of deoxyribose. Therefore, it can be inferred that the differences in the behavior of holes, electrons, and deoxyribose decomposition differed depending on the soft X-ray irradiation conditions. We achieved successful selective induction of DNA lesions by tuning soft X-ray energies. This technique is expected to be utilized as a powerful tool for investigating damage in DNA.

Reference

Fujii, K. et al., Nucleobase Lesions and Strand Breaks in Dry DNA Thin Film Selectively Induced by Monochromatic Soft X-rays, The Journal of Physical Chemistry B, vol.113, issue 49, 2009, p.16007-16015.

Formation of Basis for Nuclear Energy R&D, and Creation of Innovative Technology

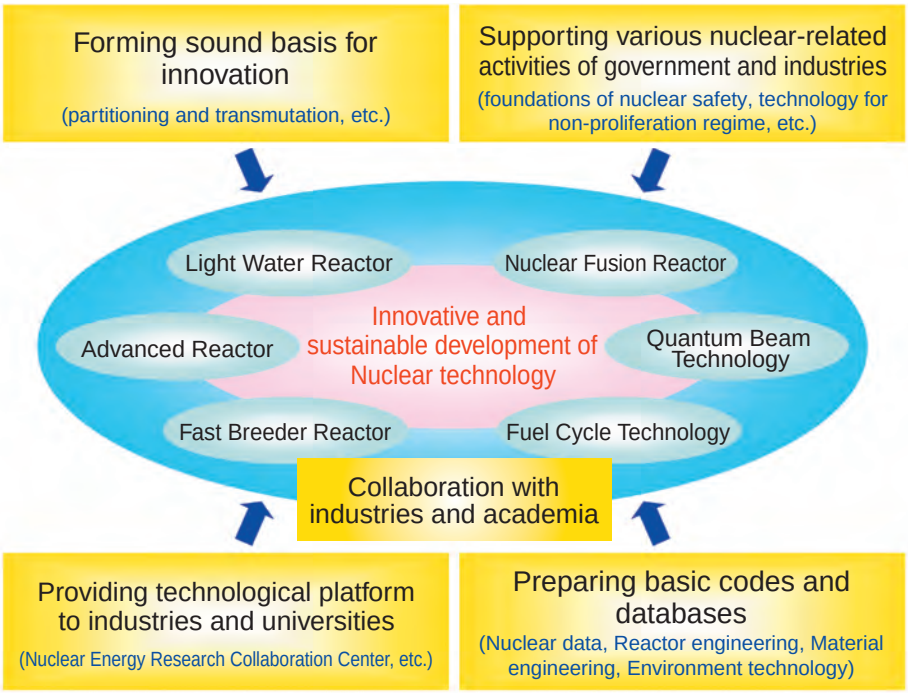

Fig.8-1 Roles of nuclear science and engineering research

The R&D activities in nuclear science and engineering research at the Japan Atomic Energy Agency comprise the four roles shown in Fig.8-1. To this end, research is being conducted in the areas of nuclear data and reactor engineering, fuels and materials engineering, and environment and radiation science. JAEA has been also promoting joint research and development with industry and academia, and the Nuclear Engineering Research Collaboration Center (NERCC) was established in 2005 to support these activities.

Nuclear data and reactor engineering

Measurements of nuclear cross-section data and compiling the data into an evaluated database (JENDL-4.0) are the major research activities in this field. Reactor physics and heat transfer are also studied. Most of the R&D activities on partitioning and transmutation to reduce the burden in the geological disposal of high-level waste (HLW) are conducted in this research field.

Fuels and materials engineering

Basic studies on advanced nuclear fuel and cycle technology (Fig.8-2) and on the various nuclear materials are included in this field. Study of vitrification processing of high-level radioactive liquid waste is also ongoing, including some activities at NERCC to assist with commercial plant operation.

Environment and radiation science

R&D on the environmental behavior of radionuclides and dose assessment is being pursued. Studies on radiation protection are also included in this field. Some of this research has been applied to more familiar issues, such as the study of carbon release from soil using carbon-14 isotopes for better understanding of the greenhouse effect, and development of a new technology for liquid waste treatment based on nuclear waste management.

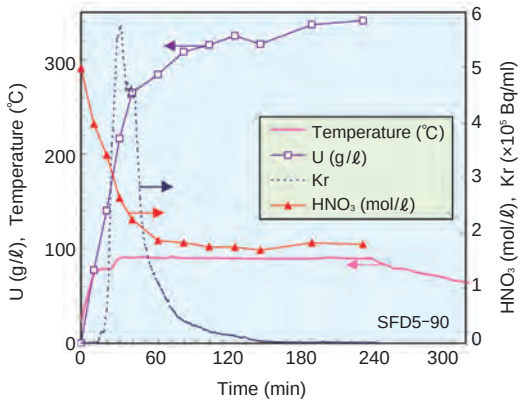

Fig.8-2 Changes in temperature and composition of working solution, and release behavior of Kr during MOX dissolution

The Handbook on Process and Chemistry of Nuclear Fuel Reprocessing containing these data is also published via the Internet. Frequent access to the website suggests that it has obtained many users including private companies.

8-1 New Nuclear Data Library for Science and Technology
—General Purpose Japanese Evaluated Nuclear Data Library JENDL-4.0—

Table 8-1 Comparison among evaluated nuclear data libraries
JENDL-4.0 contains more nuclear data than other evaluated data libraries.

Library	JEFF-3.1.1	ENDF/B-VII.0	JENDL-4.0
Developed by	Europe	USA	Japan
Released year	2009	2006	2010
No. of nuclides	381	393	406
No. of nuclides with γ-rays	139	206	354
No. of nuclides with covariances	37	26	95

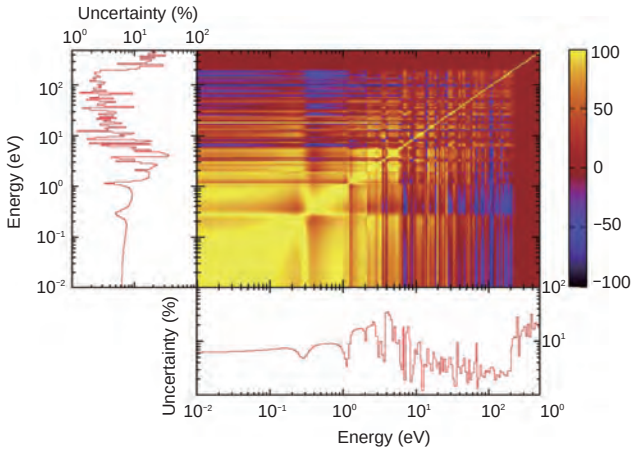

Fig.8-3 Example of covariance matrices (above)
The ^{235}U fission cross section covariance matrix is shown. The diagonal part represents the uncertainties in the cross section. The off-diagonal part shows the correlation between energy regions. Change in the cross section at an energy region affects cross sections in other energy regions.

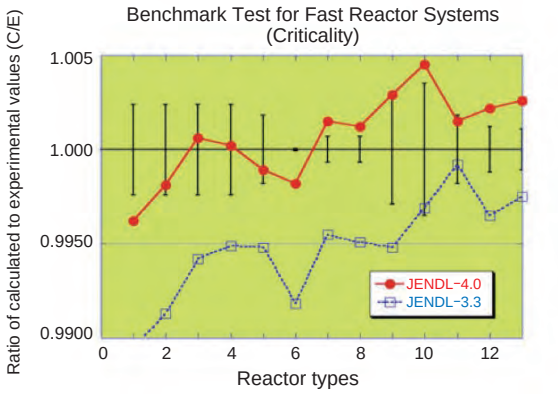

Fig.8-4 Example of criticality analysis for fast reactor systems
The ratio of calculated value (C) to experimental value (E) is shown. A value of 1.0 means good prediction performance. Calculations using JENDL-4.0 show better prediction performance than those using JENDL-3.3.

A new evaluated nuclear data library, JENDL-4.0, has been completed and released. The JENDL-4.0 library contains basic neutron reaction data, and is used in various kinds of nuclear science and technology fields.

The library contains the data of 406 nuclides. Following the release of the JENDL-3.3 library in 2002, users' needs and requests were incorporated into the new library. In particular, the data of minor actinides and fission products, which play an important role in high burnup reactors and disposal of nuclear waste, have been emphasized. Highly requested additional covariance data are also given in the new library, more than in the previous library. Table 8-1 shows a comparison among the main evaluated libraries. The JENDL-4.0 library surpasses other libraries not only in coverage of the nuclides it contains, but also in terms of covariance data and γ-ray production data.

An example of covariance data is shown in Fig.8-3. The figure shows the correlations for the ^{235}U fission cross section. The diagonal part indicates the uncertainties in the cross section itself and the off-diagonal part represents the correlation between energy regions. It shows the degree of the effect of a cross-section change in one energy region on the cross-section of another energy region.

Many benchmark tests have been performed to confirm the performance of JENDL-4.0. Fig.8-4 shows the results of tests for fast reactor systems. The ratios of calculated neutron multiplication factors to measured ones are given. A value of 1.0 means good performance. The results with JENDL-4.0 show improved performance.

The JENDL-4.0 library is an open library and can be freely used. The library can be downloaded from the website of the JAEA nuclear data center (http://wwwndc.jaea.go.jp/index.html) and other international websites like the IAEA NDS, and OECD/NEA Data Bank. The JENDL-4.0 library is thus expected to be used by researchers and engineers all over the world.

Reference

Namekawa, M., Katakura, J., Curves and Tables of Neutron Cross Sections in JENDL-4.0, JAEA-Data/Code 2010-017, 2010, 822p.

8-2 Operation of the Accurate Neutron-Nucleus Reaction Measurement Instrument Has Been Started

—To Obtain More Accurate Nuclear Data—

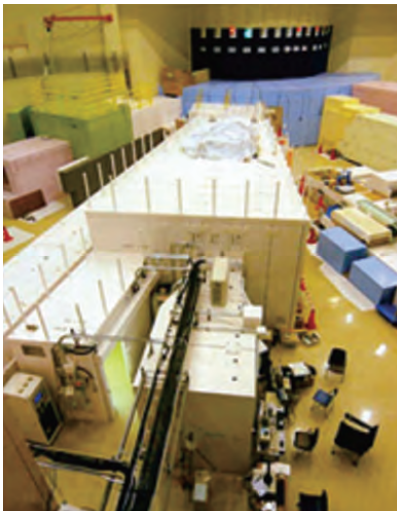

Fig.8-5 A photo of ANNRI
ANNRI is located on Beam Line No.04 of MLF in J-PARC.

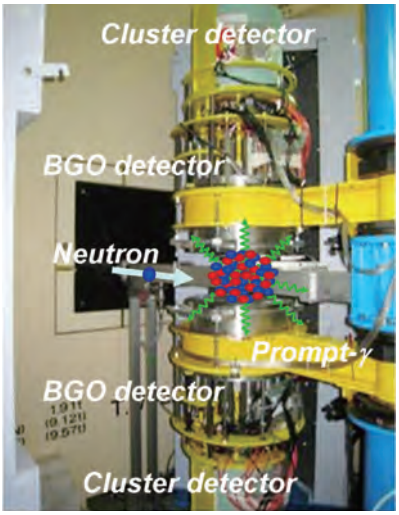

Fig.8-6 A photo of the 4π Ge spectrometer
The spectrometer consists of two cluster Ge detectors and eight coaxial Ge detectors.

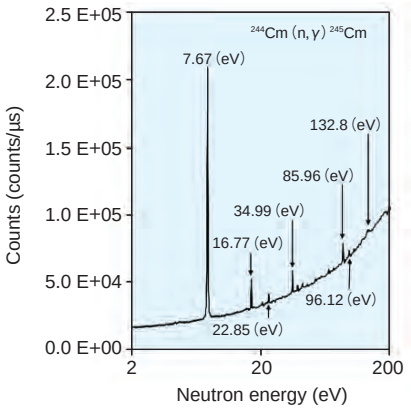

Fig.8-7 Neutron-capture γ-ray yields of a ^{244}Cm sample
The ^{244}Cm sample contained 0.6 mg curium oxide and its activity was 1.8 GBq.

Accurate data for neutron-capture cross sections are important in detailed engineering designs and safety evaluations of innovative nuclear reactor systems. In particular, neutron-capture cross sections of minor actinides (MAs) and long-lived fission products (LLFPs) have been attracting attention in the field of nuclear systems such as transmutation of radioactive waste and various innovative reactor systems. However, accurate measurements of these cross sections are very difficult due to the high radioactivity of these samples. To overcome this difficulty, the Accurate Neutron-Nucleus Reaction measurement Instrument (ANNRI) has been developed as a collaboration between Hokkaido University, Tokyo Institute of Technology, and JAEA. ANNRI is located on the Beam Line No.04 of the materials and life science experimental facility (MLF) in the Japan Proton Accelerator Research Complex (J-PARC). We have started to measure MAs and LLFPs cross sections with high intensity pulsed neutrons.

Fig.8-5 shows a photo of ANNRI and Fig.8-6 shows a photo of a large germanium (Ge)-detectors array named the 4π Ge spectrometer. The 4π Ge spectrometer is the main detector of ANNRI and is located at a flight length of 21.5 m. Using the Ge spectrometer with a neutron time-of-flight method, both energy of neutrons and prompt-γ rays are measured at the same time. The energy-integrated neutron intensities at the sample position are 4.5×10^6 n/s/cm^2 in the neutron energy range of 1.5-25 meV, and 6.6×10^5 n/s/cm^2 in 0.9-1.1 keV at a beam power of 120 kW. In the epithermal energy region, the energy-integrated neutron intensity is more than 7 times higher than the values of other instruments. Moreover, with the future 1 MW operation, these intensities are expected to increase to 4.3×10^7, and 6.3×10^6 n/s/cm^2, respectively.

As an example of neutron-capture cross-section measurements, Fig.8-7 shows neutron-capture γ-ray yields of a ^{244}Cm sample. Seven resonance peaks of ^{244}Cm are clearly observed. The 7.67 eV and 16.77 eV resonance peaks are the first such experimental results in the world. The ^{244}Cm sample contained 0.6 mg curium oxide and its activity was 1.8 GBq. The measurement time for the ^{244}Cm sample was about 33 hours.

The results of these experiments show that neutron-capture cross-sections can be deduced using ANNRI, where a small amount (less than 1 mg) of a highly radioactive sample can be used. In the near future, ANNRI will be used not only for nuclear data but also nuclear astrophysics and microanalysis.

Present study is the result of "Study on nuclear data by using a high intensity pulsed neutron source for advanced nuclear system" entrusted to Hokkaido University by the Ministry of Education, Culture, Sports, Science and Technology of Japan (MEXT).

Reference

Kiyanagi, Y., Kimura, A. et al., Neutron Nucleus Reaction Instrument, NNRI, Hamon, vol.20, no.1, 2010, p.21-24 (in Japanese).

8-3 Microscopic Observation of Deformation Process in Metallic Materials
—Computer Modeling of Defect Structure via Atomistic Simulation Methods—

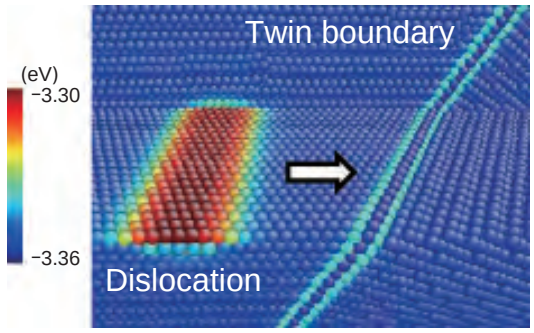

Fig.8-8 Atomic model of defect structures (dislocation and twin boundary)
An atomic model including a pure edge dislocation and a twin boundary is constructed. Atoms are color-coded according to potential energy.

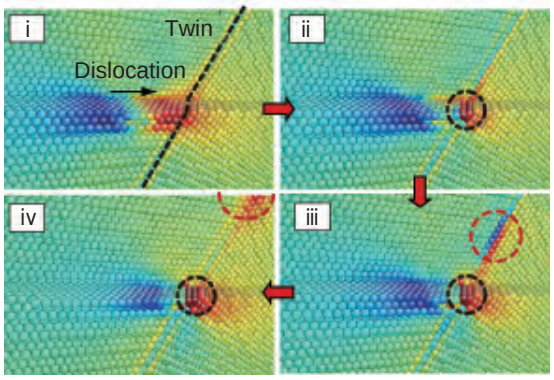

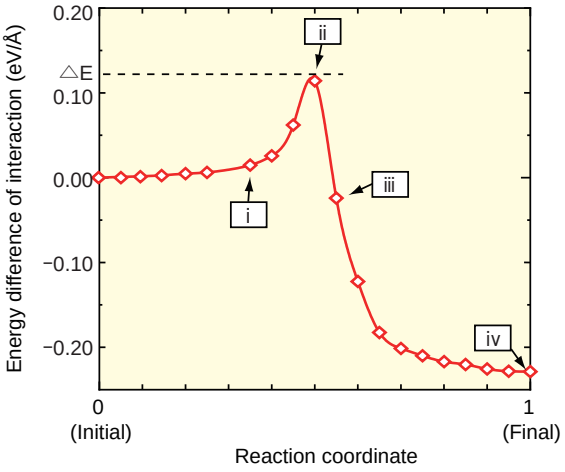

Fig.8-9 Reaction energy of the interaction between dislocation and twin boundary
The reaction energy along the minimum energy path of the interaction process per unit length of a dislocation is shown. The energy curve has a high energy peak.

Fig.8-10 Atomic configurations of the defect motion during the interaction process
Defect motion in the reaction process corresponding to the Roman numerals in Fig.8-9 is shown. The high energy state (ii) is equivalent to the moment of the interaction. Dissociated mobile and immobile dislocations are marked by red circles and black circles, respectively.

Reactor structural materials are constructed mainly from metallic materials. Most metallic materials have a defect structure in which local atomic arrangement is disordered, and mechanical properties such as plastic deformation and crack nucleation are determined by such a defect structure. Additionally, defect structures change from moment to moment under deformation. Therefore, it is important to understand the details of structural changes from the microscopic point of view. Among the various kinds of defect structures, dislocations and grain boundaries are the most significant factors in deformation characteristics and material strength. With the former, there is a disconnect region between planes in crystalline materials, and the latter are defined by the interface between two crystal grains. We investigated structural changes in these two typical defects via computational modeling. An atomic model of a dislocation and twin boundary in aluminum is shown in Fig.8-8. When shear stress is applied to the model, the dislocation is first activated and interacts with the twin boundary. An atomistic transition states method based on a nudged elastic band method was employed to evaluate the interaction process between the dislocation and the twin boundary. The energy difference along the minimum energy path of the interaction process is shown in Fig.8-9. It was found that this process needs to overcome a high energy barrier at the moment of the interaction. Atomic configurations during the interaction are shown in Fig.8-10, where the Roman numerals corresponds to those in Fig.8-9. The highest energy state occurs at the moment when the dislocation is approaching the twin boundary. We described the dissociation of a lattice dislocation into mobile and immobile dislocations. In summary, it was found that the twin boundary acts as a high energy barrier for the dislocation motion and that the dissociation of the glide dislocation gives rise to grain boundary sliding. Thus, we consider that computational simulations demonstrate great potential to understand defect dynamics under deformation at a microscopic level of view.

Reference

Tsuru, T. et al., Fundamental Interaction Process between Pure Edge Dislocation and Energetically Stable Grain Boundary, Physical Review B, vol.79, issue 1, 2009, p.012104-1—012104-4.

8-4 Rationalization of the Structural Design of Nuclear Components under Exposure to Intense Irradiation

— Development of a Concept for Assuring Integrity Applicable to Components with Reduced Ductility Due to Intense Irradiation —

Table 8-2 Systematic categorization of potential failure modes for a wide range of ductility
Failure modes for components with high and reduced ductility can be categorized according to crack initiation and loss of functions due to excessive deformation. Failure modes for each category are given in the table.

Category	Failure mode
Crack initiation	Crack initiation by a single load application
	Crack initiation by incremental deformation
	Initiation of fatigue cracking
	Crack initiation by environmental effects such as stress corrosion cracking
	Brittle fracture
Loss of functions due to excessive deformation	Excessive deformation by a single load application
	Incremental deformation
	Buckling

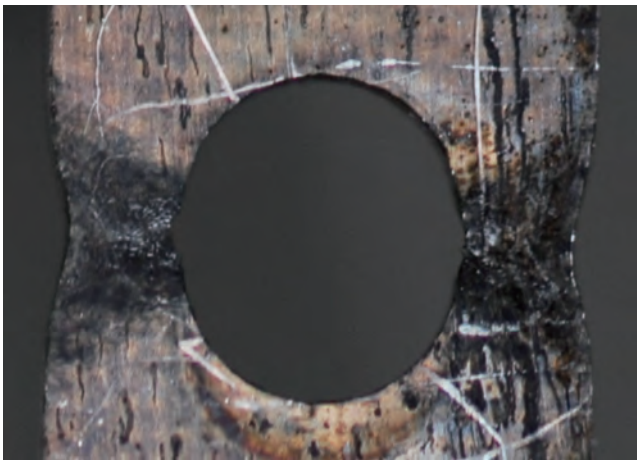

Fig.8-11 Deformation behavior of an intensely irradiated structure with a discontinuity
The structure with a hole in the center (initial diameter of the hole was approximately 2.5 mm) subjected to tensile loading shows that the center part of the structure (ligament) became unstable, leading to necking, similar to a simple tensile specimen according to the JIS standard. No cracking was observed on the surface at the maximum strain point (or at the edge of the circular hole).

Upgrading of fast breeder reactors, extension of operative duration of light water reactors, and development of fusion power systems require rationalization of component design under exposure to intense neutron irradiation. The components in use must meet the requirement that the tensile elongation of the component material be above a specified value (for example, 10%). However, the requirement is not always met in intense irradiation conditions.

Several studies reveal that under irradiation conditions up to tens of dpa (displacements per atom), even a material with reduced elongation has sufficient ductility, because even in a reduced elongation condition, the reduction in area (better ductility index) is sufficiently high. However, with further increases in irradiation neutron fluence, even the ductility is expected to gradually decrease. Therefore, a concept for assuring structural integrity has been developed for application to nuclear components where the ductility reduces as irradiation continues.

As the ductility decreases, the fracture mechanism changes (especially failure modes and deformation behavior). Therefore, although in current structural codes in which high ductility is required the tensile strength parameter as an alternative to fracture strain, has been used for generating design allowable limits, it is not appropriate to use this parameter in such reduced ductility conditions. Thus we first identified failure modes, especially with regard to how the modes change with reduced ductility, and then we elaborated a universal categorization of failure modes in order to systematically develop the concept to apply it to a wide range of ductility, ranging from high to reduced. At a low temperature where creep phenomena are not observed, we found that the modes are categorized into a crack initiation group and a loss of function due to excessive deformation group, as summarized in Table 8-2.

Next, for each failure mode, we considered what kinds of limiting parameters should be selected for generating design allowable limits. The key conclusion is that the limiting parameter should be selected by considering which occurs first: localized deformation due to tensile plastic instability, or crack initiation. Systematic selection criteria were then developed for application to a wide range of ductility. The applicability of the selection criteria was not clear in structures with discontinuous configurations which cause complicated deformation behavior, and tensile testing of an intensely irradiated structure with a discontinuity was conducted. The discontinuity was a circular hole in the center of a flat plate. The deformation of the structure just before fracture is shown in Fig.8-11. After passing the maximum load point, the plastic deformation became unstable and localized, and at that time no crack initiation was observed on the surface. Such a localized deformation or necking is often observed in tensile testing of a simple tensile test specimen according to the Japanese Industrial Standards (JIS). Accordingly, it can be concluded that the selection criteria are applicable to structures with actual configurations.

A part of the present study was performed under the sponsorship of Japan Nuclear Energy Safety Organization (JNES) Fundamental Research Project on Nuclear Safety.

Reference

Suzuki, K. et al., Intensely Irradiated Steel Components: Plastic and Fracture Properties, and a New Concept of Structural Design Criteria for Assuring the Structural Integrity, Nuclear Engineering and Design, vol.240, issue 6, 2010, p.1290-1305.

8-5 To Clarify Material Characteristics from the View Point of Microstructure
—Image Based Modeling of Ceramic Material Using X-ray CT—

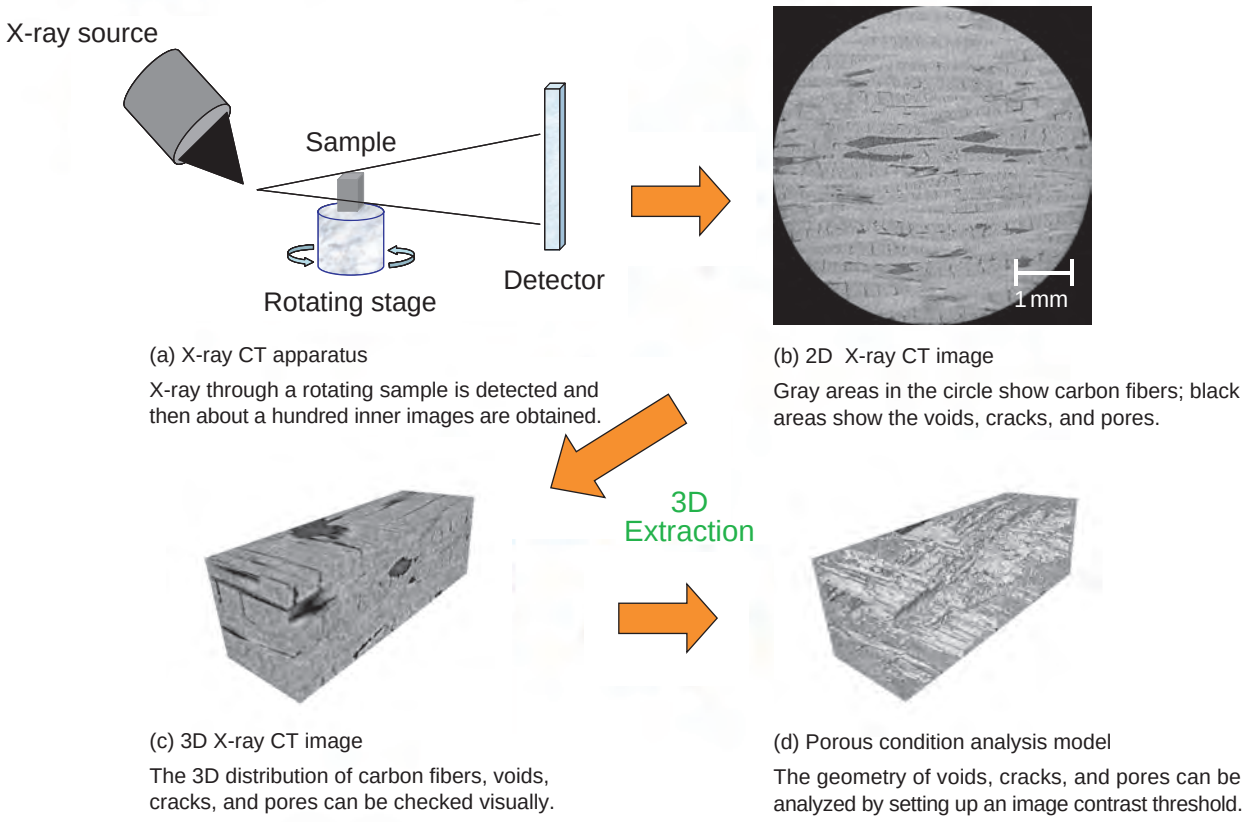

(a) X-ray CT apparatus

X-ray through a rotating sample is detected and then about a hundred inner images are obtained.

(b) 2D X-ray CT image

Gray areas in the circle show carbon fibers; black areas show the voids, cracks, and pores.

(c) 3D X-ray CT image

The 3D distribution of carbon fibers, voids, cracks, and pores can be checked visually.

(d) Porous condition analysis model

The geometry of voids, cracks, and pores can be analyzed by setting up an image contrast threshold.

Fig.8-12 Image based modeling using X-ray CT

In order to develop a Very High Temperature Reactor (VHTR), which is a promising candidate for a Generation IV nuclear energy system, studies are being carried out on the technology for lifetime extension of in-core graphite and for the application of ceramic components. It is important to evaluate irradiation-induced change in the properties of graphite materials, such as dimensional change, Young's modulus, etc., for lifetime assessment of the graphite components. These properties are strongly dependent on irradiation-induced change in the graphite microstructure (crystal grains and pores). Carbon fiber reinforced carbon composite (C/C composite) is made of carbon fibers impregnated with resin through a baking process in fabrication. It is one of the candidate materials for ceramic components of the VHTR. C/C composite contains many micro voids, cracks, and pores generated in the fabrication process, which strongly influence its material properties. It is thus necessary to develop an evaluation method for the properties of the material based on its microstructure.

A new study has just been started to try to correlate the microstructures of graphite and C/C composite to their material properties by means of image-based modeling using X-ray computed tomography (X-ray CT), in cooperation with Toyo Tanso Co., Ltd. In this correlation method, the size and distribution of crystal grains and pores are quantified in micro regions by three-dimensional (3D) X-ray CT images and the material properties are then evaluated. As the first step of this study, the applicability of image based modeling with 3D X-ray CT images (Fig.8-12) was investigated for the C/C composite, provided by Toyo Tanso. To evaluate the porous condition from the X-ray CT images, it is necessary to binarize the images to distinguish between solid elements and pores. An analytical model was successfully developed through detailed X-ray CT image analysis and by setting appropriate threshold values for image binarization. Moreover, it was confirmed that this method can be also applied to graphite material.

The model correlating the microstructures of graphite and carbon material to their properties is now being developed using the above analytical method. This methodology is expected to enable us to predict irradiation-induced change in the properties of graphite materials, and to evaluate the lifetime of graphite components. It is also useful for the design of new graphite and carbon materials, and could greatly contribute to the general industrial field.

Reference

Sumita, J. et al., Investigation of Microstructural Change by X-ray Tomography and Anisotropic Effect on Thermal Property of Thermally Oxidized 2D-C/C Composite for Very High Temperature Reactor, Journal of Nuclear Science and Technology, vol.47, no.4, 2010, p.411-420.

8-6 High Performance Extraction Separation Systems Using Ionic Liquids
—Application to Extraction of Metal Ions and Proteins—

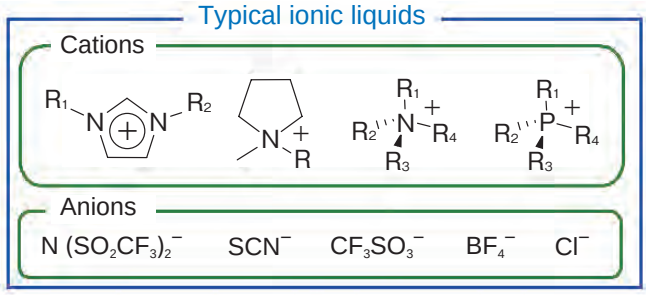

Fig.8-13 Molecular structures of typical ionic liquids

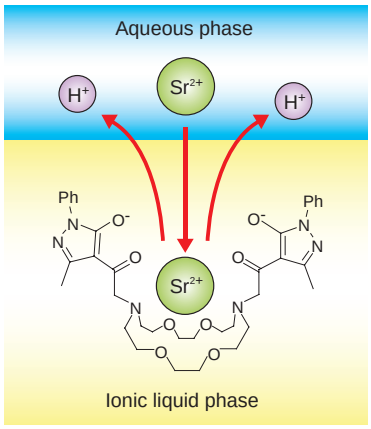

Fig.8-14 Extraction of strontium ions into ionic liquids with diazacrown ether bearing β-diketone fragments
Modification of diazacrown ether with β-diketone groups creates an intramolecular synergistic effect in an ionic liquid system, and provides remarkably high extraction performance.

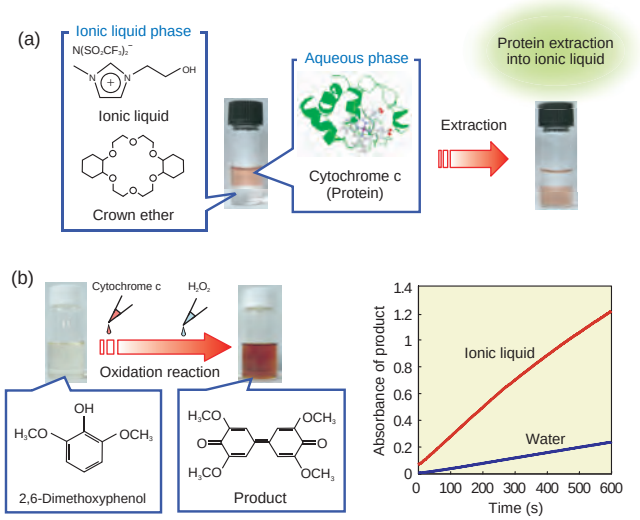

Fig.8-15 Protein extraction into ionic liquid and biocatalytic reaction
(a) Cytochrome c (red) is extracted from the aqueous phase (upper phase) into the ionic liquid phase (lower phase) through formation of a supramolecular complex with crown ethers. (b) Cytochrome c, which is an electron-transfer protein, cannot function as an enzyme. Cytochrome c in water displays minor peroxidase activity in the oxidation reaction of 2,6-dimethoxyphenol, whereas cytochrome c in the ionic liquid offers high peroxidase activity, and accelerates the oxidation reaction rate.

Ionic liquids, which are entirely composed of ions, are room temperature molten salts (Fig.8-13). Ionic liquids have potential as a green solvent, because they possess attractive properties such as negligible volatility and nonflammability. Their chemical and physical properties are effectively tunable, depending on the combination of cations and anions. For example, ionic liquids can be made hydrophobic while retaining ionicity and high polarity. Thus one can synthesize ionic liquids that are immiscible in water and organic solvents. Their unique properties have encouraged us to develop novel extraction separation systems using ionic liquids as extracting media.

Solvent extraction is one of the most effective separation methods for hydrometallurgy, reprocessing of nuclear wastes and recovery of rare metals from industrial wastes. We investigated extraction of precious metal ions, lanthanides and actinides using various extractants into ionic liquids as alternative replacements for conventional organic solvents. Application of ionic liquids was found to provide unprecedented enhancement of extraction performance compared with a conventional organic solvent system.

In solvent extraction, it has sometimes been observed that extraction performance is dramatically enhanced by using two different extractants compared with using only a single extractant. This phenomenon is known as a synergistic effect. Recently, we synthesized diazacrown ether bearing two β-diketone fragments as a novel extractant, and applied it to the extraction of strontium ions (Sr^{2+}). The extractant generates an intramolecular synergistic effect only in the ionic liquid extraction system, and demonstrated very efficient extraction of Sr^{2+} compared with an organic solvent extraction system (Fig.8-14).

Furthermore, we succeeded in extracting a protein into ionic liquids, and demonstrated that the protein in ionic liquids provides a new functionality to catalyze oxidation reactions (peroxidase). As shown in Fig.8-15, a hydroxyl-group-containing ionic liquid that has high affinity for the heme protein cytochrome c was synthesized, and the ionic liquid with a crown ether that can recognize the surface of cytochrome c was found to be capable of quantitative partitioning of cytochrome c. We clarified that cytochrome c in the ionic liquid causes a structural transformation, which triggers its functional conversion from an electron transfer protein to peroxidase.

Reference

Shimojo, K. et al, Cooperative Intramolecular Interaction of Diazacrown Ether Bearing β-Diketone Fragments on an Ionic Liquid Extraction System, Dalton Transactions, no.25, 2009, p.4850-4852.

8-7 How Does Radiation Influence Cells, the Human Body, and the Earth?
—Integration of Radiation Transport Simulations for Different Scales—

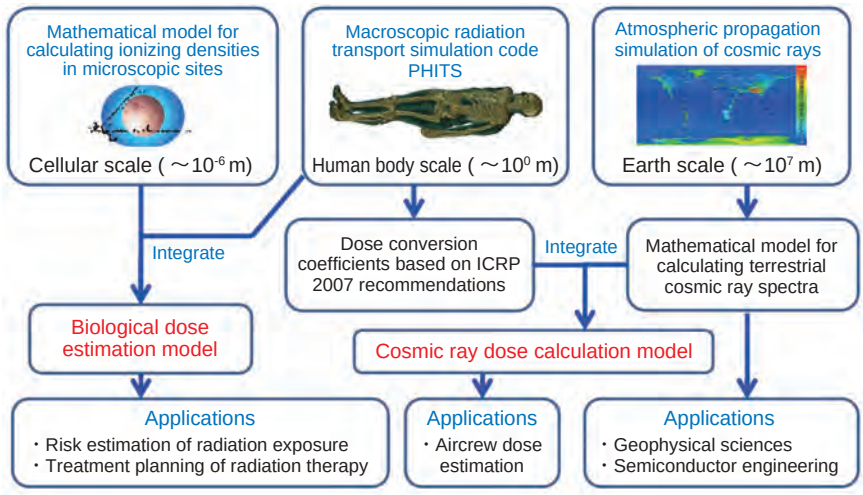

Fig.8-16 Outline of this study
The left and right sides of this figure show the outlines of the integration of radiation transport simulations between cellular and human-body scales and that between human-body and planetary scales, respectively.

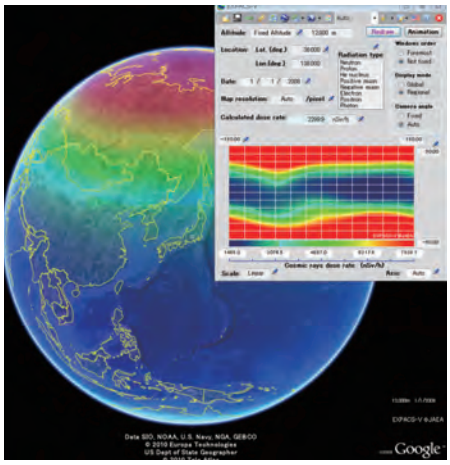

Fig.8-17 EXPACS-V screenshot
http://phits.jaea.go.jp/expacs/

Recently, high-energy particles are widely used for radiation therapy owing to their high relative biological effectiveness (RBE). On the other hand, their high RBE has adverse effects in cases of undesirable exposure, such as aircrews being exposed to high-energy cosmic rays. Integrated study of radiation transport simulations on different scales is necessary for elucidating the influences of such high-energy particles on matter.

We therefore integrated radiation transport simulations for cellular and human body level scales, and developed a biological dose estimation model for the human body based on individual cellular responses (left side of Fig.8-16). For that purpose, first we established a mathematical model that can instantaneously calculate the ionizing densities in microscopic sites on the basis of microscopic radiation transport simulations. This model was implemented in the macroscopic radiation transport simulation code PHITS, and the improved PHITS enables us to estimate the survival fractions of cells inside the human body within a reasonable computation time.

We also integrated radiation transport simulations for the human body and planetary scales, and developed a novel calculation model for cosmic ray dose rates any time and anywhere in the world (right side of Fig.8-16). For that purpose, we calculated fluence-to-effective dose conversion coefficients for various particles over a wide energy range, based on the 2007 recommendations of the International Committee on Radiological Protection (ICRP). Simultaneously, a mathematical model that can calculate terrestrial cosmic ray spectra as functions of altitude, latitude, longitude, and date was established by performing an atmospheric propagation simulation of cosmic rays using PHITS. The cosmic ray dose rates can be easily estimated using this mathematical model coupled with calculated dose conversion coefficients. Software for visualizing the cosmic ray dose rates on Google Earth™ maps was also developed, and opened to public via the Internet (Fig.8-17).

The biological dose estimation model we established can be utilized not only in radiation exposure risk estimation but also in high energy particle therapy treatment planning. The cosmic ray dose calculation model is currently employed in aircrew dose estimation in Japan to preserve their annual dose limits. The mathematical model for calculating terrestrial cosmic ray spectra is also used in various research fields such as the geophysical sciences and semiconductor engineering.

References

Sato, T. et al, Development of PARMA: PHITS-Based Analytical Radiation Model in the Atmosphere, Radiation Research, vol.170, issue 2, 2008, p.244-259.
Sato, T. et al, Biological Dose Estimation for Charged-Particle Therapy Using an Improved PHITS Code Coupled with a Microdosimetric Kinetic Model, Radiation Research, vol.171, issue 1, 2009, p.107-117.

8-8 Simple and Low-Cost New Recovery Technology "Emulsion Flow"

—Extending Radioactive Liquid Waste Treatment to Effluent Purification Technology—

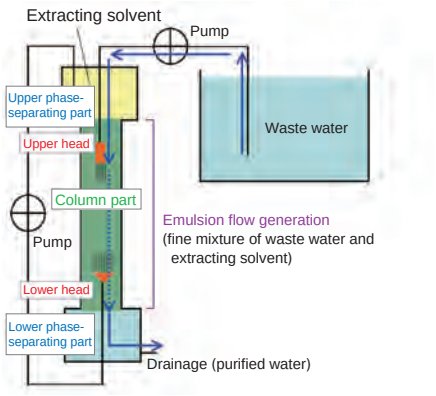

Fig.8-18 Overview of emulsion flow method
By generating fine-grained liquid droplets at a head, a flow of emulsion (emulsion flow) arises in a column part, and the emulsion then promptly disappears by itself in a phase-separating part.

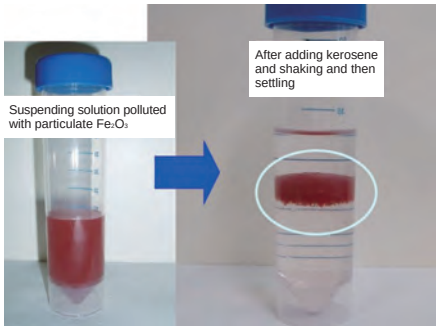

Fig.8-19 Aspects of the emulsion flow apparatus and the apparatus in use
On the top left, the inactive emulsion flow apparatus is shown. In the square box set off by a dashed line, the appearance of fine-grained liquid droplets generated at the head, the emulsion flow occurring in the column part, and the disappearance of the emulsion in the phase-separating part are shown.

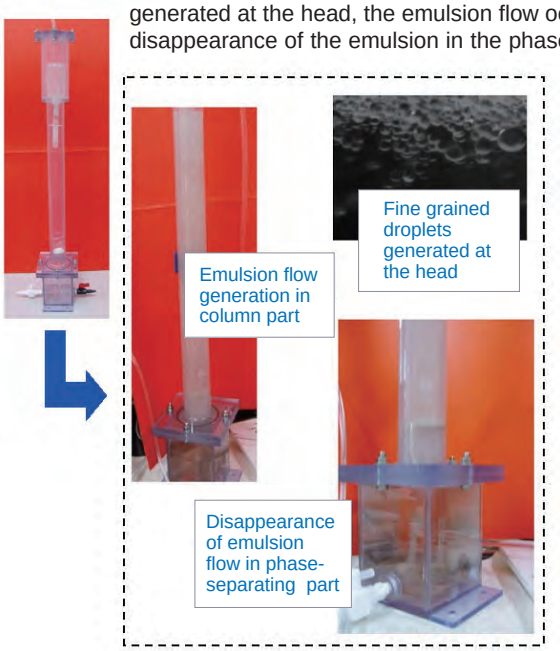

Fig.8-20 Example of particulate component removal
By adding kerosene to an aqueous suspending solution containing fine particles of Fe_2O_3 and then shaking, the particles accumulate at the liquid-liquid interface between the aqueous and organic phases, and are thus removed from the suspending solution.

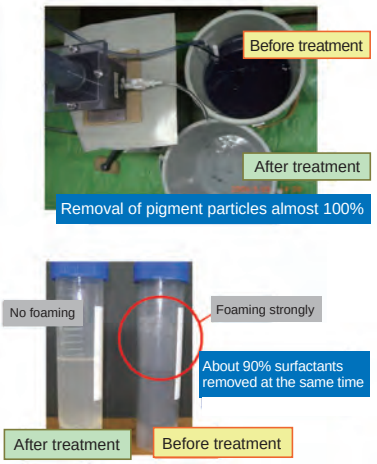

Fig.8-21 Example of purifying a paint waste solution
A paint waste solution is purified by removing both pigment particles and dissolving surfactants at the same time.

Emulsion flow is a new technology that permits low-cost, easy, and rapid recovery or removal of both dissolved and particulate components in water using a simple and compact apparatus and an organic solvent immiscible in water, such as paraffin. In emulsion flow, dissolved components such as metal ions are recovered by liquid-liquid extraction (solvent extraction) and particulate components such as suspended matter are removed by liquid-liquid interfacial aggregation. Both of these components can be recovered (or removed) at the same time.

Liquid-liquid extraction is a method for extracting a target component from an aqueous solution into an organic solvent immiscible in water, which is very popular in industry. In liquid-liquid extraction using an emulsion flow apparatus, the flow of an emulsion, which is a fine mixture of aqueous and organic phases, arises in a column part by generation of fine-grained liquid droplets at a head, and the emulsion then promptly disappears by itself when it reaches a phase-separating part (Fig.8-18 and Fig.8-19). In other words, aqueous and organic phases can be effectively mixed and emulsified by only sending liquid. Therefore, the emulsion flow is markedly low-cost and simple compared with conventional apparatuses (mixer-settler, etc.). In addition, phase separation promoted by a change in the flow rate enables a rapid treatment with a compact apparatus.

Emulsion flow was developed to be used in the treatment of radioactive waste solutions produced in the decommissioning of nuclear facilities and equipment, and has achieved remarkable progress toward practical use. Recently, emulsion flow has received much attention not only in the nuclear field but also many other industrial fields as a simple and low-cost new technology to purify drainage water and to collect rare metals from industrial waste water.

The emulsion flow method is also used for collecting particulate components like suspended matter. Fig.8-20 shows that a suspending solution polluted with Fe_2O_3 as a particulate component is purified by shaking with kerosene, i.e., Fe_2O_3 is accumulated at the water/oil interface. By doing this in an emulsion flow manner, particulate components in water can be removed effectively without any filter or flocculant. We show an instance of applying the emulsion flow to purifying a waste water containing automotive aqueous paint in Fig.8-21. The pigment particles can be removed almost completely (about 100%) from the waste water (upper part of Fig.8-21). At the same time, about 90% of surfactants dissolved in the waste water can also be removed. Before the emulsion flow treatment, there was intense foaming in waste water because such surfactants are like soaps. In contrast, after the treatment, no foaming is seen (lower part of Fig.8-21). This is evidence of the removal of the surfactants from the waste water.

References

Naganawa, H. et al., Countercurrent Emulsion Flow Continuous Liquid-Liquid Extraction Apparatus, Patent Application Publication, pub.no.JP2010-082531.
Naganawa, H. et al., Method for Continuously Collecting Particle Component in Solution, Patent Application Publication, pub.no.JP2010-082530.

Research on HTGR and Nuclear Heat Applications to Attain a Low-Carbon Society

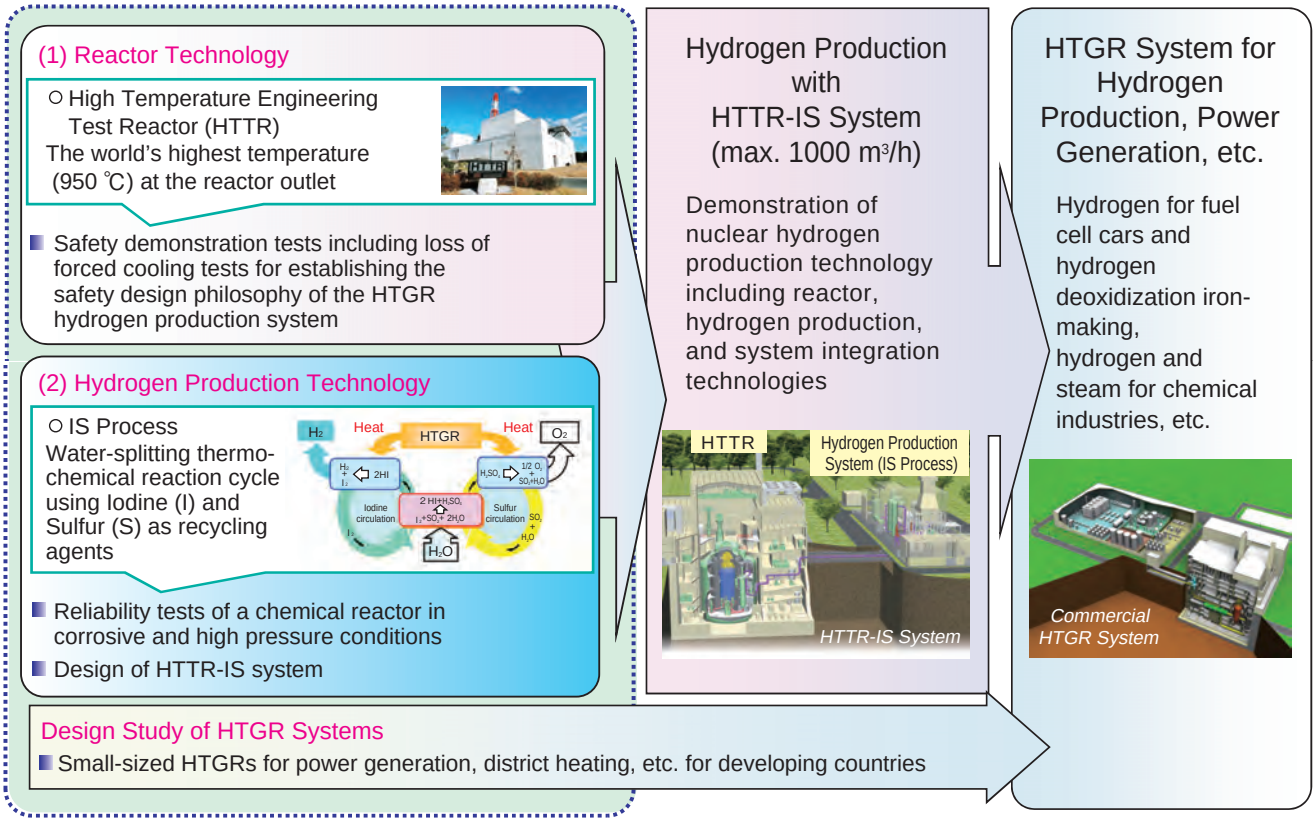

Fig.9-1 Plan of research on HTGR and nuclear heat applications
In order to diversify nuclear heat applications to non-electric fields such as transportation, iron-making, and chemical industries and attain a low-carbon society, we are carrying out research on HTGR, which can produce heat above 900 ℃, and nuclear heat applications.

The breakdown of Japan's energy consumption and CO_2 emissions in each field shows that utilization of heat in transportation and industry by combustion of fossil fuels accounts for around 70%. In order to achieve a greater than 50% reduction in overall carbon emissions to restrain global warming and attain a low-carbon society, diversification in the use of nuclear heat such as process heat and steam for chemical industries, district heating, desalination, and so on, as well as production of clean energy such as hydrogen, is indispensable. In particular, the demand of hydrogen for fuel cell cars and hydrogen deoxidization iron-making is expected to grow dramatically in the near future. Furthermore, in order to meet the growing demands for energy in developing countries while restraining global warming, deployment of nuclear power plants, especially those with small-sized reactors, is necessary because remote regions and cities in developing countries require a relatively small energy plant to produce affordable electricity and district heating, and to potentially generate new energy products to develop local economies. In particular, High Temperature Gas-cooled Reactors (HTGR), which feature superior inherent safety and economies despite their small size, can supply heat above 900 ℃ and meet the diverse energy demands described above. HTGRs can thus meet the energy production requirements for global greenhouse gas reduction.

We are carrying out HTGR research and development particularly with regard to reactor technology and heat utilization technology for the commercialization of an electricity and hydrogen cogeneration HTGR system (Fig.9-1). Japan's first high-temperature gas-cooled reactor, named the High-Temperature Engineering Test Reactor (HTTR), located at the Oarai Research and Development Center, is a graphite moderated and helium gas-cooled reactor with 30 MW thermal power and a maximum temperature of 950 ℃ at the reactor outlet. The first criticality of the HTTR was achieved in 1998, and 30 MW full power operation was attained in 2001 with a reactor outlet temperature of 850 ℃. Safety demonstration tests have been conducted since 2002. The first high temperature operation and first continuous operation at 950 ℃ for 50 days were successfully conducted in 2004 and 2010, respectively.

In terms of hydrogen production technology, a thermochemical hydrogen production cycle called the IS (Iodine-Sulphur) process has been developed step by step. In June 2004, continuous hydrogen production using a bench-scale test apparatus made of glass was successfully achieved, with a hydrogen production rate of about 30 ℓ /h for 1 week. Reliability tests of a chemical reactor in corrosive and high pressure conditions are now being conducted. The goal of the HTTR project is to demonstrate nuclear hydrogen production using the IS process connected with the HTTR by 2020, which will yield a hydrogen production rate up to 1000 m^3/h.

Design study of a small-sized HTGR system is also ongoing.

9-1 Toward Efficient Hydrogen Production in IS Process
—Development of a Radiation-Grafted Membrane for HI Concentration—

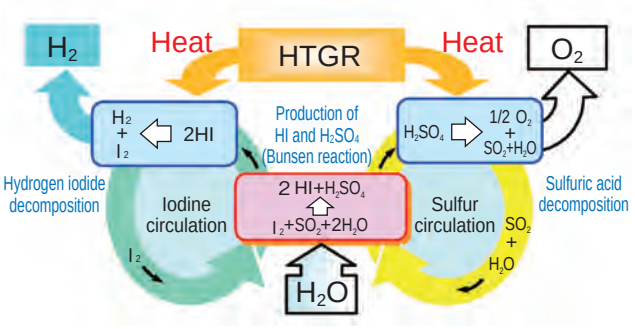

Fig.9-2 Schematic representation of the IS process
Hydrogen and oxygen are generated by thermally decomposing hydriodic and sulfuric acid, respectively, which are produced from water by a reaction with iodine and sulfur dioxide.

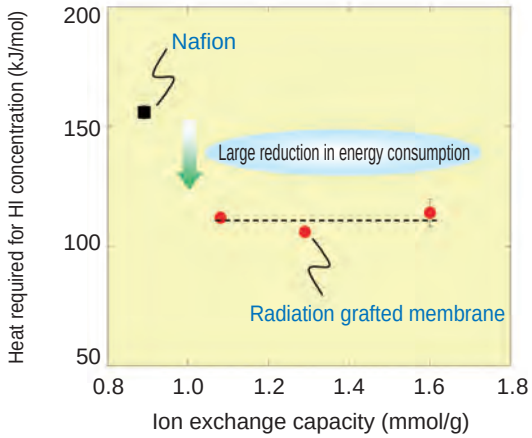

Fig.9-4 Performance comparison between radiation-grafted membranes and commercially available membranes
Compared to commercially available membranes (Nafion), the heat requirement for HI concentration can be greatly reduced by using radiation-grafted membranes.

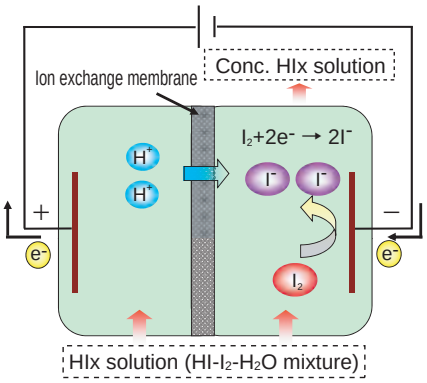

Fig.9-3 Concept of HI concentration using the ion exchange membrane
Hydriodic acid can be concentrated with the aid of a redox reaction of iodine-iodide ions at electrodes and selective proton permeation through the ion exchange membrane.

We have been investigating a hydrogen production method, the Iodine-Sulfur (IS) process, using a High Temperature Gas-cooled Reactor (HTGR) as the heat source. The IS process is a water-splitting thermochemical reaction cycle using Iodine (I) and Sulfur (S) as recycling agents (Fig.9-2). This technology is not only capable of expanding the use of nuclear energy, but can also contribute to carbon dioxide reduction through non-utilization of carbon sources such as fossil fuels.

The IS process, in which nuclear heat supplied by the HTGR is converted into hydrogen chemical energy, is expected to produce hydrogen with thermal efficiency of over 40%, exceeding that of conventional technologies such as water electrolysis. Efficient separation of HI from hydriodic acid (HI solution) is an important part of realizing this goal, and in this area we have been studying a separation technology using an ion exchange membrane (Fig.9-3).

The membrane is required to exhibit long-term stability in the HI solution and to possess high proton permeation selectivity. However, no commercially available membrane shows satisfactory performance.

Therefore, we conducted research to prepare a novel ion exchange membrane suitable for HI concentration using a radiation grafting method, which enables us to control the important membrane properties such as the ion exchange capacity (IEC), and which has been successfully applied to the preparation of ion exchange membranes for fuel cells.

Using poly (ethylene-co-tetrafluoroethylene) as the base film, cation exchange membranes with various IECs were prepared and their performance was examined. By analyzing the experimental results, it was shown that the heat energy required for the HI concentration could be significantly reduced compared to commercially available membranes (Fig.9-4).

In addition, a separate experimental study on the chemical stability of radiation-grafted membranes in an HI solution has revealed that the stability can be improved by chemical cross-linking treatment. In order to develop reliable membranes, we will continue our research on optimizing the synthesis conditions.

Reference

Tanaka, N. et al., Electro-Electrodialysis of HI-I_2-H_2O Mixture Using Radiation-Grafted Polymer Electrolyte Membranes, Journal of Membrane Science, vol.346, issue 1, 2010, p.136-142.

9-2 Towards a Stable Operation of Nuclear Hydrogen Production Systems
—Sequence Control Against Abnormal Events in Hydrogen Production Plants—

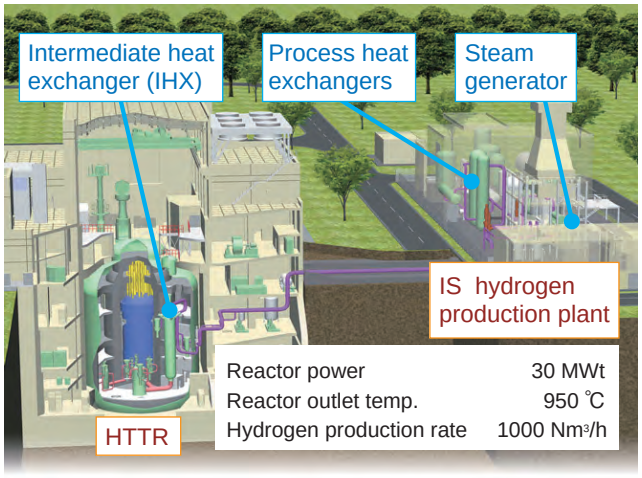

Fig.9-5 HTTR-IS nuclear hydrogen production system
The heat produced by the reactor core transfers to the secondary cooling system at the intermediate heat exchanger. The secondary coolant provides heat to process heat exchangers in the IS hydrogen production plant.

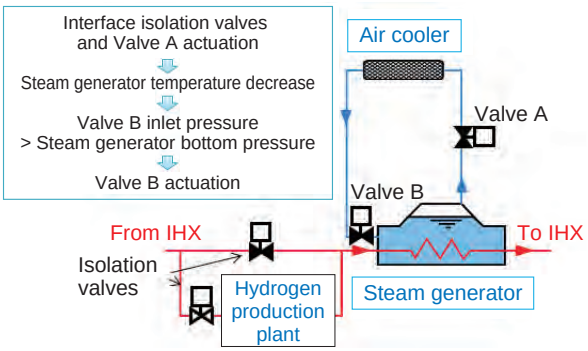

Fig.9-6 Sequence control for mitigation of load variation
Sequence control developed for mitigation of load variations induced by abnormal events in the IS hydrogen production plant.

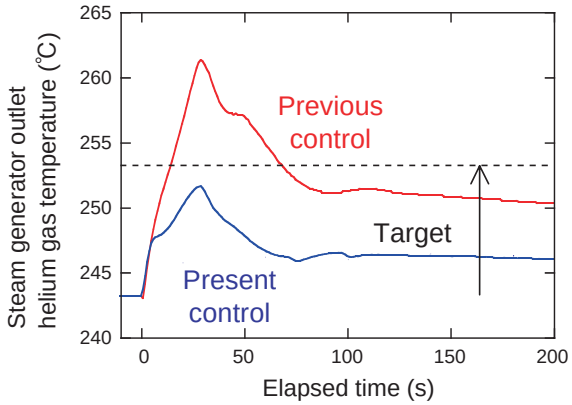

Fig.9-7 The efficacy of a proposed control (calculation)
The simulation results show that coolant temperature increase at the steam generator outlet can be suppressed by the proposed sequence control.

High temperature gas-cooled reactors are expected to significantly contribute to CO_2 emissions reduction not only in terms of power production but also by non-electric applications such as hydrogen production. JAEA has been planning to construct a hydrogen production system connected to the High Temperature Engineering Test Reactor (HTTR), the HTTR-IS system, which will be the world's first demonstration of nuclear hydrogen production (Fig.9-5).

One of the key technology requirements for the nuclear hydrogen demonstration is to mitigate the impact of thermal load variations at process heat exchangers in the IS hydrogen production plant induced by abnormal events, such as malfunctions of control systems, incorrect operations, etc. Such load variations initiate temperature transients, and the transients transfer to the primary cooling system. This would cause a reactor scram since variations are strictly limited in order to prevent structural issues because of excessive thermal stresses. Hence, mitigation of load variations is crucial for the stable operation of nuclear reactors. We have been carrying out the design of a thermal load mitigation system consisting of a steam generator and an air cooler. We also developed a plant dynamics code for the system, and the feasibility of the mitigation system has been confirmed. However, the previous control system is not acceptable in a case in which isolation from the secondary cooling system is required, as it is in the case of IS hydrogen production plants, since the increase in the rate and amount of the thermal load is significantly large.

We are developing sequential control interfacing isolation valves at Valve A, which permits mitigation of the helium gas temperature variation at the steam generator outlet. Also, actuation conditions of the valves have been identified in which stable natural circulation between the steam generator and air cooler can be performed without operator intervention (Fig.9-6). Simulation results clearly showed that continuous reactor operation can be attained in the case of abnormal events in hydrogen production plants (Fig.9-7). Further developments will include the validation of the plant dynamics code which will be used for safety evaluation of the HTTR-IS system.

Reference

Sato, H. et al., Thermal Load Control Methods for the HTTR-IS Nuclear Hydrogen Production System, Nippon Genshiryoku Gakkai Wabun Ronbunshi, vol.7, no.4, 2008, p.328-337 (in Japanese).

10 Nuclear Fuel Cycle Technological Development

Toward the Establishment of the Nuclear Fuel Cycle

We are carrying out development of technologies for reprocessing the spent fuel of light water reactors, treatment and disposal of radioactive waste, and so on, in order to establish the nuclear fuel cycle. We are also carrying out technological cooperation with Japan Nuclear Fuel Limited (JNFL), which was founded to advance the nuclear fuel cycle business.

1. Development of reprocessing technologies

To promote reprocessing and usage of plutonium for light water reactors by the private sector, taking private sector needs into account, we are instituting research and development for reprocessing uranium-plutonium mixed oxide (MOX) spent fuel for the Fugen reactor and vitrification of the high-level radioactive liquid waste. To develop the vitrification technologies we are instituting developments such as a technology for removing deposits inside the melter, a technology for measuring the shape inside the melter, measures to extend the life of the melter, and a melter structure design to decrease deposits of platinoid elements. To develop technologies for volume reduction and stabilization of low-level radioactive waste, we are investigating solidification conditions for phosphate liquid waste and slurry waste, and experimenting with nitrate decomposition of low-level liquid waste including nitrates (Fig.10-1) for the design of a cement solidification facility.

2. Technological cooperation

JAEA's technological cooperation with JNFL (Fig.10-2) includes the technological development of a new type of centrifuge equipment for uranium enrichment, support of the active test at the Rokkasho Reprocessing Plant (RRP), and designing a MOX fuel fabrication facility. Currently, we are particularly supporting the active-test of the high-level radioactive liquid waste vitrification facility at the RRP by dispatching specialist engineers in vitrification technology and teleoperation technology, mock-up testing (Fig.10-3), joint research, and so on.

In addition to the above, JAEA engineers are dispatched to the Nuclear Material Control Center and are engaged in technical support for nuclear material control in the Rokkasho district. We are also carrying out training for engineers of the Nuclear Fuel Chemical Analysis Co. (a limited liability partnership) which undertakes analysis of uranium and plutonium, etc., at the RRP.

Fig.10-1 Nitrate decomposition experiment
To reduce nitrogen of nitrate origin, we are investigating nitrate decomposition in liquid waste including nitrates for the treatment and disposal of low-level radioactive waste.

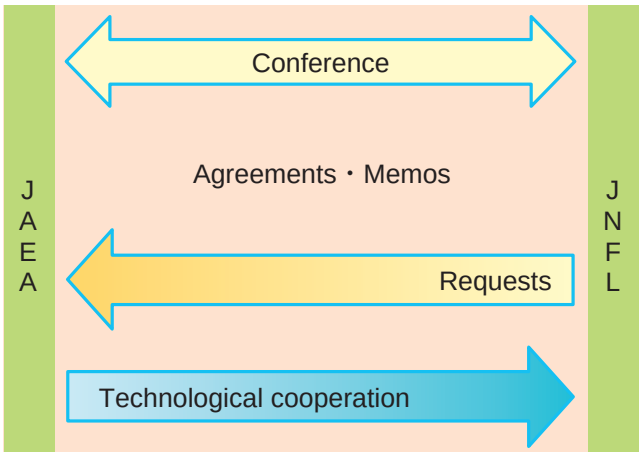

Fig.10-2 Technological cooperation with JNFL
JAEA is transferring its achievements in development of the nuclear fuel cycle to JNFL, mainly through personnel support such as education, training, and the dispatch of JAEA engineers, as well as the direct supply of information.

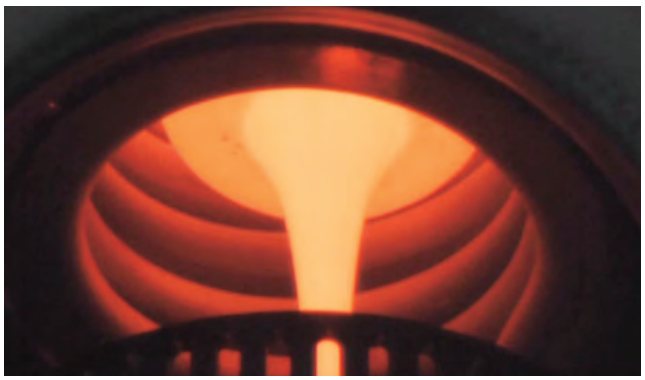

Fig.10-3 Molten glass outflow situation
Vitrification mock-up examinations are carried out as part of the technical support for the active-test of the vitrification of high-level radioactive liquid waste facility at the Rokkasho Reprocessing Plant.

10-1 Advanced Treatment Technology for Low-Level Radioactive Reprocessing Effluent
—Aiming at Establishing Cement-Based Encapsulation Technology—

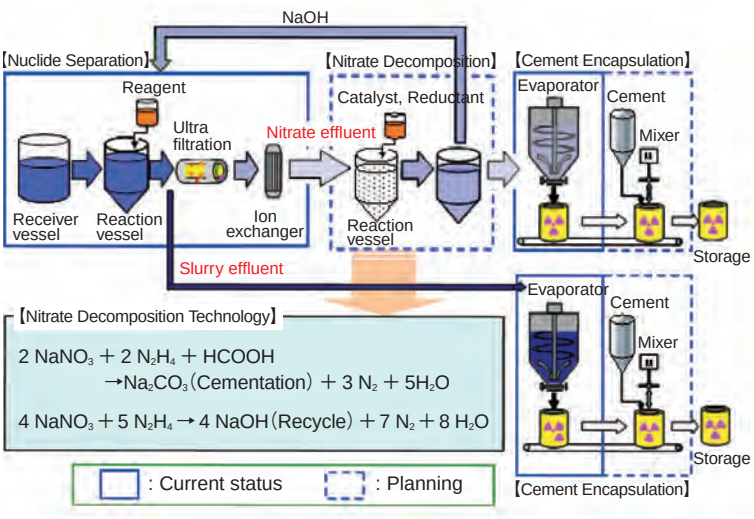

Fig.10-4 Current status and planning of the effluent treatment
Concentrated effluent and phosphate effluent at the Tokai Reprocessing Plant will be treated at the LWTF for disposal underground. To reduce the disposal cost, the concentrated effluent will be separated into a slurry effluent including radionuclides and a nitrate effluent that barely contains any radionuclides. It is planned that the nitrate in the nitrate effluent will decompose and change into carbonate to reduce nitrate-nitrogen emission at a disposal site.

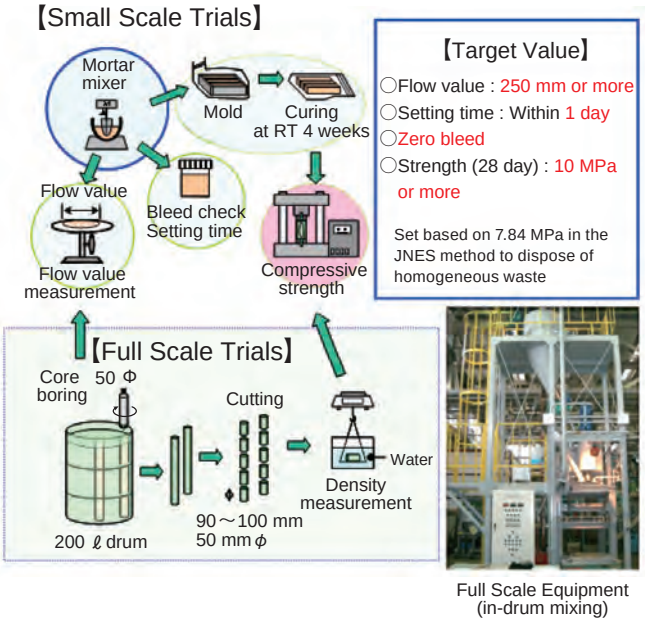

Fig.10-5 Diagram of cement based encapsulation trials

We are carrying out development work to install cement based encapsulation equipment at the Low-level radioactive Waste Treatment Facility (LWTF) (Fig.10-4). The effluent from the nuclide separation process is evaporated and encapsulated using an in-drum mixing technique. Because the ratio of water to salt is too high due to the efficiency of the evaporator, bleed water appears when commercial cement is used, and thus we adopted a special cement based on fine grains of blast furnace slag (BFS), which are capable of dealing with the surplus water. It has become possible to make a homogeneous waste form having strengths exceeding 10 MPa at a nitrate loading rate of 50 wt% (Fig.10-5). With regard to the slurry, it has become possible to make a homogeneous waste form by thickening the viscosity to prevent impurities from settling, and by adopting a paddle used for high viscosity fluids.

Carbonate effluent from the nitrate decomposition process mainly consists of carbonate precipitates and saturated solution of carbonate, having a pH of 11.5. Carbonates cause a shortage of water by hydrating 10 water molecules at temperatures under 32 ℃ and elevate the pH by reacting with calcium in a cement. We thus set the effluent temperature at 50 ℃ and adopted coarse BFS grains to deal with the shortage of water and the high pH. In small-scale trials, expansion was observed in some test pieces, and this seemed to be caused by decahydrate forming before setting, because of a rapid drop in temperature. In full-scale trials, however, such expansion in a test piece was not observed due to the retained heat in the 200 ℓ drum. The obtained solid waste achieved homogeneity and compressive strengths exceeding 10 MPa at a carbonate loading rate of 30 wt%. Further trials are planned to obtain the conditions to inhibit the expansion.

Phosphate waste (NaH_2PO_4) is produced as a result of the treatment of solvent waste, and has a pH of 4. Therefore, it is necessary to neutralize the waste before mixing to increase the pH to make it compatible with the cement powder. The loading rate is lower than 6 wt% because the phosphate interferes with the hydration and its weight increases by the formation of 12-hydrate. To improve this situation, $Ca(OH)_2$ has been used to convert the phosphate into stabile calcium phosphate having no hydrate. All the phosphate is converted into calcium phosphate, and the negative effect on hydration is eased, when the Ca/P molar ratio is more than 2.43. The waste form achieved homogeneity and compressive strengths exceeding 10 MPa at a NaH_2PO_4 loading rate of 14 wt%.

We will carry out trials to develop lower pH cement and to ascertain its suitability for disposal of waste forms.

Reference
Sugaya, A. et al., Development of New Treatment Processes for Low-Level Radioactive Waste at Tokai Reprocessing Plant, Proceedings of WM2010 Symposia, Phoenix, Arizona, USA, 2010, 12p., in CD-ROM.

Executing Decontamination & Dismantling and Radwaste Treatment & Disposal

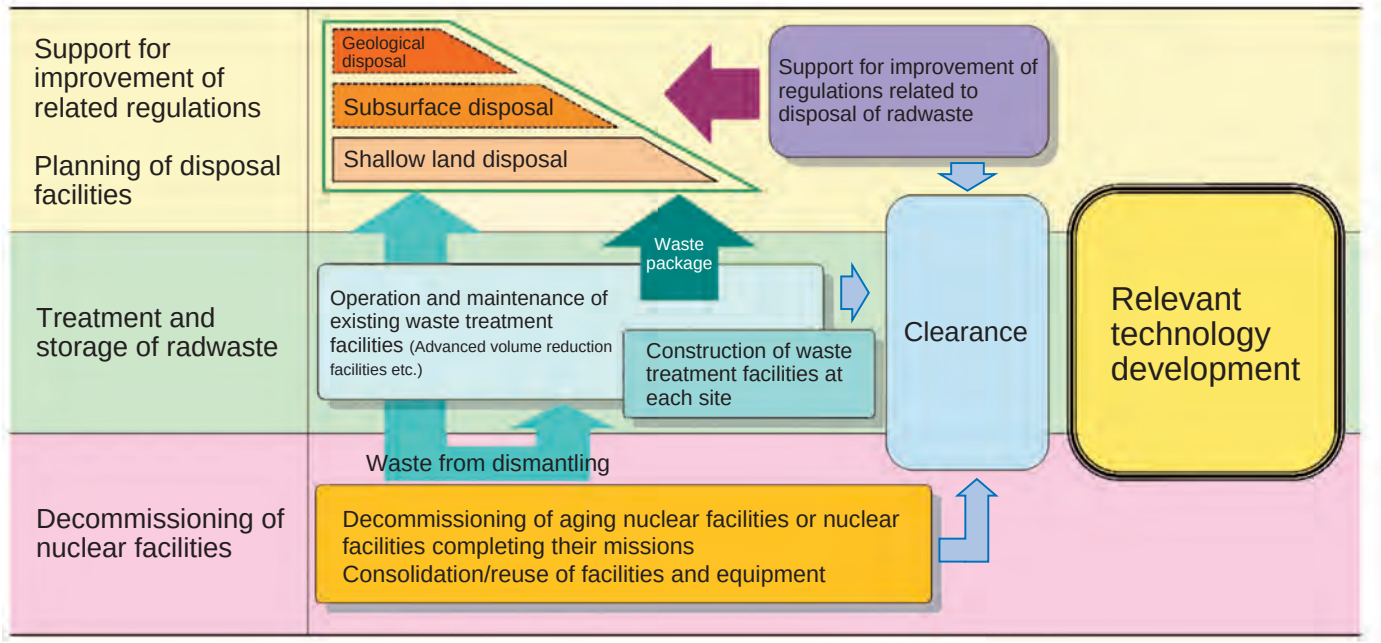

Fig.11-1 Outline of measures for decommissioning and radwaste treatment & disposal

Decommissioning and radwaste treatment/disposal are two of our major missions. In these missions, we will be disposing of radwaste arising not only from our research activities, but also those of universities, institutes, industrial facilities, etc.

We are setting up systems for the decommissioning of nuclear facilities and for radwaste management, through related technology development, planning, and construction of radwaste treatment/disposal facilities, and support for improvement of related regulations (Fig.11-1).

R&D pursuing effective judgment of clearance decommissioning

Clearance activities (reducing wastes to very small radioactive concentration levels that have a negligible effect on human health) for a large amount of waste arising from decommissioning of nuclear facilities have been planned by the JAEA. This reduction is to at or below the clearance level of the waste that arises from decommissioning. To improve the efficiency of clearance activities, a clearance level verification evaluation system (CLEVES) has been developed to support safe and secure waste clearance (Topic 11-1).

R&D for reasonable uranium waste disposal

Radioactive wastes are generated by various activities at the nuclear facilities of JAEA. Uranium waste having a long half-life is included in this waste. Safe disposal of these radioactive wastes is an important issue in atomic energy. We are conducting safety assessments to confirm the safe disposal of uranium waste over a long period of time. Because the half-life of uranium is extremely long, the engineered barriers (low diffusivity layer, low permeability layer, etc.) cannot maintain their confinement function for a long period of time (Topic 11-2).

R&D for analytical techniques for radioactive nuclides in wastes

For proper disposal of radwaste packages generated by various research facilities, an evaluation of radioactivity inventories in the waste packages is indispensable. In order to establish a practical and reliable estimation method for radioactivity inventories, we need to collect data concerning radioactivity concentrations in radwastes.

In JAEA, an analytical method that held down costs was developed as an analytical method for the important nuclides included in the melted solidified substances produced in waste treatment in advanced volume reduction facilities (AVRF).

As a result, efficiency improvements, sample pretreatment and simple speedup of methods of separating nuclides, rapid non-destructive analysis methods for long-lived nuclides, etc., were established, and these results were arranged as analysis guidelines (Topic 11-3).

11-1 Toward Effective Judgment of Clearance
—Developing a Program for Selection of NMAs—

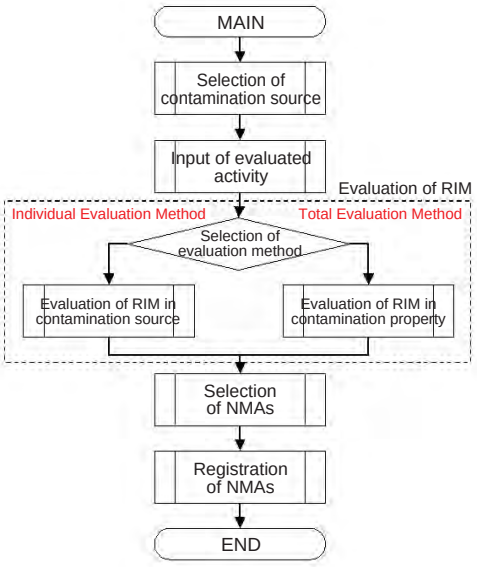

Fig.11-2 Main flow of the program for selection of NMAs
The program is built to be able to select NMAs (nuclides for measurement and assessment) according to contamination sources (fission products and corrosion products, etc.) and contamination properties (secondary contamination, activated contamination, and mixed contamination).

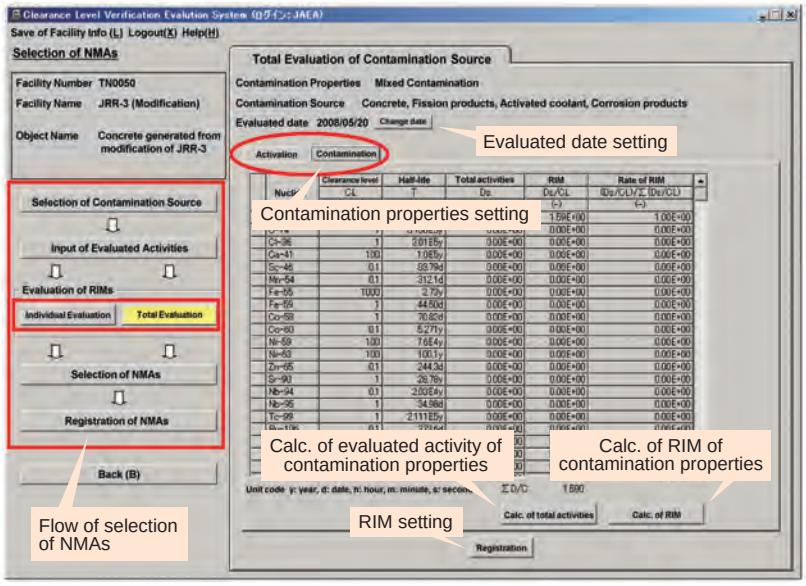

Fig.11-3 Screenshot example of evaluating RIMs by the total evaluation method
The program is structured to evaluate the RIMs of each contamination property using evaluated activities of each contamination source in the total evaluation method.

Clearance activities for a large amount of waste in the decommissioning of nuclear facilities have been planned in the JAEA. To improve the efficiency of these clearance activities, a clearance level verification evaluation system (CLEVES) has been developed to support safe and secure clearance of wastes.

The program for selecting NMAs (SNM) was created to select NMAs from 33 nuclides for which clearance levels are provided in the METI or MEXT regulations.

The SNM was created to select nuclides to be evaluated based on the relative importance measure (RIM; nuclide activity divided by clearance level) for the nuclide according to the contamination source or the contamination properties of the clearance objects.

In this SNM, taking into account characteristics such as the types and structures of reactor facilities, contamination sources are selected according to their contamination properties. Nuclide activity (D) of each contamination source is input into the program (Fig.11-2).

Next, the RIM for nuclides is evaluated by the individual evaluation method or the total evaluation method using the evaluated activities and the like.

The individual evaluation method can evaluate the RIMs in each contamination source. The total evaluation method can calculate a summation of the activity of each nuclide contamination source in the contamination properties, and can evaluate the RIM for each contamination property. Fig.11-3 shows a screenshot of evaluating the RIMs by the total evaluation method.

NMAs are subsequently selected from the 33 nuclides in descending order of the RIM rate according to the regulations of the reactor facility regulatory body.

In addition, case studies have been carried out using the SNM based on data concerning actual clearance activities with concrete generated from JAEA's modification of the JRR-3. NMAs selected by the individual evaluation method were H-3, Co-60, Sr-90, Cs-137, and Eu-152. NMAs selected by the total evaluation method were Co - 60, Cs - 137, and Eu-152.

Thus, NMAs can be selected by the individual evaluation method of the contamination source or the total evaluation method of the contamination properties. The SNM can be used in various ways according to user needs. The SNM is planned to be applied to clearance activities in the JAEA.

Reference

Tachibana, M. et al., Development of Clearance Level Verification Evaluation System I; Fabrication of Program for Selection of Nuclides for Measurement and Assessment, JAEA-Data/Code 2009-019, 2010, 52p. (in Japanese).

11-2 Reasonable Uranium Waste Disposal
—Safety Assessment for Sub-Surface Disposal of Uranium Waste—

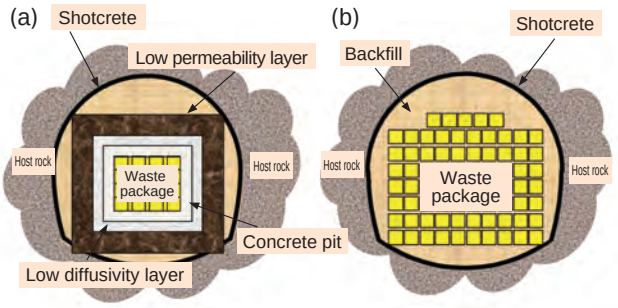

Fig.11-4 Disposal cavern concept
(a) Structure of a typical disposal cavern.
(b) Structure of the disposal cavern in this study.

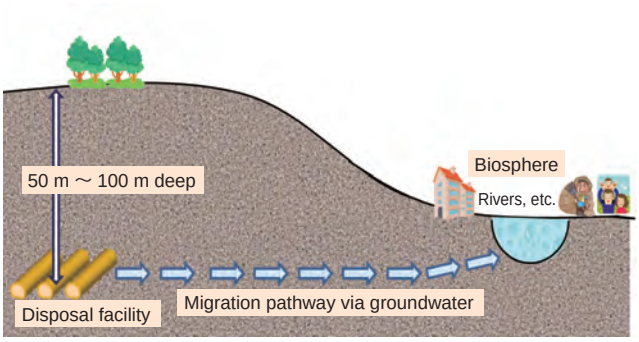

Fig.11-5 "Groundwater scenario" concept
Radionuclides will be transferred to surface water from a disposal facility via groundwater. As a result, the public will be exposed when using surface water. This typical assessment scenario is called a groundwater scenario.

Table 11-1 Scenario development and parameter set-up for safety assessment
The assessment scenarios are arranged with assumed natural events, and change events assumed in the assessment scenarios are set as parameters that change over time.

Assessment scenarios	Assumed change events	Parameter change in safety assessment
Climate change —global cooling	・Decrease in rainwater recharge (recharge volume) ・Drop in sea level	・Decrease in groundwater flow rate over time
Climate change —global warming	・Increase in rainwater recharge (recharge volume) ・Rise in sea level - Intrusion of seawater to the migration pathway	・Increase in groundwater flow rate over time ・Change in chemical condition of groundwater (from reductive to saline)
Tectonics —uplift/erosion	・Disposal cavern comes close to the ground surface due to uplift/erosion ・Increase in permeability by the weathering process (increase in groundwater flow rate) ・Decrease in distance from the disposal cavern to a river due to erosion of the ground surface	・Increase in groundwater flow rate ・Change in chemical condition of groundwater (from reductive to oxidative) ・Decrease in migration pathway length

Radioactive wastes are generated by various activities at the nuclear facilities of JAEA. Safe disposal of these radioactive wastes is an important issue for unimpeded advancement of our activity. We are carrying out safety assessments to confirm the safety of disposal of uranium waste over a long period of time.

Because the half-life of uranium is extremely long, the engineered barriers (low diffusivity layer, low permeability layer, etc.) cannot maintain their confinement function over a long period of time. We therefore devised a reasonable disposal cavern without making use of them (Fig.11-4).

The object of our study is the assessment of public exposure when radionuclides in the disposal facility migrate to the surface water via groundwater (Fig.11-5), when the disposal facility comes close to the ground surface due to uplift/erosion, and so on.

In the safety assessment, it is important to confirm that the public is safe from exposure over a long period of time. Natural events, such as climate change and geomorphological change, are assumed, and it is necessary to predict what will change, and how and when its state will change in the future, based on scientific data. Table 11-1 shows an example of arranging the assessment scenarios (a number of natural events), the related change events, and parameter changes in the safety assessment. The parameters are referenced to data supporting scientific knowledge because a concrete disposal site has not been fixed at present.

Under the conditions mentioned above, we carried out development of assessment scenarios that were assumed to correspond to the groundwater scenario, and performed parameter setting and safety assessment. As a result, we confirmed that the exposure dose to the public was very low even when various event changes were considered.

We assume that in the future it will be important to perform more detailed safety assessments considering specific parameters, the rate of change in the events, and so on.

Reference

Nakatani, T. et al., Study of Subsurface Disposal Concepts for Uranium Waste (5), JAEA-Research 2009-028, 2009, 47p. (in Japanese).

11-3 Analytical Techniques for Radioactive Nuclides in Wastes Generated from Research Facilities

—Guidelines for a Simple and Rapid Determination Method for Waste Samples—

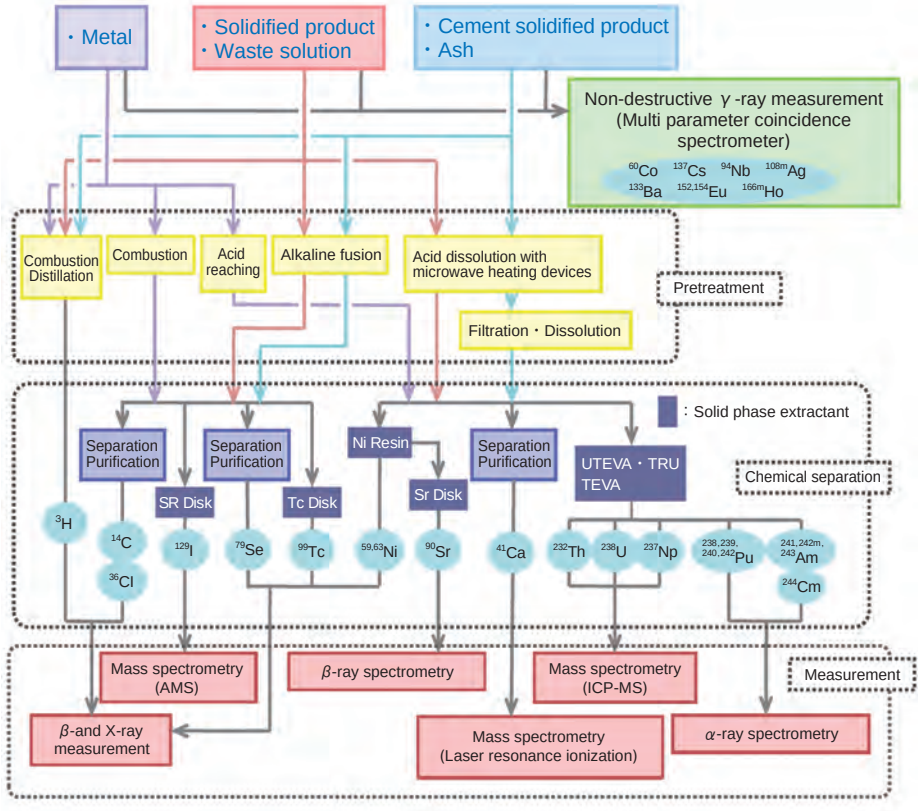

Fig.11-6 Basic radioactive waste sample analysis flow
First, the properties of radioactive waste samples are determined by a non-destructive γ-ray measurement. According to the properties of the radioactive nuclides, the samples are pre-treated by combustion, acid reaching, alkali fusion, or dissolution assisted by microwave heating. α- and β-ray emitting nuclides are separated by a Solid Phase Extraction (SPE) method and subsequently measured.

Fig.11-7 Multi parameter coincidence spectrometer
This spectrometer allows very low concentrations of nuclides in the presence of high concentrations of ^{60}Co to be detected by reducing background counts resulting from Compton scattering.

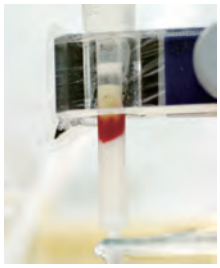

Fig.11-8 Separation of radioactive nuclides by SPE
To expedite the process of chemical separation and reduce secondary wastes, SPE resins are applied to the separation of $\alpha \cdot \beta \cdot$X-ray emitting nuclides. This picture shows that Ni is extracted by SPE resin in the red colored region.

For proper disposal of radioactive waste packages generated from various research facilities, an evaluation of radioactivity inventories in the waste packages is indispensable. In order to establish a practical and reliable estimation method for radioactivity inventories, we need to accumulate data concerning radioactivity concentrations in radioactive wastes. A total of twenty-nine nuclides (Fig.11-6) were selected as objects of analysis from preliminary safety assessment for disposal of the wastes. With conventional analytical methods, major problems in analyses of a large number of waste samples are that tedious and time-consuming pretreatment and chemical separation are needed. Therefore, we prepared a basic analytical flow and also developed constituent techniques which allow rapid analysis (Fig.11-6).

In nondestructive γ-ray measurement, a multi parameter coincidence spectrometer which consists of four Germanium detectors has been applied to increase counting efficiency. As a result, chemical separations for these γ-ray emitting nuclides are no longer needed (Fig.11-7). In order to dissolve a sample of solidified product, which is hard to dissolve by a conventional method, a new dissolution method using microwave heating devices and sealed vessels has been developed. Application of a Solid Phase Extraction (SPE) method for chemical separation of $\alpha \cdot \beta \cdot$X-ray emitting nuclides instead of solvent extraction has resulted in rapid separation and reduced secondary waste such as spent solvent (Fig.11-8). In addition to this, a new time of flight mass spectrometer based on resonance ionization and deflection by a rotating electric field has been also developed. Using these techniques, the time for the analysis of the objective nuclides has been shortened to less than one-third of conventional methods.

Based on these results, we expect that more radioactivity data for the wastes than is presently available will be effectively collected using these analytical techniques.

Reference

Kameo, Y. et al, Simple and Rapid Determination Methods for Low-Level Radioactive Wastes Generated from Nuclear Research Facilities (Guidelines for Determination of Radioactive Waste Samples), JAEA-Technology 2009-051, 2009, 81p. (in Japanese).

12 Computational Science and E-Systems Research

Extending Atomic Energy Research by Combining Computational Science, Theory, and Experimentation

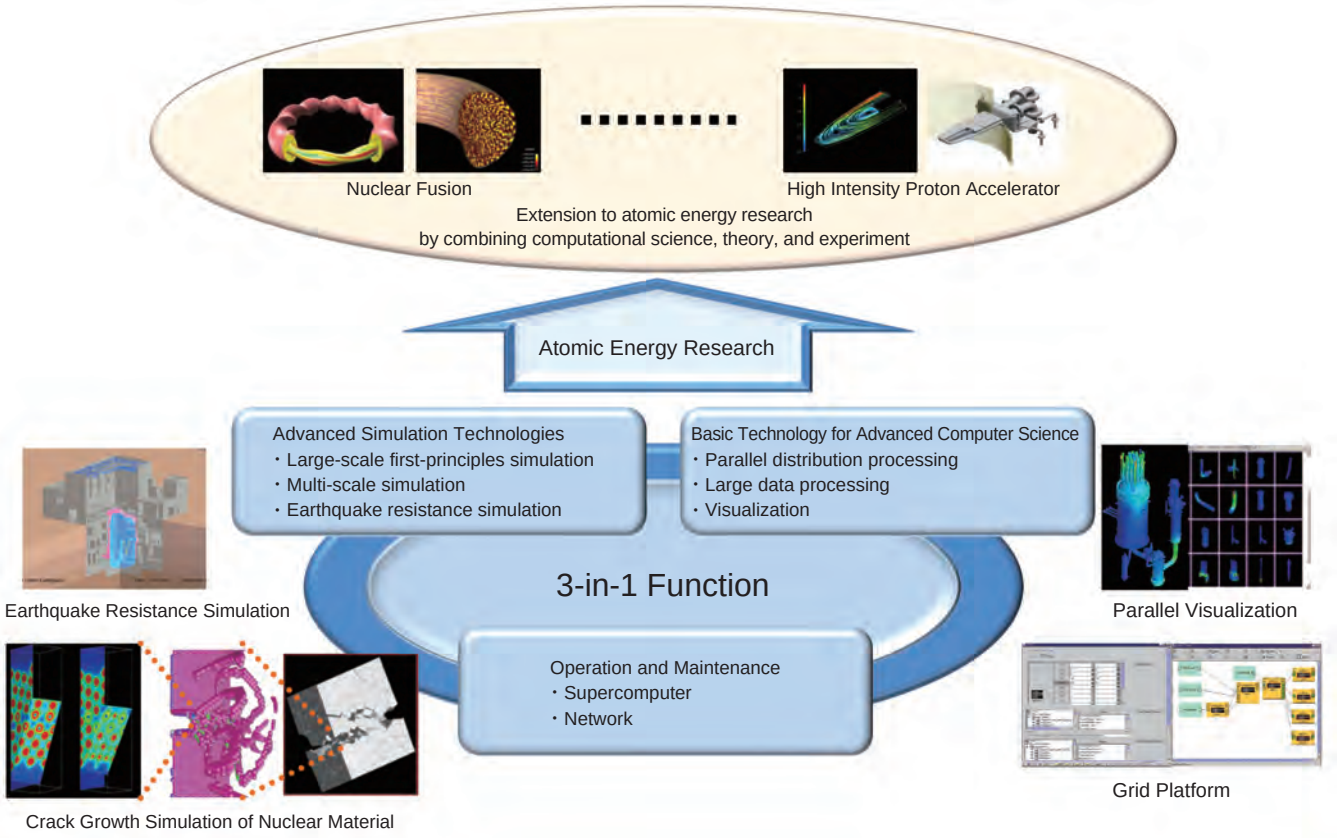

Fig.12-1 Role and achievements of computational science in supporting atomic energy research
We promote three missions while conducting atomic energy research using computational science: the development of basic technology for computer science, the development of advanced simulation technologies, and support for operation and maintenance of computer systems.

Remarkable progress has been made in simulation technologies and basic technologies that support computational science research since the invention of the supercomputer in the 1980s. Similar progress has been made in computational science, which has come to be recognized as a third research method, along with theoretical and experimental methods.

In atomic energy related fields, computational science has an important role in forecasting and analysis of phenomena that are difficult to investigate experimentally or through observation. We believe that progress in atomic energy research and development will increasingly require the use of computational science and large-scale and long-term experiments.

Therefore, in order to support such large-scale calculations, the Center for Computational Science & e-Systems (CCSE) has three missions: the development of basic technology for computational science, the development of advanced simulation technologies, and support for operation and maintenance of supercomputer systems, as shown in Fig.12-1. In addition, we combine computational science, theory, and experimentation, and work toward the development of atomic energy research that uses computational science.

For example, in the field of atomic energy, the degradation of nuclear material and nuclear fuel due to aging and the earthquake resistance of nuclear reactor facilities have been investigated both theoretically and experimentally, and the effects of the degradation of nuclear material and nuclear fuel due to aging and the earthquake resistance of nuclear reactor facilities have been analyzed. We believe that computational science will enable us to perform forecasting and analysis that have hitherto posed problems with respect to cost and scale.

Regarding the analysis of degradation of nuclear material due to aging, crack growth mechanisms in steel are investigated from the atomic scale to the macro scale.

For the purpose of analyzing the earthquake resistance of nuclear reactor facilities, a virtual vibration simulator has been constructed and long-term simulations are being carried out. The results indicate that this is an effective method for investigating the seismic responses of nuclear reactor facilities.

Moreover, we are developing new computer techniques and computer programming methods. These techniques are applied to plasma stability research and they support plasma stability research and development.

In the future, we will extend atomic energy research by developing basic technologies for computational science and advanced simulation technologies. In addition, using the techniques we develop, we will promote cooperation between research organizations inside and outside JAEA.

12-1 Toward Execution of Long-Time Atomic Energy Simulations

—Development of Fundamental Technology that Easily Executes Large-Scale Simulations—

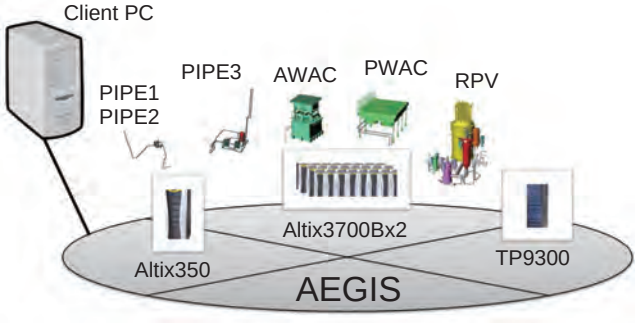

Fig.12-2 Seismic simulation for nuclear power plants
The plant is divided into 3 main equipment sections (Reactor Pressure Vessel, RPV; Auxiliary Water Air Cooler, AWAC; Pressurized Water Air Cooler, PWAC), and 3 pipes. These 6 parts are simulated concurrently. We targeted the High Temperature engineering Test Reactor (HTTR) developed by the Oarai R&D center. The required time was 10 days, which was about a 30% reduction compared with a former technology. Labor-saving in earthquake response analysis for the entire NPP, which considered the interaction between the parts, was achieved by automating control.

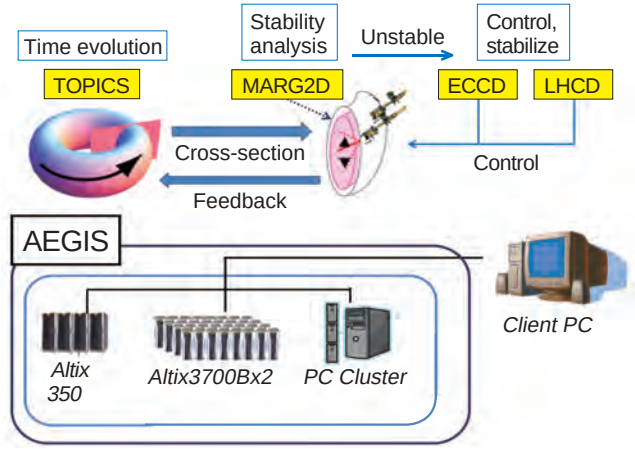

Fig.12-3 Integrated nuclear fusion simulation
This simulation is being developed by the Fusion R&D Directorate. Stabilization is required to prolong the fusion reaction when the plasma approaches the unstable stage. Although the timing of execution of stabilization cannot be predicted beforehand, using this technology we operate 3 supercomputers and execute programs that control and stabilize the plasma by electromagnetic waves automatically as the need arises. As a result, we can analyze the behavior and the stability control numerically in tens of minutes.

Nuclear energy simulations, which deal with complicated physical phenomena, require large-scale calculation and an enormous amount of data, and are difficult to carry out with a supercomputer. For example, when we verify the structural safety of nuclear power plants (NPPs) against earthquakes, we need to handle entire NPPs consisting of over 10 million components. By cooperative execution of programs that analyze each respective component (element programs), we can analyze physical phenomena such as local deformations by the interaction between parts, which had been difficult to realize using conventional component analysis technology.

To implement such simulations, we combined several supercomputers and constructed a virtual large - scale supercomputer named AEGIS. We then developed a technology for automatic control of executing cooperative/integrated programs.

The flexibility of continuing to execute element programs according to the situation is important for executing a large-scale cooperative or integrated program which requires several weeks of calculation using AEGIS. For example, because supercomputers are shared by many users, each program can be executed for only half a day. Therefore an automatic restart function is necessary when the execution of programs ends according to the limit in the execution time. Moreover when supercomputers stop for maintenance or unexpected trouble, or when execution waiting is necessary because of a high average load, a function for migrating to other supercomputers is also necessary. In AEGIS, we have implemented a function which can automatically re-execute a program based on judgement of whether or not a program has been interrupted, etc., and succeeded in implementing long-time execution of cooperative/integrated programs.

Here we show two examples. A full-scale three-dimensional vibration simulator divides facilities into several sections and concurrently computes earthquake resistance. Then the results are integrated and the earthquake resistance of a whole facility is analyzed (Fig.12-2). In integrated nuclear fusion simulation, because the stabilizing process is carried out when burning plasma approaches an instability, the execution of the element program changes according to the state of the plasma (Fig.12-3). For long-time execution of these cooperative programs, substantial modifications of the element programs were required with previous technologies. With our new technology, what previously required 100000 lines of programming has been reduced to 100 lines. This outcome can be expected to contribute to not only reducing execution time and labor saving in execution, but also to shortening the development period for the programs.

Reference

Tatekawa, T. et al., Simple Orchestration Application Framework to Control Integrated Simulations on Grid, FUJITSU Family Association, 2009, 19p. (in Japanese).

12-2 Development of Fast Eigenvalue Solver on a Cell Cluster
—Toward Real Time Plasma Stabilization on ITER—

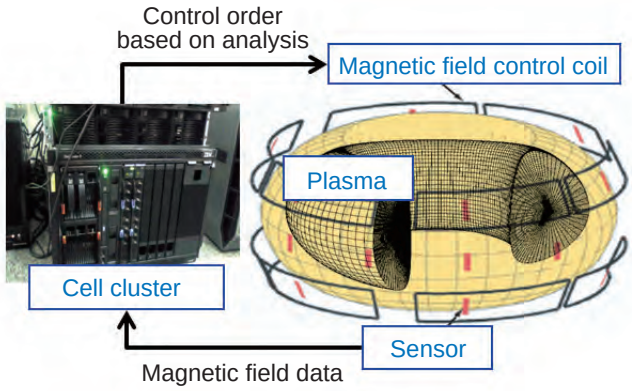

Fig.12-4 Illustration of plasma stabilizing system
In plasma fusion reactors, we stabilize fusion plasma by controlling the external magnetic coils when we detect signs of plasma instability. In order to achieve real time monitoring of instabilities, a dedicated fast computer is indispensable. We developed such a computer by connecting Cell processors, and we ultimately succeed in developing a high speed eigenvalue solver.

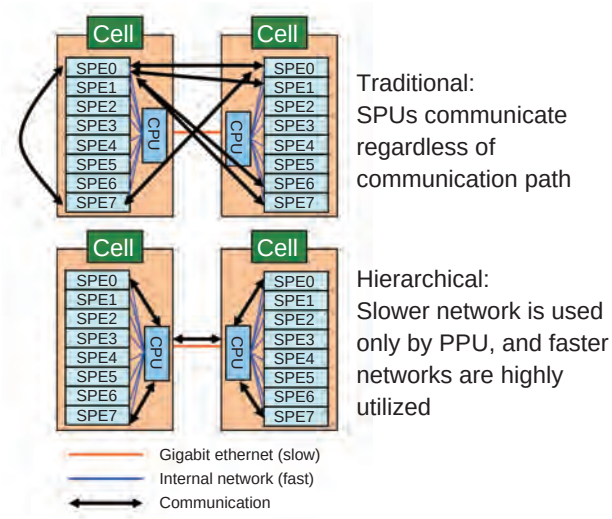

Fig.12-5 Overview of Cell cluster and hierarchical parallelization
A Cell consists of a CPU, fast floating point calculators called SPEs, and an internal fast network. Cells are connected via a general-purpose network in our Cell cluster. For high performance, we developed a hierarchical parallelization that minimizes the use of the general-purpose network and utilizes the internal network.

The International Thermonuclear Experimental Reactor (ITER) project, which is being led by seven countries including Japan, is testing the feasibility of a tokamak type fusion reactor for burning plasma for long periods. It has been noted that the operation efficiency of a tokamak fusion reactor can be degraded by the existence of plasma instabilities. One of the encouraging methods for plasma stabilization is that of control of the plasma by changing the external magnetic field when signs of the plasma instabilities appear (Fig.12-4). However, the period between the time the signs appear and the time limit to stabilization is quite short (such as only five seconds, even in a reactor as large as ITER). Thus, fine control based on accurate plasma state analysis has been considered technically challenging, because it requires higher processing power than what is provided by today's supercomputers. Recently the computational power of supercomputers has been increased by connecting many CPUs. This method is suitable for reducing calculations from one week to one day. However, it cannot be adapted to a one minute calculation, because communication overheads can become large. Moreover, supercomputers are not suitable for use in constant monitoring, because many users share them and we cannot exclusively use them for monitoring use.

We introduced the Cell processor into our computing environment to obtain more processing power beyond that of supercomputers. Moreover, Cell processors are highly cost-effective, and this enables us to build a dedicated computing environment. On the other hand, it also requires sophisticated programming techniques for high performance.

As a first step, we focused on the eigenvalue solver, because it consumes the most computational time. In order to achieve high performance with the Cell processor, we reduced communication time by introducing a hierarchical parallelization technique (Fig.12-5). Furthermore, we developed a novel eigenvalue solver that only requires mathematically inevitable communication. As a result, our eigensolver performs well, with high computational stability, although there is a trade-off between these qualities in traditional methods. Taking these techniques together, we can complete the eigenvalue within one second. We believe that we may open the way toward real time plasma stabilization. Additionally, our newly developed method can be applied to other applications in the nuclear field.

This research is based on Grant-in-Aid for Scientific Research No. 21760701 from the Ministry of Education, Culture, Sports and Technology of Japan (MEXT).

Reference

Kushida, N. et al., High Speed Eigenvalue Solver on the Cell Cluster System for Controlling Nuclear Fusion Plasma, Proceedings of 18th Euromicro International Conference on Parallel, Distributed and Network-Based Computing (PDP 2010), Pisa, Italy, 2010, p.482-488, doi: 10.1109/PDP.2010.22.

12-3 Improving Material Degradation Simulation Using Evolutional Mechanism
—Application of Genetic Algorithms to the Production of Polycrystal Structures—

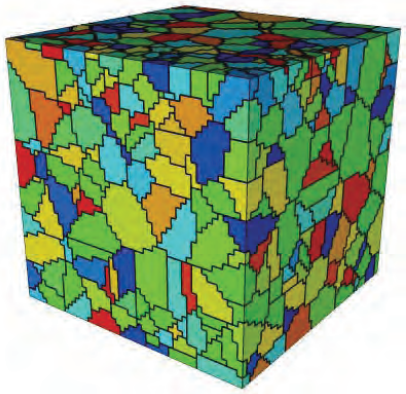

Fig.12-6 Polycrystal produced by a genetic algorithm
Polycrystals usually contain grains of various sizes. We developed a method to computationally construct realistic polycrystals composed of many grains, sufficient to conduct material simulations, for the first time.

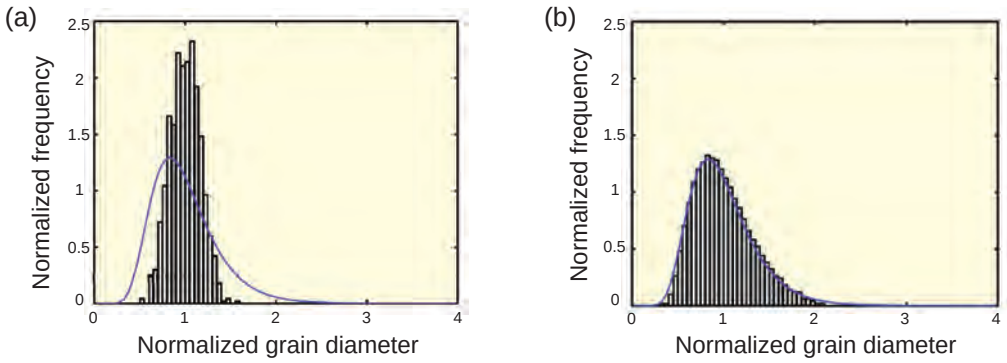

Fig.12-7 Grain size distribution before optimization (a) and after optimization (b)
Application of simple uniform random numbers to constructing polycrystals leads to a size distribution such as the histogram in (a), in which most of the grains have similar sizes; this is significantly different from the realistic size distribution denoted by the blue line. A genetic algorithm was successfully applied to reproducing polycrystals with a realistic grain size distribution, as shown in (b).

Most solid materials, including those applied to nuclear devices, are composed of many grains as seen in Fig.12-6. It is of great importance to understand the degradation mechanism of such a polycrystal, and a possible mechanism could be the reduction of atomistic bonding force at grain boundaries. To predict degradation, it is therefore necessary to reproduce grain configurations as observed in experiments and to evaluate the strength of materials based on such grain configurations. For this purpose, we attempted to develop a software program to automatically produce a polycrystal with a realistic grain configuration, which is critical to improving the prediction of nuclear materials degradation.

In the course of the software development, however, we realized that the calculation time became enormous if the conventional method was applied, and it was impossible to obtain a realistic grain configuration. Fortunately we noticed that application of a genetic algorithm (GA) could overcome this difficulty. GAs provide a numerical optimization method originating in the Darwinian theory of evolution. According to this theory, many individuals of the same species gradually adapt to their environment; GAs utilize such a process for solving numerical optimization problems.

In this particular application, we prepared in advance many unrealistic polycrystals instead of many individuals of the same species. We let some relatively favored polycrystals survive and abandoned the rest as in the theory of natural selection. The surviving polycrystals became the parents of polycrystals in the subsequent generation that were slightly different from their parents; this corresponds to multiplication in the theory of evolution. Among the individuals of the next generation, we again let some relatively favored polycrystals survive. Through iteration of this procedure, we repeatedly selected some of the best polycrystals from many samples at the same time. Thus optimization was accelerated and it was possible to obtain a polycrystal that satisfied the desired grain size distribution (Fig.12-7).

The method described above for the first time made it possible to construct realistic polycrystals composed of a few thousand grains, and to supply initial conditions for material simulations of grain growth, deformation, and fracture, all of which are critical to the development of nuclear materials.

Reference

Suzudo, T. et al., An Evolutional Approach to the Numerical Construction of Polycrystalline Structures Using the Voronoi Tessellation, Physics Letters A, vol.373, issue 48, 2009, p.4484-4488.

12-4 Curious Characters of Iron-Based Superconductors
—R&D for Application Based on Their Unique Features—

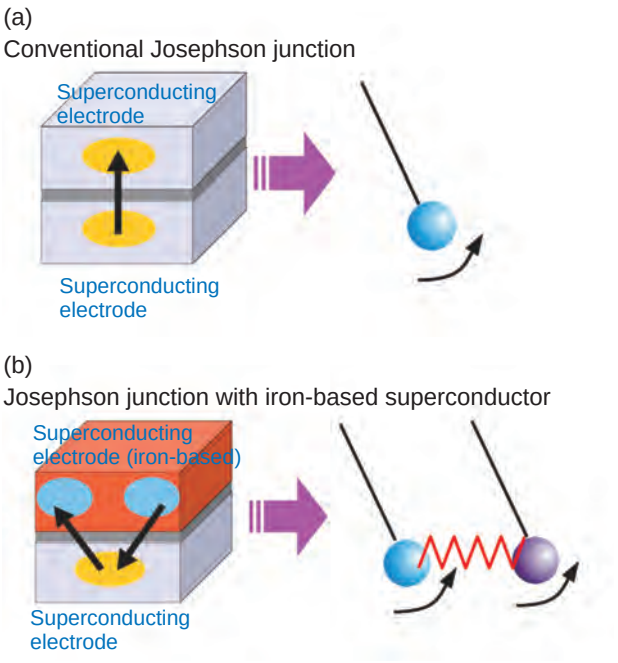

Fig.12-8 Models of Josephson junctions
A conventional Josephson junction is described by motion of a simple pendulum model (a), while a junction with iron-based superconducting materials is described by a coupled pendulum model (b).

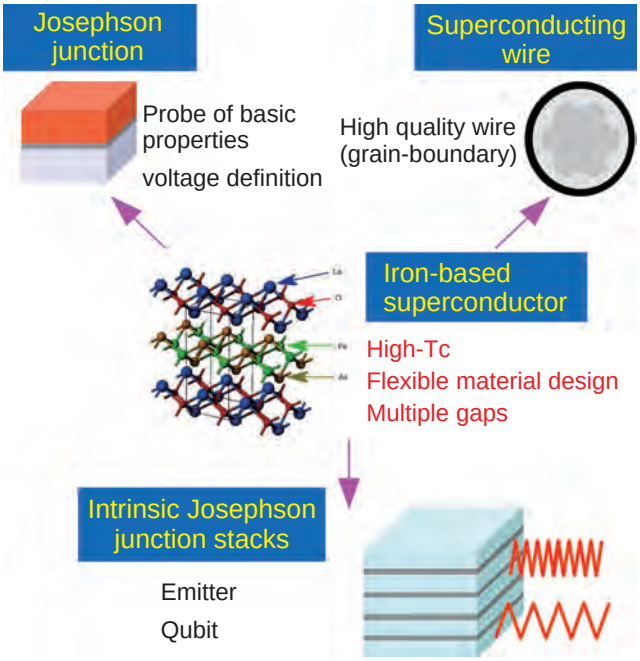

Fig.12-9 Application potential of iron-based superconductors
Various potential applications of iron-based superconducting materials, such as material properties probes, voltage definition, wires, emitters, and qubit.

Superconductivity is one of the most remarkable phenomena in condensed matter systems. A typical behavior is the sudden disappearance of electric resistance below the superconducting transition temperature. Such a property not only brings about transportation with no energy loss but also leads to sensitive detectors and devices much superior to standard ones. Presently, in the nuclear R&D field, potential applications of the superconductors are being intensively studied. In fact, a superconducting coil will be indispensable for a nuclear fusion reactor.

A new superconducting material, an iron-based superconductor was discovered in 2008. This type of a material has a very high transition temperature compared to copper-oxide superconductors and a richly varied chemical composition. One of its most curious features is that multiple (at least three) superconducting gaps coexist, although most existing superconductors have a single gap. Recently, we have been studying the device characteristics originating from their multi-gap feature, focusing on the Josephson junction, which is a typical superconducting device.

First, we directed our attention to the fact that a conventional Josephson junction is theoretically equivalent to the motion of a single pendulum, and the behavior of the superconducting tunneling current is well described by such an elementary dynamical model (Fig.12-8). The present task is to reveal how the conventional description alters when one of the superconducting electrodes is replaced by the iron-based superconductor. We successfully demonstrated that the system is described by coupled oscillators, and went on to predict various electrical and magnetic characteristics of iron-based superconducting devices.

The present contribution provides a theoretical foundation of Josephson junctions with iron-based superconductors. We believe that this study clarifies the essence of iron-based superconductors and will lead to further developments in superconducting engineering (Fig.12-9).

This work is supported by CREST "Framework Development for Multiscale and Multiphysics Simulations towards Novel Application of Superconductivity" from Japan Science and Technology Agency.

Reference

Ota, Y. et al., Theory of Heterotic Superconductor-Insulator-Superconductor Josephson Junctions between Single- and Multiple-Gap Superconductors, Physical Review Letters, vol.102, issue 23, 2009, 237003-1—237003-4.

Development of Nuclear Nonproliferation Technology to Support Peaceful Use of Nuclear Energy

Nuclear nonproliferation technology development for Japan and international applications

We have developed technologies for nuclear nonproliferation including proliferation - resistance technologies and advanced safeguards systems as well as nuclear security technologies. In the field of safeguards environmental sample analysis, we have been providing technical support to the IAEA through the IAEA Network Lab.

New efforts to develop new nuclear security technologies

At the Nuclear Security Summit in April 2010, then Prime Minister Hatoyama announced that Japan would promote research cooperation with the U.S.A. in the development of technology contributing to the advancement of the measurement and control of nuclear material, as well as technologies related to nuclear material detection and nuclear forensics, which provide identification of the origins of illicitly trafficked nuclear material. Moreover, the announcement included the establishment of a regional center this year under JAEA with the aim of providing human resources development assistance and improving infrastructure, particularly in Asia, in order to strengthen nuclear security. We are proceeding towards the realization of these pronouncements.

Contributions to the international community based on our technology and experience

We contribute to the establishment of international nuclear testing monitoring systems. As activities relating to the Comprehensive Nuclear Test Ban Treaty, we have been operating radionuclide monitoring stations and transmitting data worldwide, as well as building a national data center.

Contributions for cultivating human resources

In order to contribute to developing human resources related to nuclear nonproliferation, we offer safeguards training in cooperation with the IAEA. We have also been promoting joint efforts to cultivate researchers at universities, especially the University of Tokyo.

Domestic and international contributions utilizing management and experience of nuclear materials

As an institution that handles large volumes of nuclear materials, our own nuclear materials are strictly controlled. Moreover, we assist in streamlining inspections, such as by providing technical support to the Japanese government and to the IAEA. We also provide support to the IAEA in the field of physical protection, as well as responding appropriately in the case of revisions of Japanese laws.

From a recognized think-tank in Japan to a resource center for Asia

We research and analyze international nonproliferation and nuclear security trends in order to realize both the peaceful use of nuclear energy and nonproliferation. In Asian countries, such as Vietnam, Thailand, Indonesia, etc., we have been providing support in nonproliferation infrastructure development by implementing measures matched to the country's particular circumstances and by sharing our experience.

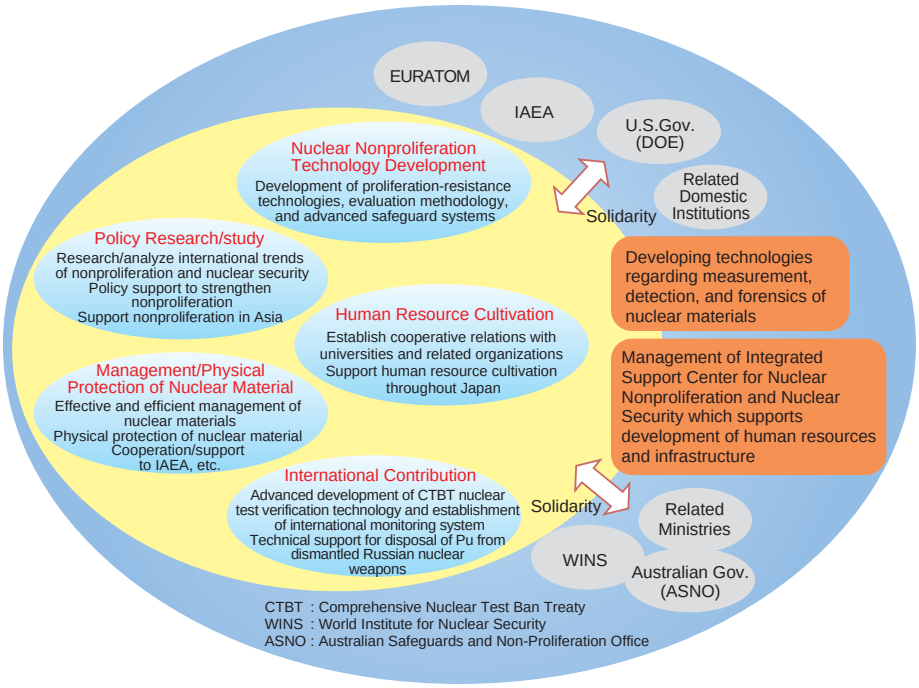

Fig.13-1 JAEA activities in scientific and technical development for nuclear nonproliferation
We have two primary missions regarding nuclear nonproliferation: to support the government in developing nonproliferation policies through research and study, and to support government and international organizations by developing nuclear nonproliferation technology.

13-1 Toward Advanced Safeguards of Future Nuclear Fuel Cycle Facilities

—Development of Safeguards Verification Technologies for Large Pu-Throughput Facilities with Treating Low-Decontaminated, MA-Bearing Nuclear Material—

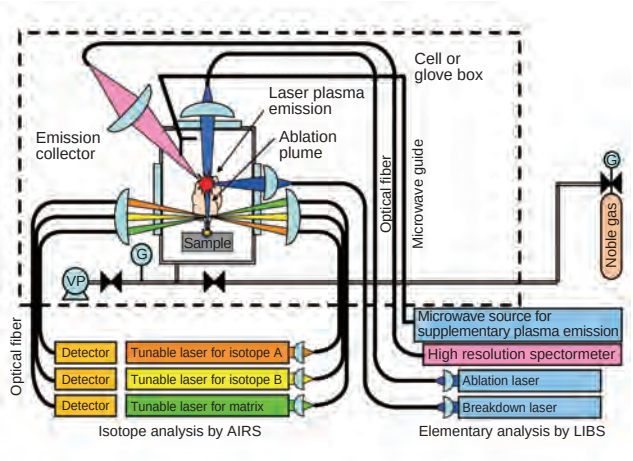

Fig.13-2 Concept of MOX sample verification system for FNFC using LIBS/AIRS
The concentration of an element (Pu) can be measured by detection of breakdown emissions from a plasma produced by interrogation with a breakdown laser onto an ablation plume generated by an ablation laser. It is also possible to analyze the isotopic composition of the element by measuring tuned laser absorption in the ablation plume for each isotope.

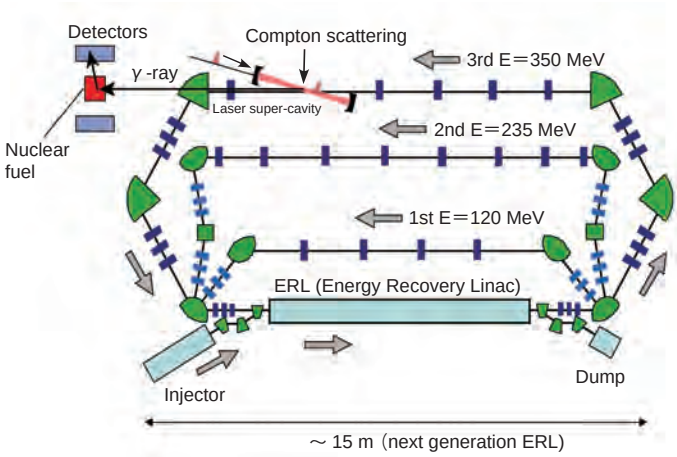

Fig.13-3 Concept of Pu NDA system for spent fuel using NRF with interrogation of LCS γ-rays
Interrogation with 2.143 MeV γ-rays, which are generated from laser Compton scattering of 350 MeV electrons with laser photons, on a spent fuel assembly causes a ^{239}Pu NRF reaction emitting the same energy (2.143 MeV) γ-rays. By counting the γ-rays emitted from ^{239}Pu, we can measure amount of Pu in the spent fuel assembly.

Some future nuclear fuel cycle (FNFC) facilities have the following characteristic features: (1) a very large Pu throughput, (2) treatment of low decontamination nuclear material (containing fission products (FPs)), and (3) recycling of minor actinides bearing material. Here we show examples of advanced safeguards technologies that are proposed or under development based on needs arising from the above features.

Feature (1) means that the accumulated amount of uncertainty in plutonium measurement errors grows very large within a short time period, which requires very frequent safeguards inspections, and thus very fast measurement/analysis technologies are necessary for material accountancy and verification.

Characteristic feature (2) means that nuclear material treated in the FNFC has strong background γ-rays originating from contained FPs. This makes the present γ-ray spectroscopy for determining the isotopic composition of Pu difficult or impossible. In addition, because of feature (3), nuclear material treated in the FNFC contains ^{244}Cm with a very high intensity of spontaneous fission neutrons (10^4 times higher than ^{240}Pu), which means that the present neutron coincidence counting method is difficult to apply to FNFC materials. Given these features, it is necessary to develop new Pu NDA technologies for FNFC materials.

Corresponding to the situations derived from the characteristic features (2) and (3), we are developing a combined method of LIBS (Laser Induced Breakdown Spectroscopy) and AIRS (Ablation Initiated Resonance Spectroscopy) for analyzing the Pu concentration and isotopic composition of Pu in (FNFC) MOX samples (Fig.13-2).

Furthermore, for some time SRD (shipper-receiver difference) has been an issue with reprocessing facilities. Accumulation in the SRD amount tends to increase with increment of reprocessed material. For FNFC reprocessing facilities treating large amounts of plutonium, the SRD issue must be addressed properly.

In addition, there are many spent fuel assemblies in storage pools of reactors with less radiation self-protection because of their very long cooling time. Diversion of fuel rods from assemblies has become a large global concern. Based on this background, development of Pu NDA technologies for spent fuel assemblies, which had been thought to be very difficult, has started.

As one of these technologies, we are proposing a NDA system with a laser Compton scattering (LCS) γ-ray source that uses nuclear resonance fluorescence (NRF) reactions by interrogation of monochromatic γ-rays tuned to the specific resonance energy (within a range of 1~3 MeV) of a target isotope such as ^{239}Pu (Fig.13-3). This system is capable of identifying individual isotopes.

Moreover, FNFC facilities need a variety of advanced safeguards technologies.

Reference

Hayakawa, T., Seya, M. et al., Nondestructive Assay of Plutonium and Minor Actinide in Spent Fuel Using Nuclear Resonance Fluorescence with Laser Compton Scattering γ-rays, Nuclear Instruments and Methods in Physics Research A, vol.621, issues 1-3, 2010, p.695-700.

14 Development of Experimental Techniques / Facilities at JAEA R&D Centers

Tsuruga Head Office

In the Fast Breeder Reactor Research and Development Center,"MONJU", the following procedures were completed: modification work as a measure against sodium leakage; an entire system function test to check the overall functioning of the plant including the modified parts (excluding the water/steam system); preparation and inspection for the System Start-up Test (SST) to confirm the condition of the valves and switches before starting plant operations; and an earthquake-proofing safety assessment related to the Niigata Chuetsu-Oki Earthquake. After that, the "MONJU" SST was restarted on May 6, 2010 for the first time in 14 years and 5 months, and it reached criticality on May 8; furthermore, the core confirmation test, which is the first step in the 3 step-SST that will be conducted for 3 years, was completed on July 22, 2010.

The Applied Laser Technology Institute was established in September 2009, with the aim of contributing to industries in Fukui Prefecture with laser technology. The "FUGEN" decommissioning project has been progressing steadily, and an aging research laboratory has been provided in coordination and cooperation with the Kansai Electric Power Co., Inc.

The Director General of "MONJU", Mr. Mukai, reporting the SST restart to then-president Mr. Okazaki on May 6, 2010.

Opening ceremony of the Applied Laser Technology Institute, held on September 29, 2009.

Tokai Research and Development Center, Nuclear Science Research Institute (NSRI)

Research reactors (JRR-3, JRR-4, NSRR), accelerators, critical experiment facilities (STACY, FCA, etc.), and research facilities (WASTEF, BECKY, etc.) in which nuclear fuel can be treated are safely and successfully operated at the NSRI. In addition, cold facilities such as the LSTF and Large Scale Reflood Test Laboratory are in operation for studies of thermal-hydraulic phenomena.

These facilities have been actively utilized in various research and development activities by researchers mainly from JAEA's Nuclear Science and Engineering Directorate, Nuclear Safety Research Center, Quantum Beam Science Directorate, and Advanced Science Research Center. NSRI personnel are carrying out developments to realize JRR-3's high-intensity cold neutron beam, and are developing neutron calibration technology for neutron dosimetry. Moreover, techniques to measure the void fraction in two-phase flow under high temperature and high pressure have been successfully developed, in order to investigate the behavior of two-phase flow under conditions simulating nuclear reactors (Topic 14-2).

Large-scale cold facilities to investigate thermal-hydraulic phenomena in nuclear reactors

Facilities in the Nuclear Science Research Institute to facilitate and support the utilization of nuclear energy and quantum beams

Other research facilities in the NSRI: JRR-4, Fast Critical Assembly (FCA), Waste Safety Testing Facility (WASTEF), Tandem Accelerator, Facility of Radiation Standards (FRS), etc.

Tokai Research and Development Center, Nuclear Fuel Cycle Engineering Laboratories

At the Plutonium Fuel Development Center, an engineering-scale test is being carried out to develop a fuel fabrication technology named the simplified MOX pellet fabrication process. Last year, 18 fuel assemblies that were fabricated using pellets obtained from the test were supplied to "MONJU" for its plant performance test. Moreover, a pressing machine with a die-wall lubrication system was installed to develop the process.

Seismic reinforcement of the Tokai Reprocessing Plant is being carried out at the Reprocessing Technology Development Center.

Various other R&D activities are being executed, such as advanced reprocessing using an aqueous method and geological disposal technologies.

Additionally, construction of an incineration facility for radioactive waste treatment is currently under planning.

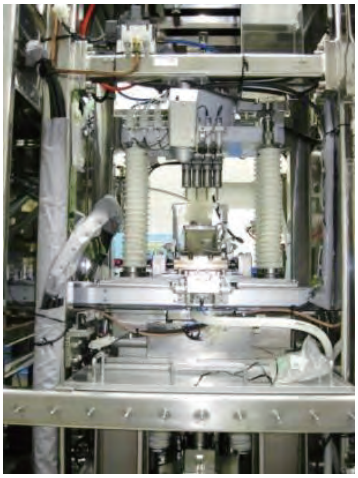

Die-wall lubrication system for engineering-scale test

J-PARC Center

All experimental facilities of the Japan Proton Accelerator Research Complex (J-PARC) have been available for user programs since the first neutrino beam was successfully produced in April 2009. For the second user program year of the Materials and Life Science Experimental Facility (MLF), 111 proposals, for the eight neutron instruments and one muon instrument, were approved in the general use category through a call for proposals and proposal review. After the proton beam intensity was ramped up to 120 kW in November 2009, a remarkable high beam availability of 86 to 92% was achieved. Currently, the J-PARC accelerators are stably providing users with beams higher than 100 kW after accomplishing the mid-term objective of a beam operation with a power of 100 kW in 2008. Moreover, in December 2009, a 300 kW proton beam was successfully accelerated and delivered to the MLF, producing the world's highest intensity neutron and muon beams at that point in time.

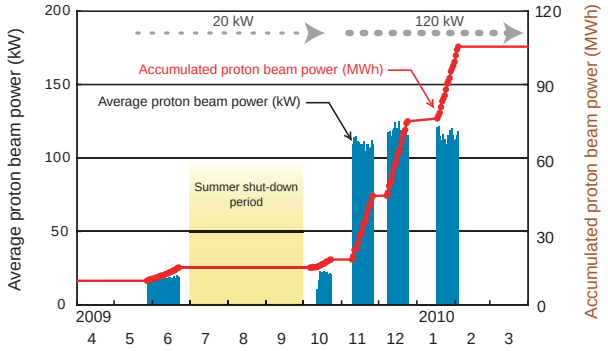

Proton beam power delivered to a pulsed spallation neutron source at the Materials and Life Science Experimental Facility in J-PARC, in FY2009

Oarai Research and Development Center

Experiments needed in the Fast Reactor Cycle Technology Development (FaCT) Project were conducted: post-irradiation examination of FBR high burn-up fuel, minor actinide containing fuel, and sodium tests. Construction began for the Advanced Technology Experimental Sodium (Na) facility (AtheNa) for coolant system equipment for the demonstration plant.

The Japan Materials Testing Reactor (JMTR) proceeded with refurbishment work for restart in FY2011. The 2nd International Symposium on Material Testing Reactors was held, in Idaho, U.S.A., including the Idaho National Lab, for information exchange and discussions related to technology implementation.

The statutory report (final report) of the results of investigating the case in which there was an obstacle on the in-vessel storage rack in the experimental fast reactor "JOYO" (which occurred in November 2007) was submitted to MEXT, and detailed design work was conducted relating to replacement equipment for the upper core structure (Topic 14-8).

The High Temperature engineering Test Reactor (HTTR) reached 50 days of full power operation with a 950 ℃ outlet coolant temperature, and obtained data on the characteristics of high-temperature equipment, for basic technology establishment and demonstration.

HTTR reached 50 days of full power operation

Naka Fusion Institute

The Naka Fusion Institute, together with the Fusion R&D Directorate, is working toward the utilization of fusion energy. As well as fusion plasma research and fusion engineering research, equipment production is advancing, in our capacity as a domestic agency of the experimental reactor ITER, which will be constructed in France. The Satellite Tokamak JT-60SA Program is being developed as a part of the Broader Approach activities, in cooperation with the EU, for the purpose of supporting and complementing ITER. In 2009, the first production of a superconducting conductor for the JT-60SA coil was successful, and two conductors were completed. Moreover, the preparation work for dismantling JT-60 proceeded, and a special area for safely keeping removed activated matter in solid containers was prepared on the premises. Storage-keeping began, and the high voltage table of the heating device and the radiation shielding wall were transferred to storage for reutilization in JT-60SA.

Inside the experimental building, where the space to carry out work on the main body of JT-60 was secured after preliminary dismantling work progressed (upper)
The first production of a superconducting conductor (450 m long) for JT-60SA, wound onto a drum 3 m in diameter (lower)

Takasaki Advanced Radiation Research Institute

Takasaki Ion Accelerators for Advanced Radiation Application (TIARA), which consists of four ion accelerators, an electron accelerator, and gamma irradiation facilities at the JAEA's Takasaki Advanced Radiation Research Institute, are open to researchers in JAEA and other organizations to perform R&D on new-functional and environmentally-friendly materials, biotechnology, the radiation effects of materials, and quantum beam analysis. Practical technology development activities are in progress relating to microbeams, single ion hits, and uniform wide-area irradiation techniques at the cyclotron, and three-dimensional in-air PIXE analysis and three-dimensional microbeam writing technology with different energy proton beams at the electrostatic accelerators. In 2009, a technique for quickly changing the ion species of heavy-ion microbeams at 1 μm size in 30 minutes was developed by a combination of cocktail-beam and flat-top acceleration technologies at the AVF cyclotron (Topic 14-10).

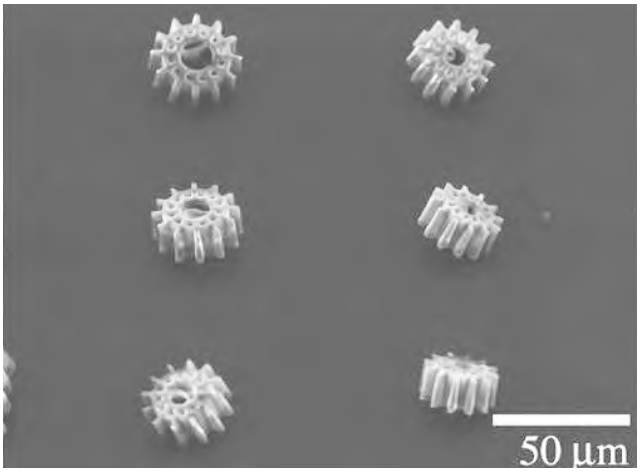

Three-dimensional fine structure organic material parts were fabricated using scanning irradiation of proton microbeams having energies of 1 and 3 MV, and subsequent chemical etching

Kansai Photon Science Institute

At our facility in the Kizu district outside Osaka, we are making improvements in advanced lasers, such as improved beam quality for high-energy lasers and increased X-ray laser repetition rates.

Moreover, the Photo-Medical Research Center is promoting the creation of a "Photo-Medical Valley" (Chapter 5) funded by the Special Coordination Fund for Promoting Science and Technology commissioned by the Ministry of Education, Culture, Sports, Science and Technology. In addition, the Consortium for Photon Science and Technology (C-PhoST) is developing high-Quality Ultra-Advanced Radiation sources (QUADRA) as a core institute.

In the Harima district, we are developing state of the art measurement techniques and equipments for materials science using intense X-rays at four JAEA beamlines in SPring-8, the world's largest synchrotron radiation facility. In addition, we are promoting the application of these techniques to specific researches in material, energy and environment using JAEA beamlines. Some of these researches are related to actinide science, and important in nuclear energy development.

JAEA Kansai Advanced Relativistic ENgineering (J-KAREN) laser system

Horonobe Underground Research Center

The Horonobe Underground Research Laboratory Project is a project utilizing research facilities deep underground and is carrying out geological disposal research and development focusing on sedimentary rock.

In FY2009, the ventilation shaft and the east access shaft were excavated to depths of 250 m and 225 m, respectively. The construction of the 140 m drift was completed by excavating from the east access shaft to the ventilation shaft in May, and by excavating to the west access shaft (before construction) in September.

The International Communication House was opened in October 2009, as a place for information exchange/communication for domestic/overseas researchers and local residents, and for supporting events such as lecture meetings and debriefing sessions.

In the next fiscal year, excavation of the east access shaft to a depth of 250 m and additional tunneling at 250 m (from the east access shaft to the ventilation shaft) will be carried out. In addition, investigations on how to control the inflow of groundwater into the underground facilities and construction of countermeasures will continue to be carried out.

In-situ tests carried out in the 140 m gallery of the Horonobe URL

Tono Geoscience Center (TGC)

The TGC's task is to provide the scientific and technical basis for safe geological disposal of high-level radioactive waste. This involves research on long-term stability of the geological environment, and researches on development and improvement of techniques for characterization of the deep geological environment and a wide range of engineering for deep underground application at an underground research laboratory in crystalline rock, referred to as Mizunami Underground Research Laboratory (MIU). As of March 2010, the Main and Ventilation Shafts had reached GL -459.6 m and -459.8 m (meters below ground level). Research and development activities were conducted, such as geological mapping during excavation and borehole investigations at the -300 m Stage (Topic 14-11).

View up inside the Main Shaft from GL -400 m

Ningyo-toge Environmental Engineering Center

We are working on engineering development for the decommissioning of the uranium conversion plant (URCP) facility and uranium enrichment plant facility in the Ningyo-Toge Environmental Engineering Center. We began the decommissioning project in the URCP facility in FY2008. The URCP facility is a commercial-scale nuclear fuel facility, and the project of decommissioning the URCP facility is the first such trial for a commercial-scale nuclear fuel facility in Japan. Therefore, it is important to collect and evaluate information on the results of the decommissioning work, because the results of the URCP facility decommissioning project will be reflected in future similar decommissioning projects. The main information collected is the number of workers, the content of the work, and the work procedures. In addition, we conduct investigations into the material and weight of dismantled equipment. The URCP facility has 37 rooms in its radiation controlled area, and we completed dismantling 14 rooms in FY2009 that were begun in FY2008. The gross weight of dismantled equipment is about 300 t. This is equivalent to about 60% of the equipment weight in the radiation controlled area of the URCP facility. We will continue to develop the engineering for dismantling at this commercial-scale nuclear fuel facility, and we will also continue to collect/evaluate information about the results of the decommissioning work.

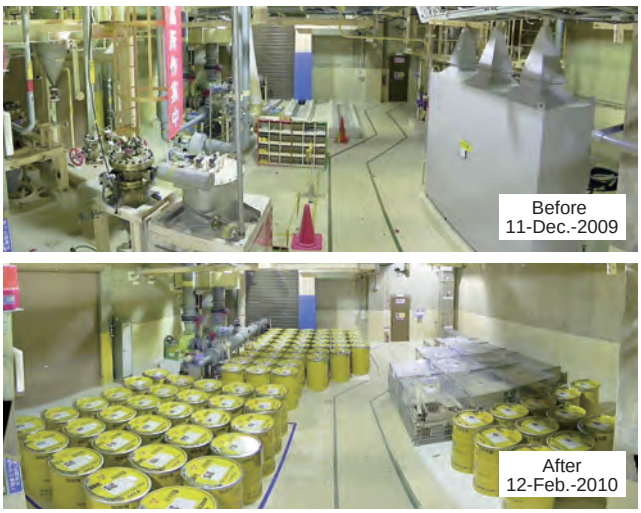

This photograph shows the states before and after dismantling in the hydration and conversion room (3rd floor). The equipment for the hydration preprocessing process and the dehydration reduction process, which made up the conversion process, were installed in the hydration and conversion room. We carried out the dismantling/removal of the utility equipment in this room in FY2008. The dismantling/removal of the processing equipment concluded in FY 2009.

Aomori Research and Development Center

In the Rokkasho district in Aomori Prefecture, all of the main buildings for the International Fusion Energy Research Centre were opened this March for the beginning of full-scale activities relating to the "Agreement for the Joint Implementation of the Broader Approach (BA) in the Field of Fusion Energy Research" between the government of Japan and the European Atomic Energy Community.

In the Mutsu district of Aomori, a research survey for reasonable/economical large assembly dismantling methodology for the operation of a waste disposal plant for research facilities, etc. has been carried out, and a clearance evaluation system database is being compiled. Such a practical decommissioning method is under progress for decommissioning the reactor facility of the nuclear-powered ship Mutsu. Also, the development of a technology to analyze ultra trace elements using accelerator mass spectrometry (AMS) is continuing, while the AMS has been opened for public use. Exchange of information between users was carried out by the hosting of the second AMS user's briefing session.

Photo at the ceremony to commemorate the completion of the International Fusion Energy Research Centre facilities

14-1 Monitoring Sensors by Optical Fiber Grating
—Application of Femtosecond Laser Processing for the Piping System—

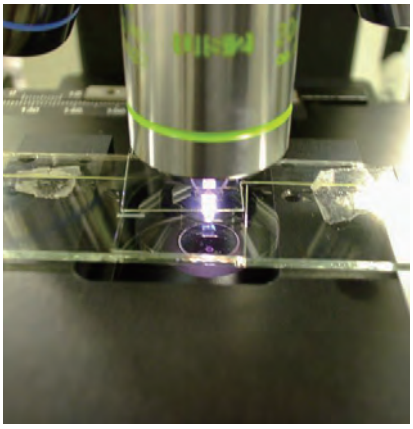

Fig.14-1 Laser fine processing
Femtosecond laser pulses were focused by a microscopic objective lens. Refractive index change was monitored at the focus points. Fine processing was successfully carried out by monitoring the intensity of the super-white continuum emitted at the optical fiber core.

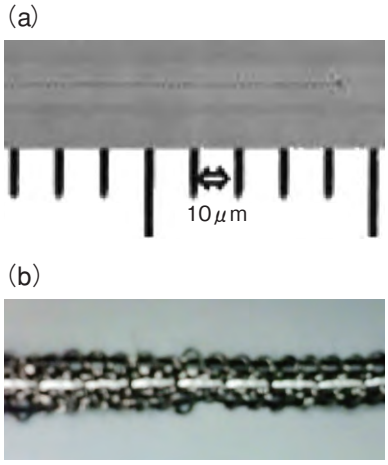

Fig.14-2 FBG along the fiber core and woven carbon fibers
(a) Perfectly aligned dots along the optical fiber core were precisely processed using a femtosecond laser. (b) Woven carbon fiber tape sufficiently improved the strength of a laser processed FBG sensor.

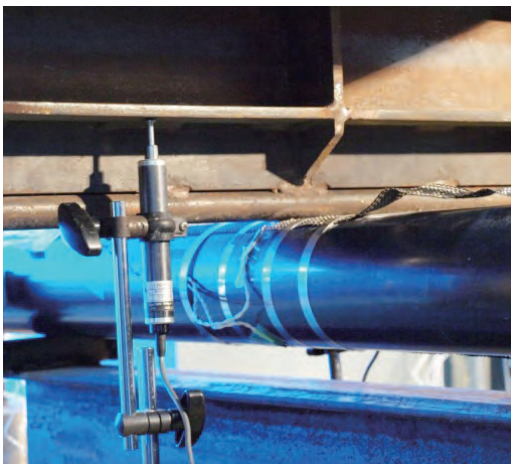

Fig.14-3 Attachment test and loading test of the FBG sensor on a mock-up pipe
The strengthened FBG sensor will be attached by high temperature cement to a mock-up cooling pipe. Loading testing is being planned.

It is very important to understand the seismic deformation of aging piping systems. For this reason, we developed prototype seismic sensors with optical fiber Bragg grating (FBG) using femtosecond laser processing. FBG sensors have periodic refractive index change in their core fiber. The refractive index change in the core fiber actually functions as a wavelength tunable reflection mirror. A fiber cable installed along a complex piping system can detect a deformation when there is a strong earthquake. The fiber laser monitor observes the wavelength shift of the reflection spectrum peak.

Two methods of FBG fabrication are well known: interference exposure and direct writing. Commercially available FBG sensors are commonly produced by interference exposure, and operation in high temperature conditions cannot help but degrade these FBG sensors. We improved the direct writing FBG fabrication method, which can produce structures with superior heat resistance. Fig.14-1 shows microscopic focusing on silica glass optical fiber. Temperature at the focus point rapidly increased to the melting point in picoseconds. Thermal expansion and cooling solidification generate changes in density where the density becomes lower at the center of the molten zone. This density change is strong enough to be maintained for a long time, which is shown in Fig.14-2(a). Ultraviolet laser pulses necessarily damage the surface layer of the optical fiber before they reach the optical fiber core, and nanosecond laser pulses cause thermal damage. In our processing, infrared femtosecond laser pulses can work well, just like a "light engraver," only for the optical fiber core, without causing thermal damage.

In addition, to combine FBG optical fiber and woven carbon fiber is very important in order to apply it to the surface of a facility's pipes. It is well known that carbon fiber has high strength and durability. Thus we hope that woven carbon fiber in a tape-like shape will be sufficiently strong and easily handled, which is shown in Fig.14-2 (b).

Moreover, we developed a compact fiber laser as a monitoring light source, which has a wavelength tunable grating at one end of its resonator. It can monitor the center wavelength of the spectrum reflected from the FBG's structure. We have a plan to apply the FBG sensor to a mock-up piping system such as the FBR secondary coolant system, which is shown in Fig.14-3. In the near future, both real time monitoring by FBG sensors and seismic monitors will be popular for the safe operation of nuclear plants.

Reference

Shimada, Y., Nishimura, A. et al., Design of Monitoring System of High Temperature Piping System by Heat Resistant Fiber Bragg Grating, Journal of Laser Micro/Nanoengineering, vol.5, no.1, 2010, p.99-102.

14-2 Development of Capacitance Void Fraction Meter for LWR Test
—Measurement under High Temperature and High Pressure Conditions—

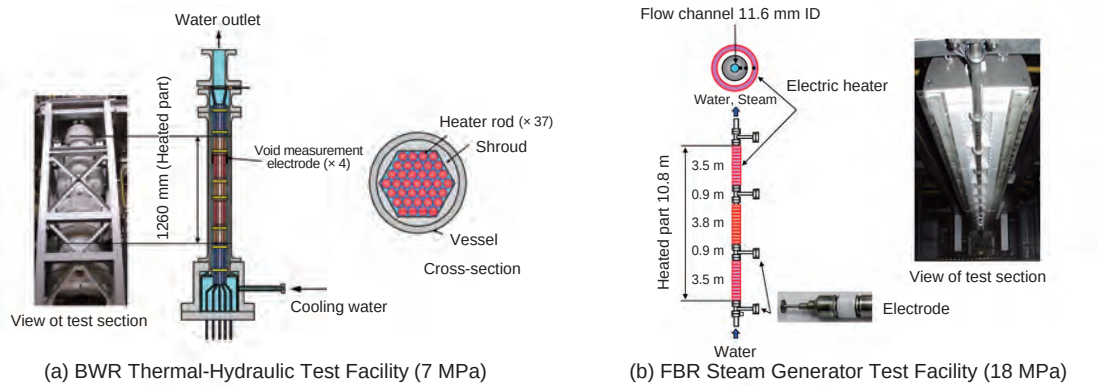

(a) BWR Thermal-Hydraulic Test Facility (7 MPa)　(b) FBR Steam Generator Test Facility (18 MPa)

Fig.14-4 Test facilities applied to the capacitance void measurement method
(a) The 37-rod-bundle electric heater in the test section is shown in (a). Circular electrodes attached to the shroud were used to measure the void fraction.
(b) The vertically stacked double small SUS pipe, which is heated by an electric heater attached to the outer pipe. The lower picture shows the void electrode.

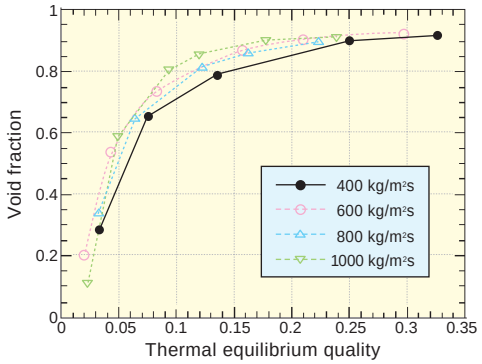

Fig.14-5 Result of void fraction measurement in BWR thermal hydraulic testing
Fig.14-5 shows results from the BWR thermal test facility shown in Fig.14-4(a). The void fraction increases with mass flow at the same quality (mass ratio in the steam), which agreed with previous experience. Note that quality increases with the heating power of the rod bundle.

In a Boiling Water Reactor (BWR), reactor power, fuel conversion ratio, and reactor cooling capacity change according to the void fraction in the core. We have developed a capacitance method (C method) to measure the void fraction under high temperature and high pressure conditions simulating those of a reactor. This C method is based on the principle that the capacitance in the two-phase flow is a function of the void fraction. Using this method, we can measure void fractions in real time, at all regions of void fractions, and with a small measurement error, which had not been realized by hitherto standard techniques.

From a calibration test of the C method using a quick shut valve, we found that the curve of capacitance vs. void fraction is represented by a fixed hyperbolic function, that this function can be applied to a high void fraction region, and that this function is uninfluenced by water quality. Furthermore, using an electrode insulator made of special ceramic material (with a thermal expansion coefficient equal to that of metal), we enabled C method measurements to be made up to 330 ℃ and 18 MPa.

We obtained void fraction data by applying the C method to the following tests.

(1) Thermal hydraulic test (Fig.14-4(a), Fig.14-5)
Development test for reduced moderation water reactor.

(2) BWR thermal hydraulics neutronics coupling test
Reactor stability test at 100% BWR output.

(3) Transient boiling test
Reactor safety test with reactivity induced by void fraction under sudden fuel rod heat. The method is based on the principle that capacitance in the two phase flow changes according to the void fraction.

(4) FBR steam generator test facility (Fig.14-4(b))
Flow instability test in a small pipe simulating the secondary loop of the FBR steam generator.

(5) Flow test for BWR plenum
Flow characteristics test in the upper plenum of the BWR core.

Void fraction measurement for micro channels was developed as an application of this method. The C method is expected to promote development of micro machines such as CPU small heat exchangers and so on.

Reference

Watanabe, H. et al., Experimental Study on Feasibility of Capacitance Void Fraction Meters, Nippon Kikai Gakkai Ronbunshu, B Hen, vol.74, no.742, 2008, p.1257-1262 (in Japanese).

14-3 Toward Highly Purified Uranyl Nitrate Hexahydrate Crystal
—Physicochemical Properties of Plutonium Cesium Nitrate—

Fig.14-6 Plutonium cesium nitrate obtained from a nitrate solution
The pale green compound shows plutonium cesium nitrate precipitated in a dissolver solution of mixed oxide fuel and recovered on a glass filter. Physicochemical properties of the compound were measured to investigate a procedure for obtaining highly purified UNH crystals.

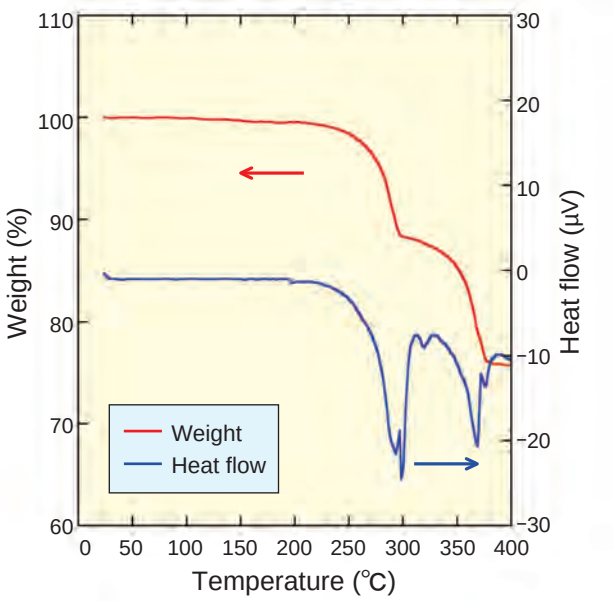

Fig.14-7 Thermal analysis of plutonium cesium nitrate
The thermal properties of plutonium cesium nitrate were analyzed. Weight loss from the compound began at around 245 ℃. This indicated that the compound exists in a solid state during the uranium crystal purification operation.

Crystallization has been studied as advanced aqueous reprocessing in order to partly separate uranium from the dissolver solution of fast breeder reactor (FBR) spent fuel. Crystallization is applied in the fields of chemicals, food, and medicine. In the 1980s, uranium crystallization was proposed by the Kernforschungszentrum Karlsruhe (KfK) in Germany for purifying the uranium product in light water reactor (LWR) fuel reprocessing. Uranyl nitrate hexahydrate (UNH) can be separated and recovered only by temperature control of the solution without a further reagent. Since the dissolver solution of FBR spent fuel contains more plutonium and fission products (FPs) than the uranium product obtained from solvent extraction by the KfK, it is important to understand the behavior of these elements. Previous studies have suggested that plutonium cesium nitrate precipitates in the uranium crystallization, and there may be issues induced by low purified UNH crystals and increasing radiation exposure during uranium product storage and fuel fabrication. Therefore, we studied the physicochemical properties of plutonium cesium nitrate in order to suppress their precipitation and removal from the UNH crystal.

Precipitation experiments were carried out at the Chemical Processing Facility (CPF). Pale green precipitate was prepared from a nitrate solution (Fig.14-6). This compound has been proven to be generated with increasing HNO_3 concentration in the mother liquor. This compound was identified $Cs_2Pu(NO_3)_6$ by elemental analysis and X-ray diffraction. The thermal properties of $Cs_2Pu(NO_3)_6$ were studied for purification operations at 60~100 ℃. Since $Cs_2Pu(NO_3)_6$ weight loss was not observed below 245 ℃ (Fig.14-7), the compound was shown to exist in a solid state during the purification operation.

The $Cs_2Pu(NO_3)_6$ experimental data will be useful for finding a way to suppress its precipitation and to recover highly purified UNH crystals.

This work was financed by the Ministry of Education, Culture, Sports, Science and Technology of Japan (MEXT).

Reference

Nakahara, M. et al., Preparation and Characterization of Dicesium Tetravalent Plutonium Hexanitrate, Journal of Alloys and Compounds, vol.489, issue 2, 2010, p.659-662.

14-4 Improvement of Pu and U Measurement Reliability

—The First ISO Accreditation of a Testing Laboratory for Nuclear Materials in Japan—

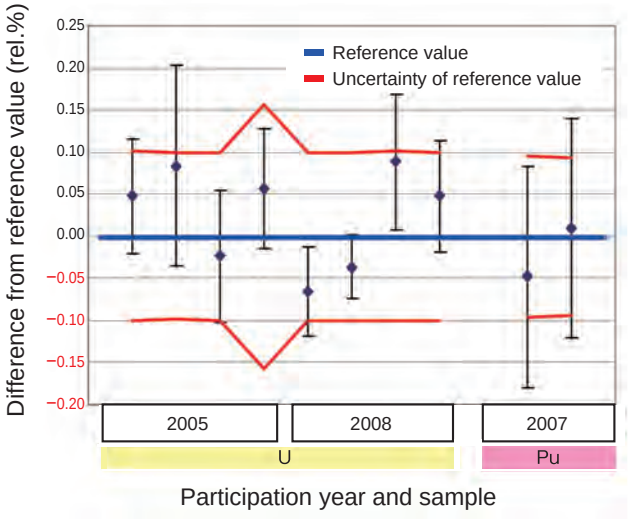

Fig.14-8 Intercomparison results
We participated in the intercomparison program organized by CETAMA, France, which uses reference material as a sample and confirmed our results are accurate and precise compared to the reference value.
(Error bar: Uncertainty of the measurement (95% confidence limit))

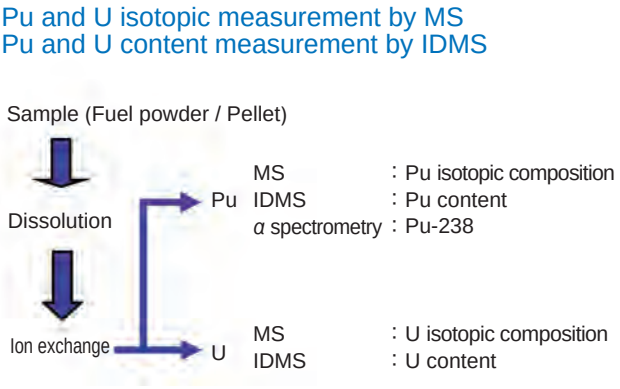

Fig.14-9 Scope of the ISO/IEC accreditation
The scope of the ISO/IEC 17025 accreditation is from receipt of a MOX fuel pellet or its fuel powder to Pu and U isotopic measurement by Mass Spectrometry (MS), as well as content measurement by Isotope Dilution Mass Spectrometry (IDMS).

Accurate and precise measurement of Pu and U are critically important for safeguards, not only for process control but also for safeguards inspection by the IAEA and the Japanese government at nuclear fuel handling facilities.

The Quality Control Section of the Plutonium Fuel Development Center has been performing quality control in accordance with ISO 9001 requirements and has technically improved the following areas.

(1) A method was established to estimate Pu and U measurement uncertainty based on the ISO/IEC Guide 98-3 in cooperative research with the NBL of the U.S. Department of Energy, which supplies reference materials internationally.

(2) We participated in the intercomparison measurement work organized by CETAMA, France, and the NBL, U.S.A., to confirm that our measurement results agree with reference values and that the analysis precision is comparable to the major international laboratories (Fig.14-8). The results were very good compared with the International Target Values for Measurement Uncertainties in Safeguarding Nuclear Materials (ITV) of ±0.36% (2σ), for Pu and U content measurement.

(3) Since the analysis procedures for Pu and U in nuclear fuel materials had not been standardized between laboratories within Japan, development of standard procedures is considered to be an important to improve the reliability of analysis results in the future. Thus, domestic standard procedures for analytical methods were developed by the "Special Committee on Quality Assurance of Accountancy Analysis for Safeguards" which was established by the Atomic Energy Society of Japan.

With this process, our analysis procedures have been confirmed to be equivalent to the standard procedure.

Based on these activities, as of March 1, 2010, we have been accredited for ISO/IEC 17025:2005 (JIS Q 17025:2005) (International Standard for the General Requirements for the Competence of Testing and Calibration Laboratories) by Japan Chemical Laboratory Accreditation (JCLA) of Japan Chemical Industry Association, as the first testing laboratory for nuclear materials in Japan. The accreditation scope is shown in Fig.14-9.

While ISO 9001 certifies the quality assurance system of an organization, ISO/IEC 17025 accreditation certifies that a laboratory has the capability to perform specific testing. Accreditation by the third-party organization is based on international standards and the reliability of results by an accredited laboratory can be guaranteed internationally.

We will contribute to accurate and reliable accountancy analysis of the nuclear materials at nuclear fuel facilities by consistently reporting reliable analysis results and improve transparency in the use of nuclear materials.

Reference

Sumi, M. et al., Experience on Preparation of LSD Spikes for MOX Samples, Proceedings of the Institute of Nuclear Materials Management, Tucson, Arizona, USA, 2009, Abstract #292, 9p., in CD-ROM.

14-5 Neutrons Clarify the Full Picture of Atomic Motions
—Novel Method for High Efficiency Inelastic Neutron Scattering Measurement Demonstrated in J-PARC—

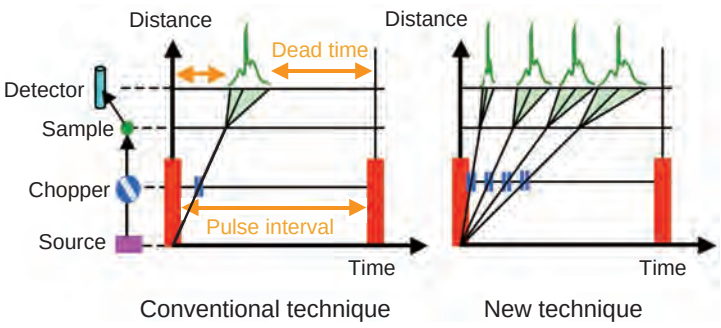

Fig.14-10 Principle of inelastic neutron scattering measurement at pulsed neutron source
The new experimental technique utilizing multiple incident energies can markedly reduce the measurement dead time, leading to enhancement of measurement efficiency.

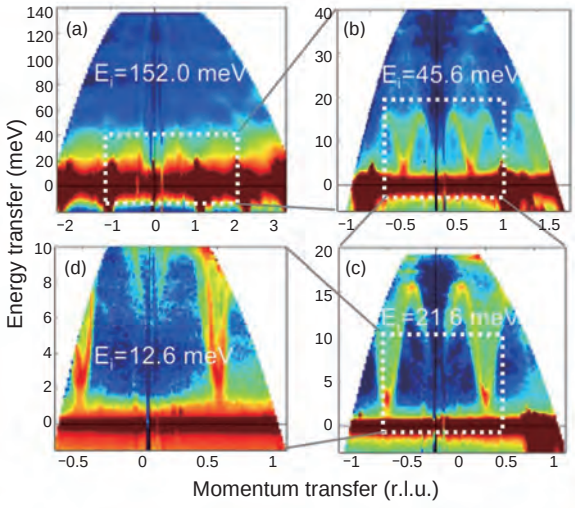

Fig.14-11 Inelastic neutron scattering spectra obtained by the new experimental technique
Four kinds of twodimensional maps that visualize the dynamical information for $CuGeO_3$ are obtained simultaneously. These data have a zoom-in/out relation with each other.

Atoms in a material vibrate while cooperatively coupled with neighboring atoms. This atomic motion in a material is closely related to unique material functions such as high-T_c superconductivity. Inelastic Neutron Scattering (INS) experiments can visualize atomic dynamical information for a material. Conventional INS experiments that use single incident energy (E_i) have the disadvantage of low measurement efficiency and so require a long measurement time and a large sample amount.

To overcome this difficulty, we proposed the idea that the simultaneous utilization of multiple E_i's can enhance the INS measurement efficiency (Fig.14-10). We refer to this experimental technique as multi-E_i measurement. The 4D Space Access Neutron Spectrometer (4SEASONS) has been designed to implement multi-E_i measurement and was constructed at the Materials and Life Science Experimental Facility in J-PARC. The INS measurement efficiency will improve in proportion to the number of E_i's. A higher chopper frequency enables higher resolution measurement and an increase in the number of available E_i's, but it also causes some loss of intensity. Thus, we have to examine the best experimental condition in advance. The dynamical information for $CuGeO_3$ single crystals observed by 4SEASONS is given in Fig.14-11. Four different two-dimensional maps of INS spectra are simultaneously obtained by the multi-E_i measurement, where it is possible to zoom in on the data at smaller E_i's in the maps with higher resolution. For example, the resolution of Fig.14-11(d) is 40 times higher than that of Fig.14-11(a). Thus, we have succeeded in obtaining a full picture of dynamical information, from overall features over a wide range to precise features in a fine range, as with an Internet map service that can freely zoom in and out in satellite photos all over the world.

The new experimental technique we have demonstrated has great potential for markedly enhancing the opportunity to discover new phenomena. When the neutron source at J-PARC is operated at the rated maximum power of 1 MW, the measurement efficiency will improve more than ten times from the current stage, and then multi-E_i measurement is expected to explore a new frontier of condensed matter science.

This work was supported by a Grant-in-Aid for Specially Promoted Research (No.17001001) from the Ministry of Education, Culture, Sports, Science and Technology of Japan (MEXT).

Reference

Nakamura, M. et al., First Demonstration of Novel Method for Inelastic Neutron Scattering Measurement Utilizing Multiple Incident Energies, Journal of the Physical Society of Japan, vol.78, no.9, 2009, p.093002-1—093002-4.

14-6 Realization of the World's Most Brilliant Neutron Source at J-PARC
—Unique Source Design and Smooth Power-Up of Accelerators—

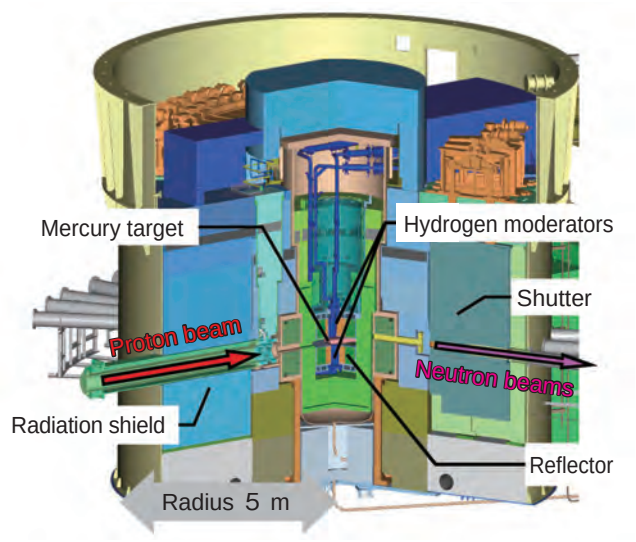

Fig.14-12 1 MW pulsed neutron source at J-PARC
A 3 GeV pulsed proton beam is injected into a mercury target to generate 10^{17} spallation neutrons per second. The neutrons are cooled by 20 K cryogenic hydrogen moderators, and pulsed cold neutron beams are then delivered to users.

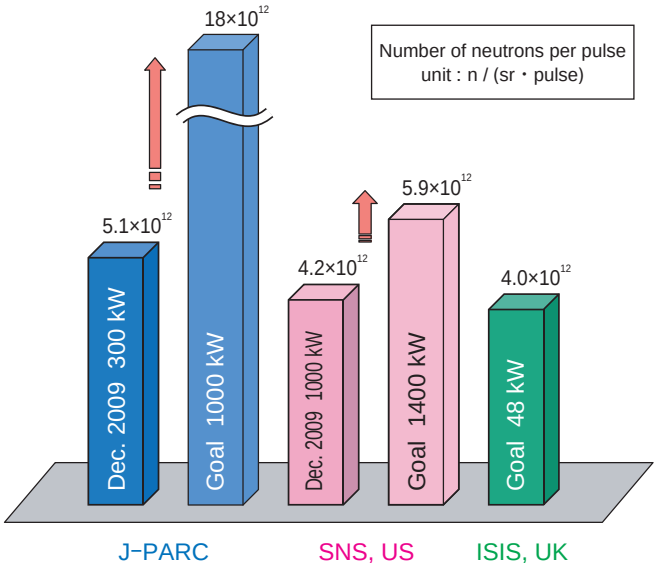

Fig.14-13 Comparison of neutron intensities of the world's major spallation neutron sources
The neutron intensity per pulse depends on the pulse repetition frequency and the source design as well as the power. On achieving the rated 1 MW power, J-PARC's neutron intensity will be outstanding.

Neutrons can be used as probes to observe the structure and motion of materials. World-leading scientific outcomes in the fields of materials and life science, and further contributions to industrial applications such as the creation of innovative materials and medicines, are anticipated from the use of intense pulsed neutron beams. To realize the world's most intense pulsed neutron beams we have constructed a neutron source (Fig.14-12) in the Materials and Life Science Experimental Facility in J-PARC. The first neutron pulse was generated in May 2008, user service operations commenced in December 2008 at 20 kW beam power, and operations have been continuing at elevated 120 kW beam power since November 2009.

A high power test operation to generate intense pulsed neutrons was conducted by increasing the beam power to 300 kW on December 10, 2009. The number of neutrons emitted from the hydrogen moderator per unit solid angle per pulse was found to be 5.1×10^{12}. As of December 2009, the corresponding neutron intensities in the world's major spallation neutron sources were 4.2×10^{12} neutrons at the SNS facility in Oak Ridge National Laboratory, US, and 4.0×10^{12} neutrons at the ISIS facility in Rutherford Appleton Laboratory, UK (Fig.14-13). Thus it was confirmed that the neutron intensity achieved at J-PARC was the world's highest. J-PARC's neutron intensity will eventually be three times that of SNS when the beam power is raised to the rated 1 MW.

The outstanding performance of the J-PARC neutron source is a result of the accelerator group's continuous efforts to increase the beam power. The number of pulses per second is suppressed to 25, compared to 60 at SNS, to increase the number of neutrons in each pulse. The Monte Carlo calculation code PHITS for tracking the behavior of protons and neutrons in matter has been developed to optimize the materials, dimensions, and configurations of the neutron source components such as the mercury target, hydrogen moderator, reflector, etc. Some unique ideas have been introduced in the design of the neutron source, such as the invention of a moderator shape to push up the neutron intensity and development of a new Ag-In-Cd alloy neutron absorbing material.

Several challenges still remain before we achieve the rated 1 MW power. We will continue our efforts to solve these issues in order to claim the highest-performance pulsed neutron source in the world.

Reference

Maekawa, F. et al., First Neutron Production Utilizing J-PARC Pulsed Spallation Neutron Source JSNS and Neutronic Performance Demonstrated, Nuclear Instruments and Methods in Physics Research A, vol.620, issues 2-3, 2010, p.159-165.

14-7 Development of Hydrogen Production Technique

—A Thermo-Chemical and Electrolytic Hybrid Hydrogen Production Process—

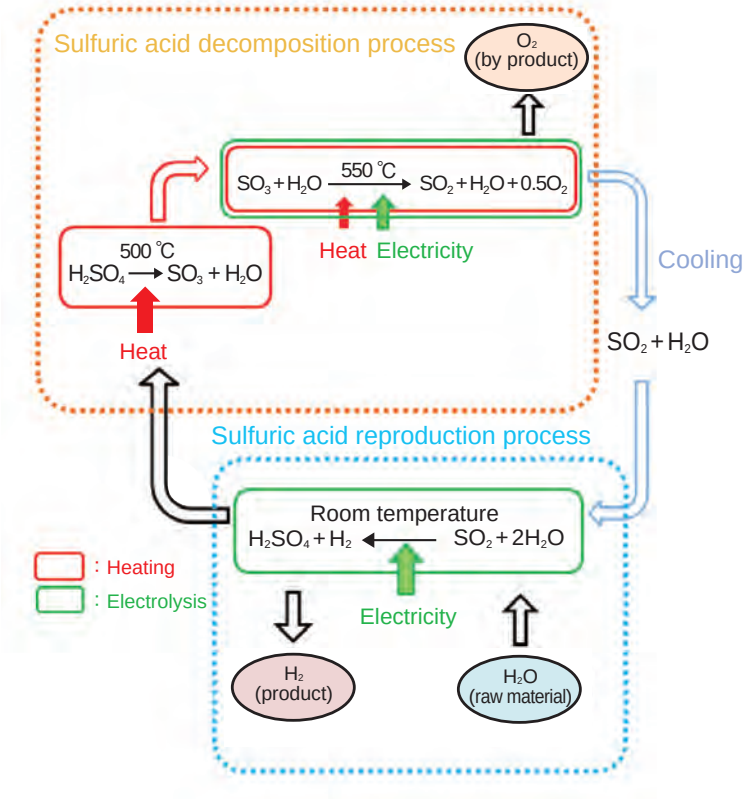

Fig.14-14　Flow of the HHLT process
Hydrogen was obtained from water using the FBR's heat and electricity.

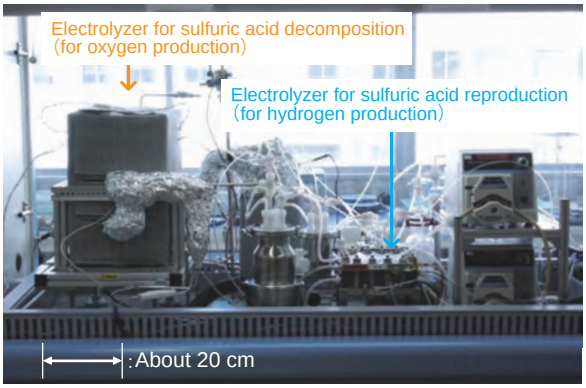

Fig.14-15　External view of HHLT engineering test apparatus
The size of this apparatus is about 1.3 m wide, 0.6 m tall and 0.7 m deep.

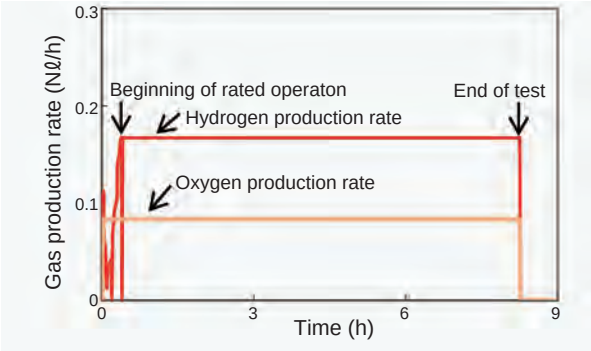

Fig.14-16　Example of hydrogen production experiment
The production rate of hydrogen and oxygen was controlled to 2:1.

Hydrogen is anticipated to be a future carbon-free energy carrier. However, at present there is a problem with carbon dioxide emissions during hydrogen production, because industrial hydrogen production uses fossil fuels. It is important to develop a future hydrogen production process without carbon dioxide emissions.

To solve this problem, we are developing a process for producing hydrogen in very large volumes from water using heat and electricity from Fast Breeder Reactors (FBRs). A thermo-chemical process is a process to decompose water chemically using multiple chemical reactions, and is expected to have higher thermal efficiency (namely lower energy consumption) than direct water electrolysis (direct water electrolysis: about 30% → our process: about 44%). A thermochemical and electrolytic Hybrid Hydrogen production process in a Lower Temperature range (HHLT) has been invented based on the Westinghouse process, which was developed for high temperature gas cooled reactors. In order to reduce the top end reaction temperature to 500~550 ℃, which is the operation temperature of FBRs, the HHLT process employs electrolysis along with thermal decomposition for the gaseous sulfuric acid decomposition step, which previously required a high temperature of over 800 ℃. We were the first in the world to achieve hydrogen production using the HHLT process.

The flow of the HHLT process is shown in Fig.14-14. Sulfuric acid is vaporized and decomposed into sulfur trioxide and water vapor, and sulfur trioxide is decomposed into sulfur dioxide and oxygen by electrolysis (sulfuric acid decomposition process). The decomposed sulfur dioxide and water vapor are cooled to room temperature, and sulfuric acid and hydrogen are produced by electrolysis (sulfuric acid reproduction process). We developed a test apparatus to confirm stable hydrogen production using the HHLT process (Fig.14-15), and achieved stable hydrogen production (Fig.14-16). Test results confirmed the stability of the process when the sulfuric acid supply flow rate was varied. Besides, the major equipments will be made of metal for practical implementation, and we evaluated the anti-corrosion performance of the materials under a highly corrosive sulfuric acid environment.

Reference

Takai, T. et al., A Hydrogen Production Experiment by the Thermo-Chemical and Electrolytic Hybrid Hydrogen Production in Lower Temperature Range - System Viability and Preliminary Thermal Efficiency Estimation-, JAEA-Technology 2008-068, 2008, 63p. (in Japanese).

14-8 Remote Inspection in the Reactor Vessel by Optical Fiber
—In-Vessel Observation in JOYO—

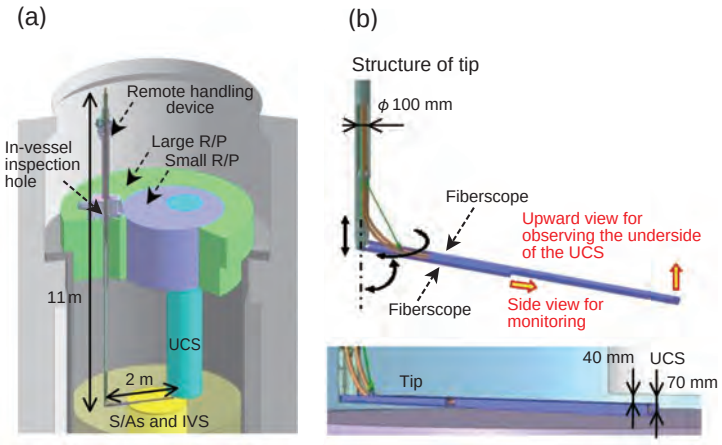

Fig.14-17 Remote handling device for observing the underside of the UCS
The remote handling device can bend its tip into an L-shape. The observation of the underside of the UCS is conducted by inserting the tip of the device into the gap between the top of the S/As and the bottom of the UCS.

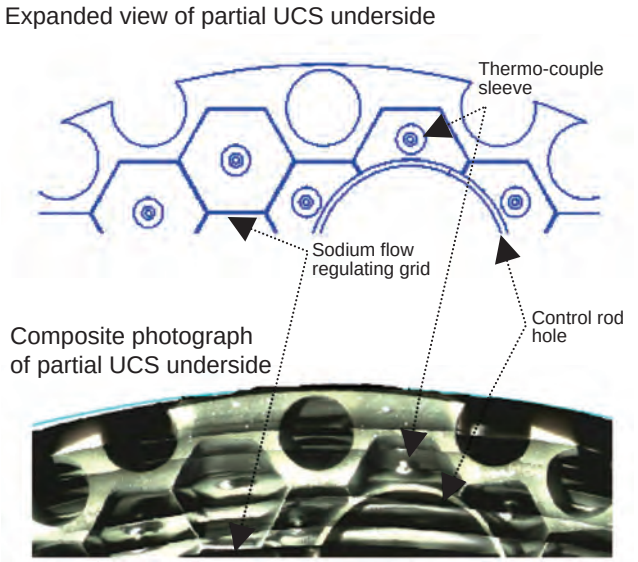

Fig.14-18 Observation results for the underside of the UCS
This figure shows a composite photograph of some of the regions on the underside of the UCS as an example, including the sodium flow regulating grid, thermocouple, and control rod guide tube.

In-vessel observation techniques for a sodium cooled fast reactor (SFR) are important issues for confirming safety and structural integrity. Since in-vessel observation of SFRs has to be conducted under high temperatures (~200 ℃) and a high radiation dose rate, the properties of the in-vessel observation equipment are required to withstand the severe conditions in the reactor. Also, because the primary sodium coolant must be contained in the reactor to remove the decay heat, it is necessary for the reactor vessel to be completely sealed during the observation. Therefore, in-vessel observation equipment is also required to pass through the fixed hole built on the rotating plug to access observation areas.

In order to verify in-vessel observation techniques in a SFR, in-vessel observations with a radiation-resistant fiberscope were carried out in the experimental fast reactor "JOYO" (sodium - cooled fast reactor; thermal power: 140 MW), with an obstacle on the in-vessel storage rack as the opportunity.

The objective was observation of the underside of the upper core structure (UCS).

As shown in Fig.14-17, a remote handling device which has a tip that can be bent into an L-shape has been developed for observation of the underside of the UCS. This device has two fiberscopes: one for an upward view and the other for a side view. The tip of the device was inserted into the 70 mm gap between the top of the S/As and the bottom of the UCS. The sodium level was kept at 50 mm below the top of the S/As during these observations. Before the observations, a full scale mock-up test was conducted to confirm the performance of the remote handling device.

As a result of these observations, the 8.0 mm thick sodium flow regulating grid on the underside of the UCS could be confirmed by radiation-resistant fiberscope while adjusting the lighting and the depth of focus as shown in Fig.14-18. These results provided valuable insights for further improvements in, and verifications of, SFR in-vessel observation techniques.

References

Itagaki, W. et al, In-vessel Visual Inspection of Sodium Fast Reactor, The 14th National Symposium on Power and Energy System, 2009, p.435-438 (in Japanese).

Takamatsu, M. et al., Development of Observation Techniques in Reactor Vessel of Experimental Fast Reactor Joyo, Journal of Power and Energy Systems, vol.4, no.1, 2010, p.113-125.

14-9 3-Dimensional Floating Support System to Permit of Thermal Expansion and Decrease of Thermal Stress

—Establishing an Evaluation Method for Thermal Displacement Behavior—

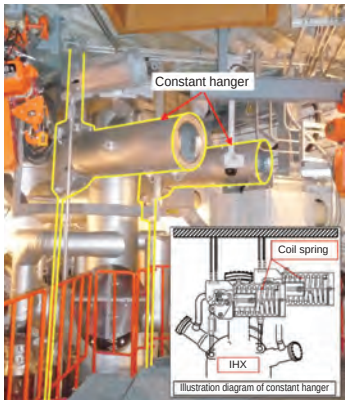

Fig.14-19 Three-dimensional floating support system
In general, a pipe elbow is employed to mitigate against thermal displacement. The HTTR adopts a three-dimensional floating support system in which the high temperature components are hung from the ceiling with a constant hanger. This makes it possible to connect components via the shortest distance using a double pipe where the internal structure is complex.

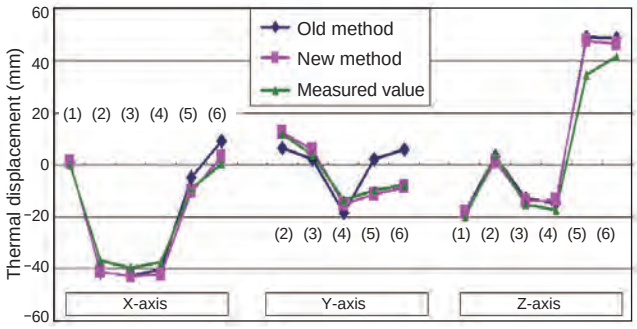

Fig.14-21 Measurement and analysis of thermal displacement
Oil snubber resistance force has a significant impact on displacement in the horizontal direction (X-axis and Y-axis). By the oil snubber in the analysis having zero resistance force, the measured value was reproduced with high accuracy.

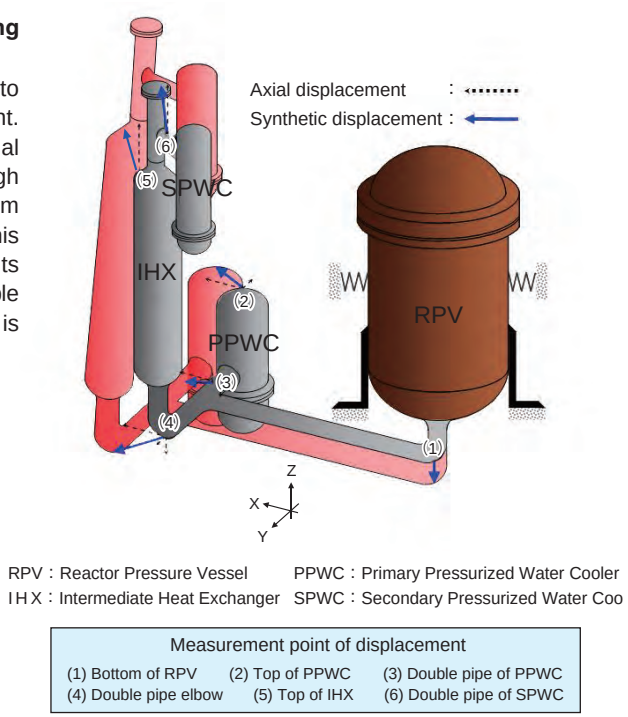

Fig.14-20 Measured value of displacement behavior
The thermal displacement behavior measured value of the high temperature component and piping is shown in red.

In the High Temperature Engineering Test Reactor (HTTR), the primary coolant temperature rises to 950 ℃ in the reactor and is returned to the reactor at 400 ℃. As the thermal displacement of the high temperature component and piping shows complex behavior, the structural support system must permit thermal expansions and must withstand earthquakes.

To make the primary cooling system in HTTR more compact, a three-dimensional floating support system has been adopted, which consists of constant hangers, rigid hangers, and an oil snubber (Fig.14-19). By means of the oil snubber, this system permits slow movement such as thermal expansion and restrains sudden movement such as earthquakes. We measured the thermal displacement of the high temperature component and piping in the HTTR (Fig.14-20).

The intermediate heat exchanger (IHX) is a long structure, so there are many intervening support structures installed around it. We have been developing an evaluation method for the thermal expansion behavior of the high temperature component and piping. In past methods, the sliding speed of the oil snubber was modeled at 1 mm/sec. In the HTTR, the temperature change in operation is slow, and the sliding resistance force becomes 4 to 5 mm/day.

Analysis was performed using ABAQUS under the following conditions: the component and piping were modeled by a beam element; hangers were modeled by a spring element; and the resistance force of the oil snubber was zero. The horizontal displacement (X-axis and Y-axis) effect of the oil snubber is analyzed with high accuracy. The Y-axis displacement, at (5) and (6), matches the measured value in the new method, and the prediction accuracy of the analysis was improved by 10% (Fig.14-21).

The thermal displacement behavior evaluation method we established contributes to the technological development of a high-temperature gas reactor, and demonstrates the practicality of the three-dimensional floating support system.

Reference

Shinohara, M. et al., Evaluation of Thermal Displacement Behavior of High Temperature Component and Piping System in HTTR, JAEA-Technology 2009-057, 2009, 33p. (in Japanese).

14-10 Quick Change of Micron-Size Ion Beam

—Integration of Cocktail Beam Acceleration and Microbeam Formation Techniques—

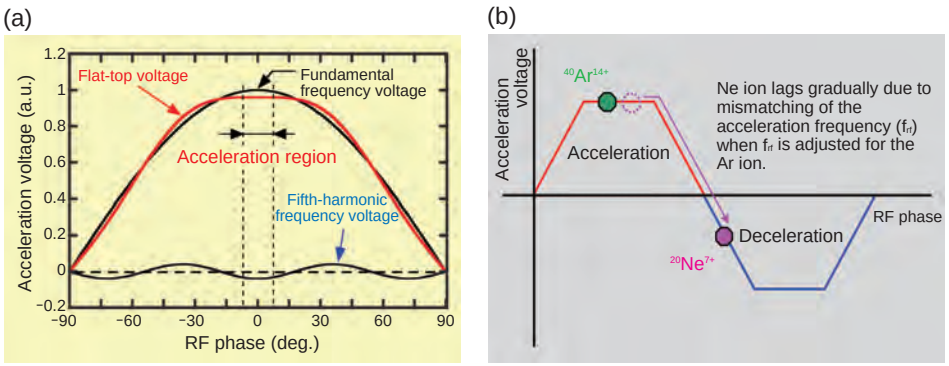

Fig.14-22 Flat-top acceleration concept and cocktail beam acceleration techniques
(a) Flat-top acceleration produces an ion beam with a narrow energy spread using a trapezoidal-like acceleration voltage. (b) Cocktail beam acceleration changes the ion species to be extracted from the cyclotron quickly by shifting the acceleration frequency.

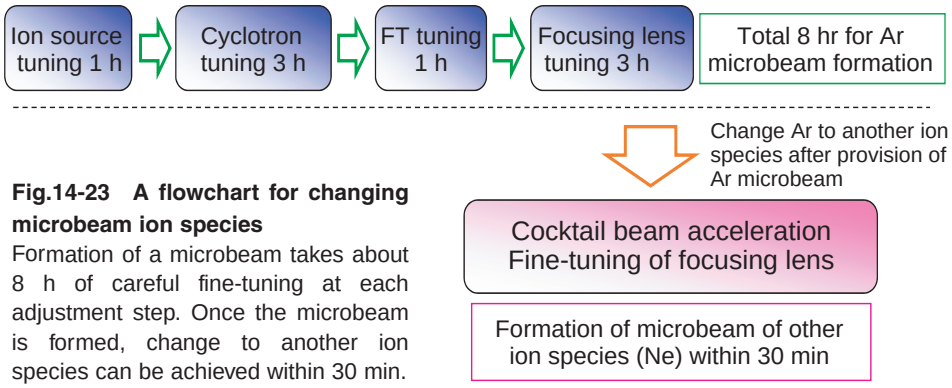

Fig.14-23 A flowchart for changing microbeam ion species
Formation of a microbeam takes about 8 h of careful fine-tuning at each adjustment step. Once the microbeam is formed, change to another ion species can be achieved within 30 min.

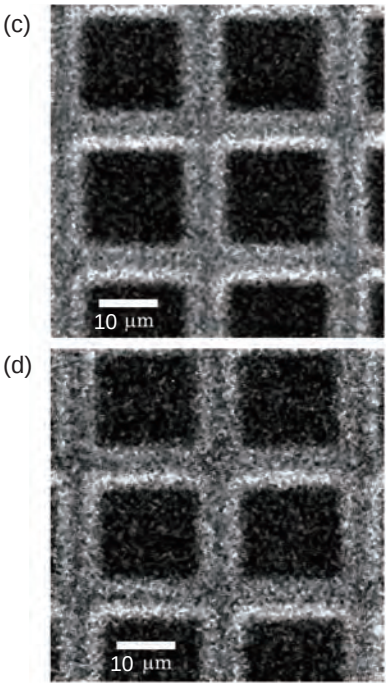

Fig.14-24 Secondary electron (SE) images of the copper grid at 1000 lines/inch obtained by irradiation with the microbeams
(c) SE image with 520 MeV $^{40}Ar^{14+}$. (d) SE image with 260 MeV $^{20}Ne^{7+}$. Both microbeam spot sizes, estimated from Gaussian fitting of brightness change at the light-dark border, are about 1 μm.

A heavy-ion microbeam with a beam spot size and hitting accuracy of about 1 μm is widely used in biotechnology and materials science research at the TIARA cyclotron facility. The microbeam is formed using a set of quadrupole magnets. The energy spread of an ion beam from a cyclotron due to rf voltage acceleration is usually on the order of 10^{-3}, and formation of a microbeam with a spot size of 1 μm is difficult because of chromatic aberration in the magnetic focusing lens. In order to reduce the energy spread to be on the order of 10^{-4}, a flat-top (FT) acceleration technique was introduced. A fifth-harmonic frequency voltage is superimposed on the fundamental to equalize the voltage in the acceleration region as shown in Fig.14-22(a). A 520 MeV $^{40}Ar^{14+}$ microbeam, which is the world's highest-energy microbeam, was formed with the FT acceleration technique. Formation of the microbeam takes about 8 h, as explained in Fig.14-23, and one species of microbeam is usually provided in an experiment. A cocktail beam acceleration technique is often used for a cyclotron to change ion species and energy quickly, as explained in Fig.14-22(b). In this technique, a few ion species having almost the same mass-to-charge ratio are injected into the cyclotron simultaneously, and only the ion species of interest, whose cyclotron resonance frequency is equal to the acceleration frequency, can be extracted from the cyclotron. The ion species to be extracted can be changed by slightly shifting the acceleration frequency. Cocktail beam acceleration was first applied to microbeam formation in order to quickly change the ion species. As a result, we have succeeded in considerably reducing the microbeam changing time to within 30 min for changing between 520 MeV $^{40}Ar^{14+}$ and 260 MeV $^{20}Ne^{7+}$ as shown in Fig.14-24.

Reference

Kurashima, S. et al., Quick Change of Ion Species of Heavy-Ion Microbeam by Cocktail Beam Acceleration Technique with the JAEA AVF Cyclotron, Nuclear Instruments and Methods in Physics Research B, vol.267, issues 12-13, 2009, p.2024-2027.

14-11 Going Deeper than -400 m Underground

—Construction of Shafts and Research Tunnels and Method for Reducing Water Inflow at the Mizunami Underground Research Laboratory—

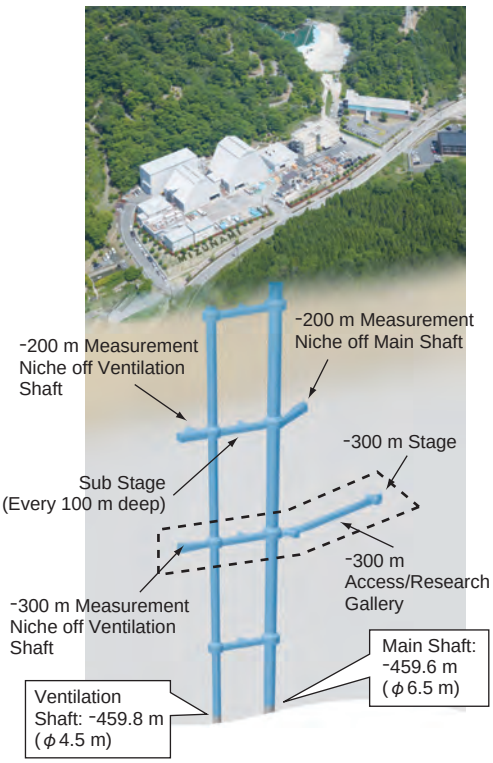

Fig.14-25 Layout of the Mizunami Underground Research Laboratory
Depth of shafts as of March 31, 2010.

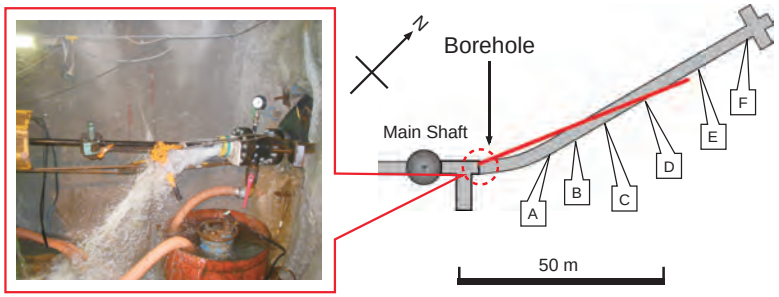

Fig.14-26 Water inflow from borehole
The rate shown in this photograph was about 1200 liters per minute.

Fig.14-27 -300 m Access/Research Gallery (Horizontal tunnel)
Borehole investigation (62.5 m long) was conducted before excavations began.

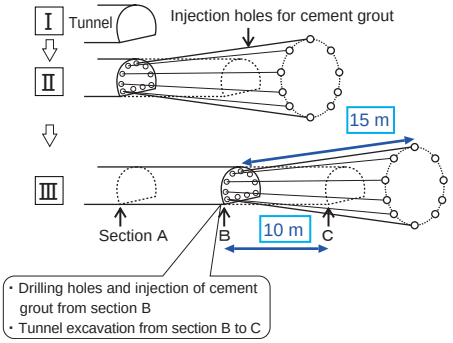

Fig.14-28 Pre-excavation grouting and tunnel excavation pattern
I→II: Injection holes about 15 m long were drilled for cement grout. Cement grout was injected into the injection holes, after which the tunnel was excavated to a length of about 10 m. III: Pre-excavation grouting and tunnel excavation steps were repeated.

The Mizunami Underground Research Laboratory, one of the main facilities in Japan for research and development of the technology for high-level radioactive waste disposal, is under construction in Mizunami City. As of March 2010, the excavation of the Main and Ventilation Shafts had reached GL -459.6 m and -459.8 m, respectively (meters below ground level, Fig.14-25).

In planning the construction, it was necessary to obtain more reliable information on the bedrock conditions in terms of the rock mass stability and hydrogeology, and therefore borehole investigations were conducted before excavations began. The results indicated that a large water inflow could be expected during the excavation of the Ventilation Shaft at around GL -200 m and from -400 m to -450 m and near the -300 m Access/Research Gallery. In order to mitigate against water inflow, pre-excavation grouting was conducted before excavation of shafts and research tunnels. Grouting refers to the injection of a material such as cement into a rock mass to stabilize and seal the rock. Our report described pre-excavation grouting and construction at the GL -300 m Access/Research Gallery.

Borehole investigations were also conducted before tunnel excavation in order to get reliable information on the bedrock conditions (Fig.14-27). The borehole drilling produced water at an inflow rate of about 1000 liters per minute (Fig.14-26). Injection holes for cement grout were drilled to a length of about 15 m, and cement grout was injected into the injection holes. Tunnel was excavated to a length of about 10 m after injection. The grouting and tunnel excavation steps were then repeated (Fig.14-28). Geological mapping during the excavation confirmed the successful injection of cement grout into the fractures. The water inflow through the grouted rock mass was reduced considerably.

In planning the construction, the water inflow reduction target was established by theoretical analysis of groundwater flow in terms of the bedrock conditions. The pre-excavation grouting was shown to be successful in subsequent excavations, and the targeted reduction was achieved. The results suggest that this methodology is effective in reducing water inflow.

Reference

Mikake, S., Ikeda, K. et al., Applicability of Countermeasure for Reduction of Groundwater Inflow and Construction of the Mizunami Underground Research Laboratory, Proceedings of the 54th Geotechnical Symposium, 2009, p.39-46 (in Japanese).

14-12 Development of Environmentally-Friendly Technique for Treating Radioactive Waste
—Development of Uranium Recovery Technique Using Ionic Liquids—

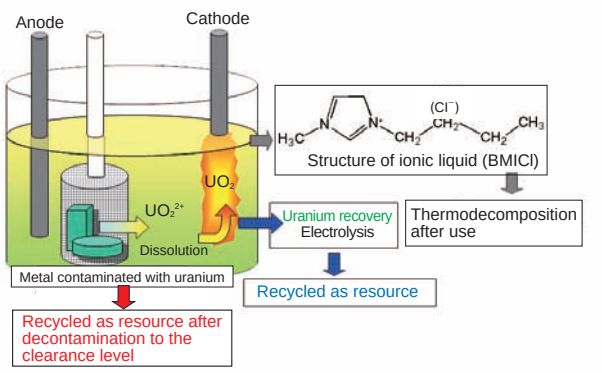

Fig.14-29 Outline of uranium recovery technique using ionic liquid
Uranium adhered to metal is removed to the clearance level, and uranium dissolved in ionic liquid is recovered by electrolysis.

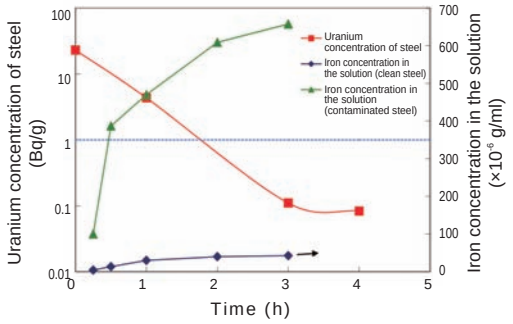

Fig.14-30 Plots of iron concentrations in ionic liquid and uranium concentrations in steels vs. time (100 ℃, in air)
The uranium concentration of contaminated steel dropped below the assumed clearance level within 3 h and iron in clean steel could not be dissolved in ionic liquid.

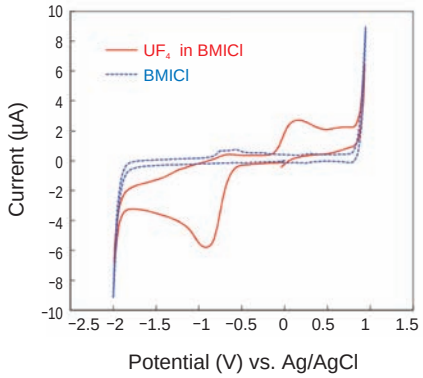

Fig.14-31 Cyclic voltammograms of the solution in BMICl (80 ℃, in air)
One reduction peak of uranium was observed around -1 V, which shows that it is possible for uranium to be recovered by electrolysis.

Among nuclear fuel cycle facilities, sludge containing uranium, or piping, towers, and vessels whose interiors are contaminated with uranium, are generated in decommissioning and operation of uranium facilities, such as uranium enrichment or uranium conversion plants. Because these wastes contain a large quantity of uranium, if the uranium they contain is removed or recovered, the recovered uranium and decontaminated metal can be recycled effectively and the amount of uranium waste will be reduced considerably.

We selected an ionic liquid known to be an environmentally-conscious solvent (a green solvent) as a treatment medium, and investigated a technique for removing uranium from waste to the clearance level (the level at which decontaminated materials are not required to be treated as radioactive waste), and a technique for recovering uranium dissolved in ionic liquid by electrolysis. Fig.14-29 shows an outline of the process. Because ionic liquids are salts that consist of only ions and have properties such as a low melting point, nonvolatility, and high conductivity, it is hoped that they can be used as safe and high-performance electrolytes.

A large proportion of metals from uranium enrichment facilities are contaminated with uranium tetrafluoride (UF_4). Dissolving steels having a surface contaminated with UF_4 in 1-buthyl-3-methylimidazolium chloride (BMICl) at 100 ℃ has confirmed that the uranium concentration in them dropped below the assumed clearance level within 3 h, and thus BMICl is highly able to dissolve UF_4 (Fig.14-30).

In addition, we confirmed a temporal change in the iron concentration in BMICl when clean steel and steel contaminated with UF_4 are dipped in BMICl, and thus clarified that the iron of contaminated steel dissolves more easily than that of clean steel. Therefore, because it is possible to dissolve only the uranium corroded part of the contaminated steel in ionic liquid, it can be anticipated that secondary waste will be reduced, since there is little extra iron dissolution (Fig.14-30).

As a result of an examination of uranium redox behavior, it has been confirmed that uranium dissolved in ionic liquid is potentially recoverable as uranium oxide by electrolysis (Fig.14-31).

From the results mentioned above, we expect that uranium can be recovered from contaminated steels and that the steels can be recycled using BMICl as a medium. It is hoped that the results will be applied in each uranium facility as an efficient method for treating uranium waste.

Reference

Ohashi, Y. et al., Application of Ionic Liquid as a Medium for Treating Waste Contaminated with UF_4, Journal of Nuclear Science and Technology, vol.46, no.8, 2009, p.771-775.

14-13 Contribution to Producing a Certificated Reference Material by AMS MUTSU
—Result of an Interlaboratory Comparison by the IAEA—

Fig.14-32 The accelerator mass spectrometer at the Mutsu Office, Aomori Research and Development Center, participated in an interlaboratoy comparison exercise
This AMS is equipped with two beam lines. The red arrow indicates the beamline for ^{129}I measurement.

Fig.14-33 Iodine extraction from seawater samples
Iodine is extracted from the upper layer (seawater) to the lower organic layer.

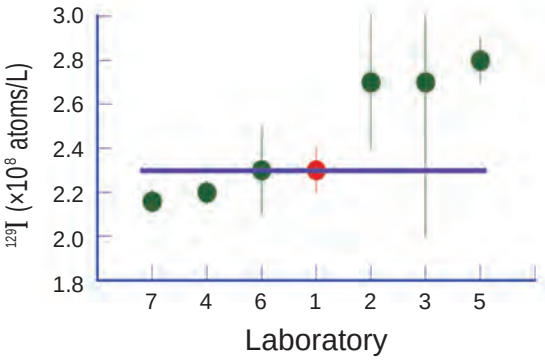

Fig.14-34 Results of the interlaboratory comparison exercise
The red point is the result of AMS MUTSU; the purple line indicates the median.

Iodine-129 (^{129}I) is one of the long lived radionuclides, and its concentration is quite low in the environment. Due to the quite low concentration of ^{129}I, it is difficult to measure ^{129}I in environmental samples by neutron activation analysis which is known to have good sensitivity for ^{129}I measurement. With the advent of Accelerator Mass Spectrometry (AMS), it is possible to measure ^{129}I in environmental samples. The AMS at the Mutsu Office, Aomori Research and Development Center, was optimized for ^{129}I measurement (Fig.14-32).

The International Atomic Energy Agency - Marine Environmental Laboratories (IAEA-MEL) produces certificated reference materials for accurate and precise determination of radionuclide samples in marine samples. However, IAEA-MEL did not have any certificated reference materials for ^{129}I. For this reason, IAEA-MEL conducted a study to produce new certificated reference material for ^{129}I in seawater samples.

To produce the certificated reference material, it is desirable to use measurements from many laboratories, but there are few laboratories that can measure ^{129}I in seawater samples. IAEA-MEL requested measurements from 8 laboratories including AMS MUTSU after sampling in the Mediterranean Sea. We carried out iodine extraction from seawater samples (Fig.14-33) and then measured ^{129}I by AMS three times. The ^{129}I concentration in the sample from AMS MUTSU was obtained to be $(2.28\pm0.14)\times10^{8}$ atoms/L based on the means and standard deviation from the three results.

In October 2009, IAEA-MEL released all data which were obtained from all participants. The results from 7 of the participants are shown in Fig.14-34. Since the concentration of the samples was determined to be 2.28×10^{8} atoms/L, the new ^{129}I certificated reference material was produced by this exercise.

The new ^{129}I certificated reference material would strongly contribute not only to evaluation of the ^{129}I concentration in environmental samples, but can also be used for oceanographic tracers in the geochemical field.

Reference

Pham, M. K., Suzuki, T. et al., Certified Reference Material IAEA-418: ^{129}I in Mediterranean Sea Water, Journal of Radioanalytical and Nuclear Chemistry, vol.286, no.1, 2010, p.121-127, doi: 10.1007/s10967-010-0621-6.

About the Design of the Cover :

The cover is designed to envisage a hopeful future shining in the sky which is a clear blue like the color of the JAEA logo. This is accompanied with white colored hexagons similar to the pattern in a tortoise shell which symbolizes the wish of people for longer lives from ancient times in Japan. Coincidentally, this shape is the same as that of core fuel assemblies for both the prototype fast breeder reactor "MONJU", and the high temperature engineering test reactor "HTTR".

The images on the cover show the element mapping of MOX-6.9wt%SiO_2 analyzed by EPMA (top left), and the HTTR-IS nuclear hydrogen production system (bottom right).

The former is the results of tests carried out to understand the behavior of silicon impurities in MOX fuel, the precipitation conditions of compounds were confirmed (Topic 1-9).

The latter is expected as clean hydrogen production technique with no carbon dioxide emissions, based on the thermochemical iodine-sulphur (IS) process using the heat from the high temperature gas-cooled reactor (Topic 9-2).

JAEA R&D Review 2010

Published by Japan Atomic Energy Agency (JAEA)
Editorial Office: Intellectual Resources Section, Intellectual Resources Department
2-4 Shirakatashirane, Tokai-mura, Naka-gun, Ibaraki-ken 319-1195, Japan
Phone: +81-29-282-6387 Facsimile: +81-29-282-5920
e-mail: ird-seika_shi@jaea.go.jp

Japan Atomic Energy Agency